University of Strathclyde

Department of Naval Architecture, Ocean & Marine Engineering

IMPROVING RELIABILITY ASSESSMENT OF OFFSHORE STRUCTURES USING BAYESIAN METHODS

By

HADI KHALILI

A thesis presented in fulfilment of the requirement for the degree of Doctor of Philosophy

Glasgow, UK

AUTHOR STATEMENT

This thesis is the result of the author's original research. It has been composed by the author and has not been previously submitted for the examination which has led to the award of a degree.

Signed: Hadi Khalili *Date*: 10 November 2021

DEDICATION

Dedicated to

My father, Samad Khalili; My mother, Sharifeh Heidari

My siblings; and my wife, Yekta

ACKNOWLEDGEMENTS

First and foremost, I would like to thank my supervisor Dr. Selda Oterkus for her help, consistent guidance, and valuable support throughout my research work.

I am especially honoured to have had Prof. Nigel Barltrop as my supervisor throughout my study. His unparalleled depth of knowledge, generosity, and vision has helped me during my research.

This study was made possible by the sponsorship and support of Lloyd's Register Foundation. The Foundation helps to protect life and property by supporting engineering-related education, public engagement, and the application of research.

The work was enabled through, and undertaken at, the National Structural Integrity Research Centre (NSIRC), a postgraduate engineering facility for industry-led research into structural integrity established and managed by TWI through a network of both national and international Universities.

Thanks to Dr. Ujjwal Bharadwaj for providing the conditions for conducting my research at NSIRC.

I would also like to thank to:

- The administrative and technical staff of the NAOME Department for their great support
- The administrative staff of the NSIRC for their great support
- All of my friends in the NSIRC and TWI for their friendship
- Finally, my family for their support

ABSTRACT

Offshore jacket platforms are commonly adopted structures for oil and gas production in shallow water depths. A large number of existing jacket platforms are operating beyond their design life due to the high cost of replacement. The safety of these structures is a major concern of the operators. Jacket structures are constructed as truss frameworks in which tubular members are welded together to create a steel frame. Fatigue damage in jacket structures is most probable to occur at the welded tubular joints due to the geometric discontinuity of the connections which produces high-stress concentrations in these intersections. Fatigue is a complicated phenomenon. As a result of the idealisations and approximations employed in the analysis process, fatigue analysis will be associated with some degree of uncertainty.

The overall aim of this research work is to develop an innovative approach to improve the fatigue reliability assessment of jacket structures using Bayesian methods to incorporate new information obtained from the inspection results.

Due to the existence of many uncertainties in the fatigue process and other uncertainties in loads and the resistance of the structure, a probabilistic approach for fatigue analysis of jacket structures is a rational and consistent basis for the inclusion of uncertainties. To develop a probabilistic approach for the reliability-based assessment, it is necessary to determine the probability of failure of each joint during the operational life of the structure. However, jacket platforms are redundant structures. Therefore, reliability analysis at a system level is more applicable than at the component level. In this research, the structural reliability analysis at the system level for a jacket platform is performed under both fatigue and extreme loading. At first, the probability of fatigue failure for each component is calculated by using the Monte-Carlo simulation. Then, important failure paths are identified by using a searching process. The system failure criterion is evaluated by comparing the platform strength and loading distributions in terms of base shear. Having calculated the structure strength and loading distributions, the annual probability of failure under an extreme wave is calculated and compared to the tolerable probability of failure.

To maintain the safety of jacket platforms in service life concerning fatigue failure, inspection is an important measure. However, the significant costs of inspections,

particularly underwater inspections, make it important to properly prioritise inspection locations and inspection frequency. The cost of an inspection is directly proportional to the number of inspections carried out. Therefore, it is required to concentrate only on fatigue-sensitive locations in the structures. At the component level, fatigue-sensitive locations are the locations that have low estimated fatigue lives. However, at the system level, critical components are those joints that have a big effect on system reliability. Due to the significant costs of inspections, the identified failure paths can be used as a database for the inspection plan.

Inspection activities provide additional information, which includes detection and measurement of crack size. After an inspection of a structure, the perception of structure condition is improved. In general, a Bayesian framework is used to update the probability distributions of the uncertainties such as crack size in a joint. The updated crack size distribution can be used to update the estimation of the probability of failure. Different methods of Bayesian inference to update the probability distribution of the crack size are presented in this research.

The credibility of the Bayesian updating process is one of the main concerns for the platforms' owners. A Bayesian process is a mathematical tool that processes the inputs and generates the outputs based on the provided inputs. Hence, if the inputs are inaccurate, the updating results are worthless and can even lead to wrong decisions for the next inspection activity. Therefore, a novel approach is developed to assess the reliability of the Bayesian methods and assure the platforms' owners regarding the updating results. This approach is capable to update the probability distributions of all uncertain parameters involved in the fatigue analysis besides the crack size. Three different categories of uncertainties are updated including, Fatigue crack size; POD curve; and uncertainties involved in the predicted model of the fatigue crack size (e.g. initial crack size, crack growth parameter, stress range, etc.). The presented methodology maximises the benefit of the inspection results by updating several uncertain parameters involved in the fracture mechanics approach. Moreover, guidance is provided to help the user to apply the proposed methodology in practice.

CONTENTS

List of Figures

List of Tables

1 . INTRODUCTION

1.1 Background and Motivations

Offshore jacket structures have been used in the oil and gas sector for decades. They are one of the most common types of structures for oil and gas production in shallow and intermediate water depths. Due to improvements in technology to recover more oil and gas efficiently, the interest in using these structures beyond their initial design lives has been increased. Hence, a large number of existing offshore structures are operating beyond their design life due to the high cost of replacement. The safety of these structures is a major concern of the operators.

Due to the existence of many uncertainties in loads applied to these structures and the resistance (strength) of the structure, a probabilistic approach for the assessment of existing offshore structures is a rational and consistent basis for the inclusion of uncertainties. Reliability assessment, which is a probabilistic approach, is often used to determine the probability of structural failure during the structure's operational life.

Fatigue failure is one of the critical failure modes in offshore structures. Offshore jacket platforms consist of tubular members that are welded together to form a steel space frame. These tubular joints are prone to fatigue damage due to the high-stress concentrations at the intersections; defects during the welding process and cyclic loading of waves apply to the structure [1].

Field observations and laboratory tests have shown that in this type of connection, a fatigue crack starts at the weld toe at the hot-spot location and gradually propagates around the intersection and through the tubular wall [2].

Fatigue issue in a tubular joint is a complex phenomenon governed by many factors. In the beginning, there may be several cracks around the intersection, but they usually join together and form a relatively long semi-elliptical surface crack [2]. Penetration of crack through the thickness causes a major reduction in joint stiffness. This stage is usually considered the end of the fatigue life of the joint [3]. Therefore, estimation of the remaining fatigue life of the joint is the main concern in the structural assessment of these platforms.

To maintain the safety of jacket platforms in service life with respect to fatigue, the propagation through the thickness of the wall needs to be monitored. To assess the state of damage, offshore platforms are periodically inspected. Regarding fatigue damage, the information from inspection consists mainly of detection and measurement of crack sizes.

1.2 Problem Description

Many offshore structures are operating beyond design life. Due to the high cost of replacement, reliability assessment is a rational and powerful tool to ensure the safety of a platform.

Fatigue failure is one of the critical failure modes in jacket structures. Fatigue is a very complicated phenomenon. As a result of the idealisations and approximations in the analysis process; the existence of many uncertainties in loads applied to such structures and the resistance of the structure, a probabilistic approach for performing fatigue analysis is a rational and consistent basis for the inclusion of uncertainties.

This study reviews a procedure to carry out a fatigue reliability analysis of welded tubular joints in a jacket offshore platform and also to quantify the effect of inspection. It introduces a probabilistic model for carrying out fatigue reliability analysis of structural joints based on fracture mechanics.

It is worth mentioning that the safety requirements of offshore structures are generally assessed at the component level and if the safety requirements are not satisfied, the structure needs strengthening to meet the additional demands. However, taking into account the design procedures and the structural redundancy, it is seen that despite the failure of a few components, the structure can undergo load redistribution and thus avoid failure. The system reliability analysis for large structures with high redundancy, such as offshore jacket platforms, may be complex due to the several structural components.

The inspection programs are crucial to monitor the fatigue performance of the tubular joints and also to extend the service life of jacket structures. Therefore, jacket platforms are periodically inspected to make sure that they can continue in service with an acceptable level of reliability. However, the significant costs of inspections,

particularly underwater inspections, make it important to properly prioritise inspection locations and inspection frequency.

Regarding fatigue damage, the information from inspection consists of detection and measurement of crack sizes. Such information can be used to update the probability distributions of crack size in a joint and of some uncertain parameters in a fracture mechanics model for crack growth.

Using the updated distributions, it is also possible to update the estimates of the time-evolving joint reliability. In this study, the Bayesian framework is used to update the probability distributions of the uncertainties using information from inspection reports. The purpose of updating is to incorporate any available inspection history into an improved estimate of the parameters.

1.3 Aim and Objectives

The main purpose of this research is to develop an innovative approach to improve the fatigue reliability assessment of jacket structures using Bayesian methods to incorporate new information obtained from inspection results.

To achieve this goal, the main objectives are defined as:

1) Developing a probabilistic fatigue model based on an appropriate limit state and considering relevant uncertainties to obtain the component probability of failure in fatigue failure mode
2) Developing a methodology to obtain the system probability of failure by considering both fatigue and extreme wave loads
3) Prioritising the inspection locations by finding out the effect of each component failure on the system reliability
4) Using conventional Bayesian methods to update the fatigue crack size distribution, and subsequently, updating the component probability of failure
5) Proposing a novel Bayesian approach for updating the distributions of all uncertain parameters involved in the fatigue analysis
6) Investigating the credibility of the proposed approach

1.4 Approach

Figure 1.1 illustrates the proposed approach for performing and updating fatigue reliability analysis of the jacket structures.

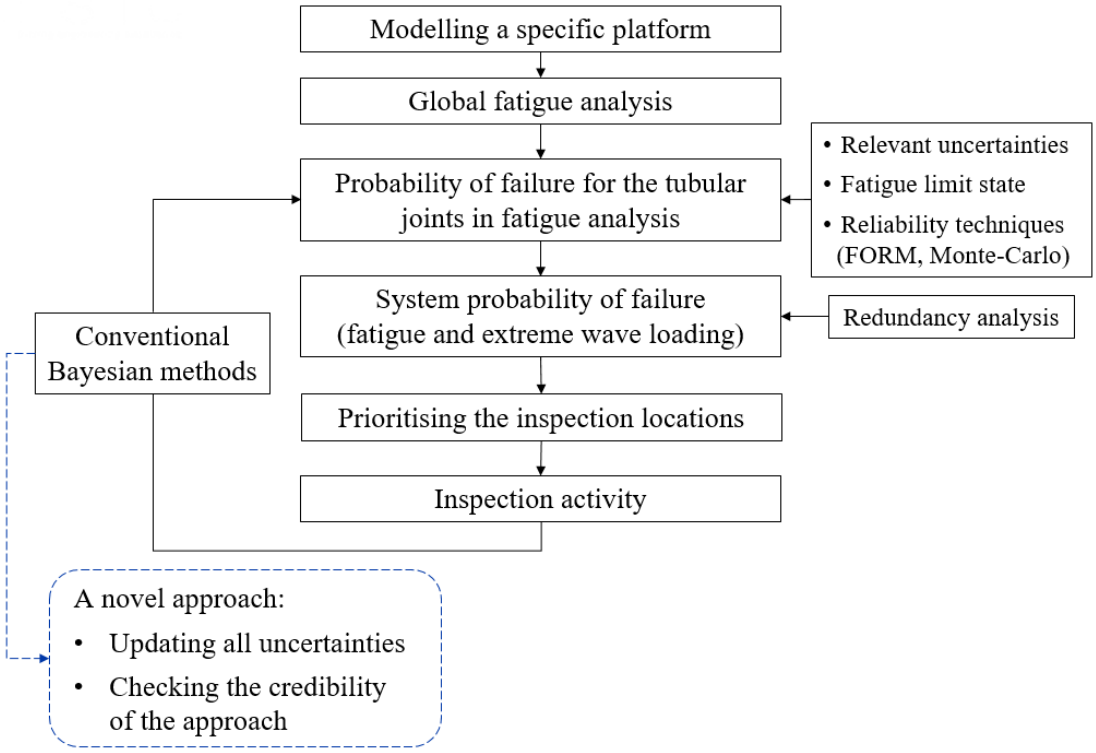

Figure 1.1. Proposed approach flowchart for fatigue reliability analysis (PhD outline)

The outline of this PhD research is explained briefly as:

Modelling a specific platform

A three-dimensional structural model of the platform is generated using SESAM software [4]. The model incorporates all primary members in the topside and the jacket. This is a geometrical space frame that integrates the jacket, the topside, and the foundation systems in one combined structure (Figure 1.2). The model's geometrical properties conform to the jacket's as-built drawings. The model also includes all gravitational and environmental loads.

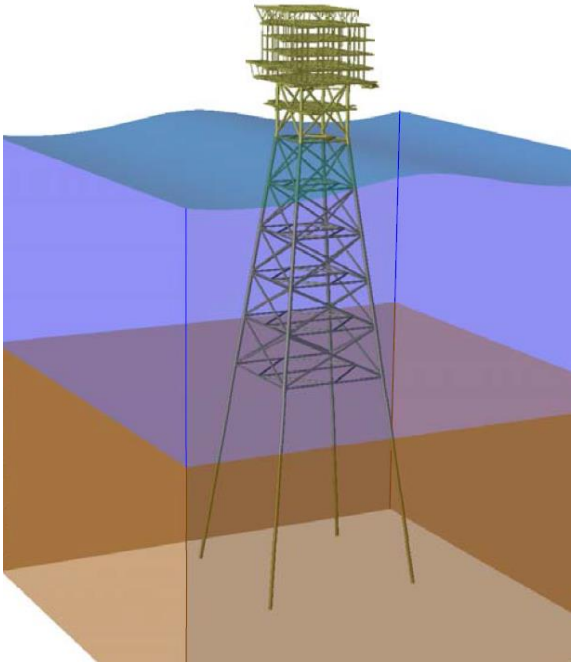

Figure 1.2. Structural model of the jacket platform in SESAM software

Global fatigue analysis

A global spectral fatigue analysis is performed using the characteristic variables. The spectral fatigue analysis is used for dynamically sensitive structures in shallow to medium water depths. The result of this analysis is the hot spot stress transfer function of each joint in the structural model.

The transfer function is obtained by finding the stress range, at the location of interest, for a range of wave frequencies and dividing the results by the wave height. Having obtained the transfer function, the hot spot stress spectrum can be achieved.

The stress spectrum then is used in the calculation of the probability of failure of the tubular joints.

Probability of failure for the tubular joints in the fatigue analysis

Due to the existence of uncertainties involved in quantifying the fatigue process, a reliability approach is adopted to assess the probability of failure. In this study, fatigue reliability analysis is performed based on the fracture mechanics approach. In the fracture mechanics approach, relationships between the average increment in crack growth during a load cycle and a global parameter are developed [5]. It will be shown

that the crack size at each time is a function of several parameters such as initial crack size, material properties, hot spot stress range, and the number of load cycles.

For calculation of the probability of failure for a tubular joint, the following steps should be considered:

- Formulation of the uncertainties involved in the fatigue process

  Reliability analysis depends on the choice of the uncertainties and their statistical descriptions [6]. Therefore, uncertainty modelling becomes an important consideration for offshore structural analysis. In dealing with the fatigue of offshore structures, there are many uncertainties involved in treating the process deterministically, such as environmental parameters, structural response calculation, stress concentration factors, crack growth parameters, etc. Some of these uncertainties are associated with the modelling of structures and the random wave environment. The others represent uncertainties in the analysis of crack growth at the tubular joint.

- Define a desirable limit state

  To evaluate the probability of failure of a component, failure needs to be defined. Failure is usually defined based on the concept of a limit state, which represents a boundary between the desired and undesired performance of a structural system or its component [6]. Several limit states such as crack size criterion, equivalent fatigue strength criterion, and failure assessment diagram, have been suggested for fatigue limit state. In this study, the crack size is considered as the failure criterion. Hence, failure occurs, as soon as the crack size is bigger than a critical value. Therefore, the probability of failure is the probability that an initial crack grows beyond the critical crack size.

- Obtain the component probability of failure

  In the structural reliability theory, there are several ways of calculating the reliability and the corresponding probability of failure, such as FORM (First Order Reliability Methods), SORM (Second Order Reliability Methods), and the Simulation Techniques (e.g., Monte-Carlo Simulation). In this study, the Monte-Carlo simulation is used to obtain the component probability of failure.

- Sensitivity analysis

  Different sources of uncertainties contribute to the fatigue reliability analysis of tubular joints of jacket platforms. The influence of these uncertainties on the overall probability of failure has been studied through sensitivity analysis.

System probability of failure

Jacket structures are redundant structures. A redundant structure has more structural members than is necessary. Therefore, if some of the structural members are damaged, the structure will not necessarily fail or collapse, since the load can be redistributed among undamaged members [7]. Calculation of system probability of failure is difficult because the number of possible failure paths would be enormous. It would be practically impossible and not necessary to identify all of them. Therefore, identification of the dominant failure paths is one of the major tasks in the system reliability analysis for such structures [8].

An approach for obtaining system reliability is introduced that can identify the dominant fatigue failure paths of the structures. In this approach, the sequence of the structural joints most likely to fail is established. For this purpose, the joint with the highest failure probability is considered to have failed. This joint and corresponding member is removed from the model and the next probable joint to failure is then searched. The procedure is repeated until a failure path is developed. A developed failure path will result in system failure.

To find out a complete failure path, after removing the critical component, the system failure criterion is checked. The system failure criterion is evaluated by comparing the platform strength and loading distributions in terms of base shear. To define a probabilistic formula for load, the global response surface method is adopted to relate the environmental load to the response of the structure. Nonlinear pushover analysis is also carried out to determine the capacity of the platform. Having calculated the structure strength and loading distributions, the annual probability of failure under an extreme wave is calculated and compared to the maximum probability of failure. When this probability exceeds the maximum acceptable probability, the platform is assumed to fail.

Prioritising the inspection locations

An inspection program is an important measure to maintain the safety of jacket platforms in service life concerning fatigue failure. However, the significant costs of inspections, particularly underwater inspections, make it important to properly prioritise the inspection locations. At the component level, fatigue-sensitive locations are the locations that have low estimated fatigue lives. However, at the system level, critical components are those that have a great effect on system reliability.

Due to the significant costs of inspections, the identified failure paths can be used as a database for the inspection plan. By identifying the dominant failure paths, the critical joints that have a greater effect on the system probability of failure are selected and therefore inspection can be focused on these joints. Therefore, instead of inspection of non-critical components, the inspection can be focused on the crucial joints.

Inspection activity

Fatigue damage accumulates during the structure's lifetime as the crack size increases. The accumulation of damage causes deterioration of the component capacity and increases the probability of failure. To assess the state of damage, offshore platforms are periodically inspected. Regarding fatigue damage, the information from inspection involves detection and measurement of crack size.

Inspection activities are performed by visual checks or more sophisticated non-destructive tests (NDT). Magnetic particle inspection (MPI), eddy current inspection (ECI), alternating current field measurement (ACFM), and flooded member detection (FMD) are the NDT methods usually used for detecting cracks in offshore structures; whilst ultrasonic testing (UT) and alternating current potential drop (ACPD) are the ones used for measuring the dimensions of the cracks [1]. The success rate of inspection techniques to detect and measure the crack size varies. For any given NDT method there is always a detectable crack size which means that smaller crack size may not be detected. Moreover, whenever a crack size is measured, it must be treated with a certain degree of uncertainty depending on the accuracy of the equipment used and the skills of the technicians.

Conventional Bayesian methods

The provided information from the inspection activities can be used to update the probability distribution of the crack size in a joint. A Bayesian framework is typically used for updating the probability distributions of the crack size in tubular joints using information from inspection reports of offshore platforms. Bayesian inference provides a formal method of belief updating when new information becomes available. The purpose of updating is to incorporate any available inspection history into an improved estimation of the parameters. There are two main approaches for obtaining the updated distribution of an uncertain parameter:

- Analytical Approach (Conjugate):

  The updated (posterior) distribution is derived in a closed-form

- Numerical Approach

  The posterior distribution is obtained numerically, and it cannot be presented in an analytical form.

For a given joint, the outcome of an inspection at any time can be:

- No crack is detected
- A crack is detected and measured

Depending on the results of inspections, an expression for the updated crack size is obtained. After updating the crack size distribution, the probability of failure for each component is updated.

After updating the distribution of the crack size, it is possible to update the estimation of joint reliability and also system reliability.

Proposing a novel Bayesian approach

The conventional Bayesian methods are used to incorporate inspection results to update the probability distribution of crack size in a tubular joint. However, several uncertain parameters exist in the estimation of the fatigue behaviour of the tubular joints. Therefore, a novel methodology is proposed to update the probability distributions of all uncertain parameters (including the crack size) when new

information becomes available. Three different categories of uncertainties are updated using this methodology:

- Fatigue crack size;
- POD curve;
- Uncertainties involved in the predicted fatigue crack size (i.e. initial crack size, crack growth parameter, stress range, and uncertainty in the estimation of the geometry function).

The credibility of the updating process is the main concern in any updating application. However, the credibility of the conventional Bayesian methods was not considered in the previous studies. The reliability of any Bayesian updating method depends on how reliable the inputs (e.g. inspection results) are. A Bayesian process is a mathematical function that processes the inputs and generates the output based on the provided inputs. Therefore, if the inputs are inaccurate, the updated results may be poor and can even lead to wrong decisions. Unlike previous studies, the reliability of the proposed approach is investigated to find out when the proposed approach might lead to poor results.

1.5 Thesis Structure

In this research, a procedure is developed to connect the component fatigue reliability, system reliability, and the mechanism to update the reliability using the inspection results.

The thesis is organised into seven chapters, the first being the introduction. It also describes the problem, research aim, objectives, and approach as well as the thesis structure.

The basic theory of probability and concept of the reliability analysis is reviewed in Chapter 2. Random variables and different distributions are explained. The fundamental concepts of the reliability analysis including load, capacity, limit state functions, reliability index, and probability of failure are introduced. Different techniques for estimation of the reliability, including First Order Reliability Method (FORM), Second Order Reliability Method (SORM), and Monte-Carlo simulation,

and advantages/disadvantages of each method are explained. Finally, some sensitivity measures are explained for the selection of important basic variables.

The main purpose of Chapter 3 is to obtain the fatigue component reliability of the tubular joints. This chapter explains the fatigue process, fatigue analysis, and reliability analysis of offshore platforms, briefly. On the subject of fatigue analysis of a tubular joint, two approaches are considered; the S-N curve approach and the fracture mechanics (FM) approach. To carry out the reliability analysis it is necessary to develop appropriate probabilistic models for the wave loads. Probabilistic modelling of the sea surface is required for fatigue analysis. Stress response of individual members is obtained using spectral analysis of offshore structures by considering a narrow-banded stress process [5].

The proposed approach for performing fatigue reliability analysis is illustrated through application to a typical jacket platform. A three-dimensional structural model of the platform is generated using SESAM software [4]. For calculation of the probability of failure for a tubular joint, the following steps are considered:

- Formulation of uncertainties involved in the fatigue failure process
- Define a desirable limit state
- Obtain the component reliability

A fatigue crack growth model is developed based on the fracture mechanics (FM) approach. This model predicts the fatigue crack size at any time for each tubular joint in a jacket platform. This crack size is considered as the failure criterion and failure occurs when the crack size is bigger than a critical value. The estimation of the reliability for individual tubular joints is obtained by using FORM and Monte-Carlo simulation. Sensitivity studies are also performed to find out the influence of the various random variables on the component probability of failure.

Due to the high redundancy of jacket platforms, the probability of failure of the whole system is more applicable than the component probability of failure. A system reliability approach is presented in Chapter 4 of this research work to calculate the probability of failure of a jacket platform considering fatigue and extreme wave loads.

The system reliability analysis for offshore jacket platforms with high redundancy may be complex due to the several structural components. Important failure paths are identified by using a searching algorithm, in which, components with the maximum change in the accumulated damage are considered as the candidate joints in the path. By removing the candidate joint, which is assumed to fail in fatigue, the probability of failure of the structure under extreme wave loading increases.

System failure criterion is evaluated by comparing the platform strength and loading distributions in terms of base shear. Nonlinear pushover analysis is carried out to determine the capacity of the platform and the annual probability of failure under an extreme wave is calculated. When the probability of failure exceeds the maximum acceptable probability, the platform is assumed to fail.

Since the components in the failure paths have a great effect on the system reliability, an inspection strategy can be proposed based on the effect of each component on the system reliability. This is an alternative inspection plan in comparison with the regular inspection plan. In this plan, due to the significant costs of inspections, the inspections are prioritised on the critical joints (joints that lead to a higher system probability of failure).

Chapter 5 shows how the inspection results can be incorporated for updating the crack size distribution in a tubular joint. Offshore platforms are periodically inspected to assess the state of damage. Regarding fatigue damage, the information from inspection consists mainly of detection and measurement of crack sizes. Such information can be used to update the probability distributions of crack size in a joint. A Bayesian framework is used for updating the probability distributions of the crack size in tubular joints using information from inspection reports.

Two different Bayesian approaches for updating the crack size distribution are introduced; the analytical method (conjugate), and the numerical method. The main advantages and disadvantages of each method are explained. Moreover, the effect of different parameters and inputs on the updated distribution of the crack size is investigated.

After updating the crack size distribution, the reliability of each component can be updated. Depending on the results of inspections, the updated reliabilities may be higher or lower than the original values.

A new methodology for updating the probability distribution of all uncertain parameters involved in fatigue analysis is presented in Chapter 6. A framework is developed for updating the probability distributions of the parameters of a fracture mechanics model and also crack size in tubular joints using information from inspection results. To find out which parameters have great influences on the updated distributions, sensitivity analyses are performed.

The credibility of the updating process is the main concern in any updating application. Chapter 6 also investigates the reliability of the proposed approach to find out when the proposed approach might lead to poor results. To help the user to implement the proposed approach in practice, guidance for using the approach is provided by explaining the framework, advantages, and limitations.

Moreover, since both Chapter 5 and Chapter 6 approaches can be used to update the crack size distribution, the results of these two chapters are compared.

Finally, Chapter 7 summarises the important findings of this dissertation and discusses future extensions of this research. It also highlights the novelty and contributions of this research.

1.6 Publications in Connection with the Research Thesis

At the time of writing, the following papers drawn from this thesis have been published in scientific journals. The list below includes the most relevant chapters of the thesis to which the publications correspond.

Journal papers

- **Khalili, H**.; Oterkus, S.; Barltrop, N.; and Bharadwaj, U. (2021). "Different Bayesian Methods for Updating the Fatigue Crack Size Distribution in a Tubular Joint", Journal of offshore mechanics and Arctic engineering, Vol.143 (2), DOI: 10.1115/1.4048155
  (Related to Chapter 5 of this thesis)

- **Khalili, H.;** Oterkus, S.; Barltrop, N.; and Bharadwaj, U. (2020). "Updating the Distributions of Uncertain Parameters Involved in Fatigue Analysis", Journal of marine science and engineering, Vol.8 (10), p.1-20, DOI: 10.3390/jmse8100778 *(Related to Chapter 6 of this thesis)*

Book Chapter

- **Khalili, H**.; Oterkus, S.; Barltrop, N.; Bharadwaj, U.; and Tipping M. (2019). "System reliability calculation of jacket platforms including fatigue and extreme wave loading", 7th International Conference on Marine Structures, Croatia. CRC Press, London, pp. 576-603. ISBN 9780367278090
  (Related to Chapter 4 of this thesis)

Abstracts and Conference presentations

- **Khalili, H.;** Oterkus, S.; Barltrop, N.; and Bharadwaj, U. "Different Bayesian Methods for Updating the Distribution of Fatigue Crack Size", National Structural Integrity Research Centre Annual Conference, 23-24 July 2020, Cambridge, UK

- **Khalili, H.;** Oterkus, S.; Barltrop, N.; and Bharadwaj, U. "Updating the Distribution of Uncertain Parameters in the Fatigue Analysis", National Structural Integrity Research Centre Annual Conference, 2-3 July 2019, Cambridge, UK

2 . CONCEPT OF RELIABILITY ANALYSIS

2.1 Introduction

The main purpose of engineering design is to provide minimum levels of serviceability and safety during the structural lifetime. There are several sources of uncertainties related to loading, material properties, engineering models, etc. These uncertainties might lead to over-design (or under-design) solutions for the considered application. Therefore, this is a difficult task to consider these uncertainties properly in engineering applications.

Reliability analysis methods provide a mathematical framework for considering these uncertainties in the design and assessment of the systems. The main objective of reliability analysis methods is to evaluate the ability of systems to remain safe during their lifetime. Different reliability methods have been established to take into account the uncertainties involved in an engineering problem.

The main objective of this chapter is to introduce the concept of reliability analysis that can be used for engineering applications. This chapter includes fundamental discussions about the reliability analysis which is mainly based on the reference books (e.g. [6], [9], [10], and [11]).

The chapter starts by introducing the basics of probability theory needed for reliability analysis (Section 2.2). Random variables and different distributions are explained in this section. Section 2.3 explains the fundamental concepts of the reliability analysis including load, capacity, limit state functions, reliability index, and the probability of failure. Section 2.4 introduces various techniques for estimation of reliabilities including First Order Reliability Method, Second-Order Reliability Method, and Monte-Carlo Simulation. Usually, several random variables exist in reliability analysis applications. To find out which of the random variables is more important in its contribution to the probability of failure, Section 2.5 explains the sensitivity measures.

2.2 Probability Theory

2.2.1 Basics

The theory of probability is based on the set theory. A set, e.g. X, is a collection of sample points with a common property. The sample points may be objects or numerical values and are generally referred as members, $x \epsilon X$.

The set of all possible members is called the universal set or sample space and it is shown by S. The set that contains nothing is the empty set or null set (Φ). An event is defined as a subset of a sample space. Each event has a set of sample points. If the event is empty, i.e., contains no sampling points, it is said that this event is impossible. If the subset contains all sample points of a sample space, the event is certain [9].

Measuring the possibility that each set will happen is the main concern of the probability theory. The algebra of sets is carried out with the following operators:

- Union ($\cup$), the OR operator
- Intersection ($\cap$), the AND operator

The complementary event to E (which is usually shown by $\bar{E}$) contains all sample points in S, which are not included in E [9]. The complement event of a set is defined in a way that:

$$E \cup \bar{E} = S$$
$$E \cap \bar{E} = \emptyset \quad (2\text{-}1)$$

The definition of probability is based on three axioms [9]. There is no matter which interpretation of probability is chosen. While it satisfies these three axioms, any results derived through the correct use of the probability theory will be mathematically valid.

- Axiom 1: The probability of an event is:

$$0 \leq P(X) \leq 1 \quad (2\text{-}2)$$

- Axiom 2: The probability of a certain event (sample space) is equal to one:

$$P(S) = 1 \quad (2\text{-}3)$$

- Axiom 3: The probability of an event which is the union of two mutually exclusive events is the sum of the probability of these two events:

$$P(X \cup Y) = P(X) + P(Y) \tag{2-4}$$

Two events are mutually exclusive when:

$$P\ (X \cap Y)\ =\ \Phi \tag{2-5}$$

If two events X and Y are not mutually exclusive, it is easy to show that the probability of their union is:

$$P(X \cup Y) = P(X) + P(Y) - P(X \cap Y) \tag{2-6}$$

To calculate the probability of the union of two non-exclusive events the probability of their intersection needs to be known. The probability of the intersection of two events can be calculated using the multiplication rule, which can be written as:

$$P(X \cap Y) = P(X|Y) \times P(Y) = P(Y|X) \times P(X) \tag{2-7}$$

where $P(X|Y)$ and $P(Y|X)$ are conditional probabilities, i.e., the probability of occurrence of one event given that the other event has occurred.

Two events are statistically independent events when the occurrence of one event does not depend on the occurrence of another event, i.e.:

$$\begin{aligned} P(X|Y) &= P(X) \\ P(Y|X) &= P(Y) \end{aligned} \tag{2-8}$$

Therefore, for statistically independent events X and Y, Eq. (2-7) can be rewritten as:

$$P(X \cap Y) = P(X) \times P(Y) \tag{2-9}$$

2.2.2 The Theorem of Total Probability

The mutually exclusive and collectively exhaustive events $X_1, X_2, \dots, X_N$ are called partitions of the sample space S (Figure 2.1). The probability of any event can then be expressed as:

$$P(Y) = \sum_{i=1}^{N} P(X_i \cap Y) = \sum_{i=1}^{N} P(Y|X_i) \times P(X_i) \tag{2-10}$$

This equation represents the theorem of total probability.

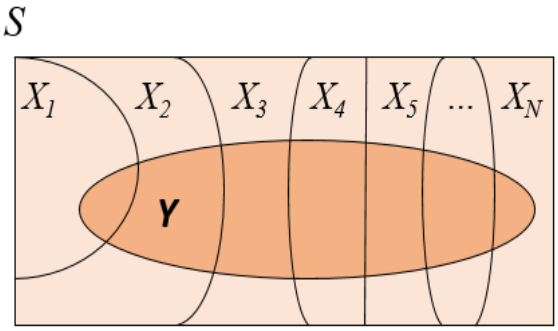

Figure 2.1. Venn diagram for the theorem of total probability

2.2.3 Definition of Probability

Three different definitions of probability exist in the literature [6]:

- Classical Definition

The classical definition goes back to Pascal and up until the 20th century. The probability theory was based on this definition. This definition comes from the games of cards and dice. According to this definition the probability of an event $X, P(X)$, is determined as the ratio of the number of favourable outcomes to the number of all possible outcomes, provided that all the outcomes are equally likely.

$$P(X) = \frac{N_X}{N} \tag{2-11}$$

where N_X is the number of outcomes at which the event X occurs and N is the number of all possible outcomes.

- Relative-Frequency Definition

The relative-frequency definition was developed by von Mises about seventy years ago [6]. It is based on experiments and easy to understand. According to this definition the probability of an event X, is simply the relative frequency of occurrence of X in the experiment, i.e., if the experiment under consideration is carried out n times and X occurs in n_X outcomes then:

$$P(X) = \lim_{n\to\infty} \frac{n_X}{n} \tag{2-12}$$

For example, to determine the probability of getting "3" as a result of dice dropping using this definition, it is necessary to drop a dice several times and as the number of dice dropping increases the probability converges to 1/6.

- Bayesian Definition

Thomas Bayes developed the mathematical framework later known as Bayesian statistics [9]. According to this definition the probability of an event is a measure of belief that the event will occur expressed in quantitative terms as a real number between 0 and 1 [9], i.e.:

$$P(X) = Measure\ of\ belief\ that\ X\ will\ occur \tag{2-13}$$

The degree of belief is a reflection of the experience, expertise, and preferences of the person. In this respect, the Bayesian interpretation of probability is subjective or person-dependent [9]. This opens up the possibility that two different persons may assign different probabilities to a given event and thereby contradicts the frequentist interpretation that probabilities are a characteristic of nature [9].

However, the Bayesian statistical interpretation of probability includes the frequentist and the classical interpretation in the sense that the subjectively assigned probabilities may be based on experience from previous experiments [9]. For example, in the dropping a dice example, a person using this definition would determine the probability of getting "3" as 1/6 by arguing that there are six possibilities. Since there is no reason to give preference to any of these six outcomes the probability should be 1/6.

The degree of belief is also referred to as a prior belief or prior probability, i.e. the belief, which may be assigned before obtaining any further knowledge [9]. The important argument in this approach is that a subjective estimate of the probability of an event (which is called a prior probability) is better than no estimate. However, as relevant data are collected and processed using the Bayesian statistical analysis, new estimates of probability (called the posterior probability) become less dependent on the prior estimate and closer to the data which is based on the relative-frequency definition.

2.2.4 Bayes' Theorem

Using the theorem of total probability, the probability of an event Y can be calculated, when it depends on mutually exclusive and collectively exhaustive events $X_1, X_2, \dots, X_N$ (with known probabilities).

It is useful to know the probability of one of the mutually exclusive and collectively exhaustive events (e.g. X_j) given that the event Y has occurred. By using Eq. (2-7):

$$P(X_j|Y) = \frac{P(Y|X_j) \times P(X_j)}{P(Y)} \tag{2-14}$$

By plugging the Eq. (2-10) into Eq. (2-14):

$$P(X_j|Y) = \frac{P(Y|X_j) \times P(X_j)}{\sum_{i=1}^{N} P(Y|X_i) \times P(X_i)} \tag{2-15}$$

The above equation is called Bayes' theorem. The theorem is very important since it provides a tool for updating the probabilities of events based on new observations [6]. Therefore, it is widely used in the reliability assessment of existing structures. In the above equation:

- $P(X_j|Y)$ is called Posterior probability of the event X_j; i.e. the updated probability of X_j after observing event Y.
- $P(Y|X_j)$ is called the Likelihood function; i.e. the probability of observing event Y given that X_j is the true state.
- $P(X_j)$ is called Prior probability of X_j; i.e. the probability of X_j before observing the event Y (new observation).

2.2.5 Random Variables

A random variable is a numerical variable whose specific value cannot be predicted with certainty before an experiment is carried out [6].

A random variable can be either a discrete or a continuous random variable. A discrete random variable has a finite or infinite countable number of values, which are often positive integers, e.g. the number of earthquakes within a certain period of time, the number of cars crossing a bridge. A continuous random variable has always an infinite number of values and is free to take on any value on the real axis, e.g. strength of materials, depth of a fatigue crack.

In this study, a random variable will be denoted by a capital letter, while a particular realisation of the random variable by the corresponding lowercase letter.

The relationship between the values of a random variable and the corresponding probabilities is described by the probability distribution of the random variable.

2.2.6 Probability Distributions

The probability distribution of a continuous random variable is usually described by the probability density function (PDF) which is the derivative of the CDF:

$$f_X(x) = \frac{dF_X(x)}{dx} \tag{2-16}$$

Therefore, the probability that X is within a tiny interval $[x, x + \Delta x]$ is equal to:

$$P(x \leq X \leq x + \Delta x) = f_X(x)\Delta x \tag{2-17}$$

For an interval of $[x_1, x_2]$ the probability that X takes on a value in this interval is:

$$P(x_1 \leq X \leq x_2) = \int_{x_1}^{x_2} f_X(x)dx \tag{2-18}$$

If the PDF of X is known, its CDF can be obtained as:

$$F_X(x) = P(-\infty \leq X \leq x) = \int_{-\infty}^{x} f_X(x)dx \tag{2-19}$$

The CDF of both discrete and continuous random variables has the following properties:

$$0 \leq F_X(x) \leq 1 \tag{2-20}$$

$$F_X(-\infty) = 0, \quad F_X(\infty) = 1 \tag{2-21}$$

$$F_X(x + \varepsilon) \geq F_X(x) \qquad for\ any\ positive\ \varepsilon \tag{2-22}$$

It is noted that the value of $f_X(x)$ is not itself a probability. Based on Eq. (2-20), CDF is a probability. Moreover, Eq. (2-22) indicates that the cumulative distribution function is monotonically increasing. Figure 2.2 shows the probability mass function and the cumulative distribution function of a discrete random variable, schematically.

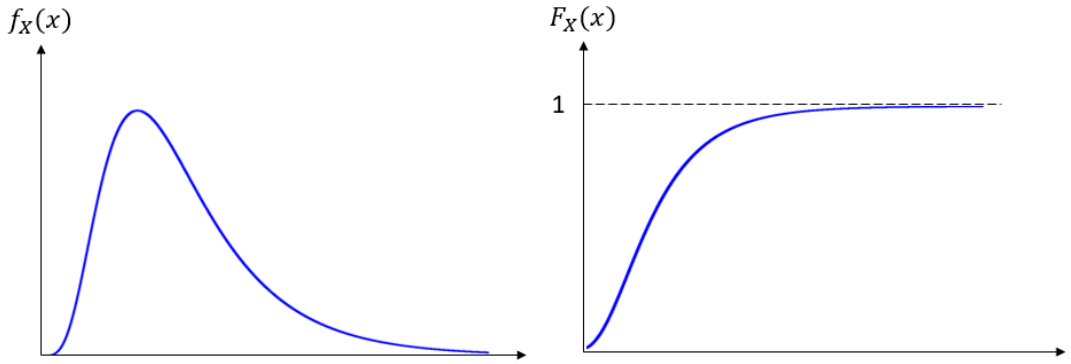

Figure 2.2. Illustration of PDF (left) and CDF (right) for a continuous random variable

2.2.7 Moments of Random Variables

Probability distributions may be also defined in terms of their moments. The i[th] moment of a continuous random variable is defined by [9]:

$$m_i = \int_{-\infty}^{\infty} X^i f_X(X) dX \tag{2-23}$$

The mean value (or expected value) of a continuous random variable is defined as the first moment [9]. The mean value is denoted as $E[X]$ and defined as:

$$E[X] = \int_{-\infty}^{\infty} x f_X(x) dx \tag{2-24}$$

The expected value can be interpreted as a weighting of x by $f_X(x)$. Therefore, the expected value of a random variable is also called the mean value of the random variable. The mean value is denoted as μ_X.

It is noted that for obtaining the mean value for a discrete random variable, Eq. (2-24) is written as:

$$\mu_X = \sum_{i=1}^{n} \left(x_i \times p_X(x_i)\right) \tag{2-25}$$

Similarly, the variance is described by the second central moment. The variance of a continuous random variable is denoted as $Var\ [X]$ and is defined as [9]:

$$Var[X] = E[(X - \mu_X)^2] = \int_{-\infty}^{\infty} (x - \mu_X)^2 f_X(x) dx \tag{2-26}$$

The square root from the variance is called the standard deviation of a random variable and is denoted as σ_X:

$$\sigma_X = \sqrt{Var[X]} \tag{2-27}$$

It is noted that for obtaining the variance for a discrete random variable, Eq. (2-26) is written as:

$$Var[X] = \sum_{i=1}^{n} \left((x_i - \mu_X)^2 \times p_X(x_i) \right) \tag{2-28}$$

The ratio of the standard deviation of a random variable to its mean is called the coefficient of variation (COV):

$$COV(X) = \frac{\sigma_X}{\mu_X} \tag{2-29}$$

The coefficient of variation provides a useful descriptor for the variability of a random variable around its expected value [9]. It is noted that the coefficient of variation is a dimensionless parameter.

2.2.8 Common Continuous Probability Distributions

2.2.8.1 Uniform Distribution

The uniform distribution is used when an experiment has an arbitrary outcome between certain bounds, $[a, b]$. The probability density function (PDF) for a uniformly distributed random variable is defined as:

$$\begin{aligned} f_X(x) &= \frac{1}{b-a}, \qquad a \le x \le b \\ f_X(x) &= 0, \qquad elsewhere \end{aligned} \tag{2-30}$$

Where a and b are the parameters of the probability density function. Figure 2.3 shows the PDF of the uniform distribution.

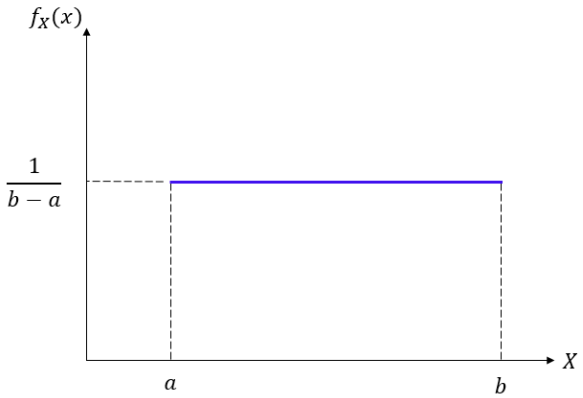

Figure 2.3. A continuous random variable with a uniform density function

By plugging the Eq.(2-30) into Eq.(2-24) and Eq. (2-26), the mean and the variance of a continuous random variable with uniform distribution are obtained as:

$$\mu_X = \frac{a+b}{2}$$
$$\sigma_X^2 = \frac{(b-a)^2}{12} \tag{2-31}$$

2.2.8.2 Normal (Gaussian) Distribution

Normal distributions are usually used to represent random variables whose distributions are not known. The normal distribution has two parameters, mean parameter (μ) and standard deviation parameter (σ). The PDF of a normal distribution is defined as:

$$f_X(x) = \frac{1}{\sqrt{2\pi\sigma^2}} \times exp\left[-\frac{1}{2}\left(\frac{x-\mu}{\sigma}\right)^2\right] \tag{2-32}$$

The random variable X is defined in the range of $(-\infty, \infty)$. Figure 2.4 shows the PDF of the normal distribution.

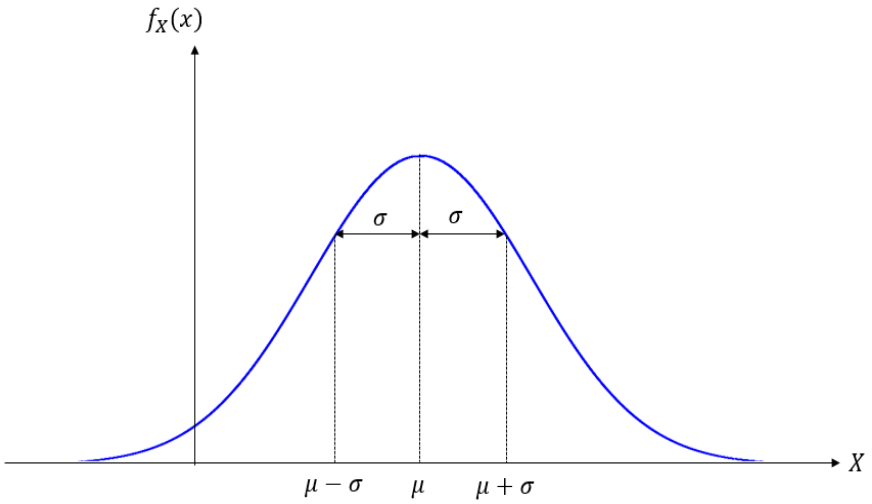

Figure 2.4. The probability density function of a normal distribution

The standard form of the normal distribution can be obtained by replacing the random variable X with an equivalent normalised value U as:

$$U = \frac{X - \mu}{\sigma} \tag{2-33}$$

Using the above transform, the mean and variance of the standard form of the normal distribution are equal to:

$$\mu_U = 0,\ \sigma_U = 1 \tag{2-34}$$

Therefore, the PDF of the standard normal variable is equal to:

$$f_U(u) = \frac{1}{\sqrt{2\pi}} \times exp\left(-\frac{1}{2}u^2\right) = \varphi(u) \tag{2-35}$$

And the standard normal CDF is:

$$F_X(x) = P(X \leq x) = \Phi\left(\frac{x - \mu}{\sigma}\right) = \Phi(u) \tag{2-36}$$

where $\varphi(u)$ is the standard normal distribution and u is a standard normally distributed variable with expected value zero and unit standard deviation. A table with numerical values of the standard normal CDF, $\Phi(u)$, is given in the literature [9]. The table can be used in two ways; find $\Phi(u)$ given u or find u given $\Phi(u)$.

2.2.8.3 Lognormal Distribution

A random variable has a lognormal distribution when its natural logarithm has a normal distribution. It is noted that the random variable X belongs to the range $[0,\infty)$. The PDF of a lognormal distribution, which depends on two parameters ξ and λ is:

$$f_X(x) = \frac{1}{x\xi\sqrt{2\pi}} \times exp\left[-\frac{1}{2}\left(\frac{\ln x - \lambda}{\xi}\right)^2\right] \tag{2-37}$$

Parameters λ and ξ and are the mean and standard deviation of $LN(X)$. These parameters are related to the mean and standard deviation of variable X as:

$$\xi = \sqrt{\ln\left(1 + \left(\frac{\sigma}{\mu}\right)^2\right)}$$
$$\lambda = \ln\mu - \frac{1}{2}\xi^2 \tag{2-38}$$

When $\sigma/\mu < 0.3$, it can be shown that:

$$\xi \cong \frac{\sigma}{\mu} \tag{2-39}$$

Figure 2.5 shows the PDF of the lognormal distribution for different amounts of parameters.

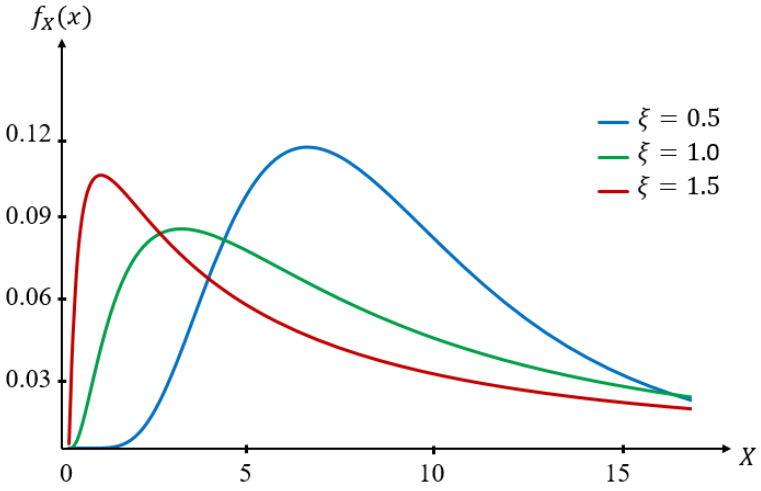

Figure 2.5. The probability density function of lognormal distribution (λ=2 for all distributions)

2.2.8.4 Exponential Distribution

The exponential distribution is the probability distribution of the time between events in a Poisson distribution. The exponential distribution has one parameter which is called the rate parameter (λ). The PDF of the exponential distribution is defined as:

$$f_T(t) = \lambda e^{-\lambda t}, \qquad t > 0 \tag{2-40}$$

The mean and standard deviation of the exponential distribution are given by:

$$\mu = \sigma = \frac{1}{\lambda} \tag{2-41}$$

Figure 2.6 shows the PDF of the exponential distribution for different amounts of the rate parameter.

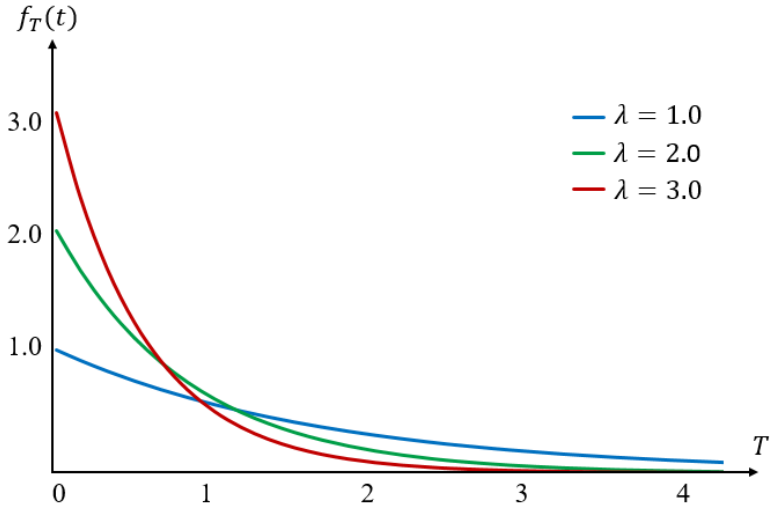

Figure 2.6. The probability density function of exponential distributions

2.2.9 Multiple Random Variables

In previous sections, it was shown how the uncertainty can be modelled by a single random variable. However, in many problems, uncertainties arise from several sources. The joint behaviour of two (or more) random variables is characterised by a joint probability distribution.

2.2.9.1 Joint Probability Distributions

In this section, joint probability distributions of two random variables will be discussed. It is noted that the joint probability results can be extended to more than two random variables.

Consider two random variables X and Y. Their joint cumulative distribution function (CDF) is defined as:

$$F_{XY}(x,y) = \mathrm{P}[(X \le x) \cap (Y \le y)] \tag{2-42}$$

For the continuous random variables, the joint probability density is obtained as:

$$f_{XY}(x,y) = \frac{\partial^2}{\partial x\, \partial y} F_{XY}(x,y) \tag{2-43}$$

The joint PDF can also be interpreted the probability of the intersection of two events:

$$P[(x \le X \le x + dx) \cap (y \le Y \le y + dy)] = f_{XY}(x,y)dxdy \tag{2-44}$$

Therefore:

$$F_{XY}(x,y) = \int_{-\infty}^{x}\int_{-\infty}^{y} f_{XY}(x,y)dxdy \tag{2-45}$$

2.2.9.2 Marginal Distributions

In some cases, it is necessary to remove consideration of one variable to study only the behaviour of the other variable. In such cases, the marginal PDF is obtained as:

$$f_X(x) = \int_{-\infty}^{\infty} f_{XY}(x,y)dy \tag{2-46}$$

2.2.9.3 Covariance and Correlation

When the uncertainty is modelled by a single random variable, the most information about the distribution of a single random variable is provided by its mean and standard deviation.

However, when there is more than one random variable, the interdependence between random variables in their joint probability distribution can be represented by the covariance as:

$$Cov(X,Y) = E[(X - \mu_X)(Y - \mu_Y)] = \int_{-\infty}^{\infty}\int_{-\infty}^{\infty} (x - \mu_X)(y - \mu_Y) f_{XY}(x,y)dxdy \tag{2-47}$$

It can be shown that for statistically independent parameters, the covariance is equal to zero. Covariance indicates the degree of linear dependency between the two random variables.

By dividing the covariance of two variables by the product of their standard deviations, a normalised version of the covariance which is called the correlation coefficient is obtained as:

$$\rho_{XY} = \frac{Cov(X,Y)}{\sigma_X \sigma_Y} \tag{2-48}$$

It can be shown that:

$$-1 \leq \rho_{XY} \leq 1 \tag{2-49}$$

The correlation coefficient shows the degree of linear dependency between two random variables.

It is noted that ρ_{XY} close to zero does not mean that there is no dependency between two random variables; although there may be some nonlinear relationship between these variables (see Figure 2.7). It is important to note that the terms statistically independent and uncorrelated are not synonymous. If two random variables are statistically independent, they must be uncorrelated. However, uncorrelated random variables are not necessarily statistically independent [6]. Figure 2.7 shows different possible correlations between two random variables.

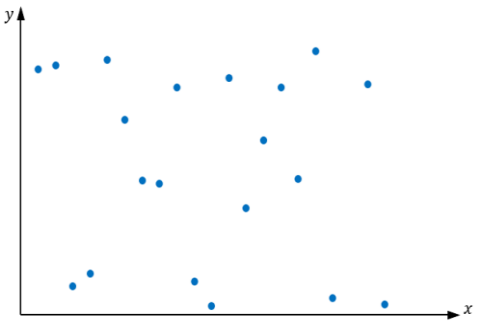

$\rho_{xy} \cong 0$

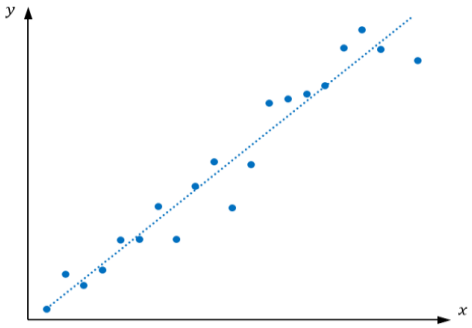

$0 \leq \rho_{xy} \leq 1$

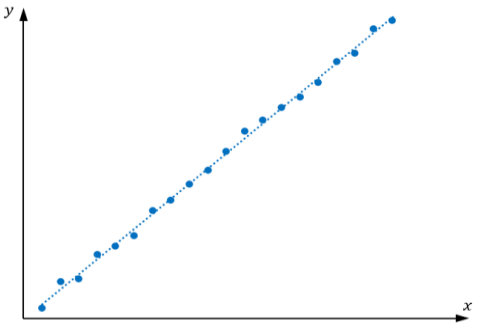

$\rho_{xy} \cong 1$

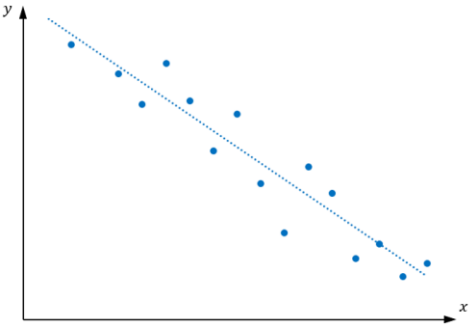

$-1 \leq \rho_{xy} \leq 0$

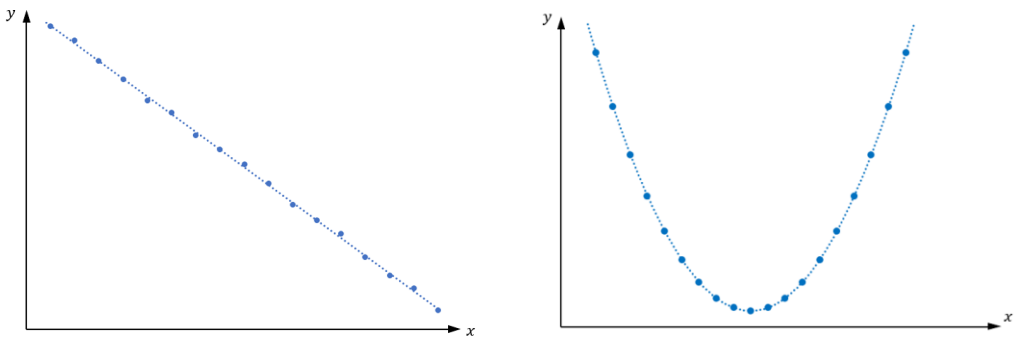

$\rho_{xy} \cong -1$ $\rho_{xy} \cong 0$

Figure 2.7. Different correlation coefficients of two random variables

It should be noted that it is rare to obtain a value of correlation coefficients equal to 0, 1, and -1. Two random variables can be assumed to be statistically independent if the absolute value of their correlation coefficient is less than 0.3. Moreover, two random variables can be assumed perfectly correlated if $|\rho_{XY}| \geq 0.9$ [6].

2.2.9.4 Common Multivariate Distributions

Multivariate distributions are more complex than distributions of a single random variable and not many of them are commonly used. One of the common multivariate distributions is a joint normal distribution. The joint PDF of two normally distributed random variables depends on five parameters which are two mean values, two standard deviations, and the correlation coefficient between two random variables. The PDF of the joint normal distribution is:

$$f_{XY}(x,y) = \frac{1}{2\pi\sigma_X\sigma_Y\sqrt{1-\rho_{XY}^2}} \times exp\left(-\frac{1}{2(1-\rho_{XY}^2)}\left[\frac{(x-\mu_X)^2}{\sigma_X^2} + \frac{(y-\mu_Y)^2}{\sigma_Y^2} - \frac{2\rho_{XY}(x-\mu_X)(y-\mu_Y)}{\sigma_X\sigma_Y}\right]\right) \quad (2\text{-}50)$$

Figure 2.8 shows the schematic shape of the PDF of the joint normal distribution for two variables.

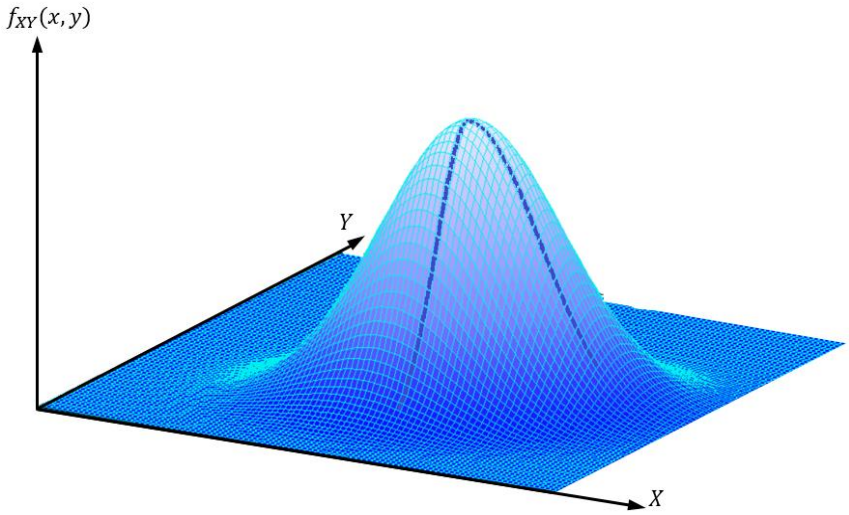

Figure 2.8. Joint normal probability density function

2.3 Fundamentals of Structural Reliability

2.3.1 Different Approaches to Structural Safety

2.3.1.1 Deterministic Approach

For many years, for the design of the structural systems, the loads and the structures' strengths are considered as deterministic values. Therefore the capacity of a system is determined in such a way that it exceeds the load with a certain margin [10]. The safety factor in this approach is defined as:

$$Safety\ Factor = \frac{Capacity}{Load} = \frac{R}{S} \tag{2-51}$$

A safety factor is considered as a measure of the reliability of the structure. In codes of practice for structural systems values for loads, strengths and safety factors are recommended. These values are determined based on experience and engineering judgement [10].

The main limitation of the deterministic approach is that it does not calculate the probability of failure. For example, if the safety factor is reduced by 20%, this approach cannot provide how much the probability of failure will increase. The method can only say that the probability of failure will increase.

2.3.1.2 Semi-Probabilistic Approach

In new codes, the characteristic values of the uncertain loads and resistances are specified and partial safety factors are applied to the loads and strengths to ensure that the structure is safe enough. The partial safety factors are usually based on experience or calibrated to existing codes [10].

Since there is uncertainty about the ultimate strength of a structure and the maximum load on the structure, these parameters are considered uncertain parameters. Imagine the mean values and standard deviations of capacity (μ_R, σ_R) and load (μ_S, σ_S) are available based on previous measurements of load and capacity.

In this approach characteristic values are defined as:

- S_K : 95% Fractiles, i.e. $P[S < S_K] = 0.95$
- R_K : 5% Fractiles, i.e. $P[R < R_K] = 0.05$

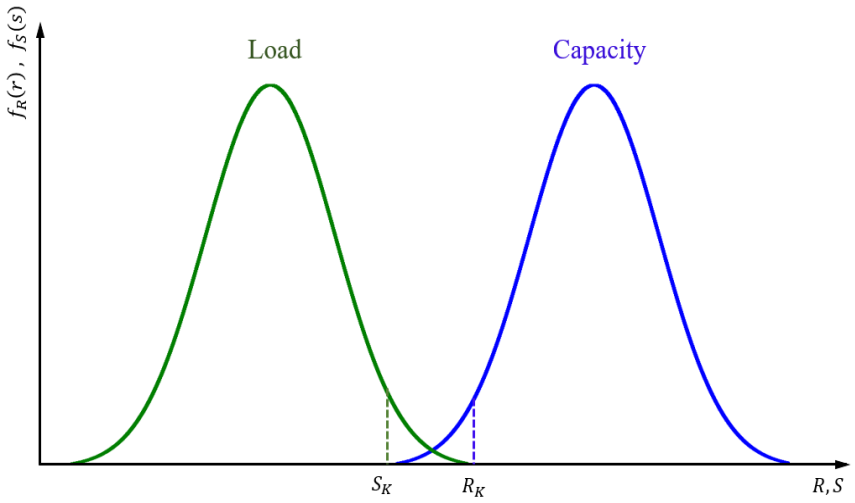

Figure 2.9. Characteristic values of capacity and load

The characteristic load is multiplied by a partial safety factor (usually greater than 1.0) to account for uncertainty in the loading estimation. The partial safety factor for the strength uncertainties is usually less than 1.0 to consider the effect of quality control during construction. To ensure safety, it is required that:

$$R_K \times \gamma_R \geq S_K \times \gamma_S \tag{2-52}$$

Where γ_R and γ_S are the partial safety factors for strength and loading variables, respectively. If this inequality is not satisfied then the characteristic design strength

R_K must be increased. This is known as a semi-probabilistic approach and it is the basis of many design codes [6].

2.3.1.3 Probabilistic Approach

It was mentioned that structural analysis has been traditionally performed based on deterministic or semi-probabilistic methods. However, in real engineering applications, there are several sources of uncertainties in the prediction of the load and the resistance of the structural systems.

For example, for an offshore platform, there are considerable sources of uncertainties in the calculation of the hydrodynamic loading on the members due to the uncertain value of marine growth, surface roughness; the uncertainties in the values of drag and inertia coefficients required in force calculations; and the simplifications made in the derivation of water particle kinematics using a wave theory. Thus the predicted forces and stresses in the members of the structure involve uncertainties.

On the other hand, the predicted strength of the structure is also subject to uncertainty due to the inherent randomness in material properties such as yield strength, fatigue strength; and the uncertainty in the soil parameters, etc.

Due to the existence of many uncertainties in loads and the resistance of the system, there is a need for the use of a probabilistic approach to ensure that the system is safe at an acceptable level of probability, during its specified lifetime.

Structural reliability analysis, which is a probabilistic approach, provides a framework for the rational treatment of uncertainties in a system. In this framework, the safety of the structure is quantified in terms of the probability of failure or reliability which is accepted as a rational measure of structural safety [7].

Since the focus of this study is on offshore structures, in the following section, the reliability analysis of a structure will be explained.

2.3.2 Structural Reliability Analysis

The reliability of a structural system is defined as the probability that the structure has a proper performance throughout its lifetime. Reliability methods are used to estimate the probability of failure. It is noted that the reliability models might have some errors.

Therefore, the estimated reliability should be considered as a measure of reliability and not as an absolute number [10].

To estimate the reliability, the following steps should be taken into account [10]:

- Identify the significant failure modes;
- Formulate failure functions (limit state functions) for each failure mode;
- Identify the stochastic variables in the failure functions;
- Specify the statistical parameters (distribution) of the stochastic variables;
- Estimate the reliability of each failure mode;
- Perform sensitivity analyses to evaluate the reliability results.

The following sections explain each mentioned step, briefly.

2.3.2.1 Definition of Failure and Limit States

Typical failure modes in reliability analysis for a structural system could be yielding, buckling, fatigue and excessive deformations [10]. The main purpose of structural reliability analysis is to evaluate the probability of failure of a structural system for these failure modes.

For this purpose event of failure should be defined. In structural reliability, failure is usually defined based on the concept of a limit state, which represents a boundary between desired and undesired performance of a structural system or component.

Three types of limit states are usually considered [6]:

1) Ultimate limit state (ULS): Failure associated with the loss of load-bearing capacity. E.g. when the load exceeds the resistance of a structural component. This failure can be related to e.g. formation of a mechanism in the structure, excessive plasticity and buckling [10].
2) Serviceability limit state (SLS): Under this condition, failure is related to a serviceability loss that does not indicate a significant decay of structural safety, e.g. excessive deflections of a beam, local damage and excessive vibrations [10].
3) Fatigue limit state (FLS): This is associated with the loss of strength under repeated cyclic loads.

It is noted that the defined failure does not necessarily mean the collapse of a structural system.

For any given realisations $\boldsymbol{x}$ of the basic variables, the structure is either in a safe region or in a failure region. The basic variable space is thus divided into two sets, the safe set and the failure set. The two sets are separated by the failure surface (limit state surface). It is assumed that the failure surface can be described as:

$$g(\boldsymbol{x}) = g(x_1, x_2, \dots, x_n) = 0 \tag{2-53}$$

Where g($\boldsymbol{x}$) is the failure function.

Usually, the failure function is defined in a way that the positive values of g($\boldsymbol{x}$) correspond to the safe area and negative values correspond to the failure area [10], i.e.:

$g(\boldsymbol{x}) < 0$: Failure area

$g(\boldsymbol{x}) = 0$: Limit state: the boundary between the safe and unsafe area

$g(\boldsymbol{x}) > 0$: Safe area

Figure 2.10 shows the limit state function when two variables are available, schematically.

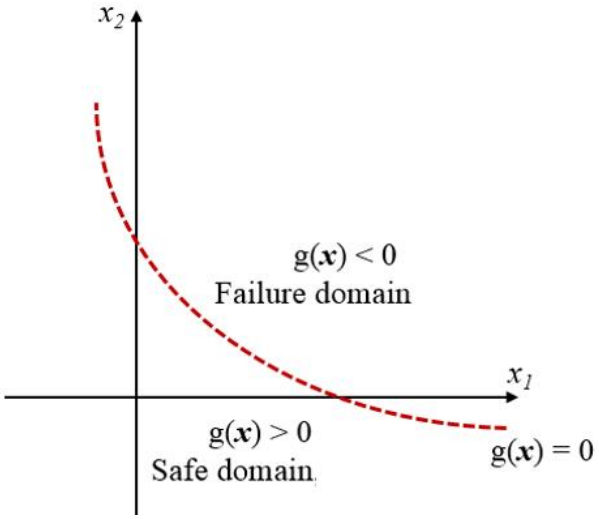

Figure 2.10. Failure function (limit state)

The limit state function usually includes several basic variables. A very simple limit state function can be defined as:

$$g = R - S \tag{2-54}$$

where R denotes the capacity of a system and S is the load acting on the system. Figure 2.11 shows how the limit state function divides the whole area into safe and unsafe areas.

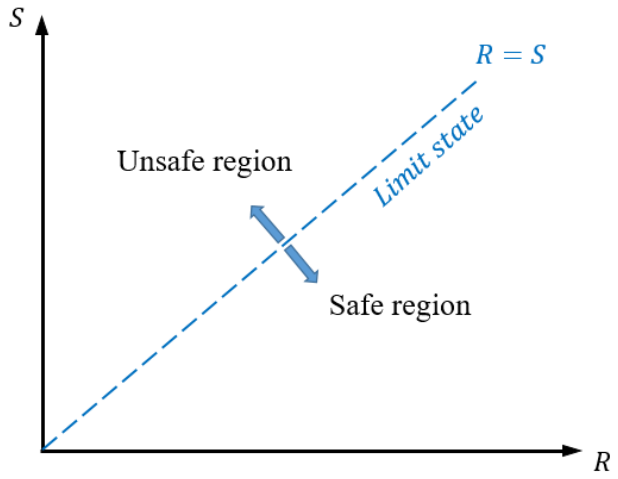

Figure 2.11. Limit state function and safe/unsafe areas in the reliability analysis

2.3.2.2 Uncertainty Modelling

The behaviour of a structural system is usually described by models (analytical, empirical or numerical). To take into account various uncertainties associated with structural properties, loads and models themselves, parameters of the models are represented by random variables. The uncertainties are usually described in terms of the probability density function of the basic variables.

In structural reliability analysis, uncertainties should be interpreted and differentiated regarding their type and origin [9]. There are different types of uncertainties including:

- Physical uncertainty (Inherent uncertainty):

  The first type of uncertainty which is also called aleatory uncertainty is uncertainty that arises from the inherent randomness of physical quantities, such as natural loads (e.g., wind, earthquake), material properties (e.g., soil, steel) [12]. The inherent uncertainty is caused by the fact that the universe is not deterministic. These uncertainties cannot be reduced through the collection of additional information [9].

- Model uncertainty;

The model uncertainties are uncertainties that are associated with the imperfect knowledge or idealisations of the mathematical models [10]. Since these uncertainties can be reduced by further research or the use of a more sophisticated model, they are called epistemic uncertainty [6].

- Statistical uncertainty.

  These uncertainties arise due to incomplete statistical information, e.g. due to a small number of material tests [9]. The collection of more relevant data via observations or tests usually enables to decrease this type of uncertainty. Therefore, the statistical uncertainty is categorised as epistemic uncertainty.

It is noted that there are other types of uncertainties such as uncertainties related to human errors in design, construction, inspection, maintenance, etc. which are beyond the scope of this study.

2.3.2.3 Human Error

Human error is another important source of uncertainty that might cause structural failures. The causes of these errors are psychological and social factors that are complex and not yet well understood [7]. Human errors, to some extent, can be controlled by better working conditions, rigorous quality control and training etc. [7].

Uncertainties due to human error are not generally accounted for in reliability analysis. Therefore, the result of a reliability analysis should be considered as a theoretical value of the reliability [7].

2.3.2.4 Reliability Estimation

It was mentioned that in the probabilistic approach to structural safety, all aspects of uncertainty in the load and capacity can be assessed. In a very simple simplest case, load (S) and capacity (R) are modelled as two random variables with probability distributions of $f_S(s)$ and $f_R(r)$, respectively. The probability of failure is the probability of being $g \leq 0$ as:

$$P_f = P(g \leq 0) = P(R - S \leq 0) = P(R \leq S) \tag{2-55}$$

A structure fails when the load exceeds its resistance (capacity). For example, if a load of a structure equals a specific value (s), the structure fails when $s \geq R$. However, R

is a random variable, therefore, the probability of failure can be calculated as the sum of all possible intersections of two events, i.e.:

$$P_f = \sum_s P[(S = s) \cap (s \geq R)] \tag{2-56}$$

Using conditional probability definition:

$$P_f = \sum_s P(S = s) \times P(R \leq s | S = s) \tag{2-57}$$

The first expression in Eq. (2-57) can be written as:

$$P(S = s) = f_S(s)ds \tag{2-58}$$

The second expression in Eq. (2-57) can be written as:

$$P(R \leq s | S = s) = F_R(s) \tag{2-59}$$

By substituting Eq.(2-59) and Eq.(2-58) into Eq.(2-57) and replacing the summation by integration:

$$P_f = \int_{-\infty}^{\infty} F_R(s) \times f_S(s)ds \tag{2-60}$$

Figure 2.12 shows the probability density functions for load and capacity and how to calculate the probability of failure.

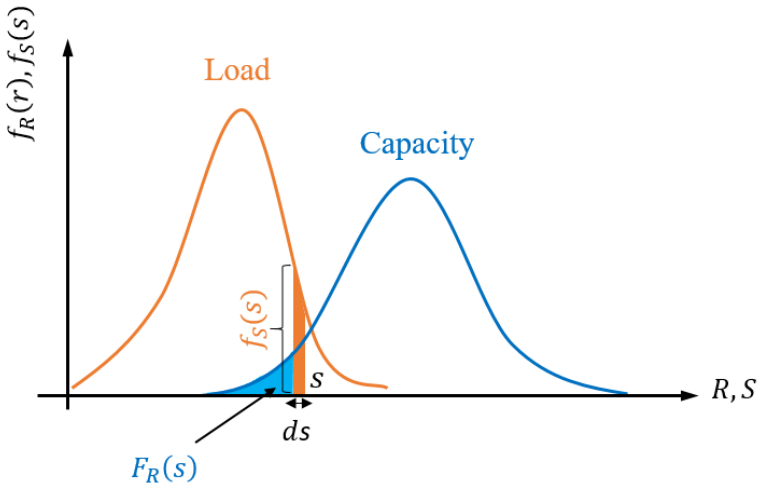

Figure 2.12. Calculation of the probability of failure

As it can be seen from Figure 2.12, for obtaining the accurate reliability results, the left tail of the capacity distribution and the right tail of the load distribution should be modelled properly.

- **Special Case - Normal Distribution**

  If the capacity (R) and load (S) are assumed as independent normal random variables, the probability of failure can easily be evaluated. In Section 2.2.8.2, it was explained that the sum of independent normally distributed random variables is normally distributed. Therefore, the limit state function ($g = R - S$) is a normal random variable with the following mean and variance:

$$\mu_g = \mu_R - \mu_S$$
$$\sigma_g^2 = \sigma_R^2 + \sigma_S^2 \qquad (2\text{-}61)$$

  where μ_R and μ_S are mean values and σ_R and σ_S are standard deviations of capacity and load, respectively. Since the limit state function is a normal random variable, based on Eq.(2-36), the probability of failure can be obtained as:

$$P_f = P[g \leq 0] = F_g(0) = \Phi\left(\frac{0 - \mu_g}{\sigma_g}\right) = \Phi\left(-\frac{\mu_g}{\sigma_g}\right) = \Phi(-\beta) \qquad (2\text{-}62)$$

  where β is called the reliability index and $\Phi(.)$ is the CDF of the standard normal distribution.

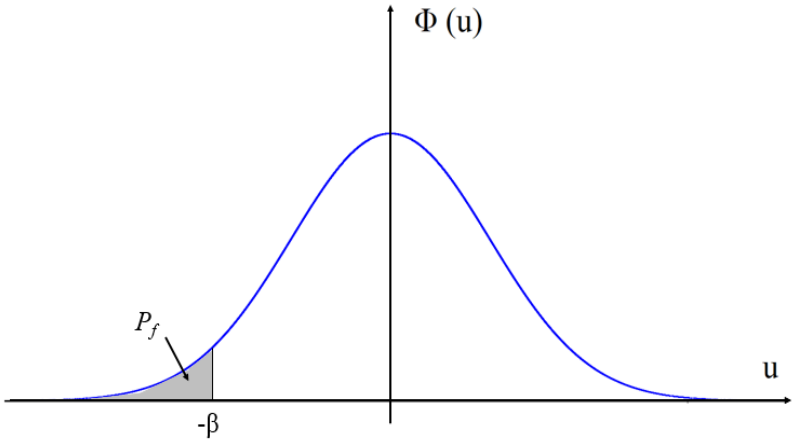

Figure 2.13. Illustration of reliability index and the probability of failure

  In this case, the reliability index can be expressed through the means and variances of the capacity and load as:

$$\beta = \frac{\mu_g}{\sigma_g} = \frac{\mu_R - \mu_S}{\sqrt{\sigma_R^2 + \sigma_S^2}} \tag{2-63}$$

The reliability index is a very important parameter in structural reliability, which is used as a measure of structural reliability instead of the probability of failure [6]. As can be seen from Eq.(2-62) there β and P_f are related to each other. Table 2.1 shows different values of probability of failure and the corresponding reliability index.

Table 2.1. Different values of probability of failure and the corresponding reliability index

Probability of Failure (P_f)	Reliability Index (β)
0.5	0
0.1	1.28
0.01	2.33
10^{-3}	3.09
10^{-4}	3.72
10^{-5}	4.26
10^{-6}	4.75

2.3.3 Levels of Reliability Methods

Methods to measure the reliability of a structure can be divided into four groups [13]:

- Level I methods: The uncertain parameters are modelled by one characteristic value, as introduced in codes based on the partial safety factor concept.
- Level II methods: The uncertain parameters are modelled by the mean values and the standard deviations, and by the correlation coefficients between the stochastic variables. The stochastic variables are implicitly assumed to be normally distributed.
- Level III methods: The uncertain quantities are modelled by their joint distribution functions. The probability of failure is estimated as a measure of reliability. This level will be considered in this research.
- Level IV methods: In these methods, the consequences of failure are also taken into account and the risk (consequence multiplied by the probability of failure) is

used as a measure of the reliability. In this way, different designs can be compared on an economic basis taking into account uncertainty, costs and benefits.

2.3.4 Techniques of Reliability Calculation

There are several ways to calculate the reliability and the corresponding probability of failure, including [6]:

- First-Order Reliability Method (FORM)
- Second-Order Reliability Method (SORM)
- Simulation Techniques

In the first two methods, transformations from the original distributions to corresponding equivalent normal distributions of uncertainties are needed at each cycle of the iteration. In FORM, the limit state function is linearised and in SORM, a quadratic approximation to the failure function is determined and then, the probability of failure is estimated [10]. In simulation technique methods, samples of the variables are generated and the relative number of samples corresponding to failure is used to estimate the probability of failure. The simulation techniques are different in the way the samples are generated [6].

2.4 Reliability Methods

In Section 2.3.2.4, the load and capacity of a structure are modelled as random variables. However, in real applications of reliability analysis, the capacity is a function of material properties and structural dimensions. Moreover, the load is a function of applied loads and materials densities [6]. Each of these parameters may be a random variable.

These random variables are called the basic random variables for the problem. In this context, the stochastic variables are denoted by capital letters, the realisations of basic variables are denoted lower case letters and vectors are denoted by bold letters.

The joint probability density function of the vector **X** of the basic random variables is denoted as $f_{\boldsymbol{X}}(\boldsymbol{x})$. Therefore, the general form of the probability of failure can be written as:

$$P_f = P[g(\boldsymbol{X}) \leq 0] = \underset{g(\boldsymbol{X})\leq 0}{\dot{\iiint}} f_{\boldsymbol{X}}(\boldsymbol{x}).\, d\boldsymbol{x} \tag{2-64}$$

In general, to obtain the probability of failure, the above integral should be calculated.

Figure 2.14 shows the joint pdf of two random variables and the limit state function, schematically.

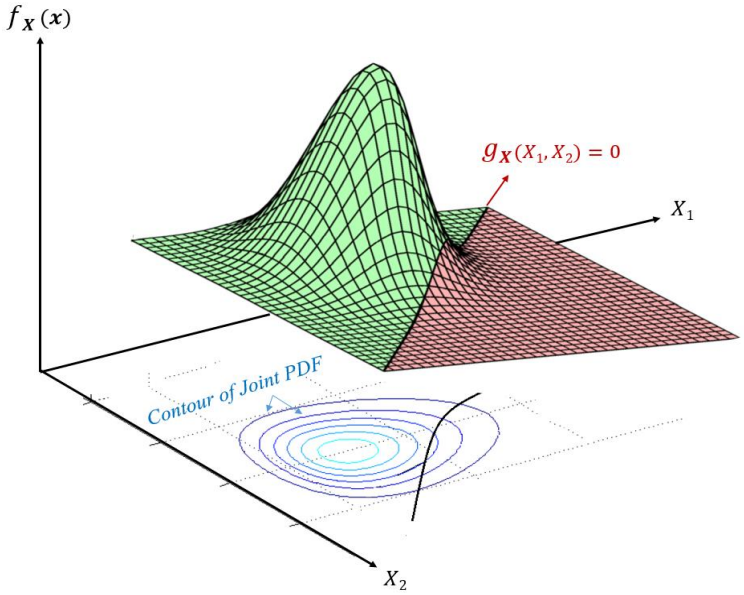

Figure 2.14. Joint PDF of random variables and limit state function

The probability integration in Eq.(2-64) is the volume underneath the surface of the joint PDF in the failure region. Figure 2.15 shows the contour of the joint PDF and the limit state function in $X_1 - X_2$ plane.

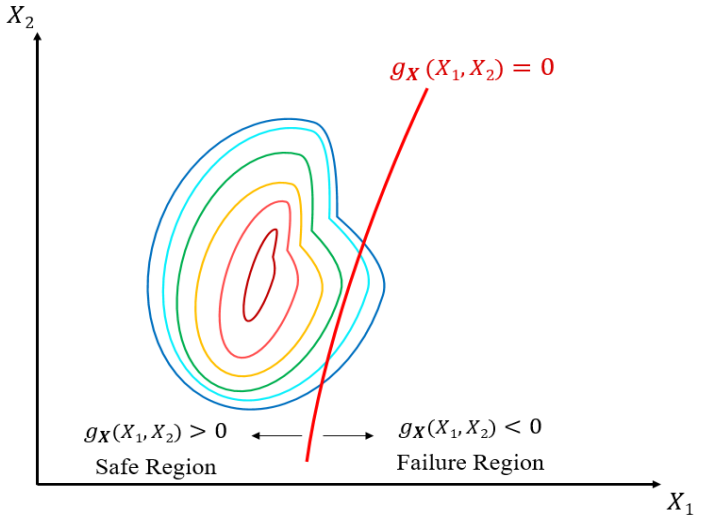

Figure 2.15. Contours of the joint pdf and the limit state function in a 2D plane

The direct evaluation of the probability integration (Eq. (2-64)) is extremely difficult due to the following items [11]:

- Since several random variables are involved in the reliability applications, the probability integration is multi-dimensional.
- The joint pdf of **X** is usually a nonlinear multi-dimensional function.
- The integration boundary ($g_{\boldsymbol{X}}(\boldsymbol{x}) = 0$) is multi-dimensional and a nonlinear function.
- In many engineering applications, there is not an explicit form for $g_{\boldsymbol{X}}(\boldsymbol{x})$. Therefore, the evaluation of the limit state function is computationally expensive.

Since it is unpractical using numerical integration to find the solution, the approximation methods have been developed in the area of structural reliability:

- First-Order Second Moment (FOSM)
- First-Order Reliability Methods (FORM)
- Second-Order Reliability Methods (SORM)
- Monte-Carlo Simulation

2.4.1 First Order Second Moment (FOSM) Method

The First Order Second Moment (FOSM) method is the first structural reliability method. The 'first order' term indicates that the method is based on a linear expansion using only the first derivative terms in a Taylor series. In this method, the higher-order derivations are neglected [6]. Due to neglecting the higher derivative terms in a Taylor series, the FOSM method does not provide an exact answer. However, it can usually give a useful approximate answer in many reliability applications [6].

It was mentioned that in the statistics terminology, mean is the first moment of the area under the probability density curve and the variance is the second moment of area about the mean. Therefore, the second-moment term indicates that each variable is described only by its mean value and variance.

2.4.1.1 FOSM Method to Obtain the Reliability Index

In Section 2.3.2.4 it was explained how the reliability index can be calculated for a special case. In that special case, the limit state function is a linear function of independent normal random variables. The FOSM method can obtain the reliability index when the limit state function is a nonlinear function of normal random variables [6].

The limit state function can be linearised using a Taylor series expansion by neglecting the higher-order derivatives as:

$$g(\boldsymbol{X}) \cong g(\boldsymbol{x}^*) + \sum_{i=1}^{n} \left\{ \left. \frac{\partial g}{\partial X_i} \right|_{\mu_X} \times \left(X_i - \mu_{X_i}\right) \right\} \tag{2-65}$$

Here, $\boldsymbol{x}^* = \{x_1^*, x_2^*, \dots, x_n^*\}$ is the expansion point, i.e. Taylor series is expanded at this point. Moreover $\frac{\partial g}{\partial X_i}$ denotes a partial derivative of the limit state function with respect to the random variable X_i. This term may be a function of the random variables. The subscript $*$ means the random variables in this function should be replaced by their values at the expansion point. It is noted that in the FOSM method the linearisation is carried out on the mean values of the random variables [6]. Therefore:

$$g(\boldsymbol{X}) \cong g\left(\mu_{X_1}, \mu_{X_2}, \dots, \mu_{X_n}\right) + \sum_{i=1}^{n} \left\{ \left. \frac{\partial g}{\partial X_i} \right|_{\mu_X} \times \left(X_i - \mu_{X_i}\right) \right\} \tag{2-66}$$

The mean value of this linear approximation of the limit state function is obtained as:

$$\mu_g = E[g(\boldsymbol{X})] \cong E\left[g\left(\mu_{X_1}, \mu_{X_2}, \dots, \mu_{X_n}\right) + \sum_{i=1}^{n} \left\{ \left. \frac{\partial g}{\partial X_i} \right|_{\mu_X} \times \left(X_i - \mu_{X_i}\right) \right\} \right] \tag{2-67}$$

Since $E[X_i] = \mu_{X_i}$, term $E\left[X_i - \mu_{X_i}\right] = 0$. Therefore, the second term on the right-hand side of the above equation is equal to zero. Eq.(2-67) can be written as:

$$\mu_g \cong g\left(\mu_{X_1}, \mu_{X_2}, \dots, \mu_{X_n}\right) \tag{2-68}$$

Eq. (2-68) indicates that for obtaining the mean value of the limit state function, the mean values of each random variable should be substituted in the limit state function.

The next step for obtaining the reliability index is to find out the variance of the limit state function:

$$\sigma_g^2 = E\left[\left(g(\boldsymbol{X}) - \mu_g\right)^2\right] = E\left[\left\{\sum_{i=1}^{n}\left(\left.\frac{\partial g}{\partial X_i}\right|_{\mu_{\boldsymbol{X}}} \times \left(X_i - \mu_{X_i}\right)\right)\right\}^2\right] \tag{2-69}$$

By expanding the above equation, two types of terms will appear, the first involving squares and the second involving cross-products as [6]:

$$\begin{aligned}\sigma_g^2 = E\Bigg[&\sum_{i=1}^{n}\left[\left(\left.\frac{\partial g}{\partial X_i}\right|_{\mu_{\boldsymbol{X}}}\right)^2\left(X_i - \mu_{X_i}\right)^2\right] \\ &+ \sum_{i,j=1;i\neq j}^{n}\left\{\left.\frac{\partial g}{\partial X_i}\right|_{\mu_{\boldsymbol{X}}}\left(X_i - \mu_{X_i}\right) \times \left.\frac{\partial g}{\partial X_j}\right|_{\mu_{\boldsymbol{X}}}\left(X_j - \mu_{X_j}\right)\right\}\Bigg] \\ &= \left\{\left[\sum_{i=1}^{n}\left(\left.\frac{\partial g}{\partial X_i}\right|_{\mu_{\boldsymbol{X}}}\right)^2\right] \times E\left[\left(X_i - \mu_{X_i}\right)^2\right]\right\} \\ &+ \left\{\left[\sum_{i,j=1;i\neq j}^{n}\left.\frac{\partial g}{\partial X_i}\right|_{\boldsymbol{\mu_X}} \times \left.\frac{\partial g}{\partial X_j}\right|_{\boldsymbol{\mu_X}}\right] \times E\left[\left(X_i - \mu_{X_i}\right)\left(X_j - \mu_{X_j}\right)\right]\right\}\end{aligned} \tag{2-70}$$

Based on the definition of variance and covariance, Eq.(2-70) can be written as:

$$\sigma_g^2 = \left\{\left[\sum_{i=1}^{n}\left(\left.\frac{\partial g}{\partial X_i}\right|_{\boldsymbol{\mu_X}}\right)^2\right] \times \sigma_{X_i}^2\right\} + \left\{\left[\sum_{i,j=1;i\neq j}^{n}\left.\frac{\partial g}{\partial X_i}\right|_{\boldsymbol{\mu_X}} \times \left.\frac{\partial g}{\partial X_j}\right|_{\boldsymbol{\mu_X}}\right] \times COV\left(X_i, X_j\right)\right\} \tag{2-71}$$

Using the definition of covariance, Eq. (2-71) can be written as:

$$\sigma_g^2 = \sum_{i=1}^{n}\sum_{j=1}^{n}\left[\left.\frac{\partial g}{\partial X_i}\right|_{\mu_{\boldsymbol{X}}} \times \left.\frac{\partial g}{\partial X_j}\right|_{\boldsymbol{\mu_X}} \times \left(\rho_{X_iX_j}\sigma_{X_i}\sigma_{X_j}\right)\right] \tag{2-72}$$

Having obtained the mean value and variance of the limit state, the reliability index can be calculated as:

$$\beta = \frac{\mu_g}{\sigma_g} = \frac{g\left(\mu_{X_1}, \mu_{X_2}, \ldots, \mu_{X_n}\right)}{\sqrt{\sum_{i=1}^{n}\sum_{j=1}^{n}\left[\left.\frac{\partial g}{\partial X_i}\right|_{\boldsymbol{\mu_X}} \times \left.\frac{\partial g}{\partial X_j}\right|_{\boldsymbol{\mu_X}} \times \left(\rho_{X_iX_j}\sigma_{X_i}\sigma_{X_j}\right)\right]}} \tag{2-73}$$

It should be noted that the calculated reliability index (and also the probability of failure) is not an exact value since the limit state function is non-linear [6].

2.4.1.2 Limitations of the FOSM Method

Since only the mean values and standard deviations are used in the FOSM method, this method is an easy method to calculate the reliability index. However, this method has some shortcomings such as:

- Random variables are assumed normally distributed;
- The limit state is linearised and higher derivative terms in a Taylor series are neglected.
- Lack of invariance problem:

  The main issue with this method is an invariance problem, i.e. the value of the calculated reliability index in this method depends on a particular formulation of the limit state function. In the other words, the equivalent limit state functions have different reliability index values, whereas, changing the formulation of the limit state function does not change the actual border between the safe and failure domains [6]. It can be shown that the obtained reliability index is different for the following limit states:

$$g_1 = R - S$$

$$g_2 = R^2 - S^2$$

  Where R and S are the capacity and load variables.

2.4.2 First Order Reliability Method (FORM)

It was mentioned that the main issue with the FOSM method is the invariance problem. To solve this problem, the First Order Reliability Method (FORM) was developed. Same as the FOSM method, the limit state function is approximated by the first-order Taylor expansion. However, here, instead of at the mean, the limit state function is linearised somewhere on the limit state surface, i.e., at a point where $g = 0$.

Two steps are considered in FORM to obtain the probability of failure [11]:

- Transferring the random variables in the original space to the standard normal space
- Linearisation of the limit state function.

After the two steps, an analytical solution to the probability integration will be easily found.

2.4.2.1 Transformation of Variables

Generally, the stochastic variables are not normally distributed. To calculate the probability of failure based on Eq.(2-64), the random variables in the original space (which is called **X**-space) are transferred to the standard normal space (which is called **U**-space). In the standard normal space, all random variables are:

- Uncorrelated
- Standard normal distributed

The transformation from the original **X**-space to the standard normal **U**-space is performed for two reasons [11]:

1) The joint PDF in the standard normal space is rotationally symmetric and it decays in the radial and tangential directions. Therefore, the point on the limit-state surface that is closest to the origin has the highest probability density. As a result, the point closest to the origin is an important point for approximating the limit-state function,
2) In the standard normal space, it is possible to develop a formula for the probability content outside a hyper-plane.

It should be noted that after the transformation, the asymmetric joint PDF in the original space (Figure 2.15) is replaced with symmetric concentric circles. Figure 2.16 shows the joint PDF contour and the limit state function in **U**-space. It is now easier to calculate the probability of failure.

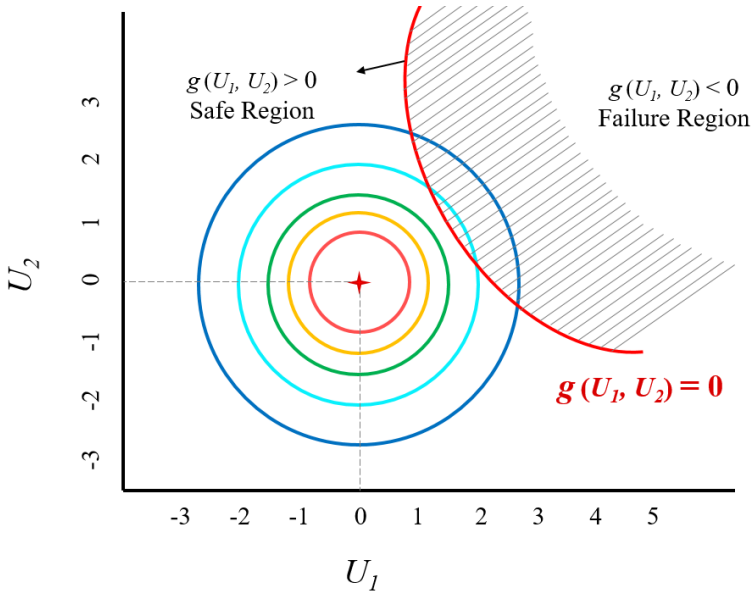

Figure 2.16. Joint PDF contour and the limit state function in **U**-space

Figure 2.17 shows the limit state functions in both **X**-space and **U**-space.

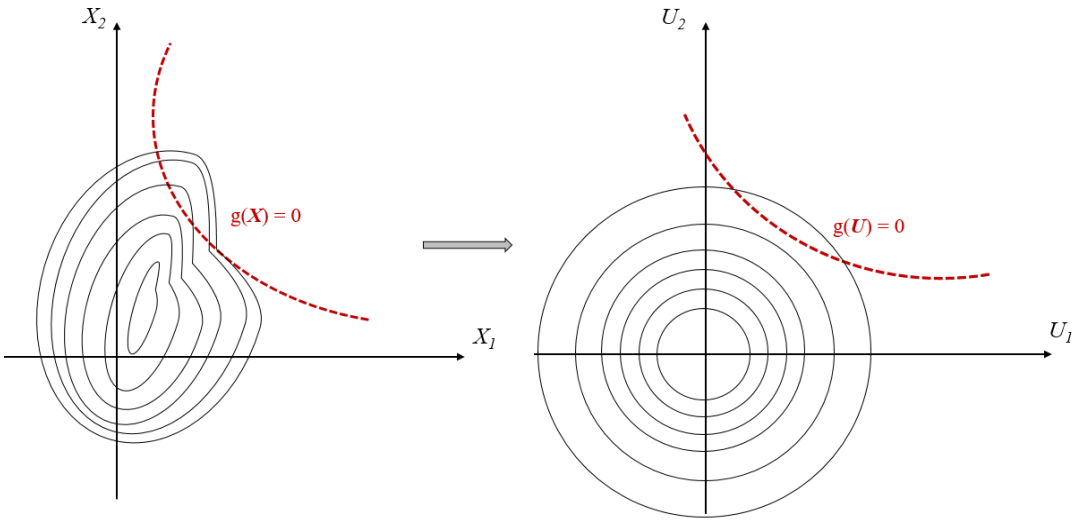

Figure 2.17. Failure functions in **X**-space and **U**-space

The transformation is based on the condition that the CDFs of the random variables remain the same before and after the transformation. The transformation can be performed in several ways, e.g. by determining eigenvalues and eigenvectors [12].

One of the useful transformations is the Rosenblatt transformation [11], which is expressed as:

$$F_{X_i}(x_i) = \Phi(u_i) \tag{2-74}$$

Therefore, the transformed standard normal variable is then given by:

$$U_i = \Phi^{-1}\left(F_{X_i}(X_i)\right) \tag{2-75}$$

After the transformation, the limit state function can be written in **U**-space. It is noted that the mathematical formulation of the original limit state will change. The probability of failure is:

$$P_f = \dot{\iiint}_{g(\boldsymbol{U})<0} \varphi(\boldsymbol{U}) d\boldsymbol{U} \tag{2-76}$$

where $\varphi(\boldsymbol{U})$ is the joint PDF of random variables in the standard normal space. Since all the random variables are independent, the joint PDF is the product of the individual PDFs of standard normal distribution and is then given by:

$$\varphi(\boldsymbol{U}) = \prod_{i=1}^{n} \frac{1}{\sqrt{2\pi}} exp\left(-\frac{1}{2}U_i^2\right) \tag{2-77}$$

2.4.2.2 Linearisation of Limit State Surface

After transferring the random variables in the original space to the standard normal space, the limit state function in **U**-space should be linearised. This linearisation is performed to make the probability integration easier to be evaluated. In the FORM method, a linear approximation (the first-order Taylor expansion) same as the FOSM method is used. However, instead of at mean, the limit state function is linearised at the design point, which is denoted by $\boldsymbol{u}^*$. The design point is unknown and it will be explained how to find it in Section 2.4.2.3.

In this section, the limit state function in the original space is denoted $g(\boldsymbol{X})$ whereas it is denoted by $G(\boldsymbol{U})$ in the standard normal space.

At first, let's assume that the design point is known. The linear Taylor series expansion around the design point can be written as:

$$G(\boldsymbol{U}) \cong G(\boldsymbol{u}^*) + \nabla G(\boldsymbol{u}^*)^T.(\boldsymbol{U} - \boldsymbol{u}^*) \tag{2-78}$$

Where $\boldsymbol{u}^* = (u_1^*, u_2^*, \dots, u_n^*)$ is the expansion point, superscript T stands for a Transpose operator and $\nabla G(\boldsymbol{u}^*)$ is the gradient of $G(\boldsymbol{U})$ at $\boldsymbol{u}^*$ which is:

$$\nabla G(\boldsymbol{u}^*) = \left(\frac{\partial G(\boldsymbol{U})}{\partial U_1}, \frac{\partial G(\boldsymbol{U})}{\partial U_2}, \dots, \frac{\partial G(\boldsymbol{U})}{\partial U_n}\right)\Big|_{\boldsymbol{U}=\boldsymbol{u}^*} \tag{2-79}$$

The alpha vector which is a unit vector is defined as:

$$\boldsymbol{\alpha} = -\frac{\nabla G(\boldsymbol{U})}{\|\nabla G(\boldsymbol{U})\|} \tag{2-80}$$

Where $\|.\|$ indicates the length of a vector.

It was mentioned that the design point is a point on the limit state surface, therefore:

$$G(\boldsymbol{u}^*) = 0 \tag{2-81}$$

By plugging Eq.(2-80) and Eq.(2-81) into Eq.(2-78):

$$G(\boldsymbol{U}) \cong [-\|\nabla G(\boldsymbol{u}^*)\|\boldsymbol{\alpha}]^T.(\boldsymbol{U} - \boldsymbol{u}^*) = \|\nabla G(\boldsymbol{u}^*)\| \times \left(\boldsymbol{\alpha}^T.\boldsymbol{u}^* - \boldsymbol{\alpha}^T.\boldsymbol{U}\right) \tag{2-82}$$

2.4.2.3 Finding the Design Point

Due to the linearisation of the limit state function, the probability of failure is not completely accurate. To minimise the accuracy loss, $G(\boldsymbol{U})$ needs to be expanded at a point that has the highest contribution to the probability integration [11]. Therefore the Taylor series is expanded at a point that has the highest value of probability density. The point that has the highest probability density on $G(\boldsymbol{U}) = 0$ is denoted as the Most Probable Point (MPP) or the design point. Therefore, it is required to maximise the joint PDF introduced in Eq.(2-77), i.e.:

$$\max_{\boldsymbol{U}} \left[\prod_{i=1}^{n} \frac{1}{\sqrt{2\pi}} exp\left(-\frac{1}{2}U_i^2\right)\right]\Bigg|_{G(\boldsymbol{U})=0} \tag{2-83}$$

Since:

$$\prod_{i=1}^{n} \frac{1}{\sqrt{2\pi}} exp\left(-\frac{1}{2}U_i^2\right) = \frac{1}{\sqrt{2\pi}} exp\left(-\frac{1}{2}\sum_{i=1}^{n} U_i^2\right) \tag{2-84}$$

Maximising the Eq.(2-84) is equivalent to minimising $\sum_{i=1}^{n} U_i^2$. Therefore the design point ($\boldsymbol{u}^*$) is obtained as:

$$\boldsymbol{u}^* = \min_{\boldsymbol{U}} \left[\sum_{i=1}^{n} U_i^2\right]\Big|_{G(\boldsymbol{U})=0} = \min_{\boldsymbol{U}} \|\boldsymbol{U}\| \Big|_{G(\boldsymbol{U})=0} \tag{2-85}$$

It was mentioned that ||.|| stands for the length of a vector, i.e.:

$$\|\boldsymbol{U}\| = \sqrt{U_1^2 + U_2^2 + \cdots + U_n^2} = \sqrt{\sum_{i=1}^{n} U_i^2} \tag{2-86}$$

Therefore the design point is obtained by solving the optimisation problem (Eq.(2-85)).

Hasofer and Lind showed that the reliability index is the smallest distance from the origin in the **U**-space to the failure surface [14]. Therefore:

$$\beta = \|\boldsymbol{u}^*\| = \sqrt{\sum_{i=1}^{n} \left(u_i^*\right)^2} \tag{2-87}$$

Figure 2.18 illustrates the geometrical concept of the reliability index.

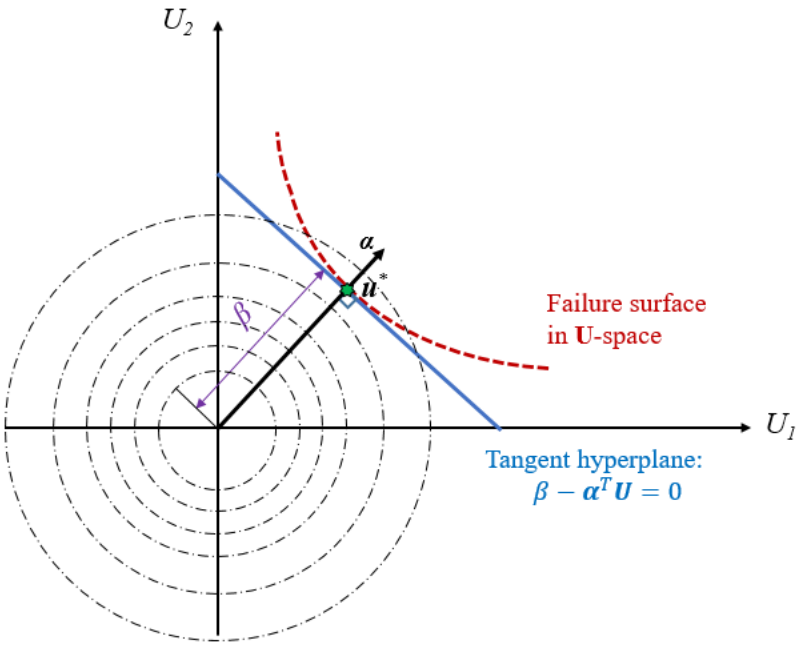

Figure 2.18. Geometrical illustration of the reliability index β

After obtaining the reliability index, the probability of failure is obtained as:

$$P_f = \Phi(-\beta) \tag{2-88}$$

Let's have look at Eq. (2-82) again:

$$G(\boldsymbol{U}) \cong [-\|\nabla G(\boldsymbol{u}^*)\|\boldsymbol{\alpha}]^T.(\boldsymbol{U}-\boldsymbol{u}^*) = \|\nabla G(\boldsymbol{u}^*)\| \times \left(\boldsymbol{\alpha}^T.\boldsymbol{u}^* - \boldsymbol{\alpha}^T.\boldsymbol{U}\right)$$

Since $\boldsymbol{\alpha}$ is a unit vector, the dot product between the parallel vectors $\boldsymbol{\alpha}$ and $\boldsymbol{u}^*$ is the length of $\boldsymbol{u}^*$. Based on Eq. (2-87), the length of $\boldsymbol{u}^*$ is equal to reliability index. Therefore Eq. (2-82) yields to:

$$G(\boldsymbol{U}) \cong \|\nabla G(\boldsymbol{u}^*)\| \times \left(\beta - \boldsymbol{\alpha}^T.\boldsymbol{U}\right) \tag{2-89}$$

Eq. (2-89) shows the linearised limit state function obtained by the FORM method.

- **Optimisation Technique**

  It was mentioned that to obtain the design point, an optimisation problem should be solved (Eq.(2-85)). A generic search technique for optimisation can be employed to determine the design point as [11]:

  $$\boldsymbol{u}_{m+1} = \boldsymbol{u}_m + s_m.\boldsymbol{d}_m \tag{2-90}$$

  where m is the iteration counter, s_m is the step size at the m^{th} iteration, and $\boldsymbol{d}_m$ is the direction vector at the m^{th} iteration. In each iteration, convergence criteria should be checked. The design point is selected when the convergence criteria are being satisfied. Two convergence criteria are considered:

  1) The trial point must be close to the limit-state surface:

  $$\left|\frac{G(\boldsymbol{u}_m)}{G_0}\right| \leq e_1 \tag{2-91}$$

  where G_0 is a scaling factor and it is usually the value of the limit state function at the mean value and e_1 is a is usually selected equal to 10^{-3} [11].

  2) The trial point is required to be the closest point on the origin:

  If the trial point is the closest point to the origin, the gradient of the limit-state function at the trial point should pass at the origin. In fact, at the design point, $\boldsymbol{u}_{m+1}$ is parallel to the gradient vector.

  The length of the **u**-vector in the direction of the **α**-vector is equal to the dot product between these vectors (i.e. $\boldsymbol{\alpha}^T.\boldsymbol{u}$). As shown in Figure 2.19, the

difference between the vector $(\boldsymbol{\alpha}^T.\boldsymbol{u})\boldsymbol{\alpha}$ and $\boldsymbol{u}$ can be assumed a reasonable convergence criterion:

$$\|\boldsymbol{u}_m - (\boldsymbol{\alpha}_m^T.\boldsymbol{u}_m)\boldsymbol{\alpha}_m\| \leq e_2 \tag{2-92}$$

where e_2 is usually selected equal to 10^{-3} [11].

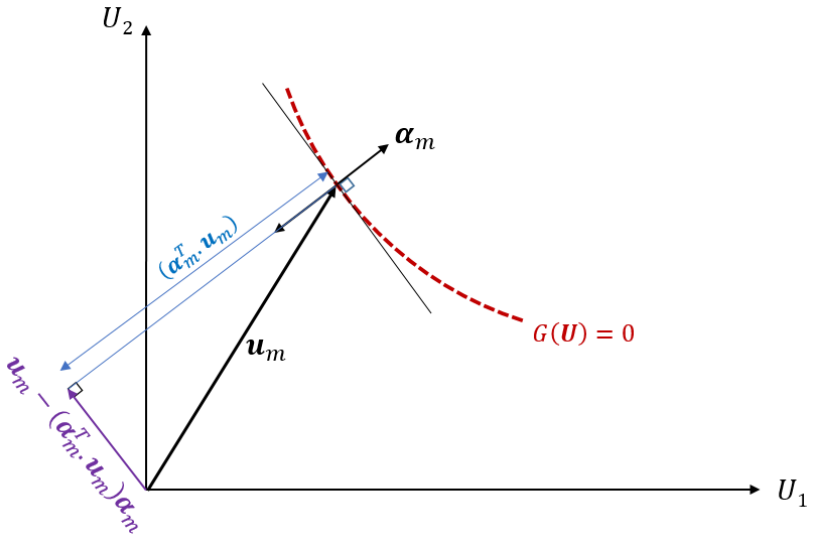

Figure 2.19. Second convergence criterion

Having obtained the design point, the reliability index can be achieved based on Eq. (2-87).

2.4.3 Second-Order Reliability Method (SORM)

Compared to a FORM estimate of the reliability of a component, the Second-Order Reliability Method (SORM) estimated the reliability by using a second-order approximation of the failure surface at the design point (expansion using the first and the second derivative terms in a Taylor series):

$$G(\boldsymbol{U}) \cong G(\boldsymbol{u}^*) + \nabla G(\boldsymbol{u}^*)^T(\boldsymbol{U} - \boldsymbol{u}^*) + \frac{1}{2}(\boldsymbol{U} - \boldsymbol{u}^*)^T.\boldsymbol{H}(\boldsymbol{u}^*).(\boldsymbol{U} - \boldsymbol{u}^*) \tag{2-93}$$

where $\boldsymbol{H}(\boldsymbol{u}^*)$ is the Hessian matrix of second-order partial derivatives of the failure surface at the design point, i.e.:

$$\boldsymbol{H}(\boldsymbol{u}^*) = \left[\begin{matrix} \dfrac{\partial^2 G}{\partial U_1^2} & \cdots & \dfrac{\partial^2 G}{\partial U_1 \partial U_n} \\ \vdots & \ddots & \vdots \\ \dfrac{\partial^2 G}{\partial U_n \partial U_1} & \cdots & \dfrac{\partial^2 G}{\partial U_n^2} \end{matrix}\right]_{\boldsymbol{U}=\boldsymbol{u}^*} \tag{2-94}$$

The result of a SORM analysis may be given as the reliability index obtained from FORM multiplied with a correction factor evaluated based on the second-order partial derivatives of the failure surface in the design point. More details of SORM analysis can be found in [13].

It is noted that the FORM method gives sensible results when the failure functions are not too non-linear. If the failure function in **U**-space is quite non-linear, then the SORM method provides more accurate results [10].

Figure 2.20 shows the first and second-order approximations of the failure surface, schematically.

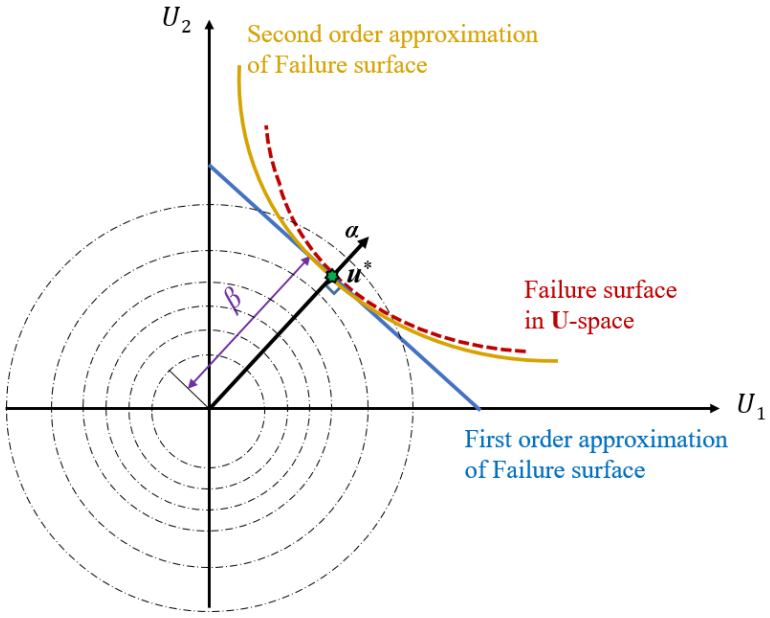

Figure 2.20. Illustration of the first and second-order approximations of the failure surface

2.4.4 Monte-Carlo Simulations

In the previous methods, iterative procedures are required to obtain the reliability index. Since in most engineering systems, variables are not normally distributed, these procedures are quite complex. For example, in both FORM and SORM,

transformations from the original distributions to corresponding equivalent normal distributions are needed at each cycle of the iteration. Moreover, the obtained solutions are not exact, albeit the approximations are usually reasonable.

The Monte-Carlo simulation can obtain very accurate solutions for the probability of failure. With the rapid development of low cost and fast computing, Monte-Carlo simulation is becoming increasingly attractive [6]. Moreover, the Monte-Carlo simulation method is a powerful tool when the failure function in the U-space has more than one β-point, i.e. there are several local, probable failure regions [10].

The name 'Monte-Carlo' was introduced in the 1940s by physicists (Stanislaw Ulam, Enrico Fermi, John von Neumann and others) working on nuclear weapon projects in the Los Alamos National Laboratory. The name is a reference to the Monte Carlo Casino in Monaco since the use of randomness and the repetitive nature of Monte Carlo simulation are analogous to the activities conducted at a casino [6].

Monte-Carlo methods are widely used to simulate engineering, physical and mathematical systems. Moreover, Monte-Carlo simulation methods are capable to perform reliability analysis regardless of the number of uncertain parameters.

The following steps are required for performing Monte-Carlo simulation [6]:

- Define random variables and their distributions
- Generate sample values of the defined random variables
- Evaluate limit state function for each set of random variables
- Estimate the probability of failure of each component

2.4.4.1 Basic Steps of Monte Carlo Simulation

In general, the process includes the following steps:

1) Assume there are m basic random variables
2) Generate a random number uniformly distributed between 0 and 1 (u_i). Index i indicates the simulation number.
3) For each basic random variable x_j $(j = 1, 2, \dots, m)$, find the value with the corresponding CDF equal to $F_{X_j}(x_j) = u_i$.

4) Substitute the generated values of the basic random variables into the limit state function.

5) Depending on the value of the limit state function, Obtain the $I(\boldsymbol{X}_i)$ as:

$$I(\boldsymbol{X}_i) = 0, \quad if \;\; g(\boldsymbol{X}_i) > 0$$
$$I(\boldsymbol{X}_i) = 1, \quad if \;\; g(\boldsymbol{X}_i) \leq 0 \tag{2-95}$$

6) Go to step one and repeat this procedure a large number of times (N).

7) Obtain the number of total simulations in which the limit state is less than zero (failure happens):

$$n_f = \sum_{i=1}^{N} I(\boldsymbol{X}_i) \tag{2-96}$$

8) Calculate the estimation of the probability of failure as:

$$P_f \cong \frac{n_f}{N} = \frac{\sum_{j=1}^{N} I(\boldsymbol{X}_j)}{N} \tag{2-97}$$

Figure 2.21 shows the frequency of the limit state function values in addition to the safe and unsafe areas, schematically.

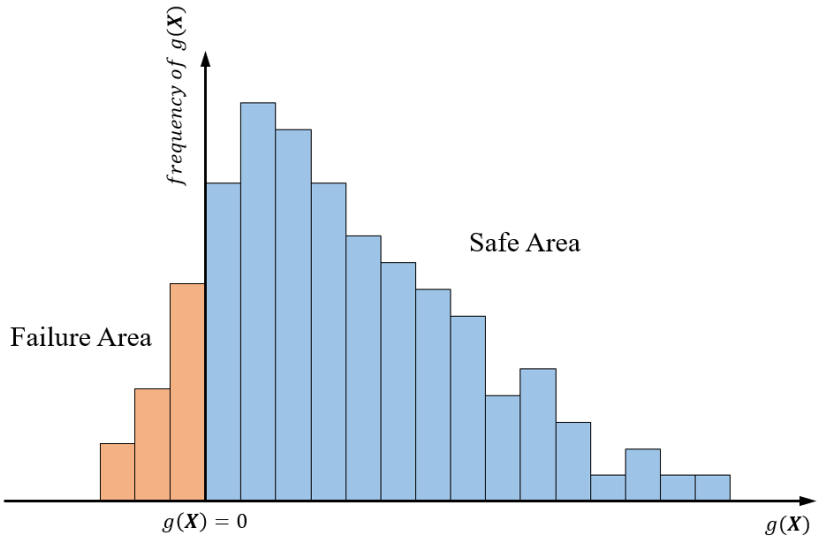

Figure 2.21. Schematic distribution of the limit state function

It should be noted that the probability of failure depends on the number of trials (i.e. N). Therefore the probability of failure can be assumed as an uncertain parameter. Hence, the calculated P_f in Eq.(2-97) is an estimation of the probability of failure. It

can be shown that the coefficient of variation of the probability of failure is calculated as [6]:

$$COV_{P_f} \cong \frac{1}{\sqrt{n_f}} \tag{2-98}$$

The COV_{P_f} represents the coefficient of variation of the estimation of the probability of failure. It is desirable to reduce the coefficient of variation to less than 0.1 to obtain a sufficiently accurate estimate of the probability of failure [6]. In most cases, this coefficient is even preferred to be smaller than 0.02 [1].

To achieve the desired level of accuracy, the number of simulations by the Monte Carlo method must be chosen high enough to keep the coefficient of variation of failure probability below 0.1.

2.4.4.2 Advantages and Disadvantages of Monte Carlo Simulation

Some advantages of using the Monte Carlo simulation method are [6]:

- Variables can have any distribution function. Even empirical distributions without explicit analytical forms can be used.
- There is no need to transfer variables into standard normal space.
- A complex limit state function can be utilised. The Monte-Carlo method is considered the most powerful technique for analysing complex problems.
- In implicit limit state functions (limit state is not expressed explicitly based on the random variables), using Monte-Carlo simulation is the only option [11].
- There is no need to calculate the gradient of the limit state at the design point.
- By increasing the number of simulations (N), the estimation of the probability of failure becomes more accurate, whereas, in FORM and SORM methods, the probability of failure is approximated.

However, this method has some disadvantages:

- A computer is needed for performing calculations.

- A large number of simulations is needed to obtain a sufficiently accurate estimate of the probability of failure, especially when the order of the probability of failure is very low. Therefore, it may require significant computational time.
- Sensitivity analysis of the reliability index to the random variables cannot be obtained [15].

2.4.4.3 Other Monte Carlo Methods

It was mentioned that to obtain an accurate and reliable estimation of the probability of failure, a large number of simulations are required especially for estimation of rare events to obtain a sufficient number of rarely failed samples.

In many structural reliability problems, the probability of failure is of an order of 10^{-5} to 10^{-4} [16]. It was mentioned that for an accurate result, the coefficient of variation of the probability of failure should be less than 0.1.

If the acceptable COV_{P_f} is assumed equal to 0.05, based on Eq. (2-98), the number of failed simulations is obtained equal to:

$$0.05 \cong \frac{1}{\sqrt{n_f}} \quad \Rightarrow \quad n_f = 400 \tag{2-99}$$

If the probability of failure is assumed equal to 10^{-4}, based on Eq.(2-97), the total number of simulations required to obtain the accurate probability of failure is approximately equal to:

$$N \cong \frac{n_f}{P_f} = \frac{400}{10^{-4}} = 4 \times 10^6 \tag{2-100}$$

Depending on the complexity of the limit state function, the computational process may become too time-consuming and not feasible to use.

To reduce the number of samples, some techniques are developed to improve the efficiency of the Monte-Carlo simulation to generate more sample points in the failure region. These techniques allow decreasing the variance of the estimate of the probability of failure without using a very large number of simulation trials. Some of these modified techniques are [10]:

- Importance sampling

- Adaptive sampling
- Directional sampling
- Latin hypercube sampling

For example, the importance sampling method attempts to increase computational efficiency by generating samples in the high-probability density regions of the failure domain. The simplest way to perform the importance sampling is to use a design point obtained by the FORM as the mean of the sampling PDF. Therefore the sampling PDF is the original PDF shifted to be centred at the design point [6]. More details about the modified Monte-Carlo simulation techniques can be found in [10] and [17].

2.5 Sensitivity Measures

Usually, several random variables exist in reliability analysis applications. In structural reliability analysis, in addition to the value of the probability of failure or reliability, it is crucial to know which of the basic random variables is more important in its contribution to the probability of failure. The main reasons for performing the sensitivity analysis are:

- Identify the factors which have the most influence on reliability,
- Identify factors that may need more research to improve confidence in the analysis,
- Identify factors that are insignificant to the reliability and can be considered as deterministic parameters.

Therefore, it is important to investigate the effect of each variable on the reliability index. A study of the sensitivity measures helps to identify the variables of the model that most significantly influence the reliability of the structure. Some sensitivity and importance measures have been reported in the literature which provides valuable additional information to help in decision making under uncertainty and these are discussed in the following [7].

The sensitivity of the reliability index with respect to stochastic variables can be evaluated by using sensitivity measures. One important sensitivity measure is the alpha vector ($\boldsymbol{\alpha}$).

Based on Figure 2.18, the design point vector can be written as:

$$\boldsymbol{u}^* = \beta\boldsymbol{\alpha} \tag{2-101}$$

Since $\boldsymbol{\alpha}$ is a unit vector, the dot product between this vector and its transpose equals to:

$$\boldsymbol{\alpha^T}.\boldsymbol{\alpha} = 1 \tag{2-102}$$

By multiplying $\boldsymbol{\alpha}^T$ into both sides of Eq. (2-101):

$$\begin{gathered}\boldsymbol{\alpha}^T.(\boldsymbol{u}^*) = \boldsymbol{\alpha}^T.(\beta\boldsymbol{\alpha}) \\ \boldsymbol{\alpha^T}.\boldsymbol{u}^* = \beta\end{gathered} \tag{2-103}$$

Therefore:

$$\left.\frac{\partial\beta}{\partial U_i}\right|_{\boldsymbol{U}=\boldsymbol{u}^*} = \alpha_i \tag{2-104}$$

Based on Eq.(2-104), the numerical value of α_i is a measure of the sensitivity of the reliability index to inaccuracies in the value of U_i at the design point. Thus the components in the **α**-vector can be considered as the relative importance of each stochastic variable on the reliability index [13].

It can be shown that the variance of the limit state function is equal to [10]:

$$Var[G(\boldsymbol{U})] \cong \|\nabla G(\boldsymbol{u}^*)\|^2 \times (\alpha_1^2 + \alpha_2^2 + \cdots + \alpha_n^2) \tag{2-105}$$

Therefore, for independent stochastic variables, α_i^2 gives the percentage of the total uncertainty associated with U_i (and X_i).

It can be shown that if $|\alpha_i| \leq 0.14$, the corresponding error in the reliability index is less than one percent. Therefore, the stochastic parameter related to this variable can be assumed as a deterministic parameter [10].

In the reliability analysis context, sometimes it can be difficult which variables represent load variables and which variables represent strength variables. It can be shown that [10]:

$\alpha_i > 0$: Load parameter

$\alpha_i < 0$: Resistance parameter

There are other sensitivity measures such as reliability elasticity coefficient and omission sensitivity factors. The omission sensitivity factor was introduced by Madsen to determine the relative error in the reliability index by treating one of the basic variables as deterministic [18].

2.6 Summary

This chapter presents the basic concepts of the probability theory, random variables and commonly-used probability distributions. Then different approaches to structural safety are described and the concepts of structural reliability theory are explained. Different sources of uncertainty associated with load and resistance modelling are described.

Different techniques for estimation of the reliability, including FORM, SORM and Monte-Carlo simulation and advantages/disadvantages of each method are explained.

Although FORM and SORM methods estimate the probability of failure by approximating the nonlinear limit state function, they provide a measure of the sensitivity of the reliability index to the random variables considered in the analysis.

Monte-Carlo simulation techniques, on the other hand, can estimate an accurate probability of failure if a large number of simulations is generated. However, a large number of simulations makes reliability analysis more time-consuming.

3 . FATIGUE RELIABILITY ANALYSIS

3.1 Introduction

Offshore jacket platforms are one of the most common types of offshore structures. They are usually constructed as truss frameworks in which tubular members are the structural elements [5]. These tubular members are welded together to create a steel frame, to transfer the gravitational and lateral loads to the pile foundations [1].

Fatigue is defined as the failure of a component under a repeated load that never reaches a level sufficient to cause failure in a single application [3]. Fatigue is the process of damage accumulation in a member which experiences variable stresses due to time-varying loading [19]. Fatigue failure occurs when the accumulated damage is exceeding a critical level.

Offshore jacket platforms are likely to fatigue damage due to the cyclic nature of wave loading on the structure. Therefore, fatigue analysis of such structures is very important in both the design and the assessment of platforms. Fatigue damage in offshore jacket platforms is most probable to occur at the welded tubular joints due to:

- Geometric discontinuity of the connections which produces high-stress concentrations in these intersections
- Presence of small initial defects at the weld toe due to the welding process

Therefore, tubular joints of offshore platforms are susceptible to fatigue damage. Due to the high-stress concentration in the welded intersections, under these cyclic wave loads, these tiny defects gradually grow into fatigue cracks, and significantly reduce the capacity of the connections. The crack propagation may reach unacceptable sizes through thickness cracks and might lead to failure of the tubular joints.

The main purpose of this chapter is to obtain the fatigue reliability analysis of the tubular joints. Section 3.2 introduces the fatigue process, how to model the wave loading in the sea environment, and how to obtain the response of the structure to the environmental loads by introducing the transfer function concept.

In Section 3.3, stress analysis of tubular joints is considered. Different types of tubular joints are introduced. The concept of hot spot stress (HSS) and stress concentration factor (SCF) is presented.

For fatigue analysis of a tubular joint, two approaches are available: the S-N approach and the Fracture Mechanics (FM) approach [5]. Section 3.4 explains the S-N approach, important factors that should be taken into consideration when using the S-N approach (e.g., wall thickness), and fatigue damage calculation.

Fatigue analysis based on the FM approach is explained in Section 3.5. The crack growth estimation, Paris law, and stress intensity factor (SIF) are introduced as well. It is noted that in this study, the FM approach is considered for performing the fatigue reliability analysis.

Considerable research effort has been made on the probabilistic approaches to fatigue reliability analysis of offshore jacket platforms. Section 3.6 explains some of these studies. Section 3.7 describes how to perform fatigue reliability analysis for a tubular joint in a jacket structure. To carry out reliability analysis it is necessary to develop an appropriate probabilistic model. In this section, sources of uncertainties in fatigue analysis are explained and the limit state function is introduced. It is worth mentioning that in this chapter, the fatigue reliability analysis is considered at the component level, i.e. the probability of failure is estimated for a specific component (tubular joint). The system reliability calculation will be discussed in Chapter 4 of this thesis.

Finally, the application of the fatigue reliability analysis to a jacket platform is provided in Section 3.8. A three-dimensional structural model of the considered platform is generated using SESAM software. A global fatigue analysis is performed by SESAM and the generated stress results are used to predict the crack size for the critical components in the considered platform. At any given time, the reliability of a tubular joint depends on the size of the fatigue crack. By performing the reliability analysis for the critical components, the probability of failure of each joint is obtained.

It is worth mentioning that in this Chapter, Sections 3.2 to 3.7 describe the theoretical aspects of the fatigue reliability analysis, whereas, Section 3.8 demonstrates the application of the theoretical aspects to the considered platform and results that have been developed by the author.

3.2 Fatigue Stochastic Process

The theory of stochastic processes is treated in several textbooks such as [20], [21] and [22]. The basics of stochastic process can be explained by taking into account the time history of a process such as shown in Figure 3.1. The value of the stochastic process at any specific time cannot be precisely predicted. However, it is possible to describe the process by its statistical properties. A process is said to be stationary if the statistical properties (e.g. mean value and standard deviation) do not vary with time [5].

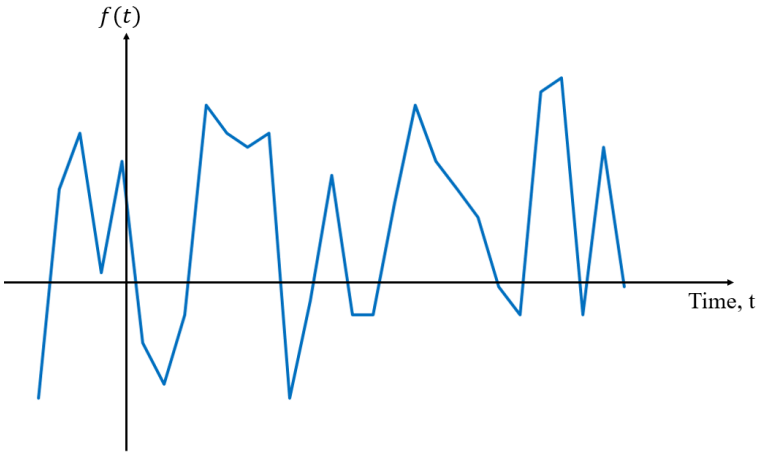

Figure 3.1. Time history of a stochastic process

Many processes can be considered stationary processes if the considered time interval is short enough. For example, the sea surface (water level) elevation can be considered to be a stationary process within time intervals of three to six hours [5].

The main characteristic of a stationary process is that it can be considered as being composed of infinite harmonic components with different frequencies [5]. It can be shown that the energy of a harmonic wave is proportional to the square of its amplitude [5]. The energy spectrum shows how this energy of a harmonic wave is distributed at various frequencies.

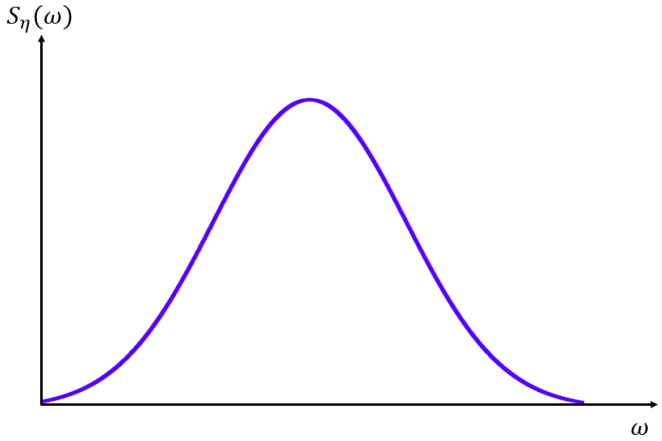

Figure 3.2. Energy spectrum for a harmonic wave

Figure 3.2 shows an energy spectrum for a harmonic wave, schematically. In the literature, the wave energy spectrum is also called wave spectral density [5]. In this figure, ω represents the angular frequency and $S_\eta(\omega)$ represents the water surface energy spectrum for a harmonic wave. The angular frequency is defined as:

$$\omega = \frac{2\pi}{T_w} = 2\pi f_w \tag{3-1}$$

where T_w and f_w are the wave period and wave frequency, respectively.

The zero-order moment of the energy spectrum (which is the area under the spectrum) represents the total energy of the process [5]. It can be shown that the zero-order moment of the energy spectrum is also equal to the variance of the process [5], i.e.:

$$m_0 = \int_0^\infty S_\eta(\omega) d\omega = \sigma_\eta^2 \tag{3-2}$$

where m_0 represents the zero-order moment of the energy spectrum and σ_η^2 represents the variance of the water surface [5].

The spectral width parameter (ϵ) of a process (any stochastic process in general) is defined as [5]:

$$\epsilon = \sqrt{1 - \frac{m_2^2}{m_0 \times m_4}} \tag{3-3}$$

where m_2, m_4 are the second-order and fourth-order moments of the energy spectrum of that process, respectively. The amount of ϵ varies between zero and one. When it is

close to zero, the spectrum is narrow and the time history of the process is relatively smooth and regular. Otherwise, the spectrum is broad and a time history is more irregular in shape [5].

For a narrow-band process, the average zero-crossing period for the water surface (T_z) is approximated by [5]:

$$T_z = 2\pi \times \sqrt{\frac{m_0}{m_2}} \tag{3-4}$$

In this chapter, the statistical properties of sea waves are modelled using short-term sea states. The duration of a sea state is normally taken as three hours [5]. Within each sea state, the water surface elevation ($\eta(t)$) is modelled by a stationary, Gaussian stochastic process. Therefore, the wave elevation is assumed normally distributed with an expected value of zero ($\mu_\eta = 0$) and standard deviation of σ_η [5].

3.2.1 Response to the Environmental Loads

In a linear system, the spectrum of the response can be obtained by using a transfer function. Linear systems are systems in which the relation between the input (excitation) and the output (response) is described by a linear differential equation [5].

In the North Sea, the surface waves are of major importance in the design of jacket structures, whereas the wind loads only represent a contribution of less than 5% of the total environmental loading [19]. Therefore, for an offshore structure, the ocean wave forces can be considered as the excitation and the stresses in a member can be assumed as the response. In general, the response process at the same frequency as the excitation process can be given by [5]:

$$Y_\omega(t) = T(\omega) \times X_\omega(t) \tag{3-5}$$

where $T(\omega)$ is the transfer function, $X_\omega(t)$ and $Y_\omega(t)$ are the excitation and response, respectively.

The value of the energy spectrum at a given frequency is proportional to the square of the amplitude of the harmonic wave at that frequency [5]. Therefore, the energy spectrum of the response process is given by [5]:

$$S_Y(\omega) = |T(\omega)|^2 \times S_X(\omega) \quad (3\text{-}6)$$

where S_Y represents the response spectrum and S_X represents the excitation spectrum.

In this chapter, the water surface is the excitation (i.e. $X_\omega(t)$) and stress is considered as the response (i.e. $Y_\omega(t)$). Therefore, Eq. (3-6) is written as:

$$S_S(\omega) = |T(\omega)|^2 \times S_\eta(\omega) \quad (3\text{-}7)$$

where S_S represents the stress spectrum and S_η represents the water surface spectrum.

Figure 3.3 shows the water surface spectrum ($S_\eta(\omega)$), the stress spectrum ($S_S(\omega)$), and the transfer function ($T(\omega)$), schematically.

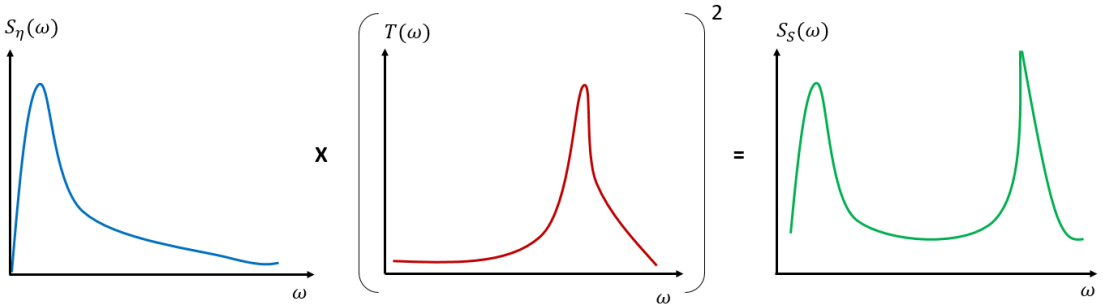

Figure 3.3. Obtaining the stress spectrum ($S_S(\omega)$), by using the water surface spectrum ($S_\eta(\omega)$) and the transfer function ($T(\omega)$)

The major task of the frequency domain analysis is the determination of the response of the structure for a unit sinusoidal wave as a function of the wave angular frequency (i.e. transfer function).

3.2.2 Modelling of Wave Loads

The real sea does not contain the regular wave. Therefore, the sea may be described in terms of the statistical properties of the sea surface elevation.

The wave period of a sea state can be defined as the time between two successive up-crossings through the still water level (zero up-crossing period). The wave height for each period is defined as the difference between maximum and minimum values within that period [5]. Figure 3.4 shows the time history of the irregular sea surface.

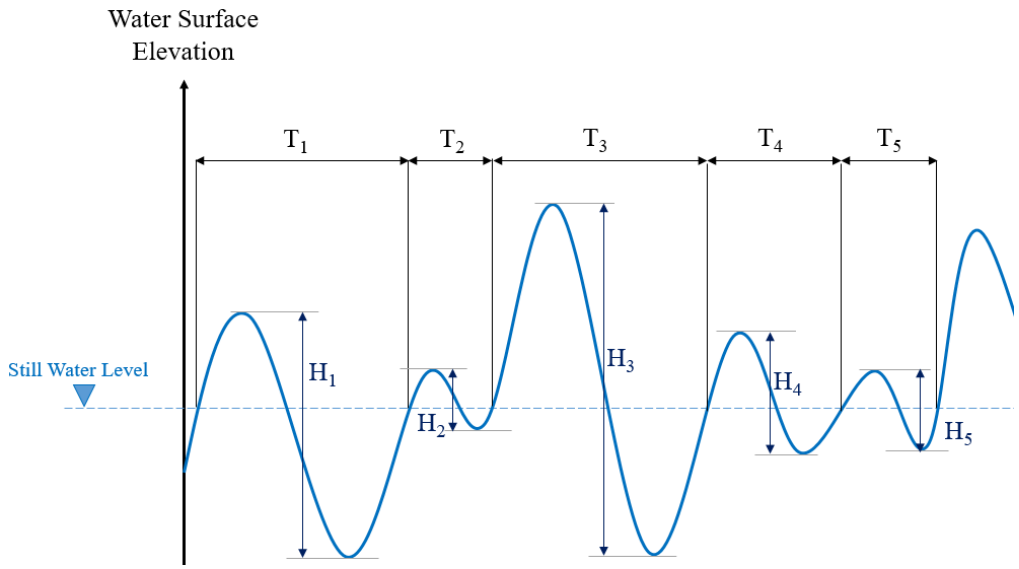

Figure 3.4. A time history of the irregular sea surface

In a short time interval (e.g. 3 hours), the statistical properties of the sea state may be considered to be constant. Therefore, the theory of stationary stochastic processes can be used to describe the sea state. For this stationary process, the following terms are defined:

- Zero up-crossing period (T_Z):

  The average value of the wave periods as shown in Figure 3.4

- Significant wave height (H_S):

  The average of the highest one-third of the wave heights as defined in Figure 3.4

- The water surface spectrum, $S_\eta(\omega)$:

  Wave spectra can be obtained by analyses of recorded wave-time histories. For design purposes, the model wave spectra are analytical expressions describing the spectral shape [5]. Several spectra have been developed and the most commonly used in the North Sea are Pierson-Moskowitz (PM) and JONSWAP spectrum. The PM spectrum applies to a fully developed sea, i.e. when the growth of waves is not limited by the size of the generation area. Therefore, the PM spectrum is usually used for fatigue analyses in the North Sea [5].

In the PM spectrum, the wave spectral density, $S_\eta(\omega)$ is defined as a function of significant wave height (H_S), mean zero-crossing period (T_Z) and wave angular frequency (ω), as [5]:

$$S_\eta(\omega) = \frac{4\pi^3 \times H_S^2}{T_z \times \omega^5} \times exp\left[-16\pi^3 \times \left(\frac{1}{T_z \times \omega}\right)^4\right] \quad (3\text{-}8)$$

The parameters H_S and T_Z are constant within each sea state.

Eq. (3-8) is obtained based on extensive oceanographic data and has been adopted as the most appropriate expression of sea surface behaviour for a fully developed sea.

Having obtained the water surface spectrum (excitation), the stress spectrum (response) can be achieved by using a frequency domain analysis. In a frequency domain analysis (spectral approach), the stress range spectrum is obtained by using water surface spectrum and the transfer function as shown in Eq. (3-7). In this approach, the wave statistics of the random sea are considered a stationary process.

Morison's equation is widely used in the design of jacket structures for calculating the wave-induced loading. Morison's equation provides reasonable results by careful selection of the drag (C_D) and inertia (C_M) coefficients in combination with an appropriate wave theory [19] as:

$$F = \frac{\rho D}{2} \times C_D \times U|U| + \frac{\pi \rho D^2}{4} \times C_M \times \frac{\delta U}{\delta t} \quad (3\text{-}9)$$

In Eq.(3-9):

- ρ: Mass density of water
- C_D: Drag coefficient
- D: Effective diameter of the cylindrical member including marine growth
- U: Velocity vector of the water normal to the axis of the member
- C_M: Inertia coefficient,
- $\delta U/\delta t$: Acceleration vector of the water normal to the axis of the member

3.3 Stress Analysis of Tubular Joints

Due to the uniform and symmetrical cross-section of tubular members, the stress concentrations are very small for these members. However tubular joints, which are welded connections, represent structural discontinuities that give rise to very high-stress concentrations in the intersection area [5].

Fatigue failure is a major problem in welded tubular joints due to high-stress concentrations at the weld toes of the intersections. Therefore, the proper design of tubular joints against fatigue failures must be based on detailed knowledge of the magnitudes of the stress at the weld toes of the connections [5].

3.3.1 Types of Tubular Joints

Offshore structures are made from welded tubular joints which are different from each other with respect to size, shape, and load-carrying capacity. These joints can be loaded in any combination of three modes which are axial loading, out-of-plane bending (OPB), and in-plane bending (IPB). Due to the complexity of joint geometry and shell behaviour of welded tubular joints that govern load response, local stresses are non-uniformly distributed. Figure 3.5 illustrates common loads in a tubular joint [3].

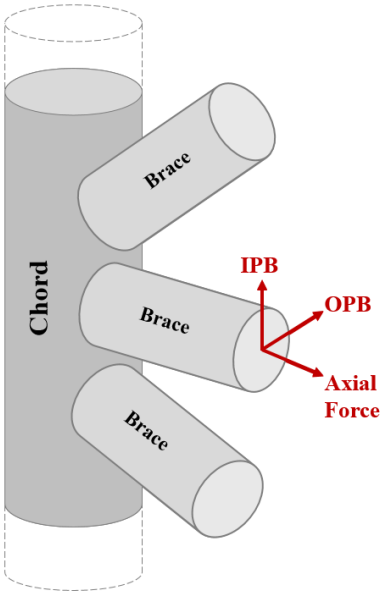

Figure 3.5. Illustration of different types of loading

Tubular joints are made in different shapes and their configurations and dimensions are usually chosen based on structural requirements [5]. Tubular joints consist of joints

between main and secondary member tubes. The member which has a larger diameter is called a chord, and the smaller-sized member is denoted as a brace [5].

Tubular joints are classified based on the geometrical configuration, the applied load, and the design types. The design types are categorised as [5]:

A) Simple welded joints: Simple (ordinary) welded joints that are used as planar or multi-planar designs are tubular members without overlap of the brace tubes and without any stiffeners or reinforcements [5]. Figure 3.6 shows some typical planar and multi-planar joint types.

B) Overlapping joints: An overlapping joint is defined based on its geometry and its force transfer. These joints are joined together at their connection with the chord. Therefore, the loads are transferred between the braces through their common weld [5].

C) Complex joints: Complex joints are the joints that have internal/external stiffeners [5].

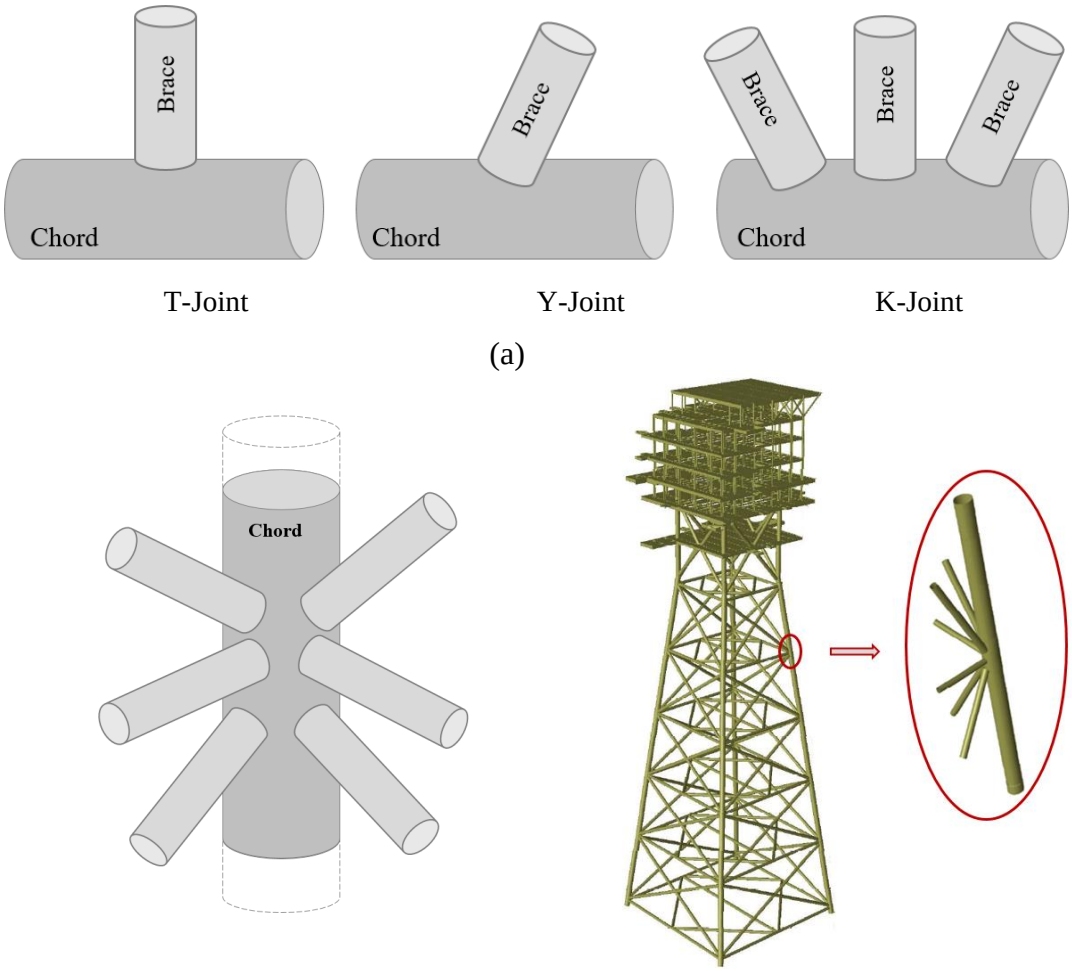

Figure 3.6. Simple welded joints, (a) planar joints, (b) a multi-planar joint, (c) offshore jacket platform

The non-uniform distribution of stress occurs both on the tubular joint surface and also through the joint thickness. Non-uniform stress distribution leads to the existence of stress concentrations, mostly along with the chord and brace weld toes [3]. These stress concentrations cause the fatigue cracks to originate and propagate. For the design and assessment of structural components, stress analysis is carried out to determine both the location and magnitude of these critical stresses.

The location of the most critical hot spots is usually unknown in advance. Therefore, several points (usually eight points) around the circumference of the tubular sections are checked for fatigue, both on the chord and brace sides of the weld. For each point, the magnitude of the critical stress is specified. Figure 3.7 shows these circumferential points for a tubular joint.

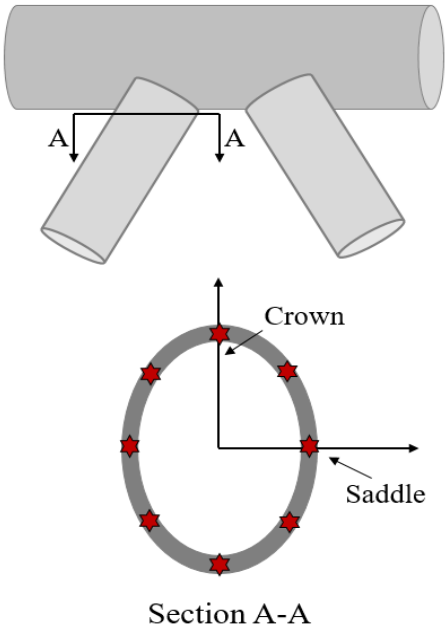

Figure 3.7. Illustration of fatigue check points

3.3.2 Stress Definition in Welded Connections

The presence of the weld at the complicated geometry of tubular joints causes major changes in the stress field in the brace and chord members. In fatigue crack growth analysis, critical stresses have to be determined for each joint. There are three main sources of stress in tubular welded joints [3]:

1) Nominal stresses: These stresses occur in the tubular members due to the members behaving as beam and column elements.

2) Geometric stresses: These stresses occur due to the deformation of the brace and chord walls at the connection. The difference in axial stiffness of the brace and bending stiffness of the chord wall, which varies along the intersection, causes major distortions of the stress field. The magnitude and distribution of these stresses are influenced by the overall geometry of the joint.

3) Notch stresses: The stresses which happen from the geometric discontinuity of the tube walls introduced by an abrupt change in the section at the weld toe. These stresses are also commonly referred to as local stresses and are a function of weld size and geometry [3].

Unlike nominal and geometric stresses, notch stresses are not propagated far through the wall thickness and, therefore, the resulting stress field is highly localised [3]. Due to the complexity and the variety of joint geometries used in the construction of offshore structures, the weld toe geometry (i.e. the weld toe radius and angle) cannot be made identical for each joint configuration [3].

Due to this difficulty in the determination of the notch stresses, a characteristic stress range is used for the fatigue analysis [3]. This characteristic stress range is known as the hot spot stress range [3].

3.3.3 Definition of Hot Spot Stress and Stress Concentration Factors

The Hot Spot Stress (HSS) is the most influential factor to control the fatigue strength of tubular joints [5]. HSS is the stress at the weld toe calculated by linear extrapolation to the weld toe of the geometric stresses [3]. It is noted that in the S-N method, the hot spot stress excludes the contribution to the stress concentration caused by the notch effect of the weld geometry [5]. Figure 3.8 illustrates the definition of hot spot stress.

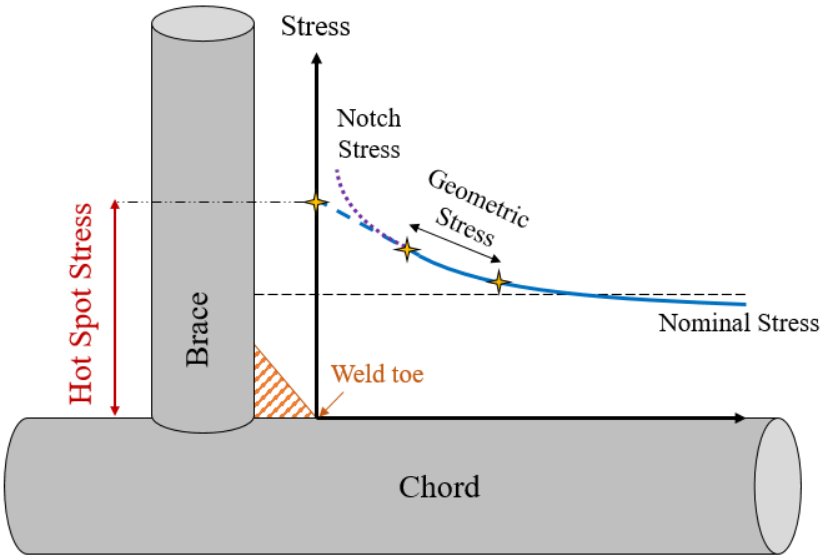

Figure 3.8. Stress distribution in chord wall

The hot spot stress definition should be based on extrapolation from a point located 0.25T from the weld toe on the chord side, and 0.25t on the brace side where T and t are the chord and brace thickness, respectively [5]. Furthermore, this distance should not be less than 4 mm [5].

In welded joints, two different hot spots are found for the brace and the chord side. The maximum stress value may be on the chord side or brace side depending on the design and geometry of the joint [5]. The hot spot stresses must be calculated individually for the chord and brace.

The stress concentration factor (SCF) is defined as the ratio of the hot spot stress to the nominal stress in the brace as [5]:

$$SCF = \frac{\sigma_{HSS}}{\sigma_N} \tag{3-10}$$

where σ_N is the nominal stress and σ_{HSS} is the hot spot stress in the brace.

Due to the complexity of the joint configurations, different guidelines provide different values for SCFs. The DNV document [23] states that stress concentration factors may be obtained from relevant tests or analyses. This code also requires the SCF not to be less than 2.5 [23].

Department of Energy Guidance [24] defines the hot spot stress as "The greatest value around the brace/chord intersection of the extrapolation to the weld toe of the geometric stress distribution near the weld toe. This hot-spot stress incorporates the overall effects of joint geometry but omits the stress concentrating influence of the weld itself which results in a local stress distribution". This definition of hot spot stress is now accepted as an offshore standard for stress analysis of offshore tubular joints.

The American Petroleum Institute [25] defines hot spot stress as "the stress in the immediate vicinity of a structural discontinuity". This code recommends the use of the finite element analysis (FEA) method to obtain hot spot stress. In general, the hot-spot stress incorporates the effects of the overall geometry but omits the stress concentrating influence of the weld itself which results in a local stress concentration.

Accurate estimation of the SCF and hot spot stresses are required to ensure adequate fatigue strength. The sensitivity of the fatigue strength to the values of the SCF is illustrated that an underestimation of 18% of the value of the SCF may cause a 100% overestimation of the fatigue life prediction [5].

3.3.4 Methods of Stress Analysis

Hot spot stress at the intersection of welded tubular joints governs fatigue strength of offshore structures [3]. Therefore, the determination of this value is a crucial step during the fatigue assessment of jacket platforms.

Due to the complexity of joint shapes and the shell behaviour of tubular joints, stress analysis of tubular welded joint intersections is difficult. A wide range of techniques has been developed and employed in assessing offshore structures. The methods vary in their degree of accuracy in modelling different geometries and loading cases [3].

Several methods have been used over the years for the analysis of stresses in welded joints. The first attempts were performed to analyse tubular joints using theoretical methods for stresses [26]. However, the determination of stresses in tubular welded joints is difficult through the use of theoretical methods. As a result, the stress analysis is usually performed by using:

- Finite element methods;
- Experimental measurements;
- Parametric equations.

3.3.4.1 Finite Element Methods

Stress analysis with the finite element methods (FEM) is the most accurate approach to determine the stress distribution and hot spot stress in tubular joints [3]. However, FEM analyses are more expensive in comparison with other methods.

3.3.4.2 Experimental Methods

Most of the early information on the performance of tubular joints and tubular joint stress behaviour was obtained by experimental measurements on steel models [3]. The increased offshore activity in the North Sea in the 1970s lead to an increased need to predict stresses in tubular joints more accurately, and different approaches [3] were being used to determine stresses in tubular welded joints using experimental methods. Experimental methods rely on the measurement of strain and hence stress concentration factors on scaled or full-scale models [3]. Elliot et al. [27] studied a range of tubular joint geometries and obtained detailed information on the distribution

of stresses on the surface and also through the chord and brace walls near the intersection.

Experimental methods on steel models normally give accurate results. Therefore, results obtained using this technique are used as a benchmark for assessing the accuracy of other methods. However, it is a very time-consuming and expensive method because extensive strain gauging is required to give detailed information on the stress distribution in the region of interest [3]. In addition, high-capacity loading machines are required to provide measurable strains in full-scale specimens [3].

Fatigue tests on large-scale tubular welded joints have been performed, for many years, to characterize the fatigue behaviour of steels used offshore. Although conducting these tests can be very expensive, crack growth behaviour in tubular welded joints is complex and cannot be reproduced by conducting tests on simple welded specimens.

3.3.4.3 Parametric Equations

Based on several independent studies, a few sets of parametric equations have been published that have varying capabilities and degrees of accuracy in analysing various joint geometries.

Parametric equations are those equations that are available for different joint types (e.g. Y-joint, T-joint, etc.). These equations estimate the SCF values based on non-dimensional parameters of the joint geometry. These non-dimensional parameters are:

$$\beta = \frac{d}{D} \qquad \gamma = \frac{D}{2T} \qquad \tau = \frac{t}{T} \tag{3-11}$$

where:

- d: Brace diameter
- D: Chord diameter
- t: Brace thickness
- T: Chord thickness
- θ: Angle between brace and chord

There are several parametric equations such as the equations of Kuang et al. [28] and Efthymiou equations [29]. For example, the SCF value for a simple Y-joint under in-plane bending moment is estimated by using the Efthymiou equation as [29]:

$$SCF = 1.45 \times \beta \times \tau^{0.85} \times \gamma^{(1-0.68\beta)} \times (\sin\theta)^{0.7} \quad (3\text{-}12)$$

Parametric equations provide a suitable analysis route for obtaining SCFs. However, available recommended equations are only suitable for simple planar joints, and FEA may be required for more complicated engineering structures. Each set of parametric equations is limited in application in one of three ways [3]:

- Restrictions in the types of joint geometry,
- Restrictions on parametric validity range,
- Restrictions on the loading configuration are covered by any set of parametric equations.

Different parametric equations will yield results that vary in accuracy, depending on the joint geometry and the validity range. However, consistency in the predicted results is also important. In comparison with other parametric equations, Efthymiou equations have considerable advantages in consistency and coverage [3]. Efthymiou equations also provided a better fit to the SCF database examined when compared to other equations. The Efthymiou equations are recommended by different standards such as API [25].

3.4 Fatigue Analysis: The S-N Approach

3.4.1 Basics

The S-N approach is traditionally used during the design of offshore welded tubular joints and connections [5]. As the design stage assumes no initial crack, the estimated fatigue damage based on the S-N approach is more consistent than the fracture mechanics approach [19]. In this approach, the fatigue life of a tubular joint is obtained based on a single parameter, i.e. the hot spot stress.

In the early 1970s, American Petroleum Institute provided the first guidance on the design of tubular joints against fatigue using S-N curves [3]. The same data used in producing the API curves were also the basis of the curves in BS 6235 [30], and DNV rules [31]. Following the increasing availability of experimental data, design codes have been revised and the guidance on fatigue design has been modified, based on available data.

The hot spot stress range along the chord/brace intersection is obtained by using Eq. (3-10). The SCF values can be obtained through FEM, experimental tests, or parametric formulas. As it was mentioned in Section 3.3.1, the fatigue life is usually checked at 8 points along the brace/chord intersection. For each point, the stresses due to the load cases (i.e. axial load, IPB, and OPB) are superimposed and the maximum HSS is selected for that specific joint [5].

Having provided the HSS range, the number of allowable cycles (N) corresponding to the hot spot stress range (S) can be obtained by using the relevant S-N curve for different structural details. Moreover, for the prediction of fatigue life of tubular joints, Miner's rule with linear cumulative damage summation is used [5].

The S-N curves are based on a statistical analysis of experimental data. The data are presented as linear relations between $log_{10}(\sigma)$ and $log_{10}(N)$ as [19]:

$$Log_{10}(N) = Log_{10}(K) - m \times Log_{10}(\sigma); \quad if \sigma > \sigma_0 \tag{3-13}$$

Where N represents the number of cycles to failure for stress range, σ, K is a constant parameter in the S-N curve, m represents the inverse slope of the S-N curve and σ_0 is the endurance limit. The stress range levels below the endurance limit do not contribute to fatigue damage. Figure 3.9 shows a schematic S-N curve.

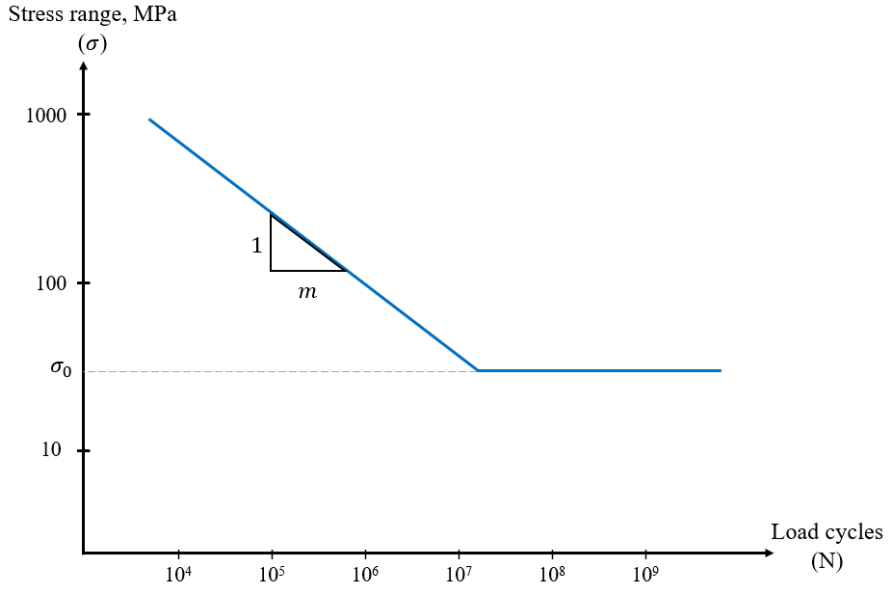

Figure 3.9. A schematic S-N curve

The numerical values for the S-N curves are summarised in several guidelines such as in DNV [23], API [25], ISO [32], etc. Figure 3.10 shows the suggested S-N curve by API for the joints in air and joints in seawater with cathodic protection [25].

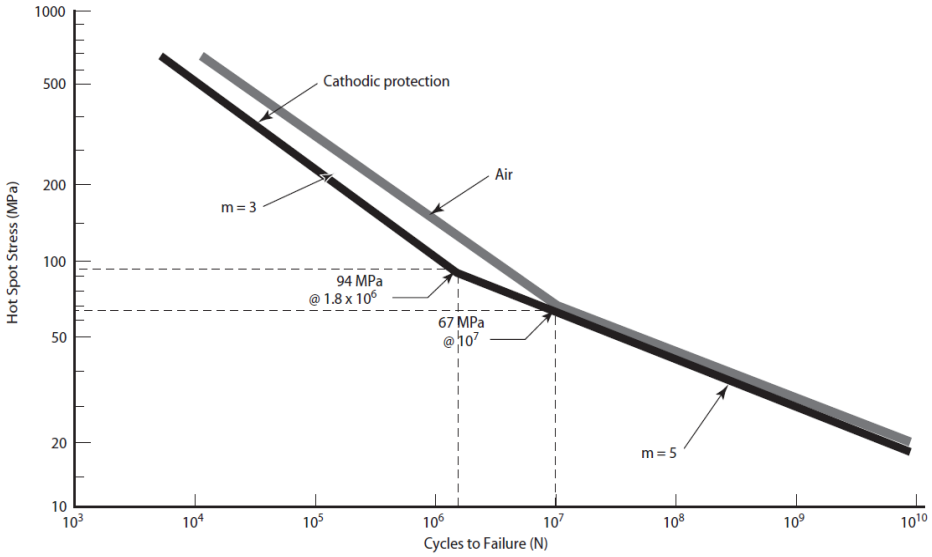

Figure 3.10. The S-N curve for a tubular joint with a thickness of 16mm (API [25])

Table 3.1 shows the value of the basic design S-N curve provided by API for a welded tubular joint [25].

Table 3.1. Values of basic design S-N curve [25]

Environment	$Log_{10}(K)$	m	N
In air	12.48	3	$N < 10^7$
	16.13	5	$N \geq 10^7$
In seawater (with cathodic protection)	12.17	3	$N < 1.8 \times 10^6$
	16.12	5	$N \geq 1.8 \times 10^6$

It is noted that in the S-N method, the number of fatigue cycles to failure is considered as the number of cycles that corresponds to the first through-wall cracking [5].

Some important factors should be taken into consideration when using the S-N curves, such as thickness effects, cathodic protection, corrosion fatigue, and variable amplitude fatigue (See [3] for more details).

3.4.2 Fatigue Life Calculation

In the S-N approach, the fatigue damage is estimated by using Miner's damage summation. Miner's rule assumes that every stress cycle causes some fatigue damage and the damages caused by various stress cycles are linearly added up together as [5]:

$$D = \sum_{i=1}^{m} \frac{n_i}{N_i} \tag{3-14}$$

where the cumulative damage, D, is determined based on the number of cycles (n_i) over N_i which is the number of cycles to failure at the stress range (corresponding with each sea state) according to the S-N curve. In Eq.(3-14) Subscript i indicates the number of sea state and m is the total number of sea states.

The Miner-Palmgren equation assumes that the failure occurs at a damage ratio of 1. However, the acceptable amount for D is usually selected between 0.5 and 1.0 [5].

3.5 Fatigue Analysis-The Fracture Mechanics Approach

The S-N approach is widely used to design welded tubular joints of offshore structures. Design standards such as API RP-2A [25] provide guidelines for fatigue analysis of offshore structures using this method. One of the most significant shortcomings of this method is that it cannot consider the changes in crack size during fatigue life and hence it cannot be used in assessing the structural integrity of cracked tubular joints in service [3]. Since the S-N approach cannot mathematically predict the changes in crack size during fatigue life, it cannot incorporate the results of any in-service inspection of the structure [1].

On the other hand, the fracture mechanics approach (FM) can relate the increase of crack size to the number of fatigue stress cycles, and therefore it can be used to quantify the fatigue crack growth process [33]. FM approach is widely used in the fatigue analysis of the tubular joints in offshore platforms. The FM approach can be used during the operational stage of a structure, to make important decisions on inspection scheduling and repair strategies [3].

Regarding fatigue damage, the inspection results include information such as observed crack size which can be incorporated to update the fatigue reliability. This update is

convenient if the fatigue model is based on the FM approach which considers the physical deterioration such as fatigue crack growth [34].

Fracture mechanics (FM) analysis is the most powerful and useful tool available for solving fatigue crack problems. It is a simulation with crack growth models for mechanical evaluation of the strengths of cracked bodies or the behaviour of fatigue cracks. The use of FM in the probabilistic analysis of structural components subjected to fatigue loading is increasing, in the offshore oil and gas industry [3].

In the FM approach, some models (e.g. average stress model [35], two-phase model [2], and modified average stress model [36]) are developed to predict the fatigue crack growth in welded tubular joints, subjected to service loading. These models are based on results obtained from finite element analysis and also include empirical results. The accuracy of these models in predicting fatigue crack growth is assessed by comparing the predicted results (obtained from these models) with experimental results [3]. In general, the existing FM models rely on using the overall equivalent stress range (for variable amplitude loading) together with a suitable crack growth law.

In welded structures, fatigue cracks almost always start at a weld defect. Once a crack is initiated, it grows slowly as the stress cycles are repeated. It was mentioned that in offshore structures the cyclic stress variations are primarily caused by waves loading. When the crack size becomes critical, an unstable fracture occurs [5]. Therefore, the fatigue fracture includes three main stages [5]:

- Crack initiation
- Crack propagation (crack growth)
- Unstable fracture

In welded joints, the presence of defects such as slag inclusions, porosity, undercuts, lack of fusion, etc. is unavoidable [7]. Since there are some defects from the manufacturing stage in the welded joints, the crack propagation represents a substantial percentage of the total fatigue life of welded joints. In tubular joints of offshore structures, the crack growth period accounts for around 90 percent of the fatigue life. The crack growth depends on the stress conditions at the crack tip. Hence, fatigue is

governed by geometry, especially any change in the geometry which introduces a concentration of the stress flow [5].

FM methods can be divided into two general categories, namely linear elastic fracture mechanics (LEFM) and elastic-plastic fracture mechanics (EPFM). Only LEFM is considered in this study which is briefly denoted as FM.

3.5.1 Factors Affecting Fatigue Behaviour

Several factors have effects on the fatigue behaviour of an element. These factors can be represented into two groups as [7]:

- Loading: Fatigue is a cumulative, time-dependent phenomenon. Each cycle of load will cause some damage. Therefore, the magnitude of load cycles has a great effect on the fatigue performance of an element. As mentioned before, for offshore structures the main fatigue loading is due to ocean waves.
- Weld Defects: Fatigue cracks in tubular joints originate from weld defects such as inclusions, undercuts, lack of fusion. The existence of these defects is unavoidable. Those defects which are present in the high-stress concentration regions may develop into fatigue cracks.

3.5.2 Crack Growth Estimation

Several relations for predicting the crack growth rate have been proposed. These relations are divided into two main categories; Theoretical relations and empirical laws [5]. Many attempts have been made to develop a law of fatigue crack growth theoretically, but none of the proposed expressions has general applicability. On the other hand, the empirical expressions (which are fitted to available data) are valid to the extent that the applications are represented in the data [5]. The scatter in the actual data indicates that the empirical expressions may have satisfactory results in a limited region or for a limited set of data. Therefore, those expressions can be utilised for that specific region (or set of data) [5].

Figure 3.11 shows a typical crack growth rate curve. This curve shows the relation of the crack growth rate versus the stress intensity factor on a logarithmic scale.

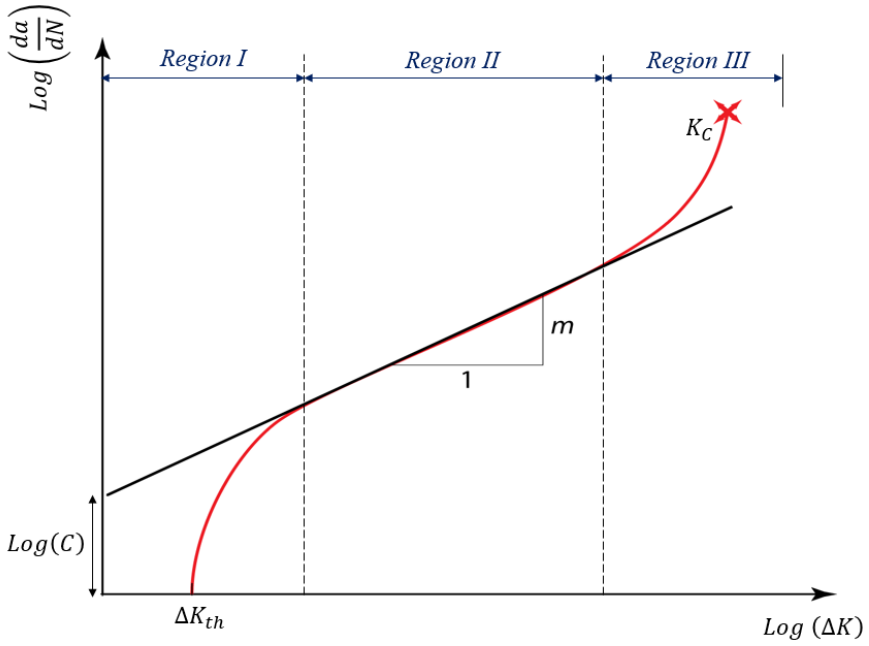

Figure 3.11. A schematic crack growth rate curve

In Figure 3.11:

- da/dN: Crack growth rate, i.e. crack growth per cycle
- ΔK: Stress intensity factor (SIF) range
- ΔK_{th}: Threshold value of ΔK
- K_c: Critical value of K, which fracture happens
- C, m: Crack growth parameters

The aforementioned curve is characterised by three different regions. In each region, the fatigue crack growth rate shows different dependencies on the stress intensity factor range [3]. These three regions are:

- Region I (threshold region):

  This region is characterised by a rapid decrease in crack growth rate with decreasing the SIF. Behaviour in this region is dependent on microstructural features [3]. Parameter ΔK_{th} is a threshold stress intensity range below which the crack will not grow. In this research, the threshold stress intensity is assumed to equal zero. The effect of the value of threshold stress intensity upon calculated crack size is very small [37].

- Region II (intermediate region):

  The majority of fatigue life (up to 80 percent) of tubular joints in offshore structures can be considered to occur in this region [3]. This region is characterised by stable crack growth and can be described by a linear equation (in a logarithmic scale).

  The most common relationship in this region, in mathematical terms, is the Paris equation which describes the crack growth rate as introduced by Newman and Raju as [38]:

$$\frac{da}{dN} = C(\Delta K)^m \tag{3-15}$$

  where C and m are the crack growth parameters which are constants for a particular material and particular testing conditions and a is the crack size [5].

  In general, the Paris equation yields conservative results [5]. As can be seen from Figure 3.11, the Paris law overestimates the crack growth rate in region I and underestimates the crack growth rate in region III.

- Region III (failure region):

  The rate of crack propagation in this region increases rapidly until fracture. This region corresponds to the unstable and rapid crack growth and is characterised by the material's fracture toughness [3].

3.5.3 Stress Intensity Factor

The fracture mechanics approach aims to define the local conditions of stress around a crack, in terms of the global parameters of loads, geometry, etc. [5]. Different approaches have been utilised in the analysis of fracture problems. These approaches introduce various fracture mechanics parameters, e.g. energy release rate (G), J-integral, crack opening displacement (COD), and stress intensity factor (K). The most popular among these parameters is the stress intensity factor [5].

A fundamental principle of fracture mechanics is that the stress field ahead of a crack can be characterised in terms of this single parameter; K [5].

It should be noted that the concept of hot spot stress is inapplicable in the analysis of stresses near the crack tip. This is due to the existence of a stress singularity. Therefore, fracture mechanics rely on analysing the stress field in the vicinity of the crack tip, rather than the infinite stress due to the stress singularity at the crack tip. The nature of the stress field depends on the mode of crack extension, loading, and deformation of crack faces [3].

There are three main modes, including Mode I (opening mode), Mode II (sliding mode), and Mode III (tearing mode). Cracks are extended or deformed in one or a combination of these modes [3]. These modes are shown schematically in Figure 3.12.

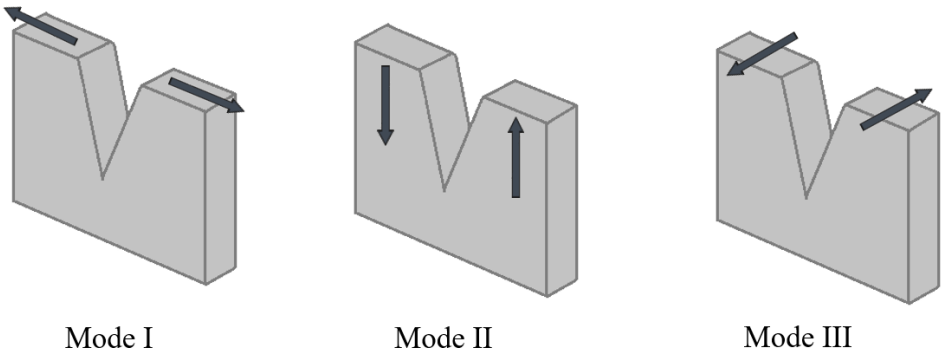

Figure 3.12. Different modes of a crack deformation

In general, Mode I is the dominant mode for most practical applications and two other modes are less significant with negligible contributions to crack growth [3].

The stress intensity factor (SIF) is the parameter adopted to describe the elastic stress field in a cracked body around the crack tip for any given mode of crack extension. In general, SIF is a function of applied stress, the size and shape of the crack, and the geometry of the cracked component [3]. Therefore, finding an accurate solution for the stress intensity factor is a difficult task.

A large number of studies have been performed to obtain the value of SIF for various amounts of load and crack shapes. In general, for mode I, the SIF for a centre crack of length $2a$, in an infinite plate subjected to a uniform stress field (σ) is given by:

$$K_I = \sigma\sqrt{\pi a} \tag{3-16}$$

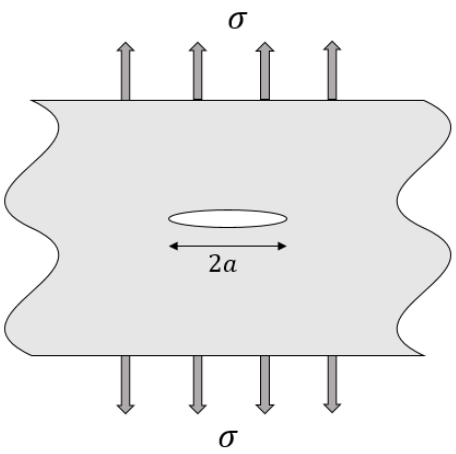

Figure 3.13. A crack of the length of $2a$ in an infinite plate under uniform stress

It is noted that the SIF in Eq. (3-16) is in the absence of all boundaries [3]. However, cracks in welded tubular joints are usually in a complex stress field that is different from the uniform stress field in an infinite plate. Therefore, for surface cracks in engineering structures, various correction factors have to be used to account for boundary effects, crack shape, and loading geometry [3]. SIF for mode I in the general case is given by:

$$K_I = Y \times \sigma\sqrt{\pi a} \tag{3-17}$$

where Y is the overall correction function which is also denoted as a geometry function [3].

The correction factor can be obtained based on experimental results or empirical solutions. Different analysis methods have been proposed to determine the correction factor for cracked tubular welded joints [3]. The correction function takes into account several aspects such as crack shape, a free front surface, finite plate width, a non-uniform stress field, etc. [5].

3.5.4 Estimation of SIF for Tubular Joints

The proposed SIF solutions in the literature are usually for plates. Therefore, they cannot be applied directly to tubular welded joints which have different boundary conditions. However, these solutions can still be used to provide estimates of stress intensity factors for the tubular joints by applying the appropriate boundary condition correction functions [3].

The calculation of stress intensity factors for the cracks in tubular joints is a difficult task due to the complex geometry and the stress distribution. Existing analytical and experimental data of the geometry function for tubular joints includes a significant scatter. The main reason is that there is no analytical solution available for the stress intensity factor for a semi-elliptical surface crack in tubular joints [1].

Several studies have been performed to use experimental solutions to calculate SIFs for tubular joints [39]. However, these solutions are based on several assumptions and are valid for specific loading joint types.

Dover and Dharmavasan [35] presented an empirical method to compute SIF in T-joint and Y-joint. The method was derived by calibrating the corresponding SIF range with the experimentally measured crack growth rate based on Paris equation for a joint with known fatigue material properties. Lee and Bowness [40] presented a simple method to estimate SIF for semi-elliptical weld toe cracks in tubular joints by aggregating the results of a large number of finite element analyses on un-cracked and cracked tubular joints. Several polynomial relations have been suggested for the geometry function in different tubular joints under axial load, IPB, and OPB based on the experimental data in [1].

3.5.5 Fatigue Life Prediction

In the FM approach, the average increment in crack growth during a load cycle is related to the range of the stress intensity factor. To predict the fatigue crack growth of a surface crack, in this study it is assumed that the crack growth per stress cycle follows the Paris equation.

Fatigue life assessment based on FM involves calculating the fatigue crack size after a certain number of fatigue cycles. The stress intensity factor range is a parameter that expresses the effect of load range on the crack. It describes the stress field associated with the cracked body at the crack tip. The stress intensity factor range is obtained as [5]:

$$\Delta K = K_{max} - K_{min} \tag{3-18}$$

It was mentioned that Mode I is the dominant mode for most practical applications and the contribution of the other two modes can be ignored [3]. Therefore, Eq. (3-17) can be written as:

$$K = K_I = Y \times \sigma\sqrt{\pi a} \tag{3-19}$$

By using Eq. (3-19), Eq. (3-18) can be written as:

$$\Delta K = Y \times (\Delta\sigma)\sqrt{\pi a} \tag{3-20}$$

By implementing a suitable crack growth law such as the Paris equation, the number of fatigue cycles required to extend a fatigue crack from an initial size (a_0) to any size (a_f) can be calculated as:

$$\begin{aligned} \frac{da}{dN} &= C(\Delta K)^m \\ \frac{da}{dN} &= C\left(Y \times (\Delta\sigma)\sqrt{\pi a}\right)^m \\ dN &= \frac{da}{C\left(Y \times (\Delta\sigma)\sqrt{\pi a}\right)^m} \\ N &= \int_{a_0}^{a_f} \frac{da}{C\left(Y \times \sqrt{\pi a}\right)^m \times (\Delta\sigma)^m} \end{aligned} \tag{3-21}$$

Since the stress range is not constant in different load cycles; ($\Delta\sigma$) can be replaced by $E[\Delta\sigma]$, which is the expected value of the stress range [41].

In general, for predicting the fatigue life in the FM approach, the following steps will be required:

- Selection of a suitable crack growth law;
- Use of suitable crack growth material constants (C and m);
- Determination of stress ranges;
- Estimation of correction factor;
- Determination of stress intensity factor range;
- Integration of crack growth rate for the applied loads.

3.5.6 Unstable Fracture

An unstable fracture occurs when a critical combination of tensile load and crack length is attained [5]. The unstable fracture may represent the end of the fatigue life of a component. This section focuses on the main failure modes of unstable fracture and simple methods for calculating the critical combinations of load and crack length. Figure 3.14 shows the load and displacement definition.

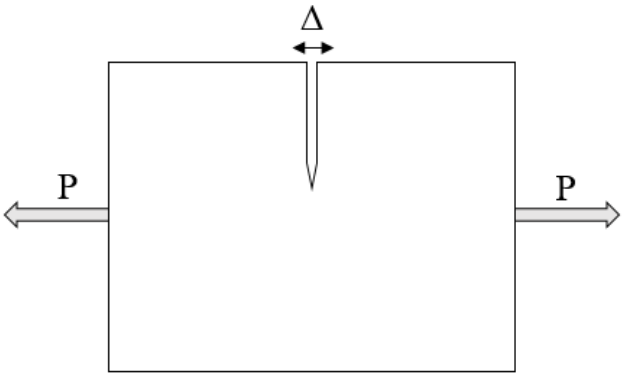

Figure 3.14. Definition of load (P) and displacement (Δ)

There are three possible modes of fracture [5]:

- Brittle fracture:

  The structure behaves in a linear-elastic manner right up to the point of fracture. In other words, the macroscopic behaviour of the body is brittle. In such cases, the microscopic mode of fracture is usually also brittle and is known as cleavage fracture [5]. Figure 3.15 shows the brittle fracture behaviour for a metal.

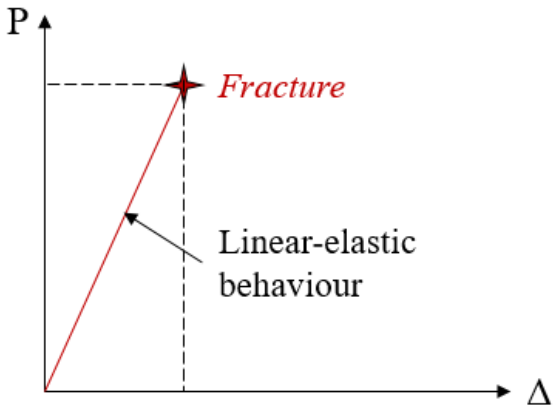

Figure 3.15. Linear-elastic behaviour for a brittle fracture

- Elastic-plastic behaviour:

  In this case, the structure shows some degree of macroscopic plasticity before fracture. However, the final fracture, which may be preceded by a small amount of ductile crack growth, is by cleavage, i.e. it is microscopically brittle [5]. Figure 3.16 shows the elastic-plastic behaviour.

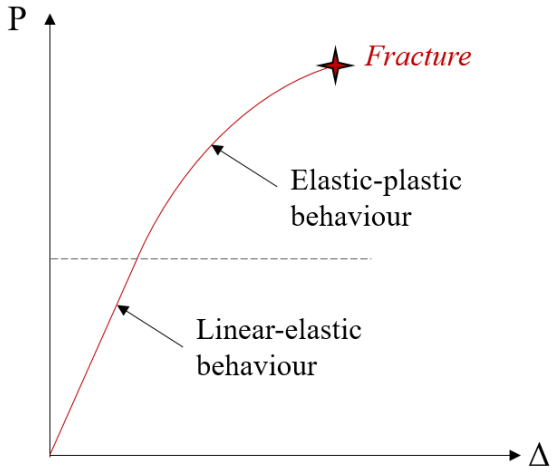

Figure 3.16. Elastic-plastic behaviour

- Ductile fracture (plastic collapse):

  In this case, the fracture is ductile behaviour. As the load increases the crack extends stably, until a point is reached when the rate of reduction of load-bearing capacity due to crack growth is equal to the rate of work hardening. At this point, the load reaches a maximum value. If the load is not dropped, the system will become unstable at this point, and the structure will fail by a combination of unstable fracture and plastic collapse. Figure 3.17 shows the plastic behaviour.

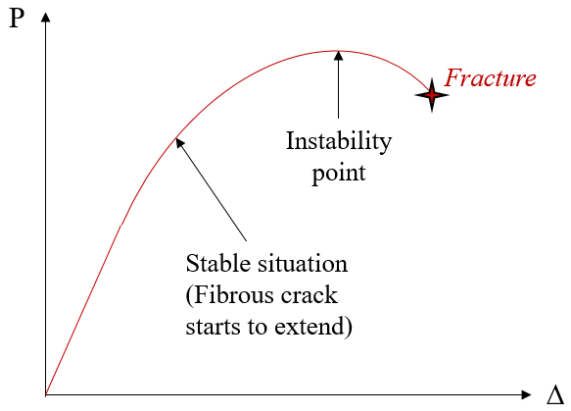

Figure 3.17. Plastic collapse behaviour

3.5.7 Fracture Mechanics Usage in Unstable Fracture

The stress intensity factor (K) for a crack in a loaded body is a function of the stresses acting on the body, the size of the crack, and the geometry of the crack and the body. If the structure behaves in a brittle fracture or a linear-elastic fashion before fracture, the fracture will initiate from a pre-existing crack or sharp defect when the stress intensity factor reaches a critical value [5].

However, if the structure shows a significant amount of plasticity, the stress intensity factor approach becomes invalid and an elastic-plastic fracture mechanics parameter must be used to describe the crack tip stresses and strains. The parameters most widely used are the J-integral and the crack tip opening displacement (CTOD). There are several methods for obtaining the J-integral and CTOD. However, the calculation of J-integral and CTOD will not be discussed in this section. For more detail see [5], [42] and [43].

3.5.7.1 Failure Assessment Diagram

The presence of a crack will reduce the plastic collapse load of the structure by reducing the net cross-sectional area. For long cracks in rather tough materials, a plastic collapse will be the predominant failure mode, and this fact should be allowed for in defect assessment.

The failure assessment diagram (FAD) combines the criteria for brittle fracture and plastic collapse into a single procedure [5]. To evaluate if a crack may cause structural failure, the FAD method can be used.

Two parameters are considered in the FAD procedure; fracture parameter (K_r) and plastic collapse parameter (S_r) which are defined as [44]:

$$K_r = \frac{K_I}{K_{Ic}} \tag{3-22}$$

$$S_r = \frac{\sigma_{app}}{\sigma_{col}} \tag{3-23}$$

where

- K_I: Stress intensity factor (mode I)
- K_{Ic}: Fracture toughness

- σ_{app}: Applied stress (or load)
- σ_{col}: Collapse stress (or load)

The FAD establishes the relationship between brittle fracture (by fracture parameter; K_r) with local plasticity (plastic collapse parameter; S_r). The plastic collapse could be in the form of global or local collapse. The fracture parameter (K_r) is an indicator of fracture under linear elastic conditions, while the plastic collapse parameter (S_r) could be defined as the ratio of applied stress to the collapse stress, where collapse stress refers to the remote stress that will cause the spread of plasticity [45].

A simple failure assessment diagram has a semi-empirical basis [5]. All points inside the FAD are considered safe; points outside of the diagram are unsafe [46]. Figure 3.18 shows a simple FAD and safe/unsafe areas.

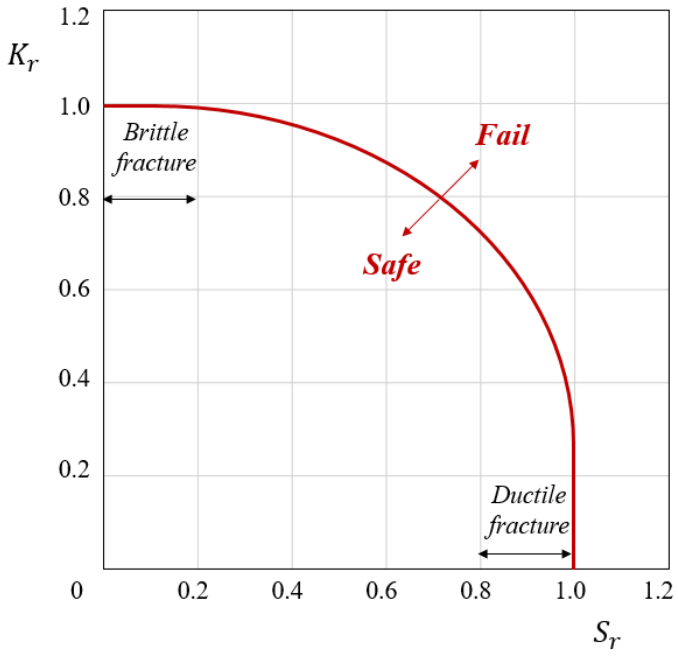

Figure 3.18. A typical failure assessment diagram

As Figure 3.18 shows for the high toughness material, the structure fails by collapse when S_r is close to 1.0. Whereas, for a brittle material failure occurs when K_r is close to 1.0. In intermediate cases, plastic collapse and fracture interact, and both K_r and S_r are less than 1.0 at failure [46].

To assess a particular flaw in a structure, one must determine the toughness ratio as well as the stress ratio. The stress ratio for the component can be defined as the ratio of the applied stress to the plastic collapse stress. Alternatively, the applied Sr can be defined in terms of axial forces or moments. If the assessment point with coordinates (K_r,S_r) falls inside of the FAD curve, the analysis predicts that the component is safe. Otherwise, if it lies outside the failure curve the structure will be unsafe [46].

The FAD typically is given by the equation of a curve as $K_r = f(S_r)$. For example, the failure curve can be expressed mathematically by [46]:

$$K_r = \sqrt{\frac{8}{\pi^2 \times S_r^2} \times \ln\left(\sec\left[\frac{\pi}{2} \times S_r\right]\right)} \tag{3-24}$$

where sec represents secant function (i.e. 1 divided by the cosine).

More detailed formulas for the failure curve are provided by BS7910:2013 [47]. BS7910 defines three different options for FAD. The simplest FAD in the BS7910:2013 does not require stress-strain data. The more complicated options (options 2 and 3) require more inputs in terms of material and stress analysis [47]. For example, option 2 requires detailed stress-strain data, especially at strains below 1% [47]. Option 3 requires elastic and elastic-plastic analysis to determine J-integral values [47].

3.6 Previous Studies on Fatigue Reliability Analysis of Jacket Structures

In a probabilistic approach, fatigue lives can be expressed as distributed parameters rather than as single nominal values, and the probability of failure of any joint before any particular time can then be estimated. Considerable work was carried out on probabilistic approaches to fatigue reliability analysis of offshore jacket platforms. In these studies, the following steps were taken into account:

- Considering the uncertainties affecting the fatigue capacity of the tubular joints
- Assigning the different distributions to the uncertain parameters
- Calculation of the probability of failure using different reliability techniques (i.e. FORM, Monte-Carlo simulation).

Aghakouchak and Stiemer [1] presented a reliability-based LEFM (linear elastic fracture mechanics) approach for fatigue analysis of structural elements in jacket platforms. They developed a method that can be used for the reliability assessment of existing structures through the incorporation of the results of in-service inspections. They considered several uncertain parameters; including initial crack size, crack growth parameters, and uncertainties in the estimation of the stress range and stress intensity factor. They also applied their methodology to a sample tubular joint in an offshore structure [1].

Rajasankar et.al [15] presented a reliability-based approach to assessing the structural integrity of offshore tubular joints. The reliability analysis was carried out using the Monte Carlo simulation technique and the first-order reliability method (FORM). The initial crack size, material properties, and loading of the tubular joint were considered as random variables in the reliability calculation. The linear elastic fracture mechanics approach was employed to evaluate the crack growth. The significance of each random variable was also investigated by performing the sensitivity analysis. The sensitivity analysis results showed that the reliability of the joint is significantly influenced by variation in the variables crack growth parameter [15].

Ahmadi et.al [33] derived a fatigue limit state function based on the FM approach and investigated the effects of assigning different values to deterministic variables involved in this limit-state function on the results of reliability analysis. The deterministic variables were the material crack growth parameter (m), and the critical crack size. It was shown that the increase of the bigger material constant (m) leads to decrease in the reliability index. Moreover, the increase of the wall thickness of tubular members increases the reliability index [33]. The effects of stress concentration factors on the reliability of the multi-planar tubular joint were also considered. The numerical simulation was adopted to obtain the SCF distribution in the considered tubular joints. 81 models of multi-planar tubular DKT-joints were generated and the SCF values were obtained by using the FEM software package. Based on the FEM results, a log-normal distribution was obtained with a mean value of 15.86 and COV (coefficient of variation) of 1.05. Therefore, it was concluded that the typical value of SCF for planar joints (which is around 2.5) is not appropriate for the multi-planar tubular joints [33].

Pillai and Prasad [34] described a methodology for the estimation of reliability of fixed offshore structures with respect to fatigue and extreme stress. The failure criteria for fatigue were formulated using the fracture mechanics principle. The total life of the structure was divided into a set of stationary sea states, occurring during storms and described by directional power spectrum. The researchers showed that among the random variables included in the fatigue failure, the material parameter (C) and stress concentration factor has the greatest effect on the probability of fatigue failure [34].

Kirkemo [48] reviewed the applications of probabilistic fracture mechanics to offshore structures. Several uncertainties in loading, initial and critical defect sizes, material parameters, and the uncertainty related to the computation of the stress intensity factor were considered. The failure probabilities based on FORM and obtained the sensitivity factors for each variable were calculated.

Siddiqui and Ahmad [49] considered the uncertainties associated with the parameters for performing the fatigue reliability assessment of the tension leg platforms. They considered two approaches for fatigue damage estimation, the S-N curve approach, and the FM approach. The researchers developed the limit state functions based on those two approaches. To estimate the reliability, they employed FORM and the Monte Carlo simulation technique. They also performed a sensitivity analysis to find out the influence of each random variable on the probability of failure. Based on the sensitivity analysis results, the reliability analysis was very sensitive to the stress range and less sensitive to the geometry function [49].

Karadeniz [50] presented a procedure for modelling the uncertainties in the fatigue analysis of offshore structures regarding the reliability assessment. The uncertainties in the fatigue damage were categorised into two main groups. The first category originated from structural and environmental sources. All uncertainties in structural transfer functions and the uncertainties occurring in the wave loading were considered. The second category of uncertainties was related to the fatigue damage phenomenon (uncertainties related to the damage model). The reliability calculation for a jacket-type structure was performed as a demonstration. It was revealed that the inertia force coefficient of Morison's equation, parameters of the fatigue-damage model, and the

foundation seem to be the most dominant uncertainty sources in the fatigue reliability calculation of jacket type structures [50].

Lin et.al [51] presented a reliability-based approach to assessing the structural integrity of tubular joints with cracks in aging offshore platforms. Two different fatigue failure models were established regarding the crack propagation size and equivalent fatigue strength. The results of two reliability models were compared. It was shown that the reliability index obtained from the crack size model is much lower than that from the equivalent fatigue strength model. The reliability analysis by two different maintenance schedules (equal inspection interval and failure probability threshold) was updated. The results showed that the reliability index of tubular joints could be increased with enough inspection and maintenance measures [51].

Dong et.al [52] predicted the fatigue reliability of welded multi-planar tubular joints of the support structure of a fixed jacket offshore wind turbine in the North Sea. Hot spot stresses at the critical location by summation of the single stress components from axial, IPB (in-plane bending), and OPB (out of plane bending) were derived. The effects of planar and multi-planar braces were also considered. For this purpose, a two-parameter Weibull function was considered to model the long-term statistical distribution of the hot spot stress ranges [52].

It was mentioned that significant work was carried out on fatigue reliability analysis of tubular joints in offshore jacket platforms. Nevertheless, to achieve the aim of this research (improving reliability assessment of offshore structures using Bayesian methods) it is required to develop a probabilistic approach to obtain the fatigue probability of failure.

3.7 Fatigue Reliability Calculation

The tubular joints in jacket platforms are likely to fatigue damage due to high-stress concentration and cyclic wave loading. A fatigue crack starts at the weld toe at the hot spot location and gradually propagates around the intersection and through the tubular wall. Fatigue is a complicated phenomenon. As a result of the idealisations and approximations employed in the analysis process, fatigue analysis will be associated with some degree of uncertainty.

Due to the existence of many uncertainties in the fatigue calculation process, a probabilistic approach for fatigue assessment is a consistent basis for the inclusion of uncertainties. Reliability analysis, which is a probabilistic approach, has been extensively used in the design and assessment of offshore structures to assess the probability of failure. Computation of fatigue reliability is also useful for planning in-service inspection.

Since the FM approach considers the changes in crack size during fatigue life, the fatigue reliability analysis is performed based on this approach. For performing the reliability analysis in the FM approach, the developed crack size can be considered as a measure for the fatigue damage accumulation which is a physical measurable parameter [19]. The degree of accumulated fatigue damage in a joint can then be updated based on the outcome of inspections.

This section shows how the fatigue reliability analysis for a tubular joint in offshore jacket platforms can be performed. For this reason, important uncertainties are represented by random variables based on their probability distributions such as mean values and standard deviations. It is noted that the obtained probability of failure is dependent on the chosen uncertainty modelling [19]. The probability of failure for a component is then defined as the probability that an initial crack grows beyond the critical crack size.

3.7.1 Source of Uncertainties

Fatigue failure is one of the most important issues in offshore platforms. Since the environmental loading and conditions are random and time-dependent, a reliability approach can be employed. Since the reliability analysis depends on the choice of the items of uncertainty and their statistical description, uncertainty modelling becomes an important consideration for offshore structural analysis [50].

There are many uncertainties involved in the fatigue reliability analysis of tubular joints of offshore structures. Figure 3.19 shows different sources of uncertainties in fatigue analysis.

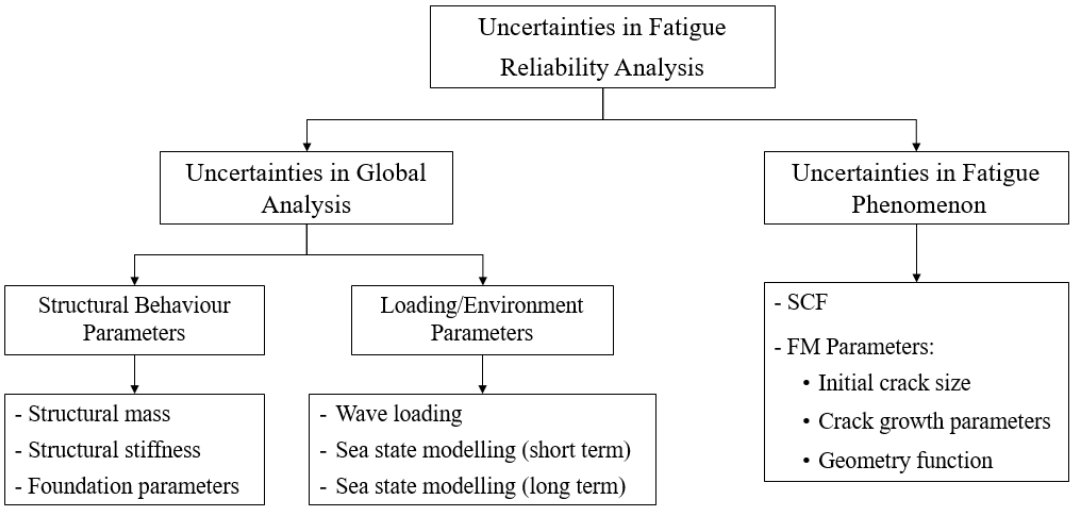

Figure 3.19. Different sources of uncertainties in fatigue analysis

The uncertainties in the fatigue reliability analysis can be classified into two categories:

a) Uncertainties related to the global analysis:

These uncertainties can be further subdivided into two categories:

- Structural behaviour: These uncertainties affect natural frequencies and structural transfer functions. Uncertainties such as:
  - System stiffness: Major uncertainty sources in the system stiffness matrix are joint flexibilities. Several tubular members are connected together at joints of the structure by welding. In theory, these connections are assumed as rigid connections, whereas the actual behaviour of the joints under the wave loading displays some flexibility in the vicinity of connections due to local deformations of members [50].
  - Mass: The mass matrix contains uncertainties due to added masses (structure–water interactions) and the structural mass [50]. Moreover, the live load of the deck during a service life is an uncertain value.
  - Foundation parameters: The other uncertainty source in offshore platforms is the foundation parameters. The soil parameters are introduced by lateral and axial springs with their values are obtained from geotechnical surveys [50].

- Loading and environmental origin: Uncertainties associated with wave loading and the modelling of random waves are considered in this category. Wave loading and the description of the sea state are the major uncertainty sources in this group. The main uncertainties in this category are:
  - Wave loading: The fatigue damage in offshore structures is mainly caused by random wave loads. In general, wave loads on tubular members are calculated using Morison's equation (Eq.(3-9)). Uncertainties in the wave loading arise from the force coefficients (C_D and C_m) and the marine growth thickness.
  - Sea state modelling: Wave conditions are described within a set of stationary short-term sea states. For each short-term sea state, the water level can be assumed to be a stationary Gaussian process with a zero mean. Each sea state is characterised by the sea state parameters, i.e. significant wave height (H_S), Mean zero up-crossing period (T_Z) and the wave spectrum. There is always uncertainty in the estimation of these sea state parameters.
  - Long-term uncertainties: The long-term stress range distribution is defined based on a weighted sum of Rayleigh distributed stress ranges for each short-term condition [19]. In the long term, the fatigue damage is accumulated depending on the probabilities of occurrences of each sea state. For each sea state, the long-term probabilities of the different main wave directions are given with a wave scatter diagram for each direction. A wave scatter diagram defines the occurrence probability for each set of H_S and T_Z values.

b) Uncertainties related to the fatigue phenomenon:

This category of uncertainties is related to the fatigue phenomenon itself and it is not related to the global analysis. There is uncertainty associated with the modelling of the FM-fatigue approach, regarding the initial crack size and the fatigue crack growth material parameters. Moreover, there is uncertainty in the estimation of geometry function.

3.7.2 Predicted Crack Size

It was explained that in the linear elastic fracture mechanics approach, the Paris equation can be used to describe the rate of fatigue crack growth. The stress intensity factor range is obtained by using Eq. (3-20). By substituting this value in Paris equation as in Eq. (3-15), fatigue crack growth for a load cycle becomes:

$$\frac{da}{dN} = C\left(Y \times \sqrt{\pi a}\right)^m \times (\Delta\sigma)^m \tag{3-25}$$

Due to the existence of several sea-state conditions, the platforms are exposed to several loading conditions. Therefore, the stress range in a platform is not constant and it varies for each sea state condition. Therefore, the stress range is replaced with the expected value of the stress range, i.e.:

$$\begin{aligned} \frac{da}{dN} &= C\left(Y \times \sqrt{\pi a}\right)^m \times E[\Delta\sigma^m] \\ \frac{da}{\left(Y \times \sqrt{\pi a}\right)^m} &= C \times E[\Delta\sigma^m] \times dN \end{aligned} \tag{3-26}$$

The relation between crack size and the number of cycles for the propagation of a crack can be obtained by integration of Eq. (3-26) as:

$$\int_{a_0}^{a_t} \frac{da}{\left(Y \times \sqrt{\pi a}\right)^m} = C \times E[\Delta\sigma^m] \times N \tag{3-27}$$

By assuming Y does not change with crack size [51] and by integrating Eq.(3-27) from the initial crack size (a_0), to the crack size at time t (a_t), the crack size value at time t can be obtained as:

$$a_t = \left\{ a_0^{1-\frac{m}{2}} + \left(1 - \frac{m}{2}\right) \times Y^m \times \pi^{\frac{m}{2}} \times C \times E[\Delta\sigma^m] \times N \right\}^{\frac{1}{1-\frac{m}{2}}} \tag{3-28}$$

3.7.3 Limit State Definition

In a deterministic approach for the design of tubular joints against fatigue failure, all the loading parameters are taken at their mean values while the resistance parameters are taken at values corresponding to mean minus two standard deviations [47].

Moreover, the tubular joints are designed in a way that the computed fatigue lives are two to ten times higher than the planned service life of the structure. Due to the

existence of several sources of uncertainty, both in the loading and fatigue resistance parameters, a probabilistic approach to fatigue design is considered appropriate. In this section, the fatigue limit state is presented using a fracture mechanics approach.

To estimate the probability of failure of a component, a failure event should be defined. Failure is usually defined based on the concept of a limit state, which represents a boundary between the safe and unsafe performance of a component [41].

A variety of criteria such as crack size criterion, equivalent fatigue strength criterion, damage criterion, and failure assessment diagram, have been proposed to describe the fatigue failure for the tubular structures with cracks [51]. Here, for the component reliability analysis, the crack size can be considered as the failure criterion which is acceptable for low toughness material [1]. This means that failure occurs, as soon as the crack size is bigger than a critical value. Therefore, the fatigue limit state function is described:

$$g = a_c - a_t \tag{3-29}$$

where a_c is critical crack size. The critical crack size could be based on serviceability criteria (e.g. through the thickness crack or economic repair limits) or ultimate collapse criteria (e.g. unstable fracture) [19]. Critical crack size is usually considered equal to the wall thickness [19].

In Eq.(3-29), a_t is the crack size after N cycles of loading which is a function of the random variables such as initial crack size, fatigue material properties, etc. (Eq.(3-28)).

Laboratory tests have shown that a fatigue crack starts at the weld toe at the hot spot location and gradually propagates around the intersection and through the tubular wall. In the beginning, there may be tiny cracks around the intersection, which usually join and form a semi-elliptical surface crack [1]. When this crack penetrates through the thickness of the tubular wall, a major reduction in joint stiffness is observed. The crack propagation through the thickness is considered as the end of the fatigue life of the joint based on the limit state function provided in Eq.(3-29).

Figure 3.20 shows the crack growth stages in a tubular joint. At stage (I), a fatigue crack starts at the weld toe at the hot spot location. This crack propagates through the thickness of the tubular wall (stage II) which is assumed as the end of fatigue life of

the joint. It is noted that after through-thickness, the joint can still work until real failure (Stage III). However, this stage is not considered in the fatigue life of tubular joints [52].

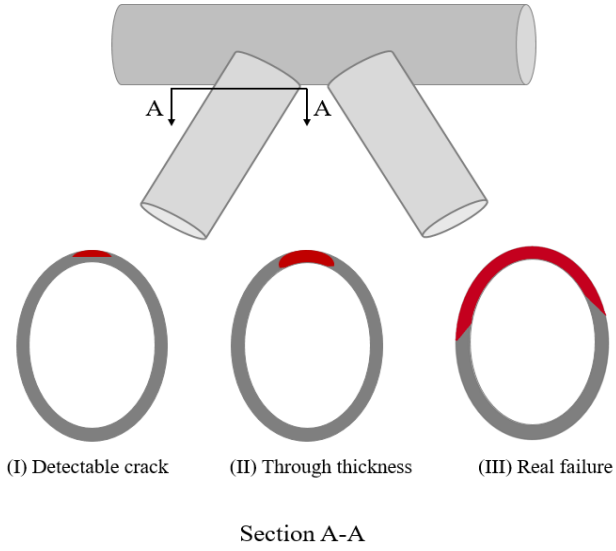

Figure 3.20. Crack propagation stages in a tubular K-joint

By plugging Eq.(3-28) into Eq. (3-29), the fatigue limit state function is written as:

$$g = a_c - \left\{ a_0^{1-\frac{m}{2}} + \left(1 - \frac{m}{2}\right) \times Y^m \times \pi^{\frac{m}{2}} \times C \times E[\Delta\sigma^m] \times N \right\}^{\frac{2}{2-m}} \quad (3\text{-}30)$$

Having obtained the limit state function, the failure probability (the probability that the crack size exceeds a critical size) is defined as:

$$P_f = P(g \leq 0) = \Phi(-\beta) \quad (3\text{-}31)$$

where P_f represents the probability of failure, β is called the reliability index and Φ (.) is the CDF (cumulative distribution function) of the standard normal distribution.

The reliability can be calculated by using the probability of failure as:

$$R = 1 - P_f \quad (3\text{-}32)$$

3.7.4 Reliability Calculation Methods

There are different methods to calculate the reliability and the corresponding probability of failure, such as FORM [9] and Monte Carlo simulation [9]. These methods were explained in Chapter 2 of this study. Both methods have some advantages and disadvantages. For example, although FORM estimates the probability

of failure by approximating the nonlinear limit state function, it provides a measure of the sensitivity of the reliability index to the random variables [6]. Monte Carlo simulation techniques can estimate the accurate probability of failure; however, a large number of iterations is required in this method. Therefore, the reliability analysis is more time-consuming [6].

3.8 Application of the Fatigue Reliability Analysis to a Jacket Platform

3.8.1 Finite Element Model

To demonstrate the fatigue reliability calculation of offshore structures, an example of a jacket offshore platform is considered. The example platform is a four-legged living quarter that is supported by a jacket structure with battered legs. The configuration of the platform is presented in Table 3.2.

Table 3.2. The structural arrangement of the example platform

Item	Description
Platform function	Living quarter platform
Water depth	70 m
No. of Legs	4
Foundation system	- Outside diameter: 91.4 cm - Pile thickness: 2.54 cm - Pile depth: 64m
Soil description	- Clay: 0-18.4 m - Silt: 18.4-31.2 m - Clay: 31.2-56.1 m - Sand: 56.1-66.0 m
Bracing type	X brace
Jacket levels	- Level 1: (+) 3.0 - Level 2: (-) 10.7 - Level 3: (-) 24.4 - Level 4: (-) 38.1 - Level 5: (-) 51.8 - Level 6: (-) 70.0
Leg Spacing	- 15.2m x 15.2m at level 1 - 33.1m x 33.1m at level 6
Material	Carbon Steel Grade S355 (Yield strength 355 MPa)
Mass of the deck	2200 ton
100-year return period wave	- Wave height: 12.2 m - Wave period: 11 sec
Fatigue wave loading	See Section 3.8.2

A three-dimensional structural model of the platform is generated using SESAM software [4]. The model incorporates all primary members in the topside and the jacket such as legs, vertical and horizontal bracings, piles, deck main girders, and topside truss members. This is a space frame that integrates the jacket, the topside, and the foundation systems in one combined structure.

The members such as boat landings, stiffeners, handrails, deck grating, and barge bumpers that do not contribute to the structural stiffness and load-bearing have been modelled either as dummy elements. However, their environmental and gravity loads are taken into consideration. The model geometrical properties conform to the jacket as-built drawings. Figure 3.21 shows the finite element model of the considered jacket platform.

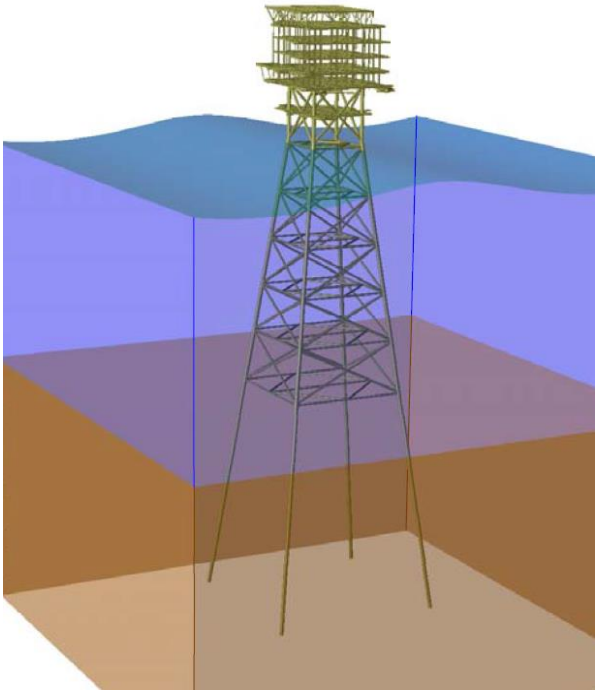

Figure 3.21. Structural model of a jacket platform in SESAM software

3.8.2 Global Fatigue Analysis

A global spectral fatigue analysis is performed using deterministic values for loading and structural parameters. The spectral fatigue analysis is used for structures in shallow to medium water depths [41].

The stress ranges are computed using a stochastic frequency domain approach [5]. The environmental loading is modelled in terms of a set of stationary sea states, each sea

state being characterised by a significant wave height, a mean zero up-crossing period, wave direction, and a wave spectrum. Here, a Pierson-Moskowitz wave spectrum [5] is assumed for each sea state. The probabilities of occurrence of the sea states are obtained by a wave scatter diagram [5].

Table 3.3 shows the wave probability in each direction for the considered platform.

Table 3.3. Probability of occurrence for different directions

Wave approaching direction	Probability of occurrence
North	0.065
North-west	0.066
West	0.029
South-west	0.019
South	0.746
South-east	0.024
East	0.018
North-east	0.033

Table 3.4 shows the characteristics of the sea states approaching from the northwest direction (scatter diagram). It is noted that the scatter diagrams are available for all eight directions. However, the scatter diagram of only one direction is shown in this section (Table 3.4). In total, 115 sea states are considered in this study for all directions which 11 of these sea states are from the northwest direction.

Table 3.4. A wave scatter diagram of sea states (North-west direction)

Sea State	H_S (m)	T_z (sec)	Probability of occurrence (Fraction of time, (f_i))
1	2.75	6.5	0.0019
2	2.75	7.5	0.0265
3	2.75	8.5	0.0054
4	3.25	7.5	0.0060
5	3.25	8.5	0.0123
6	3.75	7.5	0.0001
7	3.75	8.5	0.0087
8	3.75	9.5	0.0009
9	4.25	8.5	0.0013
10	4.25	9.5	0.0019
11	4.75	9.5	0.0006
Total probability of occurrence:			0.0656

The result of the fatigue analysis is the hot spot stress transfer function of each joint in the structural model which is acquired by using the SESAM software. For each member end and wave direction, transfer functions for the forces are computed by software. The transfer function is obtained by finding the stress range, at the location of interest, for a range of wave frequencies and dividing the results by the wave height. Figure 3.22 shows the obtained transfer function by SESAM software for beam BM24 (BM24 location is seen in Figure 3.24).

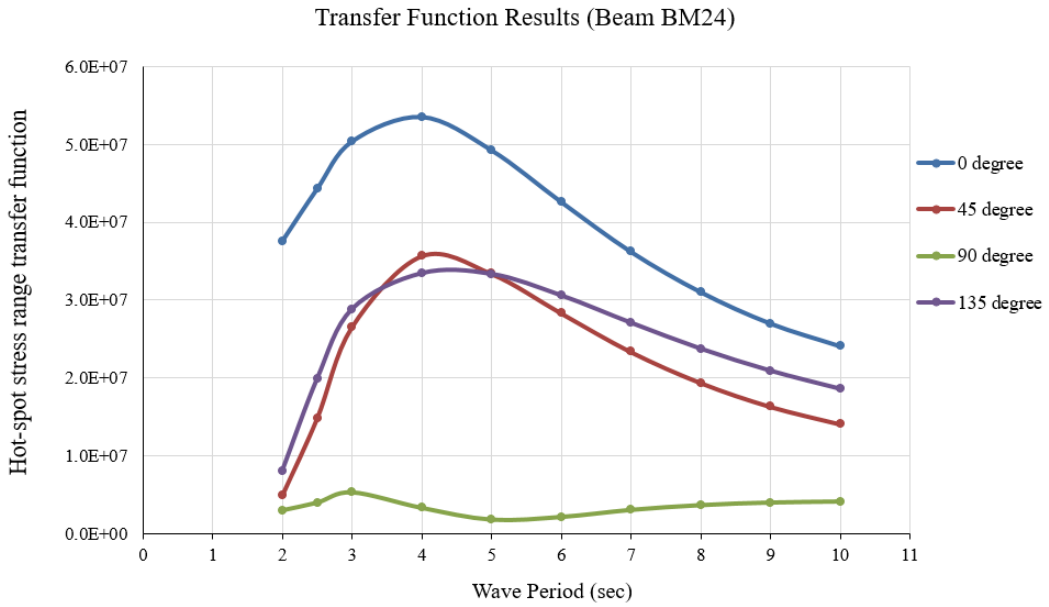

Figure 3.22. Obtained transfer function for beam BM24 (SESAM output)

After obtaining the transfer functions for each hot spot, these transfer functions are used with the sea spectrum (Pierson-Moskowitz wave spectrum) to compute a stress spectrum in each sea state (Eq.(3-6)).

The wave loading for offshore jacket structures is considered narrowly banded [19]. For a narrow-banded Gaussian process, the stress ranges are Rayleigh distributed [5]. The mean value of the fatigue stress range of the ith sea state (which is a Rayleigh distributed variable) can be calculated as [53]:

$$E[\Delta\sigma_i{}^m] = \left(2\sqrt{2}\right)^m \delta_i^m \times \Gamma\left(1+\frac{m}{2}\right) \qquad (3\text{-}33)$$

Here, m is the material property in Paris law, Γ is the Gamma function, $\Delta\sigma_i$ is stress range for ith sea state, $E[.]$ is the expected value operator, and δ_i is the root mean square value of stress under the ith sea state, i.e.:

$$\delta_i = \sqrt{(m_0)_S} = \sqrt{\int_0^\infty S_S(\omega) d\omega} \tag{3-34}$$

where $(m_0)_S$ is the zero-order moment of the stress spectrum, and $S_S(\omega)$ is the stress spectrum.

For calculation of the fatigue life, the total number of stress cycles needs to be estimated [19]. The mean number of stress cycles for a stationary stress process can be obtained as [3]:

$$N_i = T_s \times \nu_{0i} \tag{3-35}$$

where N_i is the number of waves in the ith sea state, T_S is the lifetime of structure in year and ν_{0i} is zero mean crossing frequency of stress process in the ith sea state. The value of zero mean crossing frequency is obtained by using Eq. (3-4) as:

$$\nu_{0i} = \frac{1}{T_z} = \frac{1}{2\pi}\sqrt{\frac{m_2}{m_0}} \tag{3-36}$$

where m_0, m_2 are the zero-order moment and second-order moment of the stress spectrum, respectively [3].

Since there are several sea states in the sea environment (e.g. see Table 3.4), the concept of the equivalent stress range can be utilised. In the equivalent stress range approach (for the fatigue crack growth analysis of tubular welded joints subjected to variable amplitude loading), each individual stress range is considered based on the probability of occurrence of the corresponding sea state [54]. It is noted that this method does not account for any load sequence, i.e. it assumes that this effect is negligible. Using this approach, the expected value of the equivalent stress range can be predicted as:

$$E[\Delta\sigma^m] = \sum_{i=1}^{N_{sea}} E[\Delta\sigma_i{}^m] \times f_i \tag{3-37}$$

where $E[\Delta\sigma^m]$ is the equivalent total stress range, N_{sea} is the number of sea states (which is 115 in this study), and f_i is the probability of occurrence of each sea state (the fraction of time in which the i^{th} sea state is observed). By plugging Eq.(3-33) into Eq.(3-37), the expected value of the stress range for all sea states is obtained as:

$$E[\Delta\sigma^m] = \sum_{i=1}^{N_{sea}} \left(2\sqrt{2}\right)^m \times \Gamma\left(1+\frac{m}{2}\right) \times (f_i \times \delta_i^m) \tag{3-38}$$

The SESAM software can provide the zero-order and second-order moments (m_0, m_2) of stress spectrum for each sea state.

Figure 3.23 shows the moments of the stress range for each sea state for beam BM24 (results for sea states No.27 to No.101 are not shown in this figure).

Moments of response spectrum

Member: BM24 Position:1 CHORD-SIDE Hotspot:1

Seastate	Dir	m0	m1	m2	m4
1	1	0.41423E+14	0.89449E+14	0.20726E+15	0.14352E+16
2	1	0.36699E+14	0.61748E+14	0.11413E+15	0.55096E+15
3	1	0.29089E+14	0.40598E+14	0.63691E+14	0.24177E+15
4	1	0.11599E+15	0.19515E+15	0.36072E+15	0.17413E+16
5	1	0.91937E+14	0.12831E+15	0.20129E+15	0.76411E+15
6	1	0.72590E+14	0.86634E+14	0.11900E+15	0.37813E+15
7	1	0.22445E+15	0.31326E+15	0.49144E+15	0.18655E+16
8	1	0.17722E+15	0.21151E+15	0.29054E+15	0.92317E+15
9	1	0.34735E+15	0.41456E+15	0.56945E+15	0.18094E+16
10	1	0.28251E+15	0.29298E+15	0.35814E+15	0.98582E+15
11	1	0.57420E+15	0.68529E+15	0.94134E+15	0.29911E+16
12	2	0.26146E+14	0.55589E+14	0.12672E+15	0.85108E+15
13	2	0.23961E+14	0.39882E+14	0.72562E+14	0.33591E+15
14	2	0.18863E+14	0.26267E+14	0.40834E+14	0.14909E+15
15	2	0.75728E+14	0.12605E+15	0.22933E+15	0.10617E+16
16	2	0.59618E+14	0.83016E+14	0.12906E+15	0.47121E+15
17	2	0.46398E+14	0.55595E+14	0.76151E+14	0.23417E+15
18	2	0.14555E+15	0.20268E+15	0.31508E+15	0.11504E+16
19	2	0.11328E+15	0.13573E+15	0.18592E+15	0.57169E+15
20	2	0.90965E+14	0.95053E+14	0.11641E+15	0.31195E+15
21	2	0.22202E+15	0.26603E+15	0.36440E+15	0.11205E+16
22	2	0.17829E+15	0.18630E+15	0.22817E+15	0.61142E+15
23	2	0.29473E+15	0.30797E+15	0.37718E+15	0.10107E+16
24	2	0.44027E+15	0.46006E+15	0.56344E+15	0.15098E+16
25	2	0.36670E+15	0.33745E+15	0.37277E+15	0.88789E+15
26	3	0.12277E+14	0.24879E+14	0.53697E+14	0.32057E+15
.....					
Continued					
.....					
102	7	0.11895E+15	0.13708E+15	0.17708E+15	0.45065E+15
103	7	0.97839E+14	0.98656E+14	0.11408E+15	0.25109E+15
104	7	0.16173E+15	0.16308E+15	0.18859E+15	0.41506E+15
105	8	0.26453E+14	0.56408E+14	0.12895E+15	0.86988E+15
106	8	0.24581E+14	0.40708E+14	0.73878E+14	0.34237E+15
107	8	0.20239E+14	0.27692E+14	0.42437E+14	0.15268E+15
108	8	0.77689E+14	0.12866E+15	0.23349E+15	0.10821E+16
109	8	0.63967E+14	0.87521E+14	0.13412E+15	0.48253E+15
110	8	0.51936E+14	0.60642E+14	0.81053E+14	0.24143E+15
111	8	0.15617E+15	0.21367E+15	0.32744E+15	0.11781E+16
112	8	0.12680E+15	0.14805E+15	0.19788E+15	0.58942E+15
113	8	0.24852E+15	0.29018E+15	0.38785E+15	0.11553E+16
114	8	0.20602E+15	0.20900E+15	0.24801E+15	0.63432E+15
115	8	0.34056E+15	0.34549E+15	0.40998E+15	0.10486E+16

Figure 3.23. Different order moments for stress range (beam BM24-SESAM output)

Having obtained these moments, the root mean square value of stress (δ_i) and zero-up crossing frequency of stress (ν_{0i}) is calculated by using Eq.(3-34) and (3-36), respectively. Table 3.5 shows the results of fatigue analysis in terms of the stress range for one specific direction.

Table 3.5. Spectral moments of stress spectrum in one specific direction (north-west)

Sea State	Root mean square value of stress, δ_i (MPa)	Zero mean crossing frequency of stress, ν_{0i}
1	22.57	0.17
2	20.83	0.16
3	19.45	0.14
4	24.62	0.16
5	22.98	0.14
6	28.41	0.16
7	26.52	0.14
8	24.97	0.13
9	30.05	0.14
10	28.30	0.13
11	31.63	0.13

After obtaining the root mean square value of stress for each sea state, the expected value of the stress range for all sea states in all directions is calculated by using Eq.(3-38). Having obtained the root mean square value of stress (δ_i) and zero mean crossing frequency (ν_{0i}) for each sea state, the fatigue crack size at each time can be obtained as:

$$a_t = \left\{ a_0^{1-\frac{m}{2}} + \left(1-\frac{m}{2}\right) \times Y^m \times \pi^{\frac{m}{2}} \times C \times E[\Delta\sigma^m] \times N \right\}^{\frac{1}{1-\frac{m}{2}}} \tag{3-39}$$

where $E[\Delta\sigma^m]$ and N for a narrow banded process is defined by Eq. (3-38) and Eq.(3-35), respectively. By plugging Eq. (3-38) and Eq.(3-35) in Eq. (3-39), the fatigue crack size is obtained as:

$$a_t = \left\{ a_0^{1-\frac{m}{2}} + \left(1-\frac{m}{2}\right) Y^m \times \pi^{\frac{m}{2}} \times C \times T_s \times \left(2\sqrt{2}\right)^m \Gamma\left(1+\frac{m}{2}\right) \times \sum_{i=1}^{N_{sea}} (\nu_{0i} \times \delta_i^m \times f_i) \right\}^{\frac{2}{2-m}} \tag{3-40}$$

The value of v_{0i} and δ_i is obtained by using SESAM software. The value of f_i which is the probability of occurrence of each sea state is obtained from the available wave climatology data for the considered platform.

By summation of term $\sum_{i=1}^{N_{sea}}(v_{0i} \times \delta_i^m \times f_i)$ for all sea states, the predicted crack size for each tubular joint can be calculated as shown in Eq. (3-40). In Eq. (3-40), the values of initial crack size (a_0), material properties (C, m), and the lifetime of structure in year (T_S) are the same for all tubular joints. The only difference is the value of $\sum_{i=1}^{N_{sea}}(v_{0i} \times \delta_i^m \times f_i)$ which is unique for each tubular joint.

In the next step, the value of $\sum_{i=1}^{N_{sea}}(v_{0i} \times \delta_i^m \times f_i)$ is calculated for all tubular joints in the considered platform to find out the most critical joints in fatigue analysis.

Table 3.6 demonstrates the five joints with the maximum value of the $\sum_{i=1}^{N_{sea}}(v_{0i} \times \delta_i^m \times f_i)$ summation, i.e. the five joints which have the biggest value of crack size.

Table 3.6. Five tubular joints with the maximum value of the $\sum_{i=1}^{N_{sea}}(v_{0i} \times \delta_i^m \times f_i)$

Member Name	Joint Name	$\sum_{i=1}^{N_{sea}}(v_{0i} \times \sigma_i^m \times f_i)$, MPa
BM36	Jt3	317.4
BM12	Jt3	303.6
BM34	Jt14	270.8
BM24	Jt14	258.6
BM35	Jt4	214.2

Figure 3.24 shows the location of these five components in the considered platform.

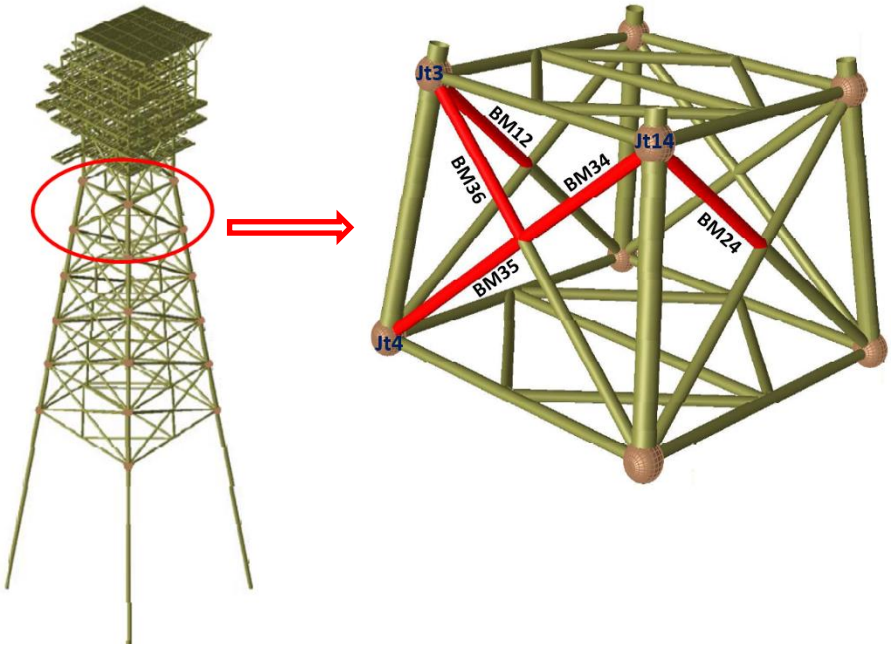

Figure 3.24. Location of most critical components in fatigue analysis

3.8.3 Reliability Analysis

The purpose of this section is to calculate the fatigue probability of failure for the most critical joints in the considered example platform (Table 3.6). To obtain the probability of failure of a tubular joint, the following steps are considered:

- Assign an appropriate distribution for each uncertainty involved in the fatigue process
- Define a desirable limit state
- Obtain the probability of failure for each joint and the corresponding reliability

The above-mentioned steps are explained in the following subsections, separately.

3.8.3.1 Uncertainties in Fatigue Analysis and their Distributions

The reliability analysis depends on the choice of the uncertainties and their statistical distributions [41]. Therefore, uncertainty modelling is very important for offshore reliability analysis. As provided in Section 3.7.1 that there are many uncertainties involved in treating the fatigue life prediction of tubular joints such as:

1) Uncertainties in global analysis:

- Structural behaviour (e.g., Mass, stiffness, foundation parameters)

- Loading and environmental origin (e.g., Wave loading, sea state modelling)

2) Uncertainties related to the fatigue phenomenon:

- Uncertainties related to the fatigue phenomenon (associated with the modelling of the FM-fatigue approach, e.g., initial crack size)

To demonstrate the application of the fatigue reliability analysis, the following uncertainties are considered in this research:

1) Uncertainties in global analysis

- Uncertainties involved in global analysis (ε_{GA}):

  The major task in the frequency domain analysis is the determination of the transfer function [5]. It is noted that the relationship between the wave height and wave-induced force is non-linear due to the drag term in the Morison equation (Eq.(3-9)). Therefore, the drag force should be linearised. The linearisation of the drag term introduces uncertainties in the response modelling for members [19]. There are also uncertainties in the calculation of hydrodynamic loading, finite element idealisation of the structure, nonlinear soil-pile interaction behaviour, etc. (Figure 3.19).

  To consider all these uncertainties in global analysis, a single variable (ε_{GA}) is introduced. The obtained stress range from the global fatigue analysis is then multiplied by this variable. It is reasonable to assume ε_{GA} to be a log-normally distributed variable [55].

2) Uncertainties in the fatigue phenomenon

- Initial crack size:

  In the FM approach, one important variable which affects the fatigue life of a component is the initial crack size [19]. The initial crack size which is denoted as a_0 is not a well-known parameter and therefore there is uncertainty associated with the modelling of the initial crack size. The initial crack size is a manufacturing property. It is representing the process defects such as inclusions, as well as damage caused during fabrication [19]. Lognormal, exponential, and Weibull distributions have been used by

researchers to fit the initial defect data. In this study, a lognormal distribution is assumed for the initial crack size (Table 3.7).

It is noted that the surface defects are usually more critical than embedded cracks as they are often located at stress concentrations and are normal to the principal stress. Experience has shown that almost all fatigue cracks resulted from an initial surface defect [19]. Therefore, the initial fatigue quality is expressed through the depth of the initial surface flaw [19].

- Crack growth parameter:

  Crack growth data for welded joints is expressed through the material parameters (m and C) in the Paris equation. Crack growth data are generated in the laboratory under constant cyclic loading on simple specimens which is different from the real situation. There is always uncertainty in the definition of reasonable distributions for the material parameters based on available laboratory test results [19]. Ideally, large samples of data from field measurements or full-scale experiments are needed to obtain the distribution of the material parameters.

  To simplify the fatigue analysis, m is usually taken as a constant parameter and all the variation in crack growth rate is considered in variable C (see [31], [47]). The distribution of the material parameter (C) approximately follows a lognormal distribution [19].

- Geometry function

  The value of the geometry function depends on the crack shape and stress field geometry [3]. However, for the type of cracks in the tubular members of offshore structures, the variation in magnitude of the geometry function is not very large [35]. Therefore, the geometry function does not vary with crack shape or size [51]. To simplify the problem, the shape of the fatigue crack is assumed to be semi-elliptical and remains semi-elliptical during crack propagation. The geometry function is usually modelled as a lognormal distribution [56].

- Uncertainties involved in local stress analysis (ε_{SCF}):

The nominal stresses from the global analysis are multiplied with SCF to account for local effects. Stress concentration factors are usually obtained by parametric equations (see Section 3.3.4.3). Comparison of SCFs predicted by parametric equations with test results show considerable scatter (see [28], [57], [58]). Therefore, the SCF value for each joint is uncertain. Uncertainties associated with the modelling of the SCFs are considered by definition of a random variable (ε_{SCF}).

Although both categories affect the reliability analysis, since this research aims to improve the reliability analysis using Bayesian methods to incorporate new information (mainly consisting of detection and measurement of crack sizes), the second category of uncertainties is more important. Therefore, it is convenient to model all uncertainties in global analysis with a single variable [55].

Though assigning a single variable for combining all uncertainties in the global analysis has some limitations, sensitivity analysis results show that the uncertainties in the fatigue phenomenon are the most important source of uncertainty in the fatigue reliability calculation of this example structure (Table 3.11).

Table 3.7 summarises the statistical characteristics of the uncertainties which are considered in this study. Different guidelines and studies, introduce various distributions for each uncertainty. For instance, the assigned distributions for the crack growth parameters are based on available laboratory test results. Large samples of data from field measurements or full-scale experiments are needed to obtain the distribution of the material parameters. Therefore, different statistical characteristics (i.e., mean, and standard deviation) have been employed by experts which are based on the experimental results collected in laboratory tests.

Table 3.7. Statistical characteristics of random variables [N, mm]

	Random Variable	Symbol	Type	Mean	COV	Ref
Uncertainties in global analysis	Uncertainties involved in global analysis	ε_{GA}	Lognormal	1.0	0.1	[1]
Uncertainties in fatigue phenomenon	Initial crack size	a_0	Exponential	0.11	1.0	[19]
	Crack growth parameters	C	Lognormal	$8.1\text{x}10^{-12}$	0.6	[15], [51]
		m	Fixed	3	---	[15], [51]
	Geometry function	Y	Lognormal	1.0	0.1	[1]
	Uncertainties involved in local stress analysis	ε_{SCF}	Lognormal	1.0	0.1	[1]

3.8.3.2 Correlations between the Uncertain Parameters

Correlation between the uncertain parameters is an important factor in performing the reliability analysis. Where two variables are correlated, a parameter to measure their correlation degree is needed.

Crack growth parameters (i.e., C and m) are the most important inputs in the crack growth model and subsequently in through life failure probability calculations of a structure containing a flaw [59].

Since the proposal of the Paris-Erdogan law in 1962, several studies have been performed to quantify these two parameters and to find out the possible correlation relationship between them. Cortie and Garrett performed a comprehensive review of these efforts until 1988 [60]. Gurney suggested that m can be selected in a range between 2.5 to 3.6 for real structural steels [61].

There are two approaches in dealing with these two parameters [62]:

1) In the first approach, C and m are considered as two correlated stochastic variables using a correlation equation:
   Several models are available in the literature. For instance, Tanaka and Matsuoka suggested the following correlation equation between C and m [63]:

$$\ln C = -8.682 - 6.924 \times m \tag{3-41}$$

Baker and Stanley performed a test programme of 35 welded and non-welded test specimens and suggested the following equation [64]:

$$\ln C = -8.48 - 6.91 \times m \tag{3-42}$$

2) In the second approach, which is a common approach, m is treated as a deterministic value and C is considered as the stochastic variable, commonly modelled by a lognormal distribution. Different recommended practices such as DNV [19], and BS 7910 [47] suggest this approach.

In this work, the second approach (i.e., a deterministic value for m and a lognormal distribution for C is considered). There is almost no correlation between material properties (i.e., C and m) and initial crack size [62]. Since the focus of this research is on investigating the credibility of the Bayesian methods, no correlation is considered between the uncertain parameters.

3.8.3.3 Fatigue Limit State

A variety of criteria such as crack size criterion, equivalent fatigue strength criterion, damage criterion, and failure assessment diagram, have been proposed to describe the fatigue failure for the tubular structures with cracks [51]. In this study, the crack size can be considered as the failure criterion which is acceptable for low toughness material [1].

The fatigue limit state is defined in Eq. (3-29). According to this equation, failure occurs as soon as the crack size is bigger than a critical value. By applying the considered uncertainties in the fatigue crack size, the limit state function is written as:

$$g = a_c - \left\{ a_0^{1-\frac{m}{2}} + \left(1 - \frac{m}{2}\right) \times Y^m \times \pi^{\frac{m}{2}} \times C \times \left[(\varepsilon_{GA} \times \varepsilon_{SCF})^m \times E[\Delta\sigma^m] \right] \times N \right\}^{\frac{2}{2-m}} \tag{3-43}$$

where the statistical characteristics of the uncertain parameters are introduced in Table 3.7.

3.8.3.4 Calculation of the Component Probability of Failure

The fatigue probability of failure for each component can be estimated by using both FORM and Monte Carlo simulation methods. The advantage of using FORM is sensitivity analysis, whereas Monte Carlo simulation is performed to check the obtained results from FORM.

There are several programs for obtaining the probability of failure of a component. "Rt" program [65] is a framework for utilising probabilistic models with reliability analysis. It also can be used in risk assessment. In this program, the considered uncertainties are defined based on their distributions. Then by defining the desirable limit state function, the probability of failure (and also the reliability) can be obtained based on FORM or Monte-Carlo simulation [65].

As was mentioned in Section 2.4.4, to obtain an accurate and reliable estimation of the probability of failure, a large number of simulations are required for obtaining the probability of failure using the Monte-Carlo simulation technique.

The acceptable COV_{P_f} is assumed equal to 0.05. Therefore, based on Eq. (2-98), the number of failed simulations is obtained equal to:

$$0.05 \cong \frac{1}{\sqrt{n_f}} \quad \Rightarrow \quad n_f = 400 \tag{3-44}$$

The probability of failure is on an order of 10^{-4}. Therefore, based on Eq.(2-97), the total number of simulations required to obtain the accurate probability of failure is approximately equal to:

$$N \cong \frac{n_f}{P_f} = \frac{400}{10^{-4}} = 4 \times 10^6 \tag{3-45}$$

Hence, the number of simulations is introduced equal to 10^7 in the Rt software.

Table 3.8 shows the calculated probability of failure for the most critical components in this platform after 5 years (T_s= 5 years).

Table 3.8. Fatigue probability of failure for the most critical components (T_s = 5)

Member Name	Joint Name	Probability of Failure	
		FORM	Monte Carlo Simulation
BM36	Jt3	2.1×10^{-4}	1.8×10^{-4}
BM12	Jt3	1.7×10^{-4}	1.5×10^{-4}
BM34	Jt14	1.0×10^{-4}	8.3×10^{-5}
BM24	Jt14	8.1×10^{-5}	6.7×10^{-5}
BM35	Jt4	3.2×10^{-5}	2.7×10^{-5}

Having obtained the probability of failure, the reliability index can be calculated by using Eq. (3-31). Table 3.9 shows the reliability index for the most critical components in this platform after 5 years.

Table 3.9. Reliability index for the most critical components (T_s = 5)

Member Name	Joint Name	Reliability Index	
		FORM	Monte Carlo Simulation
BM36	Jt3	3.53	3.57
BM12	Jt3	3.58	3.62
BM34	Jt14	3.72	3.76
BM24	Jt14	3.77	3.82
BM35	Jt4	3.99	4.03

It is noted that the reliability analysis can be carried out for each tubular joint in the considered platform. However, only the results of the five critical components (which were shown in Figure 3.24) are presented.

Table 3.9 shows the reliability index for the most critical components at a specific time (after 5 years). This calculation can be also performed for different years in the platform's lifetime.

The reliability index for the critical component (BM36-Jt3) is calculated for different numbers of years as the fatigue life of the structure. Table 3.10 shows the reliability index for the critical component (BM36-Jt3) at different years. It can be seen that the reliability index decreases with time (as the structure gets older and consumes its design life).

Table 3.10. Reliability index for the critical component (BM36-Jt3) at different years

Year in Service (T_s)	Reliability Index (FORM)
5	3.53
10	3.21
15	2.93
20	2.62
25	2.30
30	2.18

3.8.4 Sensitivity Measurements

Since several random variables exist in reliability analysis applications, in reliability analysis, in addition to the value of the probability of failure, it is crucial to know which of the basic random variables is more important in its contribution to the probability of failure. Sensitivity analyses [12] are performed to find out the importance of each variable on the reliability analysis. There are several measurements to show the importance of each variable on the probability of failure (See Chapter 2). One of these measurements is α-vector measure. It was shown in Chapter 2 that the components in α-vector can be considered as the relative importance of each variable on the probability of failure. Table 3.11 shows the α-vector measures for each random variable.

Table 3.11. Sensitivity measurement of the uncertain parameters on the probability of failure

Uncertainty Category	Random Variable	α-vector
Uncertainties in the global analysis	Uncertainties involved in global analysis (ε_{GA})	0.35
Uncertainties related to the fatigue phenomenon	Initial crack size (a_0)	0.45
	Crack growth parameters (C)	0.65
	Geometry function (Y)	0.35
	Uncertainties involved in local stress analysis (ε_{SCF})	0.35

As explained in Chapter 2, α-vector values indicate the importance of each uncertain parameter on the probability of failure.

Therefore, based on the results of the sensitivity analysis (Table 3.11), among the considered random variables, the crack growth parameter is the most important source of uncertainty in the fatigue reliability calculation of this example structure. This is followed by the initial crack size.

Sensitivity factors for all random variables are positive which means that these variables are load parameters (See Chapter 2). This is because the resistance parameter in this problem is a critical crack size (a_c) which is assumed as a constant parameter equal to the joint wall thickness.

3.9 Summary

Fatigue is an important failure mechanism in offshore structures. Fatigue damage occurs due to the cyclic nature of wave loading on the structure. This wave loading creates stress ranges at the hot spot regions and results in crack initiation. The crack initiation is followed by crack propagation through the thickness of the tubular wall which is assumed as the end of fatigue life of the tubular joints.

To carry out a fatigue analysis for a jacket structure, some assumptions are considered in the fatigue model such as:

- For a short-term period, the sea surface is considered as a realisation of a zero-mean stationary Gaussian process. The sea surface elevation is characterised by the frequency spectrum and it is described by two parameters, the significant wave height and zero-mean up-crossing period for a given wave direction.
- The long-term probability distribution of the sea states is known.
- To use the frequency approach for obtaining the stress response, the wave loading on structural members is linearised.
- Paris equation is assumed as the basis of the fatigue crack growth model. The Paris equation is recommended for the fatigue analysis of offshore structures by several codes of practice (e.g. [19], [47]). The crack growth exponent (m) is considered as a constant and the threshold stress intensity is assumed to equal to zero.

The fracture mechanics approach is used to obtain the crack size and the fatigue limit state is defined based on crack size. Several uncertainties are considered in the limit state function. It is noted that some uncertainties (e.g. a_0, C, Y) contribute in the limit state function explicitly whereas other uncertainties such as wave loads, sea state characteristics affect stress range.

The probability of failure for each tubular joint is obtained by using FORM and Monte-Carlo simulation. Sensitivity analyses are performed to show the effect of each uncertain parameter on the fatigue reliability results. Based on the analysis results, uncertainties in the crack growth parameter and initial crack size have a relatively greater effect on the reliability calculation.

4 . SYSTEM RELIABILITY CALCULATION

4.1 Introduction

In Chapter 3 of this study, only one failure mode (fatigue failure) for a single structural component was considered. Relevant uncertainties were introduced and a limit state function was defined. Then by using the different reliability methods (e.g. FORM and Monte-Carlo), the probability of failure for each tubular member was estimated, separately.

Nevertheless, most of the offshore jacket structures in the real situation are redundant structures [7]. A redundant structure has more structural members than is necessary. Therefore, if some of the structure members are damaged, the structure will not necessarily fail or collapse, since the load can be redistributed among undamaged members [7]. In offshore structures, members are connected and therefore, each member has its own limit state function. In offshore structures, conventionally, system reliability analysis is estimated based on either fatigue loading or extreme environmental loading [66].

Due to the high level of redundancy in offshore jacket platforms, the probability of failure of the whole system is more applicable than the component probability of failure. In this chapter, a system reliability approach is presented to calculate the probability of failure of a jacket platform considering a combination of fatigue and extreme wave loads. In the development of a failure tree of these structures, the initial failures occur by fatigue at the critical joints and the weakened structure collapses under the extreme wave loading.

Section 4.2 introduces the fundamental of the structural system and the reliability calculation for each system.

Considerable research effort has been made on the application of system reliability methods for offshore structures. Section 4.3 explains some of these studies.

Section 4.4 explains how to obtain the system probability of failure for a jacket structure considering both fatigue and extreme wave load. For this purpose, at first, the fatigue probability of failure of each component is obtained by using the Monte-Carlo simulation. Then, important failure paths are identified by using a searching

process in which, components with the maximum change in the accumulated damage are considered as the candidate joints in the path. Finally, the system failure criterion is evaluated and compared to the maximum acceptable probability of failure.

Section 4.5 demonstrates the application of the proposed approach to a jacket platform and the results of the system reliability. A three-dimensional structural model of the considered platform is generated using SESAM software [4]. Nonlinear pushover analysis is also carried out to determine the capacity of the platform and the annual probability of failure under the extreme wave is calculated. To carry out the pushover analysis, USFOS software is employed [67]. Section 4.5 also describes the inspection plan for a jacket platform. Underwater inspection is an expensive activity and the cost of the inspection is proportional to the number of inspections [15]. Therefore, it is required to concentrate on fatigue-sensitive locations in the structures. Furthermore, different non-destructive (NDT) techniques are explained in this section.

It is worth mentioning that in this Chapter, Sections 4.2 to 4.4 describe the theoretical aspects of the fatigue reliability analysis, whereas, Section 4.5 demonstrates the application of the theoretical aspects to the considered platform and results that have been developed by the author.

4.2 Different Types of Systems

A system is defined as a set of elements working together as parts of a mechanism. In theory, there are two fundamental systems [6]:

- Series systems:

  A series system is a system in which failure happens when one of the elements in the system fails. A series system is also named the weakest link system because its failure corresponds to the failure of its weakest component [6]. Examples of a series system are chains and statistically determinate structures. If any member in these structures fails the structure will fail.

- Parallel systems:

  On the other hand, in a parallel system, all elements of the system must fail for the failure of the system.

These two systems are fundamental. In reality, the failure of any complex system can be represented in terms of a combination of these two systems [7].

4.2.1 Modelling of Series Systems

The combination of failure elements in a series system can be understood from the statically determinate (non-redundant) structure. A structure with n_{series} elements is a statically determinate structure when the whole structure fails as soon as any structural element fails, i.e. the structure has no load-carrying capacity after failure of one of the structural elements [6]. The illustration of a series system is shown in Figure 4.1.

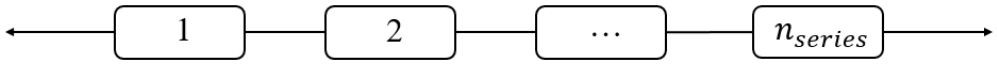

Figure 4.1. Weakest link system modelled as a series system of failure elements

Let's consider a series system of n_{series} elements. The failure of each element is modelled with its limit state function.

$$P_f(E_i) = P(g_i \leq 0), \quad i = 1,2,\dots,n_{series} \tag{4-1}$$

where E_i is the failure event of the ith element, P_f represents the probability of failure and g_i is the limit state function for the ith element.

The series system fails if just one of the elements fails, i.e. the probability of failure of the series system is the union of the individual element failure probabilities:

$$\left(P_f^{sys}\right)_{series} = P[(g_1 \leq 0) \cup (g_2 \leq 0) \cup \dots \cup (g_n \leq 0)] \tag{4-2}$$

where $\left(P_f^{sys}\right)_{\boldsymbol{series}}$ represents the system probability of failure and $\cup$ is the union operator (see Chapter 2).

Figure 4.2 illustrates the failure domain (hatched areas) for a series system with three elements which is the union of the individual element failure domains. In this figure, X_1 and X_2 are uncertain parameters.

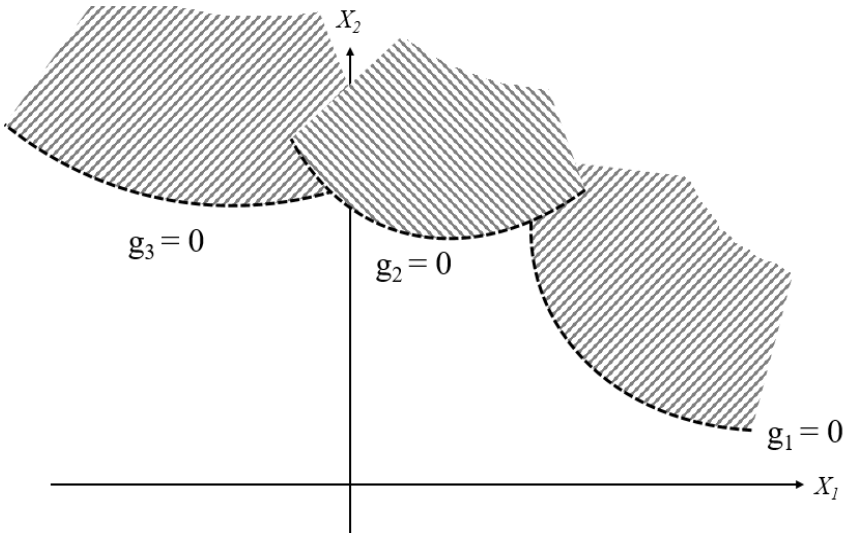

Figure 4.2. Illustration of the failure domains in a series system

4.2.2 Modelling of Parallel Systems

A parallel system is a system in which all elements have to fail before the whole system fails. Failure of the statically indeterminate (redundant) structures can be assumed as a parallel system. A parallel system with $n_{parallel}$ elements is shown in Figure 4.3.

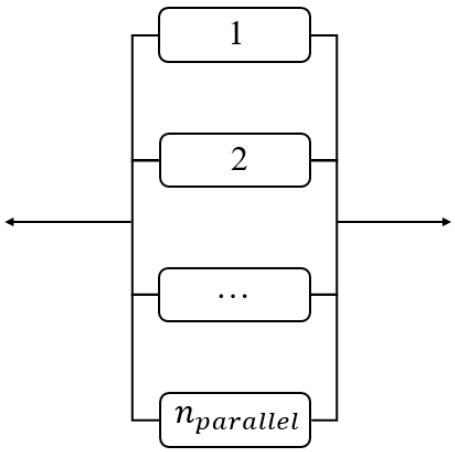

Figure 4.3. Failure of a redundant structure modelled as a parallel system

Now, consider a structural system where the system reliability model is a parallel system of $n_{parallel}$ elements. The parallel system fails if all of the elements fail, i.e. the probability of failure of the parallel system is the intersection of the individual element failure probabilities:

$$\left(P_f^{sys}\right)_{parallel} = P[(g_1 \leq 0) \cap (g_2 \leq 0) \cap \ldots \cap (g_n \leq 0)] \quad (4\text{-}3)$$

where $\left(P_f^{sys}\right)_{parallel}$ represents the system probability of failure and $\cap$ is the intersection operator (see Chapter 2).

Figure 4.4 illustrates the failure domain for a parallel system with two elements which is the intersection of the individual element failure domains. In this figure, X_1 and X_2 are uncertain parameters.

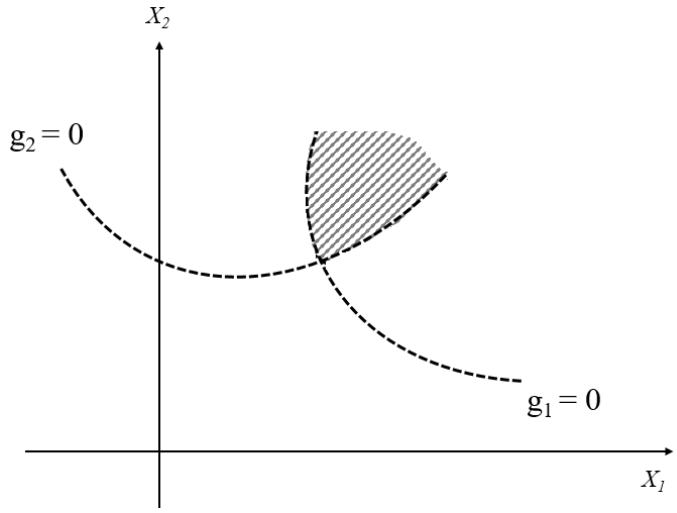

Figure 4.4. Illustration of the failure domains in a parallel system

4.2.3 Modelling of General Systems

In a redundant system with a large number of components, failure of the system occurs after a certain number of elements have failed. The failure event of such a system can be represented in terms of the "minimal cut-sets" of the system [6]. A real redundant structural system generally has many cut-sets, i.e. different sequences of element failure. Each cut-set can then be modelled by a parallel system. If one of these parallel systems fails then the whole system fails, i.e. the overall systems reliability model is a series system of the failure modes or parallel systems. This is schematically shown in Figure 4.5.

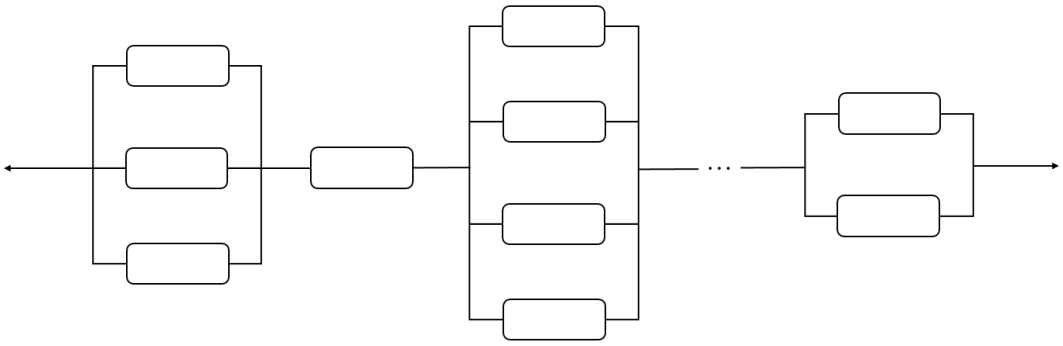

Figure 4.5. Illustration of the systems reliability model as a series of parallel systems

The probability of failure of a general system is then given by:

$$\left(P_f^{sys}\right)_{general} = P\left[\bigcup_{i=1}^{m}\left(\bigcap_{j=1}^{k_i}\left(P(g_{ij} \le 0)\right)\right)\right] \tag{4-4}$$

where $\left(P_f^{sys}\right)_{general}$ represents the system probability of failure, m is the number of cut-sets (failure sequences), k_i is the number of elements in each sequence and g_{ij} is the limit state function of the component j[th] in cut-set No. i.

4.2.4 Reliability Calculation of the Systems

Depending on the system configuration, the system probability of failure can be obtained based on equations (4-2), (4-3), and (4-4). When correlation exists between the components, calculation of the system probability of failure (or system reliability) is quite difficult [6]. The estimation of system probability is dependent on the correlation of the elements.

Simple bounds can be introduced to find out the upper and lower bounds of the system probability of failure introduced in the above equations. It is noted that there are some better bounds for estimation of system probability of failure such as Ditlevsen bounds [68].

For a series system, the probability of failure is within the following bounds [66]:

$$\max_i \left[P_f(E_i)\right] \le \left(P_f^{sys}\right)_{series} \le 1 - \prod_{i=1}^{n}\left(1 - P_f(E_i)\right) \tag{4-5}$$

The lower bound corresponds to a situation that all failure components are fully correlated. In this case, all the failure cases represent the same failure and all the

components will fail if one of them fails. Therefore the maximum probability of failure can be selected as the system probability of failure. The upper bound corresponds to a situation that all failure components are statistically independent.

The reliability of a series system decreases with an increasing number of its elements. For a given system, with a fixed number of components, system reliability decreases with decreasing correlation between pairs of elements.

On the other hand, the simple bounds for a parallel system can be introduced as [66]:

$$\prod_{i=1}^{n}\left(P_f(E_i)\right) \leq \left(P_f^{sys}\right)_{parallel} \leq \min_i \left[P_f(E_i)\right] \tag{4-6}$$

The lower bound represents the case where the components are uncorrelated and the system fails only when all the components fail. The upper bound represents the case in which all components are fully correlated. In this case, the safest component controls the reliability of the system.

The reliability of a parallel system increases with an increasing number of its components. For a given system, with a fixed number of elements, the system reliability decreases with an increasing correlation between pairs of elements.

4.3 Previous Studies on System Probability of Failure of Offshore Structures

Several research studies in offshore reliability analysis have been focusing on component reliability analysis where a fatigue limit state or an extreme wave limit state was considered to calculate the probability of failure (See Chapter 3). For statistically determinate structures, the reliability at the component level is sufficient since the failure of one member will lead to the whole structure failure. However, this is not the case for highly redundant structures such as offshore jacket platforms. The failure of one or a few members does not necessarily result in the collapse of the entire system. Therefore, for these structures, reliability analysis at the system level is more applicable. Reliability analysis at the system level takes into account the failure of one component on others and the entire system as a whole system.

Structural failure is a progressive process and a sequence of individual components is required to fail before overall failure. After the failure of the first element, the load

shared by this member is re-distributed to the remaining elements and the structure continues to support loads until a sufficient number of elemental failures occur and the structure fails. A failure path is defined as the failure sequence of members in the structure until it collapses.

The calculation of the system reliability has many theoretical and practical challenges. One of the difficulties is that for a redundant structure, a large number of sequences leading to failure exist and it is not practical to include all of them in the analysis [69]. However, only a few of the failure sequences have significant contributions to the total failure probability. The probability of those failure paths and the method of determination of the important failure paths are the basis of system reliability analysis [69]. The system failure event is then calculated as the union of these identified important sequences [70].

Considerable research effort has been made on the application of system reliability methods to fixed offshore structures. However, these efforts have mainly concentrated on the reliability analysis of the structure under one failure mode, i.e. considering either fatigue loading or extreme environmental loading.

4.3.1 System Reliability Analysis Considering Fatigue Failure

Wang and et.al considered fatigue failure as a common failure mode for offshore jacket platforms and calculated the system fatigue reliability analysis for this type of structure. They proposed a new searching method for the system reliability analysis of structures to identify the dominant fatigue failure paths and evaluate the probability of system failure through failure paths. The main feature of their method was the system decomposition. The system decomposition was implemented by dividing the failure elements into two sub-systems according to the construction and fatigue failure characteristics of jacket structures. It was shown that system decomposition improved calculation efficiency [8].

Marquez and Sorensen studied the system reliability for offshore wind turbines regarding fatigue failure. They formulated the limit state equations for components fatigue failure based on bi-linear S-N curves in offshore wind farms. They tried to find the important sequences of failure by utilising branch and bound technique and then they calculated system reliability through a combination of important failure paths

leading to system failure. The system reliability in a jacket-type wind turbine substructure was estimated using a series system [71].

Shabakhty attempted to develop a system reliability approach to monitor the safety of jack-up platforms under fatigue and fracture degradation. He assumed a semi-elliptic shape to model the crack propagation in depth and circumference of crack shape. He used Monte-Carlo Simulation to estimate the statistical crack size in accordance with the fatigue limit state. The important sequences of failure were identified using branch and bound technique and finally, the system reliability was estimated through a combination of important failure paths leading to system failure [56].

4.3.2 System Reliability Analysis Considering Extreme Load Failure

A simplified system approach was developed by Bomel Ltd. in a joint industry project to obtain environmental load factors for fixed steel offshore structures. A global failure function was defined by the difference between the structural reserve strength (resistance) and the environmental load, in which the reserve strength was evaluated by deterministic pushover analyses. In this project, both load and resistance refer to overall base shear [72].

Kurian and et al performed the structural reliability of an existing jacket platform, by determining the system probability of failure and its corresponding reliability index. They used pushover analysis to determine possible failure paths of the structure under extreme wave loading. They established three failure paths of the platform under extreme wave loading and used the simple bound formula to determine the failure probability and reliability index [69].

4.3.3 System Reliability Analysis Considering both Fatigue and Extreme Load Failures

In the above-mentioned studies, the focus of system reliability analysis was on estimating the reliability considering either fatigue loading or extreme environmental loading. However, for offshore structures, a combination of these two failure modes is more critical. Some studies were performed by considering both fatigue and extreme wave loadings.

Karamchandani et al. considered a combination of fatigue and extreme loading. They presented a formulation for a sequence of failures for three different failure modes; failure under fatigue, failure under extreme environmental loads, and combined sequence of failure. To obtain the system reliability, they assumed that the initial failures happen in fatigue and subsequent failures occur under extreme environmental loads. Then, they applied the approach to a steel jacket platform. They found that for an individual member (component level), the most probable cause of failure is fatigue, but for overall structural failure, overload and a combination of fatigue and overload are more important. However, they assumed the platform fails after only two-component failures, which is not a correct assumption [70].

Oakley et al. proposed a simplified method of estimating the system reliability of a structure. They considered both fatigue and extreme loading. The members were divided into groups, each group consisting of the diagonal bracings between any two levels of one frame. The structure was assumed to fail when any group failed. Then, they compared the simplified method results with results from a rigorous analysis [73].

4.4 System Probability of Failure Considering Fatigue and Extreme Wave

As mentioned in Section 4.1, the reliability analysis can be calculated either at the component level or system level. The reliability analysis at the component level cannot reflect the reliability of the system as a whole. For statistically determinate structures, the reliability of individual members is sufficient since the failure of one component will lead to the whole structure failure. However, for highly redundant structures, the failure of one or a few members does not necessarily lead to the collapse of the system.

System redundancy is the ability of the structure to redistribute the applied load after the failure of one of its elements. A redundant structure is capable to continue to carry loads after the failure of its members. After a failure of a component, the load supported by the failed element will be distributed to adjacent members. A considerable degree of redundancy is often built into the design of jacket structures. The need for redundancy arises for several reasons [7]:

- The probability of the actual loads exceeding the design loads,

- The inevitable nature of fabrication defects such as welding defects at the joints,
- Deterioration during service as a result of corrosion and fatigue initiating from defects.

The ultimate capacity of the structure depends on the post-failure behaviour of the primary members and joints, the structural configuration, and the degree of redundancy.

Calculation of system reliability analysis for large structures with high redundancy may be complex due to an enormous number of possible failure paths. It is practically impossible and not necessary to identify all possible failure paths. Including all the possible failure paths in the analysis is not feasible, since many of these paths have a low probability of occurrence [69]. Therefore, identification of the dominant failure paths is one of the major tasks in the system reliability analysis for this type of structure [8].

4.4.1 Global Fatigue Analysis

The first step in the estimation of the system reliability is to perform the reliability analysis at the component level. As it was mentioned, fatigue failure is considered at the component level.

To evaluate the probability of failure of a component, a failure event should be defined. In this study, the fatigue limit state is defined based on the crack size, which is obtained by the fracture mechanics approach. It is assumed that failure occurs, as soon as the crack size is bigger than the critical value. Therefore, the fatigue limit state function is described as:

$$g = a_c - a_t \tag{4-7}$$

Where a_c represents the critical crack size. Critical crack size is usually considered as the wall thickness [47]. Failure occurs when the crack size is bigger than the critical crack size, i.e. when $g \leq 0$.

By defining fatigue limit state function and uncertainties, the probability of failure can be obtained by performing the Monte-Carlo simulation method. In this study, Rt software [65] is used to perform the Monte-Carlo simulation. The calculation of the component reliability was explained in detail in Chapter 3.

For performing fatigue analysis, a spectral fatigue analysis can be employed. The spectral fatigue analysis is used for structures in shallow to medium water depths [74].

In spectral fatigue analysis, the major task is the determination of the response of the structure for a unit sinusoidal wave as a function of wave period (or wave frequency). This function is called the response transfer function [19]. In spectral fatigue analysis, transfer functions can be obtained for each sea state. The transfer function is established by finding the stress range, at the location of interest, for a range of wave frequencies, and dividing the stress range results by the wave height. See Chapter 3 for more details.

For each sea state, the sea surface elevation is characterised by the frequency spectrum (e.g. Pierson-Moskowitz or JONSWAP spectrum) [19]. Having the transfer function and wave spectrum, the response spectrum (which is the hot spot stress spectrum) can be obtained as:

$$S_S(\omega) = |T(\omega)|^2 \times S_\eta(\omega) \tag{4-8}$$

where $S_s(\omega)$ is the stress spectrum; $S_\eta(\omega)$ is water surface elevation spectrum; $T(\omega)$ is transfer function and ω is the angular frequency of the wave. Having obtained the stress spectrum, the stress range value can be obtained (see Chapter 3 for more details).

4.4.2 Identification of Most Probable Fatigue Failure Paths

Complex structural systems consist of a large number of structural elements. Therefore, the structure can fail in several different ways. Because of the considerable degree of redundancy, there is usually a large number of possible combinations of element failures that can result in the failure of these structures.

Usually, few of these failure sequences have significant contributions to the total failure probability. Therefore, in most structural reliability analyses, a searching process is required to identify important failure sequences, and the system failure event is then approximated as the union of these identified important sequences [70].

After each component failure, all the surviving elements can be chosen to form the next component to fail, the failure events can be represented in the form of a failure tree with each branch of the tree representing a failure sequence.

There are different techniques to identify the dominant failure paths. Identification of the failure paths can be performed using an incremental load method (Moses 1982), unzipping method [66], branch and bound method [75], and truncated enumeration method [76]. The basic concepts of these methods are similar [70].

The incremental load method uses an incremental elastic analysis of the structure [70]. Using mean values of the random variables as the analysis basis, the most highly stressed member is considered to have failed. It is then replaced by its post-failure strength and the loading is further increased until the next element fails. The procedure is repeated until a failure path is developed. Since the mean values of the variables are used, the results obtained from this method are deterministic and the stochastic characteristics are unable to be considered. The method is not suitable for the analysis of offshore structures with a large number of uncertainties.

The branch and bound method repeats elastoplastic analysis of the structure to determine the sequence of structure components most likely to fail, and hence to develop the failure paths [70]. The main features of this method are branching and truncation. The branching from each node of a failure tree generates new failure paths. A new branch is generated by adding one more element to the selected path. Because all of the surviving elements considered would be the next failure element, a large number of failure paths will be generated. The truncation of failure paths starts after the first complete failure path has been identified. Almost all the possible failure paths can be identified in this way. However, this method, although theoretically rigorous, is prohibitively expensive for the analysis of complex structures with high redundancy, such as offshore jackets.

However, these methods have some shortcomings. For example, Branch-and-Bound Method, although theoretically rigorous, is prohibitively expensive for the analysis of complex structures with high redundancy, such as offshore jackets [8]. Kim et al. proposed a new searching technique, where the dominant failure modes are rapidly identified through a genetic algorithm. Multiple dominant failure modes are then recognised in the lessening order based on their likelihood. The searching process ends as the contributions by newly identified modes become negligible [77].

In this thesis, the sequence of structure joints most likely to fail is established. The probability of system failure is then estimated as the union of a finite number of critical failure path events. Since other paths are neglected, the resulting estimate is a lower bound of the probability of system failure.

As described in Chapter 3, the crack size of each component is expressed as a function of basic random variables. The sequence of failures occurs if each of these individual crack sizes reaches critical crack size during the lifetime of the structure. Monte-Carlo simulation is used to compute the fatigue failure probabilities of each component. For identification of the important sequences, the branch and bound method is utilised.

In this thesis, for branching from a selected incomplete failure path of length, all the surviving elements of the structure are candidate elements and new paths are formed by combining each element to the chosen path respectively. As only some of the branches will be developed into complete paths eventually, it is not necessary to combine all of the surviving elements to develop new branches. Therefore, it is important to select a limited number of surviving elements to develop a limited number of new branches to reduce calculation consumption [70].

The starting point is the intact structure in which none of the elements have failed. By performing component reliability analysis for the intact platform, the joint with the highest fatigue failure probability is selected as a starting component for further branching. After the failure of the first component, the applied loading will be transferred by the remaining members, i.e. redistribution of the load through the structure occurs. In the damaged structure, each remaining member has already some accumulated fatigue damage, and due to the redistribution of the stresses in the structure, the rate of damage accumulation will change [19].

Two criteria are introduced for the selection of the next probable joint to failure which are the change ratio in damage and accumulated damage of surviving elements. The procedure is repeated until a failure path is developed.

(I). Change Ratio in Damage

This criterion states that only those joints, which have a large change ratio in the damage (after the failure of the critical component), are selected. The change ratio of the damage of joint *i* after the failure of joint *j* is defined as [8]:

$$r_{ij} = \frac{|D_{i/j} - D_i|}{D_i} \quad (4\text{-}9)$$

where D_i is the fatigue damage of a specific member (member i) before the j^{th} joint fails, $D_{i/j}$ is the damage after the j^{th} joint failure. The change ratio of the damage of all the intact elements is calculated. The failure paths are chosen based on the following criterion [8]:

$$r_{ij} > \alpha_c \times \max_i (r_{ij}) \quad (4\text{-}10)$$

where α_c is the selection ratio that is used to control the number of surviving elements. If α_c considered equal to zero, it means that all the surviving elements are included; if it is assumed equal to one, only the surviving element with the highest change ratio of the damage rate is selected. In this study, α_c is considered equal to 0.7.

(II). Element Accumulated Damage

The accumulative damage of the surviving element is a supplement to the above criterion for considering that some surviving elements with large accumulative damage but less change ratio of the damage rate would also develop a path with a considerable failure probability. The deterministic accumulate damage of the ith surviving element of the surviving structure corresponding to the failure path is calculated by setting all random variables to their mean values [70].

A failure path that results in structural collapse is called a complete failure path and further branching from this path is terminated while an incomplete failure path is taken up for further branching [7]. Figure 4.6 shows a failure tree in which various branches illustrate different failure paths of the structure.

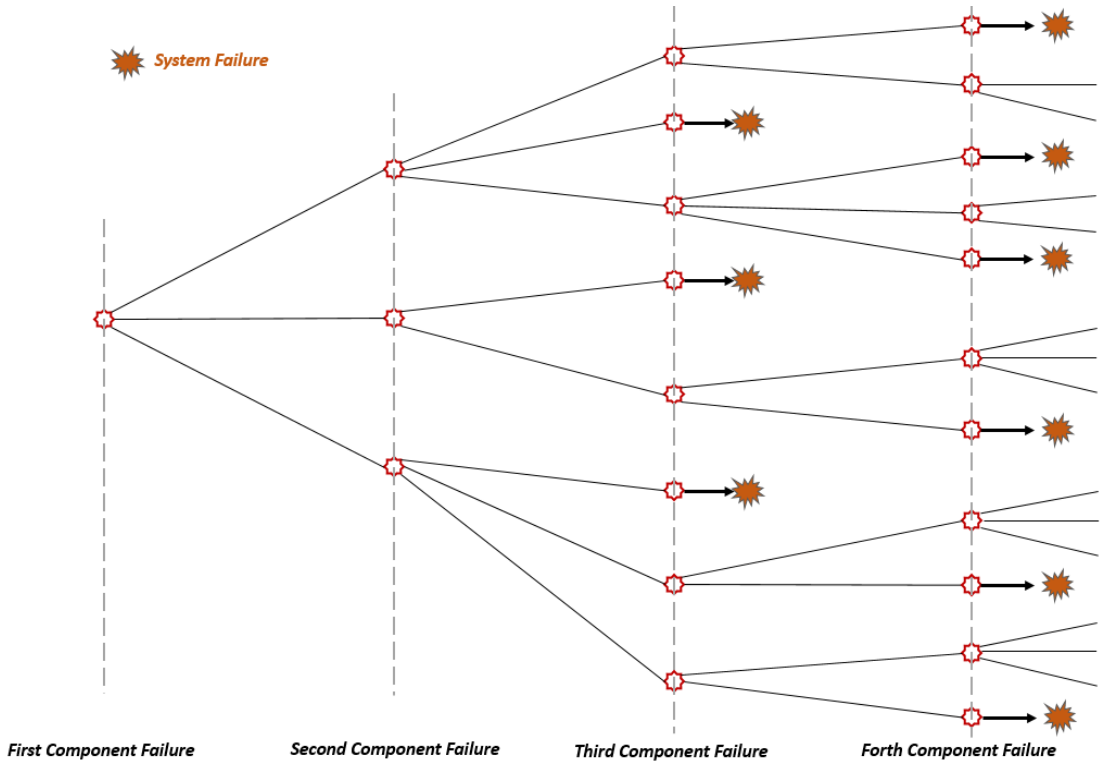

Figure 4.6. Development of the failure-tree

4.4.3 Extreme Wave Load Analysis

For performing extreme wave (environmental) load analysis, the load and response of the structure should be modelled. The extreme load can be introduced by a random magnitude, which relates wave load to the 100-year wave height. In this study, the extreme wave is a wave corresponding to an annual exceedance probability of 10^{-2} (100-year return period wave).

In this analysis framework, failure is assumed to occur by yielding at a section which is a function of axial force and the bending moment at the section. After the first failure, the force distribution in the structure changes, which leads to an increase in the stresses of the adjacent members of the failed member. The changes in the stress depend on the structure configuration, the location of the failed member, and the post-failure behaviour of the failed member.

Pushover analysis is established to perform extreme wave load analysis. This analysis provides an insight into the load-bearing performance of the platform, indicates the weak links, failure modes, and the post-failure behaviour of the structure. The procedure adopted for the pushover analysis consists of the 100-year storm load, for

the extreme environmental condition, which is incrementally introduced to the platform. The environmental load is gradually increased to induce member yielding or buckling and to eventually lead to the global collapse in the platform. The progressive collapse analysis of an offshore structure is usually carried out using a non-linear finite element program.

4.4.4 Probability of Failure under Extreme Wave Load Analysis

One approach to estimate the probability of failure under extreme wave load is in terms of structure capacity [74]. The capacity of the structure is determined by nonlinear pushover analyses.

The previous studies for jacket structures have shown that the ultimate capacity, or collapse capacity, of the structures, can be related directly to the total base-shear on the structures [19]. Therefore, the extreme limit state can be written in terms of the base shear demand that needs to be checked against the base shear capacity at collapse. Therefore, the limit state can be defined as [74]:

$$g_{extreme} = BS_{Capacity} - BS_{Load} \quad (4\text{-}11)$$

In this equation, $g_{extreme}$ represents the limit state function under extreme wave load, $BS_{Capacity}$ and BS_{Load} are uncertain parameters that refer to the base-shear capacity and base-shear load, respectively. The platform fails when the exerted load is greater than the platform capacity.

Therefore, the extreme probability of failure is the probability of $g_{extreme}$ being less than zero:

$$P_f = P(g_{extreme} < 0) = P(BS_{Capacity} < BS_{Load}) \quad (4\text{-}12)$$

The structure has a random capacity ($BS_{Capacity}$) which is the largest load the structure can withstand without system failure. The value of capacity depends on the capacities of the members in the system. In this study, the base shear capacity ($BS_{Capacity}$) will be assumed as a lognormal random variable. A COV of 15-20% is consistent for jacket platforms [74]. In this study, COV is considered equal to 0.20.

4.4.5 Global Response Surface

To establish the probability distribution of the annual maximum base-shear load acting on a given structure, a proper description of the environmental situation is needed [19].

The global response surface method relates the environmental load to the wave height [78]. For a given wave period and current speed, the base-shear load can be approximated as [19]:

$$BS_{Load} = \Gamma \times (c \times H_{max}^{\alpha}) \tag{4-13}$$

Here, c and α are deterministic constants describing how base shear varies with wave height [74]. To determine the response of the structure, 40 sets of environmental loads (wave heights) are generated based on Gumbel distribution, and structural analysis is carried out. From the analysis, 40 sets of base shears are obtained. The coefficients c and α are determined using MATLAB Curve Fitting Tool [79].

The parameter Γ, is a factor representing the uncertainty involved in estimating base shear from wave height when we use deterministic amounts for c and α. Γ is modelled as a lognormal random variable with a mean equal to 1.0 and COV equal to 0.25 [74].

Having obtained the base shear capacity and base shear load, the probability of failure for the extreme load can be obtained by using the Monte-Carlo simulation.

4.4.6 System Failure Criterion

An incomplete failure path will be completed when the system failure occurs. The common criterion of system failure is a major loss of global stiffness. The global stiffness is measured by the increase in deflection at the centre of the deck due to a unit increase in load. It is observed that usually, there is little change in stiffness during the first few member failures but after the failure of several members, a large change in stiffness often occurred. This large change in stiffness is used to detect system failure [78].

The other criterion for system failure could be using target reliability levels in design codes. Several codes and standards such as Eurocode [80] and DNV [81] introduce target reliability levels for the different types of platforms. Target reliabilities are required to be met in the assessment of offshore platforms to make sure that certain

safety levels are achieved. The values of target reliabilities depend on the consequence and nature of the failure. The consequence of failure is evaluated concerning human injury, environmental impact, and economic loss [19].

For example, the target annual reliability for a redundant structure with the high consequence of failure corresponds to the probability of failure of 10^{-4} [16]. Therefore, in this study, a maximum acceptable probability of failure (P_{max}) equal to 10^{-4} per year is used. It means that at each step of failure path development (after the failure of each component), the annual probability of failure of the platform under an extreme wave is calculated and compared to the maximum acceptable probability of failure. If the annual probability of failure in each step of the failure path is less than P_{max}, the platform is considered a safe system. An incomplete failure path is assumed to fail when annual probability exceeds the maximum acceptable probability of failure, i.e.:

$$\left(P_f\right)_{Annual} > P_{max} \tag{4-14}$$

4.4.7 Estimation of the System Probability of Failure

To calculate the system probability of failure considering both fatigue and extreme wave load, the conditional probability of extreme loads can be used. These conditional probabilities are multiplied by the probability of fatigue failures, and the products are summed to obtain the system probability of failure [82]. Therefore, the system probability of failure can be obtained as:

$$P\left(F_{sys}\right) = \sum_{k=0}^{n} P(F_k) \times P(Ext \mid F_k) \tag{4-15}$$

In this equation, $P(F_k)$ is the probability of failure of "k" joints in fatigue loading; e.g. F_0 is an event in which no component fails in fatigue (Intact case); F_1 is an event in which only one component fails in fatigue, etc. Moreover, "Ext" is an event in which platform fails under an extreme wave and $P(Ext \mid F_k)$ is the probability of failure under extreme loading given that "k" joints failed in fatigue.

By expanding Eq. (4-15), the system probability of failure can be written as:

$$P(F_{sys}) = P(F_0) \times P(Ext \mid F_0) + P(F_1) \times P(Ext \mid F_1) + P(F_2) \times P(Ext|F_2) + \cdots \quad (4\text{-}16)$$

Here, the probability of failure for each fatigue failure case ($P(F_0)$, $P(F_1)$, etc.), is obtained based on the Monte-Carlo simulation (by using fatigue limit state function) and for each fatigue failure case. The conditional probability, $P(Ext \mid F_k)$; is calculated based on extreme limit state function by using Monte-Carlo simulation. The total probability of system failure over the entire range of fatigue failure is then computed using Eq. (4-15).

4.5 Application of the Proposed Approach to a Jacket Platform

To apply the methodology described in Section 4.4, a jacket platform is considered. The considered structure is a four-legged living quarter, steel jacket platform. It is located in a water depth of 70 m. The choice of this platform is motivated by the degree of structural redundancy, which is believed to be a typical jacket platform.

Figure 4.7 shows the flowchart of the proposed approach for a jacket platform. The following sub-sections explain this flowchart.

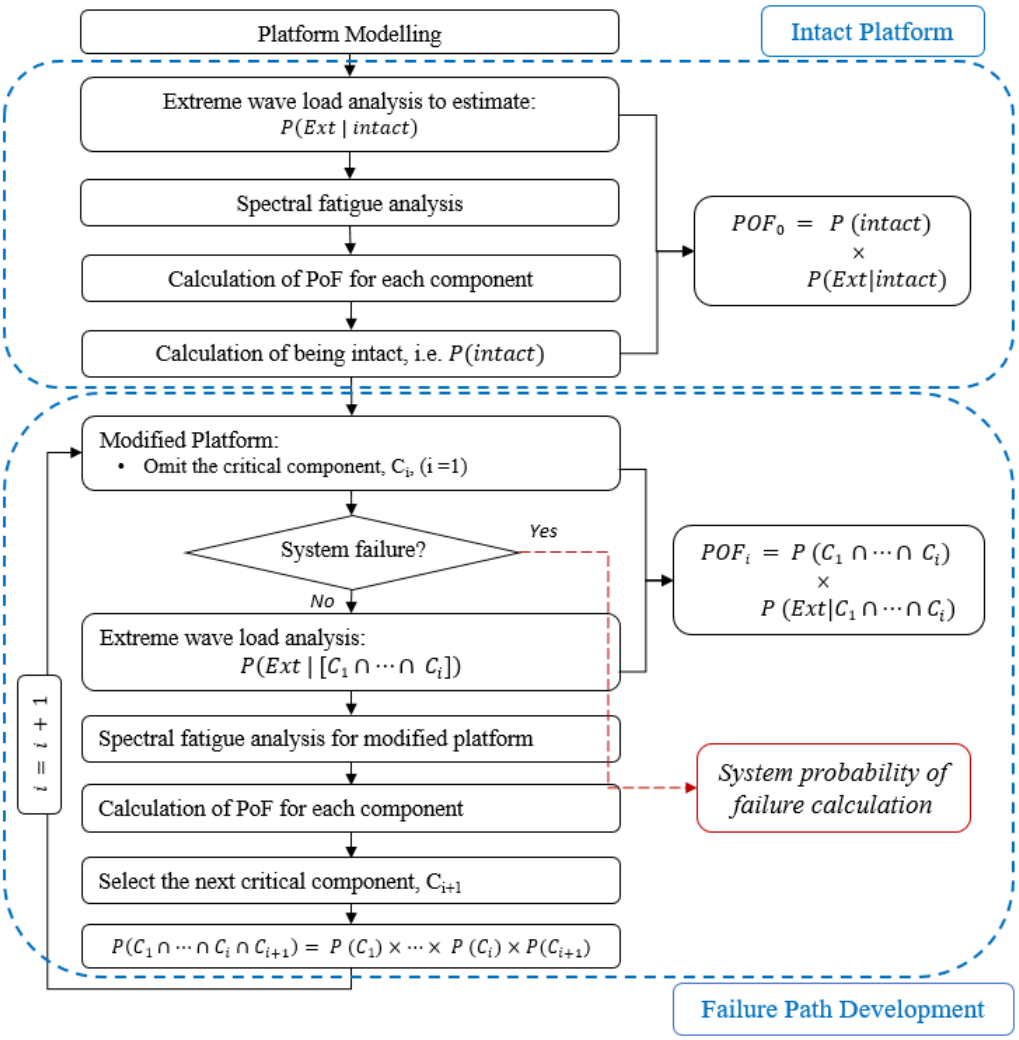

Figure 4.7. Flowchart of the proposed approach for the considered jacket platform

4.5.1 Platform Modelling

The considered jacket platform in Chapter 3 is used here as shown in Figure 4.8. A three-dimensional structural model of the platform is generated using SESAM software [4]. The model incorporates all primary members in the topside and the jacket. This is a space frame, which integrates the jacket, the topside, and the foundation systems in one combined structure. The model geometrical properties conform to the jacket as-built drawings.

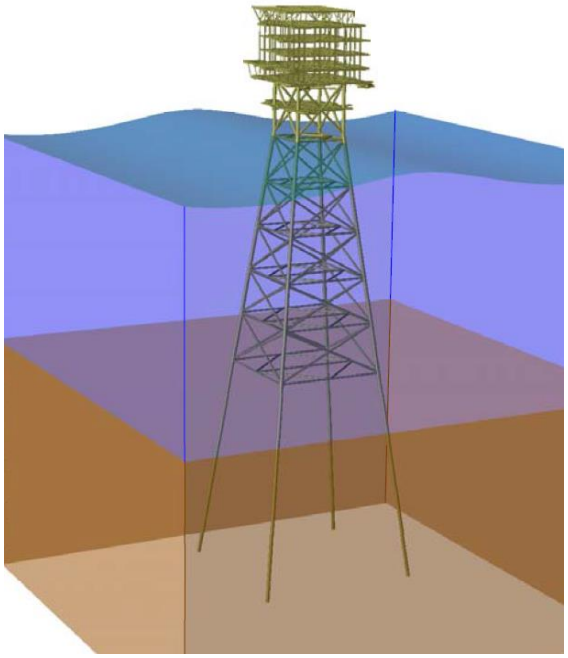

Figure 4.8. Structural model of a jacket platform in SESAM software

The main characteristic of the jacket platform is given in Table 4.1.

Table 4.1. Main characteristics of the considered jacket

Item	Description
Platform function	Living quarter platform
Water depth	70 m
No. of Legs	4
Foundation system	- Outside diameter: 91.4 cm - Pile thickness: 2.54 cm - Pile depth: 64m - Grouted to jacket legs
Soil description	- Silt: 0-1 m - Clay: 1-18.4 m - Silt: 18.4-31.2 m - Clay: 31.2-56.1 m - Sand: 56.1-66.0 m
Bracing type	X brace
Jacket levels	See Table 3.2
Material	Carbon Steel Grade S355
Mass of the deck	2200 ton
100-year return period wave	- Wave height: 12.2 m - Wave period: 11 sec
Fatigue wave loading	See Section 3.8.2

4.5.2 Intact Platform

At first, it is assumed that the platform is in an intact condition, i.e. no failure happened and all components are in safe conditions.

4.5.2.1 Extreme Wave Load Analysis

Monte-Carlo simulation is employed to calculate the probability of failure under extreme load in the intact case, i.e. $P(Ext|intact)$. For this purpose, the extreme limit state function is used (Eq. (4-11)). In this function, $BS_{Capacity}$ and BS_{Load} should be calculated.

To obtain $BS_{Capacity}$, a pushover analysis is performed. To carry out the pushover analysis, USFOS software is employed [67]. USFOS is a finite element program specifically developed for estimating the ultimate strength of space frame structures and identifying the associated collapse mechanisms. The software is capable to perform non-linear collapse analysis, in which, the structure and members are incrementally loaded beyond their yielding capacity [67].

Based on the USFOS analysis results, the collapse base shear ($BS_{Capacity}$) of this platform (in intact case) is found as 13.1 MN. Figure 4.9 shows the finite element model of the platform in pushover analysis.

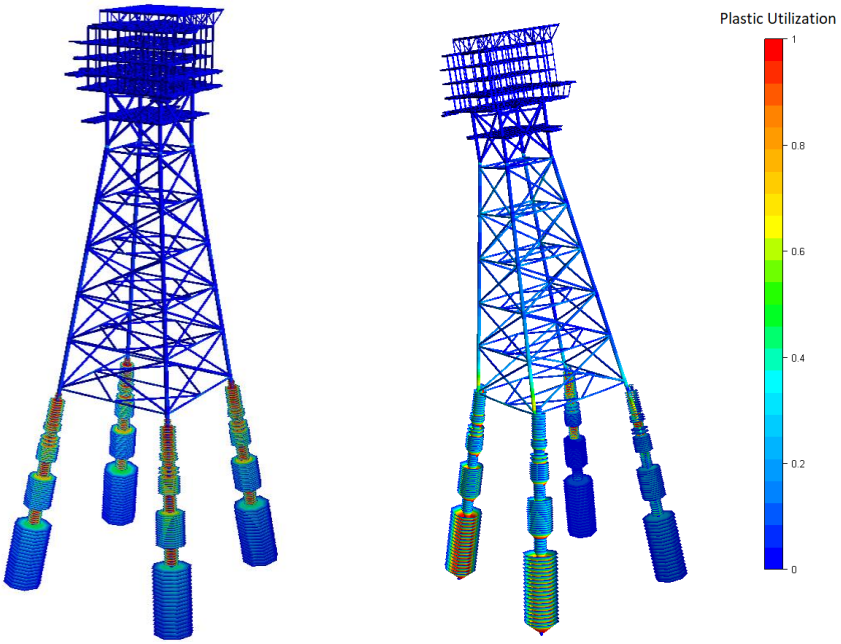

Figure 4.9. Structural model for pushover analysis, the first step of analysis (left), and the collapse of the jacket in the last step of analysis (right)

For calculation of load base shear, Eq. (4-13) is used which relates base shear to wave height. To determine the response of the structure, 40 sets of wave loads are generated based on Gumbel distribution, and structural analysis is then carried out. From the analysis, 40 sets of base shears are obtained. In this thesis, a Gumbel distribution with $\mu = 12.0$ and scale parameter (β) of 1.2 is considered for maximum wave height, H_{max} [83].

By performing a linear regression between wave height and base shear, the amount of c and α is estimated equal to:

$$c = 0.035 \qquad \alpha = 1.93 \tag{4-17}$$

Table 4.2 shows the characteristics of random variables in extreme wave load analysis.

Table 4.2. Statistical characteristics of random variables in extreme wave analysis (intact case)

Random Variable	Type	Mean	COV
$BS_{Capacity}$	Lognormal	13.1 MN	0.20
Γ	Lognormal	1.0	0.25
H_{max}	Gumbel	$\mu = 12.0$, $\beta = 1.2$	---
α	Fixed	1.93	---
c	Fixed	0.035	---

Figure 4.10 shows the distributions of the load and capacity bases shears.

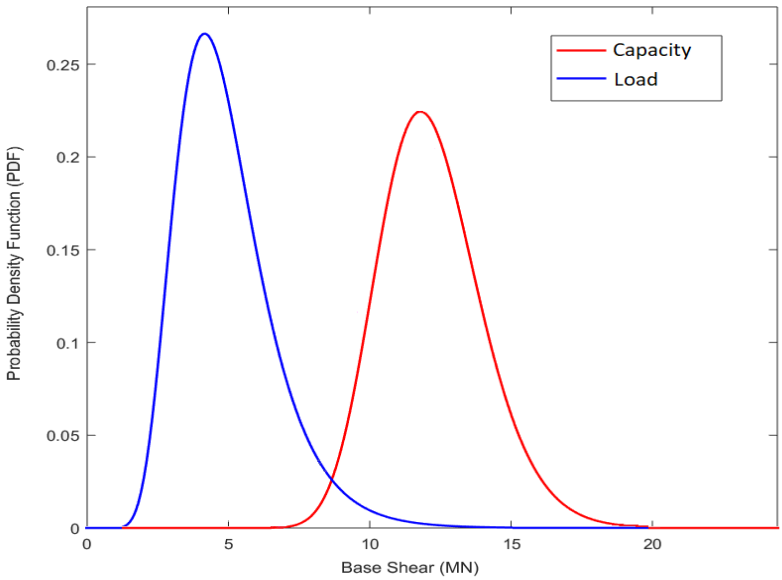

Figure 4.10. Probability density functions for load and capacity base shear

Using defined variables in Table 4.2 and the extreme limit state function (Eq. (4-11)), by performing the Monte-Carlo technique with 10^7 simulations (using Rt software [65]), the probability of failure of the platform under extreme wave loading in the intact case is obtained as:

$$P\ (Ext \mid intact) = 4 \times 10^{-5} \tag{4-18}$$

4.5.2.2 Spectral Fatigue Analysis

Spectral fatigue analysis for the jacket platform is performed using SESAM software [4]. The stress parameters are computed using a frequency domain approach. The environment is modelled in terms of a set of stationary sea states, in which each sea state is characterised by significant wave height, period, and direction. The probabilities of occurrence of the sea states are usually obtained by measurement and summarised as a wave scatter diagram. In each sea state, a Pierson-Moskowitz wave spectrum is assumed (for more detail, see Chapter 3).

Table 3.4 shows the characteristics of the sea states approaching from the northwest direction.

Table 4.3. Characteristics of sea states (Northwest direction)

Sea State	Significant wave height, H_S (m)	Dominant period, T_Z (sec)	Fraction of time, f_i
1	2.75	6.5	0.0019
2	2.75	7.5	0.0265
3	2.75	8.5	0.0054
4	3.25	7.5	0.0060
5	3.25	8.5	0.0123
6	3.75	7.5	0.0001
7	3.75	8.5	0.0087
8	3.75	9.5	0.0009
9	4.25	8.5	0.0013
10	4.25	9.5	0.0019
11	4.75	9.5	0.0006

For each member end and wave direction, SESAM computes transfer functions and spectral moments. Having obtained the spectral moments, the standard deviation and zero mean crossing frequency of the stress for each sea state can be calculated (see

Chapter 3). Table 3.5 shows the results of fatigue analysis in terms of the stress spectrum for one specific wave direction.

Table 4.4. Spectral moments of stress spectrum in one specific direction (north-west)

Sea State	Root mean square stress, δ_i (MPa)	Zero mean crossing frequency, ν_{0i}
1	22.57	0.17
2	20.83	0.16
3	19.45	0.14
4	24.62	0.16
5	22.98	0.14
6	28.41	0.16
7	26.52	0.14
8	24.97	0.13
9	30.05	0.14
10	28.30	0.13
11	31.63	0.13

It is noted that the term $\sum_i(\nu_{0i} \times \delta_i^m \times f_i)$ is calculated by summing all sea states in all directions (see Chapter 3 for more details).

4.5.2.3 Calculation of Fatigue Probability of Failure for Each Joint

Now, the probability of failure of each joint is obtained using the Monte-Carlo simulation. To perform the Monte-Carlo simulation, fatigue limit state function and fatigue uncertainties need to be defined. Fatigue limit state function is introduced in Eq. (4-7). Table 4.5 represents the fatigue uncertainties considered in this study.

Table 4.5. Statistical characteristics of random variables, Units [N, mm]

Random Variable	Symbol	Type	Mean	COV	Reference
Initial crack size	a_0	Exponential	0.11	1.0	[19]
Crack growth parameters (Material properties)	C	Lognormal	8.1×10^{-12}	0.6	[15], [51]
	m	Fixed	3	---	[15], [51]
Geometry function	Y	Lognormal	1.0	0.1	[1]
Uncertainties involved in global analysis	ε_{GA}	Lognormal	1.0	0.1	[1]
Uncertainties involved in local stress analysis	ε_{SCF}	Lognormal	1.0	0.1	[1]

After performing the Monte-Carlo simulation, the probability of failure for each joint is obtained. Table 4.6 demonstrates the probability of failure for the most five critical components in this platform.

Table 4.6. Fatigue probability of failure for the most five critical components

Component Name	$\sum_i v_{0i} \times \delta_i^m \times f_i$ (MPa)	Probability of Failure
BM36-Jt3	317.4	0.022
BM12-Jt3	303.6	0.018
BM34-Jt14	270.8	0.0100
BM24-Jt14	258.6	0.0079
BM35-Jt4	214.2	0.0026

Figure 3.24 shows the location of critical components in fatigue analysis.

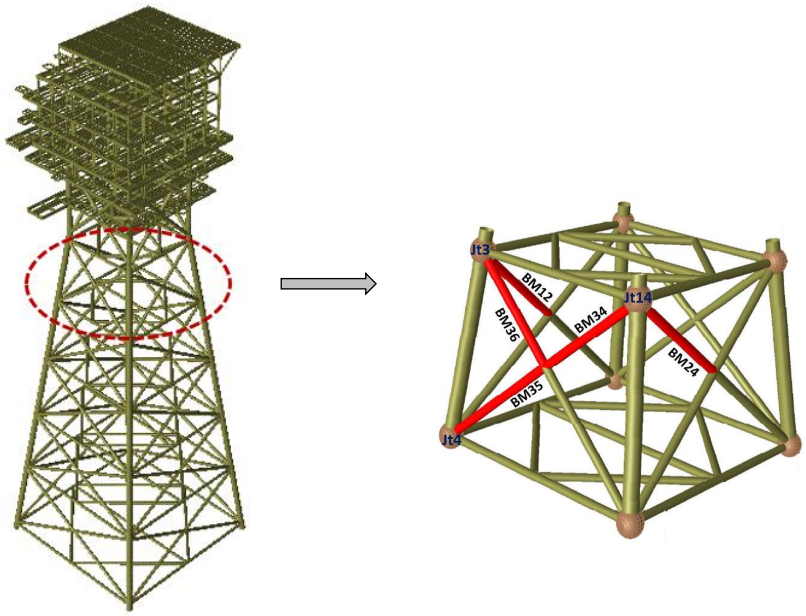

Figure 4.11. Location of the most critical components in fatigue analysis (piles were not shown)

4.5.2.4 Calculation of Probability of Failure for the Intact Platform

The platform is intact when no component (C_i) fails in the fatigue loading. Therefore, the probability of being intact is:

$$P(intact) = P([C_1\ is\ safe] \cap [C_2\ is\ safe] \cap \ldots \cap [C_n\ is\ safe])$$

$$P(intact) = (1 - P_1) \times (1 - P_2) \times \ldots \times (1 - P_n) = \prod_{i=1}^{n}(1 - P_i) \quad (4\text{-}19)$$

In which, P_i is the probability of failure of the ith component in fatigue and n is the number of components in the jacket platform. After calculating $P(intact)$, probability of failure considering both extreme wave load and fatigue load, in the intact case, is calculated as:

$$POF_0 = P(intact) \times P(Ext \mid intact) \quad (4\text{-}20)$$

4.5.3 Failure Path Development

4.5.3.1 Modified Platform

Based on Table 3.6, the most critical component (BM36-Jt3) is selected as the first component in the failure path. The modified platform is a platform in which this component (BM36-Jt3) has been removed. Figure 4.12 shows the modified platform.

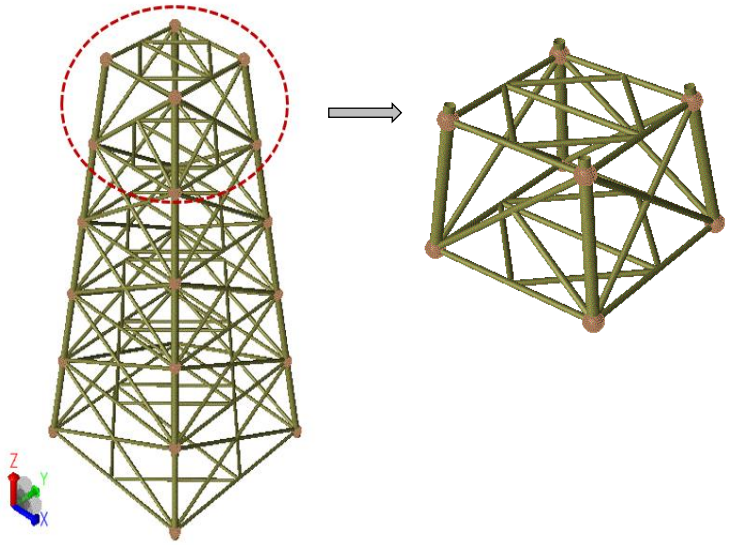

Figure 4.12. The modified platform (topside and piles were not shown)

4.5.3.2 Check the System Failure Criterion

After removing the critical component, the system failure criteria should be checked. For this purpose, the probability of failure under extreme wave load (Eq. (4-12)) is compared to the maximum acceptable probability of failure (Eq. (4-14)). As it was

explained in Section 4.4.6, the maximum acceptable probability of failure for a redundant structure is considered equal to $P_{max} = 10^{-4}$.

If the platform fails (i.e. the annual probability of failure is bigger than P_{max}), the system probability of failure is obtained based on Eq. (4-15). Otherwise, the following process is continued which includes:

4.5.3.3 Extreme Wave Load Analysis

In this step, another extreme wave analysis is performed for the modified platform (platform without component BM36-Jt3) in USFOS software. The same process as Section 4.5.2 is repeated for the calculation of the probability of failure. The only difference here is that due to removing one specific component, $BS_{Capacity}$ in this step (12.95 MN) is less than the previous amount of $BS_{Capacity}$ in intact case (13.1 MN).

Monte-Carlo simulation is performed and the probability of failure under extreme wave load given one component failed in fatigue is obtained (i.e. $P(Ext|C_1)$). After obtaining $P(Ext|C_1)$, the probability of failure under both extreme wave load and fatigue load (in a case that only one component fails in fatigue) is calculated as:

$$POF_1 = P(C_1) \times P(Ext \mid C_1) \tag{4-21}$$

Figure 4.13 shows the probability distributions of load and capacity in the intact and two damaged cases. Figure 4.13 shows that the platform capacity decreases when the number of failed components in fatigue increases. Therefore, the conditional probability of failure increases by increasing the number of failed components in fatigue, i.e.:

$$P\,(Ext \mid [C_1 \cap \ldots \cap C_{n+1}]) \;>\; P\,(Ext \mid [C_1 \cap \ldots \cap C_n]) \tag{4-22}$$

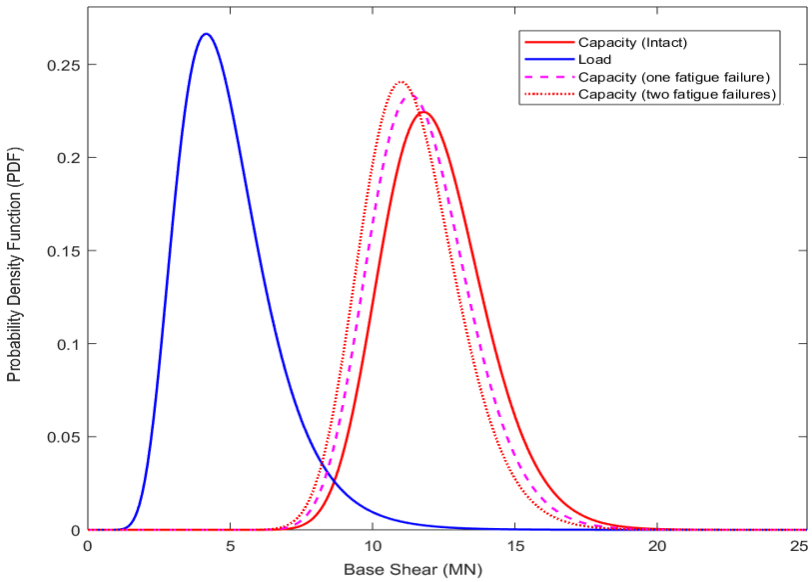

Figure 4.13. Probability density functions for load and capacity base shear in different damage scenarios

4.5.3.4 Spectral Fatigue Analysis

The next step is finding the next critical component in the failure path. For this purpose, another fatigue analysis is carried out (for the modified platform). The results of the spectral fatigue analysis are the standard deviation and zero mean crossing frequency of the stress for each sea state.

4.5.3.5 Calculation of Probability of Failure for Each Component

The probability of failure for each component is obtained by using a fatigue limit state (Eq. (4-7)) and Monte Carlo simulation.

4.5.3.6 Select the Next Critical Component, C_{i+1}

The next critical component in the failure path is selected based on the selection criteria explained in Section 4.4.2. It is assumed that the probability of failure of components is independent of each other, i.e.:

$$P\left(C_1 \cap \ldots \cap C_i \cap C_{i+1}\right) = P(C_1) \times \ldots \times P(C_i) \times P(C_{i+1}) \tag{4-23}$$

After repeating the searching process, fatigue failure paths are obtained.

4.5.4 System Probability of Failure (Specific Failure Path)

The failure path is completed when the whole structure fails. It was mentioned that the platform is assumed to fail when the probability of failure of the modified structure

under an extreme wave (i.e. $P(Ext \mid [C_1 \cap \dots \cap C_n])$) is greater than the maximum acceptable probability of failure (P_{max}).

The probability of failure of a platform considering both extreme wave and fatigue loading can be obtained based on Eq. (4-15). The probability of failure of each failure path is obtained as:

$$\begin{aligned} P(F_{sys}) = \sum_{k=0}^{n} P(F_k) \times P(Ext|F_k) = \\ P(intact) \times P(Ext \mid intact) \\ + P(C_1) \times P(Ext \mid C_1) \\ + P(C_1 \cap C_2) \times P(Ext \mid C_1 \cap C_2) + \cdots \\ + P\left(C_1 \cap C_2 \cap \dots \cap C_{n_{path}}\right) \times P\left(Ext \middle| C_1 \cap C_2 \cap \dots \cap C_{n_{path}}\right) \end{aligned} \quad (4\text{-}24)$$

The above equation can be written as:

$$P(F_{sys}) = POF_0 + POF_1 + POF_2 + \dots + POF_{n_{path}} \quad (4\text{-}25)$$

In Eq. (4-25), n_{path} is the number of components in a complete failure path, i.e. number of components that should be failed before the system failure.

4.5.5 System Probability of Failure – All Failure Paths

For a redundant structure, there are several alternate sequences leading to collapse. the event that the structure failure occurs is the event that one of these collapse sequences occurs [70].

Including all the possible failure paths in the analysis is not feasible. Therefore, only the dominant failure paths are considered in the system reliability estimation.

To find out the dominant failure paths, a searching technique is required, in which, components with the maximum change in the accumulated damage are considered as the candidate joints in the path. Identification of the failure paths can be performed using the unzipping method [66], branch and bound method [75], and truncated enumeration method [76].

The described methodology in Sections 4.4 and 4.5 is a procedure to calculate the probability of failure for one specific path. To calculate the total probability of failure, a complete failure tree should be produced based on the sequence of the failures and the probability of failure of all failure paths.

The important sequences of failure scenarios are found using the branch tree [8]. The branch tree is established through the failure probability determined for the fatigue failure mode.

To find out the dominant failure paths:

1) The starting point is the intact structure (none of the elements have failed). By performing component reliability analysis for the intact platform, the joint with the highest fatigue failure probability is selected as the first component in the sequence.
2) After the failure of the first component, redistribution of the load through the structure occurs. In the damaged structure, each remaining member has already some accumulated fatigue damage, and due to the redistribution of the stresses in the structure, the rate of damage accumulation will change.
3) To develop the failure path, the next candidate joint in the failure path, components with the maximum change in the accumulated damage are considered.
4) Depending on the considered value for α_c which is used to control the number of surviving elements (Eq. (4-10), several components would be considered as the second component in the failure path.
5) A failure path that results in structural collapse is called a complete failure path and further branching from this path is terminated.

Figure 4.14 shows the important failure sequences identified through the branch tree. Each branch represents a possible failure path, and each node is the failed component.

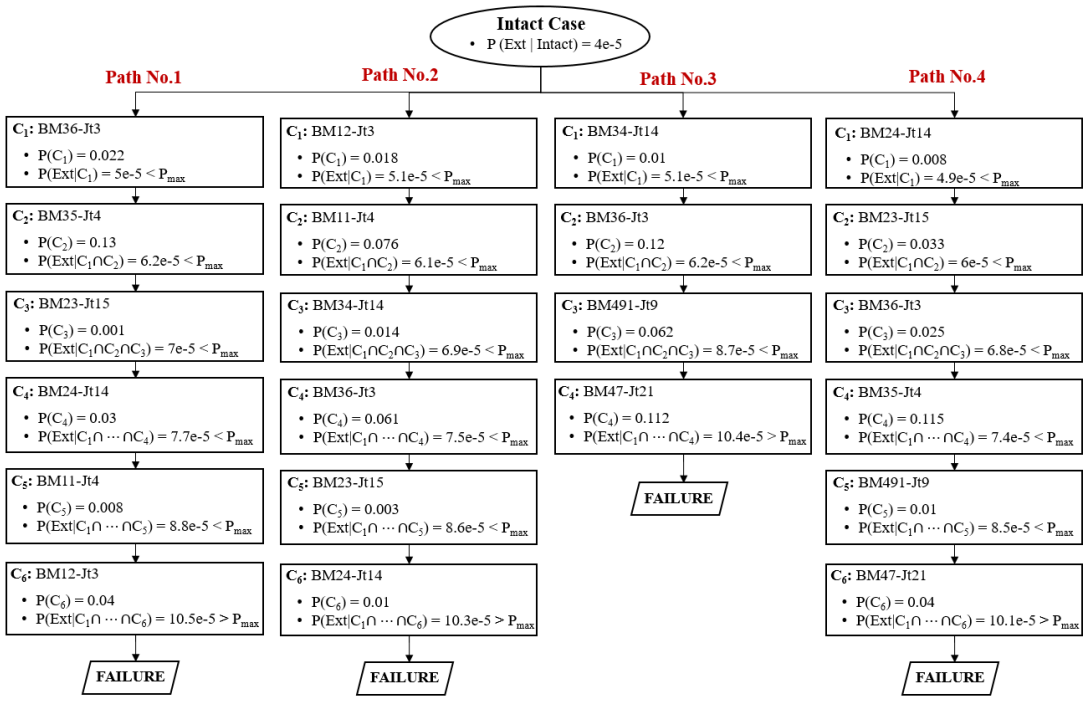

Figure 4.14. Branch tree obtained for fatigue failure and system failure under extreme wave load

For instance, for developing Path No.1, the critical component in the intact case is selected (see Table 4.6). In the next step, the failed component, and the corresponding member (i.e., BM36-Jt3) are removed and another fatigue analysis is performed for the modified platform. Table 4.7 shows how the damages for different components would change when the critical component in the intact case (i.e., BM36-Jt3) is removed.

Table 4.7. Change in the damage ratio after removing the critical component

Intact Case		Modified platform (BM36-Jt3 was removed)	Change in damage ratio
Component	Damage (D_i)	Damage ($D_{i/j}$)	$r_{ij} = \frac{\lvert D_{i/j} - D_i \rvert}{D_i}$
BM36-Jt3	5.76	----	----
BM12-Jt3	5.44	4.2	0.23
BM34-Jt14	4.3	11.5	1.67
BM24-Jt14	4.01	3.85	0.04
BM35-Jt4	3.99	**12**	**2.01**
BM491-Jt9	3.8	3.83	0.01
BM11-Jt4	3.78	3.84	0.02
BM506-Jt9	3.57	3.63	0.02
BM47-Jt21	2.75	2.76	0.00

BM23-Jt15	2.58	2.64	0.02
BM29-Jt15	2.44	1.48	0.39
BM519-Jt21	2.29	2.32	0.01
BM509-Jt9	1.74	1.73	0.01
BM493-Jt8	1.68	1.7	0.01
BM496-Jt9	1.67	1.68	0.01
BM508-Jt8	1.61	1.64	0.02
BM8-Jt4	1.35	1.33	0.01
BM32-Jt4	1.27	1.38	0.09

As Table 4.7 shows the next component in the sequence is BM35-Jt4 since it has the maximum change in the accumulated damage.

To find out the third component in the failure path, the same calculation is performed. The incomplete failure path will be completed when the system failure occurs (see Section 4.4.6).

Figure 4.14 shows the identified dominant failure sequences. As shown in Figure 4.14, for the first, second, and fourth failure paths six component failures are required for the system failure ($n_{path} = 6$ in Eq. (4-24)), whereas for the third failure path, four component failures are required.

For each failure path the last probability in Eq. (4-24), i.e., $P\left(Ext\middle|\, C_1 \cap C_2 \cap \ldots \cap C_{n_{path}}\right)$ is greater than the maximum acceptable probability of failure, P_{max} as shown in Figure 4.14.

4.5.5.1 Dominant Failure Paths

Four dominant failure paths are generated for the presented jacket platform in Section 4.5. For all failure paths, the described procedure (Figure 4.7) is employed. The probability of failure for all failure paths is shown in Table 4.8, Table 4.9, Table 4.10, and Table 4.11.

Table 4.8. The system probability of failure for the first failure path

Sequence	Component	P ($C_1 \cap \ldots \cap C_i$)	P(Ext| $C_1 \cap \ldots \cap C_i$)	POF_i = [P ($C_1 \cap \ldots \cap C_i$)] x [P(Ext| $C_1 \cap \ldots \cap C_i$)]
No component failure	----	P (intact) = 0.934	4×10^{-5}	3.74×10^{-5}
One component fails in fatigue, (i=1)	C_1: BM36-Jt3	P (C_1) = 0.022	5×10^{-5}	0.11×10^{-5}
Two components fail in fatigue, (i=2)	C_2: BM35-Jt4	$P(C_1 \cap C_2)$ = 0.022 (= min[$P(C_1)$, $P(C_2)$])	6.2×10^{-5}	0.14×10^{-5}
Three components fail in fatigue, (i=3)	C_3: BM23-Jt15	$P(C_1 \cap \ldots \cap C_3)$ = 0.001 (= min[$P(C_1)$,…, $P(C_3)$])	7×10^{-5}	0.007×10^{-5}
Four components fail in fatigue, (i=4)	C_4: BM24-Jt14	$P(C_1 \cap \ldots \cap C_4)$ = 0.001 (= min[$P(C_1)$,…, $P(C_4)$])	7.7×10^{-5}	0.0077×10^{-5}
Five components fail in fatigue, (i=5)	C_5: BM11-Jt4	$P(C_1 \cap \ldots \cap C_5)$ = 0.001 (= min[$P(C_1)$,…, $P(C_5)$])	8.8×10^{-5}	0.0088×10^{-5}
Six components fail in fatigue, (i=6)	C_6: BM12-Jt3	$P(C_1 \cap \ldots \cap C_6)$ = 0.001 (= min[$P(C_1)$,…, $P(C_6)$])	10.5×10^{-5}	0.011×10^{-5}
$P(F_{sys}) = POF_0 + POF_1 + POF_2 + \ldots + POF_6$				= 4.03×10^{-5}
Corresponding reliability index ($\beta = -\emptyset^{-1}[P(F_{sys})]$)				= 3.95

Table 4.9. The probability of failure for the second failure path

Sequence	Component	P ($C_1 \cap \ldots \cap C_i$)	P(Ext| $C_1 \cap \ldots \cap C_i$)	POF_i = [P ($C_1 \cap \ldots \cap C_i$)] x [P(Ext| $C_1 \cap \ldots \cap C_i$)]
No component failure	----	P(intact) = 0.934	4×10^{-5}	3.74×10^{-5}
One component fails in fatigue, (i=1)	C_1: BM12-Jt3	P(C_1) = 0.018	5.1×10^{-5}	0.09×10^{-5}
Two components fail in fatigue, (i=2)	C_2: BM11-Jt4	$P(C_1 \cap C_2)$ = 0.018 (= min[$P(C_1)$, $P(C_2)$])	6.1×10^{-5}	0.11×10^{-5}
Three components fail in fatigue, (i=3)	C_3: BM34-Jt14	$P(C_1 \cap \ldots \cap C_3)$ = 0.014 (= min[$P(C_1)$,…, $P(C_3)$])	6.9×10^{-5}	0.10×10^{-5}
Four components fail in fatigue, (i=4)	C_4: BM36-Jt3	$P(C_1 \cap \ldots \cap C_4)$ = 0.014 (= min[$P(C_1)$,…, $P(C_4)$])	7.5×10^{-5}	0.11×10^{-5}
Five components fail in fatigue, (i=5)	C_5: BM23-Jt15	$P(C_1 \cap \ldots \cap C_5)$ = 0.003 (= min[$P(C_1)$,…, $P(C_5)$])	8.6×10^{-5}	0.026×10^{-5}
Six components fail in fatigue, (i=6)	C_6: BM24-Jt14	$P(C_1 \cap \ldots \cap C_6)$ = 0.003 (= min[$P(C_1)$,…, $P(C_6)$])	10.3×10^{-5}	0.031×10^{-5}
$P(F_{sys}) = POF_0 + POF_1 + POF_2 + \ldots + POF_6$				= 4.21×10^{-5}
Corresponding reliability index ($\beta = -\emptyset^{-1}[P(F_{sys})]$)				= 3.93

Table 4.10. The probability of failure of the third failure path

Sequence	Component	P ($C_1 \cap \ldots \cap C_i$)	P(Ext| $C_1 \cap \ldots \cap C_i$)	POF_i = [P ($C_1 \cap \ldots \cap C_i$)] x [P(Ext| $C_1 \cap \ldots \cap C_i$)]
No component failure	----	P(intact) = 0.934	4×10^{-5}	3.74×10^{-5}
One component fails in fatigue, (i=1)	C_1: BM34-Jt14	$P(C_1) = 0.01$	5.1×10^{-5}	0.051×10^{-5}
Two components fail in fatigue, (i=2)	C_2: BM36-Jt3	$P(C_1 \cap C_2) = 0.01$ (= min[$P(C_1)$, $P(C_2)$])	6.2×10^{-5}	0.062×10^{-5}
Three components fail in fatigue, (i=3)	C_3: BM491-Jt9	$P(C_1 \cap \ldots \cap C_3) = 0.01$ (= min[$P(C_1)$,…, $P(C_3)$])	8.7×10^{-5}	0.087×10^{-5}
Four components fail in fatigue, (i=4)	C_4: BM47-Jt21	$P(C_1 \cap \ldots \cap C_4) = 0.01$ (= min[$P(C_1)$,…, $P(C_4)$])	10.4×10^{-5}	0.104×10^{-5}
$P(F_{sys}) = POF_0 + POF_1 + POF_2 + \ldots + POF_4$				$= 4.04 \times 10^{-5}$
Corresponding reliability index ($\beta = -\emptyset^{-1}[P(F_{sys})]$)				= 3.95

Table 4.11. The probability of failure of the fourth failure path

Sequence	Component	P ($C_1 \cap \ldots \cap C_i$)	P(Ext| $C_1 \cap \ldots \cap C_i$)	POF_i = [P ($C_1 \cap \ldots \cap C_i$)] x [P(Ext| $C_1 \cap \ldots \cap C_i$)]
No component failure	----	P(intact) = 0.934	4×10^{-5}	3.74×10^{-5}
One component fails in fatigue, (i=1)	C_1: BM24-Jt14	$P(C_1) = 0.008$	4.9×10^{-5}	0.039×10^{-5}
Two components fail in fatigue, (i=2)	C_2: BM23-Jt15	$P(C_1 \cap C_2) = 0.008$ (= min[$P(C_1)$, $P(C_2)$])	6×10^{-5}	0.048×10^{-5}
Three components fail in fatigue, (i=3)	C_3: BM36-Jt3	$P(C_1 \cap \ldots \cap C_3) = 0.008$ (= min[$P(C_1)$,…, $P(C_3)$])	6.8×10^{-5}	0.054×10^{-5}
Four components fail in fatigue, (i=4)	C_4: BM35-Jt4	$P(C_1 \cap \ldots \cap C_4) = 0.008$ (= min[$P(C_1)$,…, $P(C_4)$])	7.4×10^{-5}	0.059×10^{-5}
Five components fail in fatigue, (i=5)	C_5: BM491-Jt9	$P(C_1 \cap \ldots \cap C_5) = 0.008$ (= min[$P(C_1)$,…, $P(C_5)$])	8.5×10^{-5}	0.068×10^{-5}
Six components fail in fatigue, (i=6)	C_6: BM47-Jt21	$P(C_1 \cap \ldots \cap C_6) = 0.008$ (= min[$P(C_1)$,…, $P(C_6)$])	10.1×10^{-5}	0.081×10^{-5}
$P(F_{sys}) = POF_0 + POF_1 + POF_2 + \ldots + POF_6$				4.09×10^{-5}
Corresponding reliability index ($\beta = -\emptyset^{-1}[P(F_{sys})]$)				= 3.94

4.5.5.2 Total System Probability of Failure

In terms of series and parallel systems, a failure path which is a sequence of individual failures that leads to structural collapse forms the parallel system. That means all the components in the failure path need to be failed before overall failure occurs.

Due to the high redundancy of the jacket structures, several alternate sequences (failure paths) leading to collapse exist. The event that the structure failure occurs is the event that one of these collapse sequences occurs. Therefore, the combination of all these sequences represents a series system.

In other words, it is assumed that the structural system is a series of parallel systems, in which each parallel system represents a failure path.

Since a correlation exists between the important failure paths, the calculation of the exact amount of the system probability of failure is quite difficult. The estimation of system probability is, therefore, dependent on the correlation of the important failure paths. In this case, the system probability of failure is determined using the bound formulas (e.g., Simple bound, Ditlevsen bounds, etc.) for the series systems.

Simple bounds are useful to find out the upper and lower bounds of the system probability of failure. In the simple bounds, only two situations are considered:

- Failure paths are fully correlated.
- Failure paths are statistically independent.

For a series system, the probability of failure is within the following bounds [66]:

$$\max_i \left[P_f(E_i)\right] \leq \left(P_f^{sys}\right)_{series} \leq 1 - \prod_{i=1}^{n} \left(1 - P_f(E_i)\right) \qquad (4\text{-}5)$$

The lower bound corresponds to a situation in which all failure components are fully correlated. In this case, all the failure cases represent the same failure, and all the components will fail if one of them fails. Therefore, the maximum probability of failure can be selected as the system probability of failure. The upper bound corresponds to a situation in which all failure components are statistically independent.

The reliability of a series system decreases with an increasing number of its elements. For a given system, with a fixed number of components, system reliability decreases with decreasing correlation between pairs of elements.

The upper and lower bound of the probability of failure (simple bound) can be obtained based on Eq. (4-5) as:

$$\underset{k=1,\dots,4}{max}\left(P_k(F_{sys})\right) \le P_{System}(F_{sys}) \le 1 - \prod_{k=1,\dots,4}\left(1 - P_k(F_{sys})\right) \tag{4-26}$$

Where $P_{System}(F_{sys})$ is the total system probability of failure and $P_k(F_{sys})$ represents the probability of failure for each path.

Using Eq. (4-26), the system probability of failure of the jacket platform is calculated between the below ranges:

$$4.21 \times 10^{-5} \le P_{System}(F_{sys}) \le 16.4 \times 10^{-5} \tag{4-27}$$

However, due to the existence of correlations between the failure paths, it is better to use other bounds formulas for estimation of system probability of failure such as Ditlevsen bounds [10].

The Ditlevsen lower bound for the series system is obtained as [68]:

$$P_{System}(F_{sys}) \ge \underset{k=1,\dots,4}{max}\left(P_k(F_{sys})\right) + \sum_{i=2}^{4}\left\{\emptyset\left(-\beta_i\right) - \sum_{j=1}^{i-1}\emptyset_2\left(-\beta_i, -\beta_j; \rho_{ij}\right)\right\} \tag{4-28}$$

The Ditlevsen upper bound for the series system is obtained as [68]:

$$P_{System}(F_{sys}) \le \sum_{k=1}^{4} P_k(F_{sys}) - \sum_{i=2}^{4}\max_{j<i}\emptyset_2\left(-\beta_i, -\beta_j; \rho_{ij}\right) \tag{4-29}$$

In the above equations:

$$max\left(p_i, p_j\right) \le \emptyset_2\left(-\beta_i, -\beta_j; \rho_{ij}\right) \le p_i + p_j$$

$$p_i = \emptyset\left(-\beta_i\right) \times \emptyset\left(-\gamma_j\right) \tag{4-30}$$

$$p_j = \emptyset\left(-\beta_j\right) \times \emptyset\left(-\gamma_i\right)$$

Where:

$$\gamma_i = \frac{\beta_i - \rho_{ij}\beta_j}{\sqrt{1-\rho_{ij}^2}}$$
$$\gamma_j = \frac{\beta_j - \rho_{ij}\beta_i}{\sqrt{1-\rho_{ij}^2}} \quad (4\text{-}31)$$

It is noted that for the lower Ditlevsen bound, the upper bounds of $\emptyset_2(-\beta_i, -\beta_j; \rho_{ij})$ are used and for the upper Ditlevsen bound, the lower bounds of $\emptyset_2(-\beta_i, -\beta_j; \rho_{ij})$ are used [10].

As it can be seen from the above equations, to use the Ditlevsen bound formulas, the correlation coefficients between the dominant failure paths are required.

Table 4.12 shows the components in the dominant failure paths.

Table 4.12. Components in the dominant failure paths

Component	Existence in failure paths			
	Path #1	Path #2	Path #3	Path #4
BM36-Jt3	✓	✓	✓	✓
BM35-Jt4	✓	---	---	✓
BM23-Jt15	✓	✓	---	✓
BM24-Jt14	✓	✓	---	✓
BM11-Jt4	✓	✓	---	---
BM12-Jt3	✓	✓	---	---
BM34-Jt14	---	✓	✓	---
BM491-Jt9	---	---	✓	✓
BM47-Jt21	---	---	✓	✓

Since the jacket platforms are highly redundant structures, calculation of the correlation coefficients between different failure paths (e.g., ρ_{12}; the correlation between path 1 and path 2) is difficult. To estimate the correlation coefficients, the similarity coefficients for binary data can be used [84]. The similarity coefficients for binary data are calculated as the number of cases in which a component exists in both cases over the total number of cases [84]. For instance, the similarity coefficient for paths No.1 and No.2 is 5/7.

Table 4.13 shows the similarity coefficients for the dominant failure paths.

Table 4.13. Similarity coefficients for the dominant failure paths

ρ_{12}	ρ_{13}	ρ_{14}	ρ_{23}	ρ_{24}	ρ_{34}
$^5/_7 = 0.71$	$^1/_9 = 0.11$	$^4/_8 = 0.5$	$^2/_8 = 0.25$	$^3/_9 = 0.33$	$^3/_7 = 0.43$

Having estimated the correlation coefficients, values of γ_i and γ_j are calculated using Eq. (4-31). Table 4.14 shows the values γ_i and γ_j for the failure paths. The table is a matrix that γ_i is shown in the lower triangle and γ_j is shown in the upper triangle.

Table 4.14. Calculated values of γ_i and γ_j

		γ_j		
	---	1.61	3.53	2.28
	1.61	---	3.06	2.79
γ_i	3.53	3.06	---	2.50
	2.28	2.79	2.50	---

Table 4.15 shows the bounds for $\emptyset_2(-\beta_i, -\beta_j; \rho_{ij})$ for the dominant failure paths by using Eq. (4-30) and (4-31).

Table 4.15. The upper and lower bounds of the $\emptyset_2(-\beta_i, -\beta_j; \rho_{ij})$

Failure path i, j	p_i	p_j	$max\ (p_i,\ p_j)$	$p_i + p_j$
1, 2	9.2×10^{-6}	10.5×10^{-6}	10.5×10^{-6}	19.7×10^{-6}
1, 3	1.6×10^{-7}	2.1×10^{-7}	2.1×10^{-7}	3.7×10^{-7}
1, 4	8.3×10^{-7}	9.2×10^{-7}	9.2×10^{-7}	1.7×10^{-6}
2, 3	9.0×10^{-8}	9.9×10^{-8}	9.9×10^{-8}	1.9×10^{-7}
2, 4	2.3×10^{-6}	2.0×10^{-6}	2.3×10^{-6}	4.3×10^{-6}
3, 4	5.1×10^{-7}	4.2×10^{-7}	5.1×10^{-7}	9.3×10^{-7}

Having obtained the bounds for $\emptyset_2(-\beta_i, -\beta_j; \rho_{ij})$, the lower Ditlevsen bound is estimated using Eq. (4-28) as:

$$P_{System}(F_{sys}) \geq 4.21 \times 10^{-5} + (4.03 \times 10^{-5} - 19.7 \times 10^{-6}) + (4.04 \times 10^{-5} - (3.7 + 1.9) \times 10^{-7}) + (4.09 \times 10^{-5} - (1.7 + 4.3 + 0.93) \times 10^{-6})$$

$$P_{System}(F_{sys}) \geq 13.6 \times 10^{-5}$$

The upper Ditlevsen bound is estimated using Eq. (4-29) as:

$$P_{System}(F_{sys}) \leq 4.21 \times 10^{-5} + 4.03 \times 10^{-5} + 4.04 \times 10^{-5} + 4.09 \times 10^{-5} - (10.5 \times 10^{-6}) - max(2.1 \times 10^{-7}, 9.9 \times 10^{-8}) - max(9.2 \times 10^{-7}, 23 \times 10^{-7}, 5.1 \times 10^{-7})$$

$$P_{System}(F_{sys}) \leq 15.1 \times 10^{-5}$$

Therefore, using the Ditlevsen bounds formula, the system probability of failure of the considered jacket platform is estimated in the below ranges:

$$13.6 \times 10^{-5} \leq P_{System}(F_{sys}) \leq 15.1 \times 10^{-5}$$

It is seen that the Ditlevsen bounds provide a narrower range than the simple bounds (Eq. (4-27). Since the Ditlevsen bounds consider the correlation between the failure paths, they are much more precise than the simple bounds, but require the estimation of $\emptyset_2(-\beta_i, -\beta_j; \rho_{ij})$ [10].

4.5.5.3 Limitations

Jacket platforms are typically redundant structures, and structural failure is a progressive process. A sequence of individual member failures is required before overall structural failure. Usually, several sequences leading to collapse exist. Estimation of the system probability of failure is a difficult task due to:

- For redundant structures, there are several sequences leading to failure
- It is not practical to include all the sequences in the analysis

Since a few of these failure sequences have significant contributions to the total failure probability, a search technique is used to identify important failure sequences.

In general, there are some limitations in the estimation of the system probability of failure [8]:

- The possible failure paths for jacket structures with high redundancy would be enormous.
- Some important failure paths might be ignored if rapid truncation criteria are used.
- The procedure for estimating the system probability of failure is computationally expensive.
- Due to not considering all possible sequences, the system failure is approximated as the union of the important sequences.

- Due to not considering the correlation between the dominant failure paths, simple bounds are generally too wide.
- To find out a narrow range for system probability, better bounds such as Ditlevsen bounds. However, since the second-order calculation (i.e., $\emptyset_2(-\beta_i, -\beta_j; \rho_{ij})$ values) is required which is a time-consuming task.

4.5.6 Inspection Plan

Fatigue is a complicated phenomenon and there are several sources of uncertainty in the fatigue calculation process. Therefore, small changes in basic assumptions can have a significant influence on the predicted crack size and consequently on the probability of failure. Due to the uncertain parameters involved in the fatigue calculation process, there will be uncertainty about when and where fatigue cracks will occur in a structure.

Inspection activities can be performed to find out the level of degradation and to assure that existing defects in the structure do not exceed the critical size during the service life. Inspection program usually involves checking of any structural damage, adequacy of the cathodic protection system, corrosion damage, extent of marine growth, sea bed scour, damage to tubular joints due to overloading or fatigue crack growth, etc.

Since the focus of this study is on the fatigue degradation in the tubular joints, this section considers the inspection methods to find out the fatigue cracks. The purpose of the inspection is then to detect a crack that is likely to have developed during the structure's lifetime [15].

Inspections can be divided into two categories:

- Close visual inspection to detect hidden damage
- Close visual and non-destructive testing to detect developing cracks or hidden damage

For both categories, prior cleaning is usually carried out before performing inspections.

4.5.6.1 Non-Destructive Test

The inspection methods involve visual inspection or more detailed inspection methods. The in-service inspections are commonly carried out by applying the Non-Destructive Tests (NDT).

Different NDT techniques may be relevant for different types of offshore structures. Magnetic particle inspection (MPI), eddy current inspection (ECI), alternating current field measurement (ACFM), and flooded member detection (FMD) are some NDT methods usually used for detecting cracks in offshore structures [1].

MPI is a suitable technique for detecting surface flaws. In this technique, a magnetic field is induced in the body to be examined, either by passing a large electric current through it or by attaching magnets. Iron filings in light oil or water suspension are applied to the surface. The iron filings will gather around the defects and make them visible [1].

ECI is frequently used for inspection of fatigue cracks during service life as this method can detect cracks through the coating. However, if defects are detected, a further assessment by MPI is recommended. The practical advantage of MPI is that it does not require a clean surface [5]. ACFM may also be used in and out of water. The use of ACFM requires minimal cleaning and the method can be applied over paint and other coatings up to several millimetres in thickness [85]. FMD is considered efficient at hot spots where potential fatigue cracks are likely to grow into air-filled members.

4.5.6.2 Probability of Detection

The findings and the reliability of the inspection results highly depend on the method employed for inspection and the quality of crew involved with [15]. The success rate of inspection techniques to detect and measure the crack size varies. For any given NDT method there is always a critical crack size below which a crack may not be detected. It is noted that there is a certain degree of uncertainty for a measured crack which depends on the accuracy of the equipment used and the skills of the operators [1].

The reliability of a specific NDT method is described by the ability to detect an existing crack as a function of the crack size and by the uncertainty associated with the sizing of an identified crack [19].

The detection ability (quality of NDT methods for detection of cracks) of the NDT methods is defined through the Probability of Detection (POD) curves which corresponds to the distribution function of detectable crack size (a_d).

Different industrial projects have been carried out to obtain the POD curves for various NDT techniques such as [86], [87], and [88]. Some guidance on POD and uncertainty of sizing of defects is also included in BS 7910 [47], NORSOK N-006 [89], and DNVGLRP- C210 [90].

NORSOK N-006 presented POD curves for inspection on the following form [89]:

$$POD(a_d) = 1 - \frac{1}{1 + \left({a_d}/{X_0}\right)^b} \tag{4-32}$$

In this equation:

- a_d: Detectable crack depth
- X_0: Median value for the POD
- b: Distribution parameter

where the values for X_0 and b depend on the NDT technique.

Table 4.16 shows the typical values for X_0 and b for different inspection techniques in offshore platforms. The corresponding POD curves are shown in Figure 4.15.

Table 4.16. Distribution parameter for MPI method [85]

Description	X_0	b
At ground welds or similar good conditions above water	0.40	1.43
Normal working conditions above water	0.45	0.90
Below water or less good working conditions above water	1.16	0.90

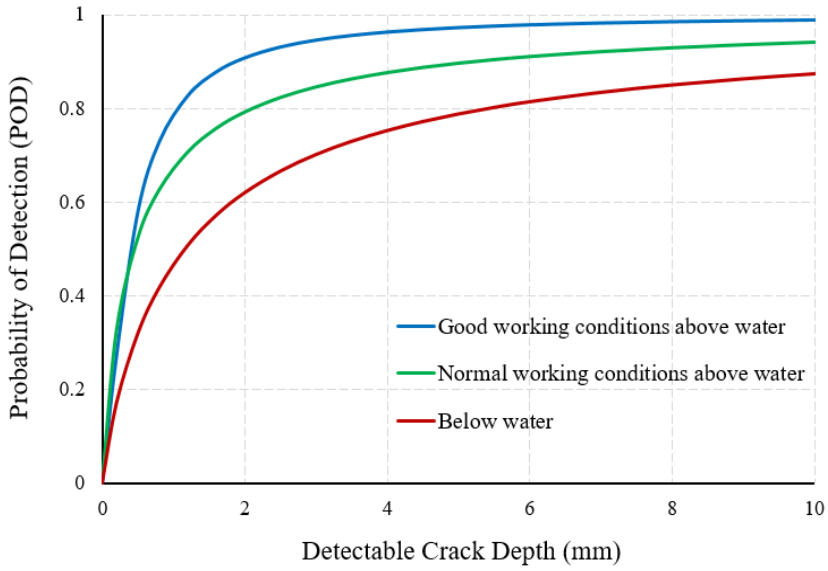

Figure 4.15. POD curves for MPI method in different conditions

Each inspection method is associated with a given probability of detection depending on the size of the crack and depending on whether the inspection is carried out above or below water.

The distribution of the detectable crack can be also modelled by an upward bounded exponential distribution as [82]:

$$POD\ (a_d)\ =\ 1 - exp\left(-\frac{a_d}{a_{md}}\right) \tag{4-33}$$

where a_{md} is model parameters (mean detectable size) which may be determined by tests and different for each technique. The value of the mean detectable size is typically between 1.4 to 2 mm. Mean detectable depth of 1.95 mm was considered for a POD curve with exponential distribution based on data from 3411 underwater NDT inspections of tubular joints in jacket platforms [82].

It is noted that the actual conditions during the inspection may be different from the testing conditions which are the basis of developing the POD curves. The quality of NDT methods depends on the conditions during the inspection. For example, the underwater inspections of jackets, are carried out under difficult conditions, due to the presence of marine growth, bad visibility, wave motions, etc. [82]. Before performing an underwater inspection, a time-consuming cleaning of the welded joints is needed which causes the high costs of underwater inspections.

4.5.6.3 Use of Inspection Results

Due to the existence of several uncertainties in the fatigue process, the predicted fatigue crack size might not represent the real crack size. Offshore platforms are periodically inspected throughout their lifetime. Regarding fatigue damage, the inspection results involve the detection and measurement of fatigue cracks. The inspection results can be used to revise and improve the estimation of the crack size. In general, a Bayesian procedure is utilised to update the fatigue crack size distribution in the light of inspection results. The Bayesian methods for updating the crack size distribution will be explained in Chapter 5.

When no crack is found, there may be a case that the fatigue model is conservative, however, if no crack is found, there is a probability that there is a crack but it is not detected.

4.5.6.4 Inspection Time

The object of structural inspection is to control the probabilities of failure [51]. Generally, two approaches exist for the inspection time (inspection intervals). The first approach is to set the inspection interval to a fixed and equal period value of ΔT, e.g. every four years. The interval is defined based on the consequence of failure of the platform.

The other approach which is called the reliability-based inspection approach is to set the annual failure probability threshold to be a fixed value and the inspection is carried out when the failure probability is more than the threshold. The members of the structure are classified into different categories depending on their contribution to the system reliability. The minimum target reliability of the members of each category is fixed depending on their importance [15]. Several studies have been carried out in reliability-based inspection planning and its implementation for offshore platforms (See [91], [92]).

The optimum time to make the inspection is when the probability of failure reaches the target annual probability of failure. Figure 4.16 shows the inspection plan for a tubular joint in case of no crack detection.

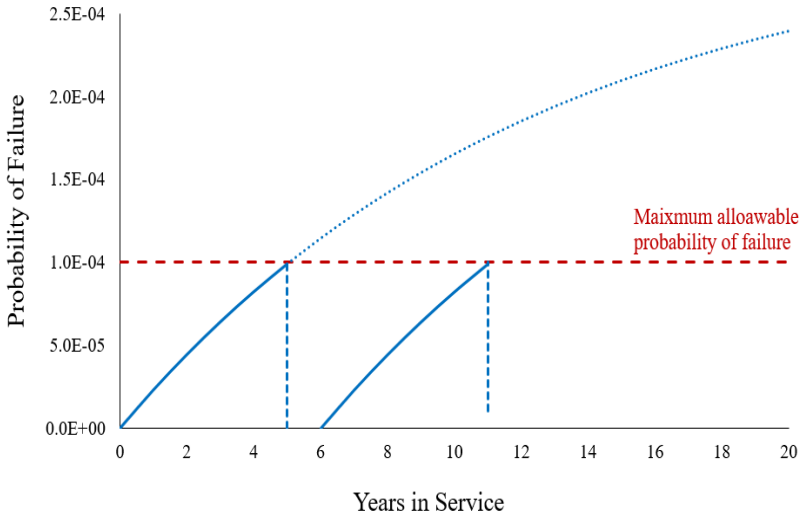

Figure 4.16. Inspection plan for a specific joint assuming no crack findings at inspections

4.5.6.5 Prioritising the Inspection Locations

The cost of an inspection is directly proportional to the number of inspections carried out and the quality of personnel and equipment employed for the inspection [15]. Therefore, it is required to concentrate only on the fatigue-sensitive locations in the structures. At the component level, the fatigue-sensitive locations are the locations that have low estimated fatigue lives. However, at the system level, critical components are those that have a big effect on system reliability.

Due to the significant costs of inspections, the identified failure paths can be used as a database for the inspection plan. By identifying these dominant failure paths, the critical joints that have a greater effect on the system probability of failure are selected and therefore inspection can be focused on these joints.

For the considered platform in this study, it is observed that the most probable failure paths of the considered platform pass through the top bay. Therefore, the inspection effort should focus on the joints in the upper bay because the failure of these joints would initiate or propagate a failure sequence, resulting in system failure. Table 4.17 shows the importance of each critical component on the system reliability.

Table 4.17. Importance of the critical components in the system failure

Component	Location	Existence in failure paths	Inspection importance
BM36-Jt3	Top bay	Exist in 4 possible paths (all paths)	Crucial
BM23-Jt15	Top bay	Exist in 3 possible paths	Important
BM24-Jt14	Top bay	Exist in 3 possible paths	Important
BM35-Jt4	Top bay	Exist in 2 possible paths	Relatively important
BM11-Jt4	Top bay	Exist in 2 possible paths	Relatively important
BM12-Jt3	Top bay	Exist in 2 possible paths	Relatively important
BM34-Jt14	Top bay	Exist in 2 possible paths	Relatively important
BM491-Jt9	Top bay	Exist in 2 possible paths	Relatively important
BM47-Jt21	Top bay	Exist in 2 possible paths	Relatively important

4.6 Summary

In this chapter, a system reliability approach is developed to calculate the probability of failure of a jacket platform considering fatigue and extreme wave loads. To specify a formulation for the fatigue limit state, the fracture mechanics is used to obtain the crack size. A joint fails when the crack size exceeds the critical crack size. Different uncertainties in fatigue are introduced and the probability of failure of each joint is obtained by using the Monte-Carlo simulation.

Due to the high redundancy of the offshore jacket platform, the probability of failure of the whole system is more applicable than the component probability of failure. Important failure paths are identified by using a searching algorithm, in which, components with the maximum change in the accumulated damage are considered as the candidate joints in the path.

By removing the candidate joint, which is assumed to fail in fatigue, the probability of failure of the structure under extreme wave loading increases.

The system failure criterion is evaluated by comparing the platform strength and loading distributions in terms of base shear. To define a probabilistic formula for load, the global response surface method is adopted to relate the environmental load to the response of the structure. Nonlinear pushover analysis is also carried out to determine the capacity of the platform. Having calculated the structure strength and loading distributions, the annual probability of failure under an extreme wave is calculated and

compared to the maximum probability of failure. When this probability exceeds the maximum acceptable probability, the platform is assumed to fail

To estimate the system probability of failure, four significant failure sequences are identified in the branch tree leading to structural collapse. The system probability of failure is approximated based on the union of the probability of failure of the important paths using the simple bounds formula.

The results of the system reliability analysis show that the calculated system failure probability in a combination of fatigue and extreme wave loads gives a much lower failure probability than the component probability of failure in fatigue loading.

Since the components in the failure paths have a great effect on the system reliability, an inspection strategy is proposed based on the effect of each component on the system reliability. This allows alternative inspection plans to be evaluated and compared to the regular inspection plans.

5 . BAYESIAN INFERENCE

5.1 Introduction

In Chapter 2, the concept of reliability analysis is explained and the application of the reliability analysis at the component level and system level is demonstrated for an offshore platform in Chapter 3 and Chapter 4, respectively.

Reliability analysis, which is a probabilistic approach, is a consistent basis for the inclusion of uncertainties. Since the reliability analysis results depend on the choice of the uncertain parameters and their statistical description, uncertainty modelling becomes an important consideration for reliability analysis [92].

As it is explained in Chapter 2, three different definitions of probability exist in the literature; classical definition, relative-frequency definition, and Bayesian definition. This chapter mainly focuses on Bayesian inference. Bayesian inference is a statistical inference in which Bayes' theorem is employed to update the probability for a hypothesis when more information becomes available.

The main purpose of this chapter is to explain Bayesian inference and to investigate the effects of different assumptions and methods.

Section 5.2 introduces the Bayesian framework and the terminology in this context. There are two main approaches for updating the distribution of an uncertain parameter; the analytical approach and the numerical approach. These two approaches and their advantages and disadvantages are also introduced in this section.

Section 5.3 provides some of the previous studies that have been performed to incorporate the information from inspection results to update the fatigue crack model and the reliability analysis results.

The application of Bayesian updating is demonstrated in Section 5.4. This section investigates how the crack size distribution in a tubular joint can be updated when additional information such as inspection results becomes available. The inspection data is used to improve the previous estimate of an uncertain parameter which is crack size. The updating process is carried out in both analytical and numerical approaches and the results of the two approaches are compared. In real situations, due to the expensive cost of the underwater inspection, there are a few inspection results

available for each tubular joint. Section 5.4 also demonstrates how to use the inspection results of similar tubular joints to update the crack size distribution for different locations. After updating the crack size distribution, the reliability analysis can be updated using the crack size distribution. An application of updating the reliability as a function of time is also presented in Section 5.4.

Several important parameters (e.g. selection of the prior distribution, inspection outcomes, POD curves, and the number of inspections) have effects on the updated distribution of the uncertain parameter. The sensitivity of the Bayesian updating to the inputs is investigated in Section 5.5.

It is worth mentioning that in this Chapter, Section 5.2 and Section 5.3 explain the Bayesian framework, whereas, Section 5.4 and Section 5.5 demonstrate the application of the Bayesian approach to the considered tubular joint that has been developed by the author.

5.2 Bayesian Framework

5.2.1 Basics

Thomas Bayes (1702–1761) was a British mathematician who is well known for his paper "An essay towards solving a problem in the doctrine of chances" [93], which was published two years after his death. In this work, it was stated that the probability of an event (first event) conditional on another event (second event) is simply the ratio of the probability of both events to the probability of the second event, which is the definition of conditional probability. It was shown that conditional probability can be expressed regardless of the order in which the events occur.

In the area of statistical analysis, there are three main approaches for the definition of probability; Classical, Relative frequency, and Bayesian inference approach. These approaches are explained in Chapter 2. The first two methods can be only applied to an event whose random experiments are available. On the other hand, Bayesian inference allows the definition for the probability of an event or a statement, in which a random experiment is not available. This offers a different dimension of probability for the degree of belief, which is regarded as plausibility [94].

The Bayesian theory has had great advancement after the significant work by Jeffreys [95], Cox [96], and Jaynes [97]. Since then, different Bayesian methods have been developed and widely applied to many different areas of engineering, especially in statistical physics (e.g. [98] and [99]), structural dynamics [100], and medical sciences (e.g. [101] and [102]).

Bayesian inference is very useful in structural engineering. As mentioned in Chapter 3, there are many uncertainties in structural engineering applications such as an offshore platform. For example, load excitation, such as time-varying waves, cannot be predetermined. Material properties such as yield stress are difficult to determine to a precise level. The size of cracks in welded connections is also uncertain. There are also modelling errors, such as SCF (Stress Concentration Factor) assumptions. Therefore, the Bayesian method is useful for explicit action of the modelling and quantification of the uncertainties.

The idea of Bayesian updating is similar to our thinking process. We have a perception of a specific matter based on our experience. When a new event happens (i.e., new data is obtained), it modifies our perception. In other words, our perception is not only determined by the latest piece of information but also depends on the original perception. In Bayesian analysis, the original perception is regarded as the prior information and the new piece of information is utilised to update our perception or mathematical model.

In general, model updating is performed for two main purposes. The first one is to identify physical parameters, e.g., stiffness of a structural element. Using these parameters, the condition of the element can be monitored from time to time. For example, a reduction indicates possible damage to the member. However, reduction may be due to statistical uncertainty. Therefore, it is necessary to quantify the uncertainty of the estimation so that one can distinguish whether the parameter change is due to the deterioration of the structural member [94]. Another purpose of model updating is to obtain a mathematical model to predict the behaviour of an element (or system). In this case, parameters may not necessarily be physical, e.g., coefficients of regressive models.

5.2.1.1 Conditional Probability

Consider A and B as two events. The conditional probability of event A provided the occurrence of event B is given by:

$$P(A|B) = \frac{P(A \cap B)}{P(B)}, \quad [if\ P(B) \neq 0] \tag{5-1}$$

Conditional probability does not necessarily imply a reason-consequence relationship. However, if the conditional probability is large, there is a possibility of event A being a consequence of B or the opposite.

The law of total probability is usually used in the context of conditional probability. If event A is subdivided into n mutually exclusive events $(A_1, A_2, \ldots, A_n)$, then the probability of event B is given by [103]:

$$P(B) = \sum_{i=1}^{n} P(B \cap A_i) = \sum_{i=1}^{n} P(B|A_i) \times P(A_i) \tag{5-2}$$

Therefore, Bayes' theorem can be obtained as:

$$P(A|B) = \frac{P(A \cap B)}{P(B)} = \frac{P(B|A) \times P(A)}{\sum_{i=1}^{n} P(B|A_i) \times P(A_i)} \tag{5-3}$$

The law of total probability is also used for continuous events. In this case, Eq. (5-3) is written as:

$$f(x|y) = \frac{f(y|x) \times f(x)}{\int_{-\infty}^{\infty} f(y|x) \times f(x) \times dx} \tag{5-4}$$

where $f(x)$ and $f(y)$ is the probability density function that describes the random variable x and y, respectively.

5.2.1.2 Bayesian Inference

When additional information such as experimental data, and inspection results become available, the obtained information can be used to improve the previous estimate of uncertain parameters. The framework for updating the distribution of estimated parameters is called the Bayesian framework [104]. A Bayesian framework is a powerful tool for uncertainty management. Bayesian inference provides a normative and formal method of belief updating when new information, becomes available [105].

In the Bayesian framework, the uncertain parameters are treated as random quantities [94].

The distribution that describes our knowledge after incorporating new data is called posterior distribution. The posterior distribution of the uncertain parameter given new information is available can be obtained by using Bayes' theorem as [94]:

$$f(\theta|x) = \frac{f(x|\theta) \times f(\theta)}{f(x)} = \frac{Likelihood \times Prior}{Normalisation} \tag{5-5}$$

With:

$$f(x) = \int_{-\infty}^{\infty} f(x|\theta) \times f(\theta) \times d\theta \tag{5-6}$$

In the Bayesian context:

- θ represents the uncertain parameter which its probability is affected by new data;
- $f(\theta)$ represents the prior probability distribution, and it is the estimate of the probability of the uncertain parameter before the new data is available;
- x represents the new data;
- $f(\theta|x)$ represents the posterior probability distribution, which is the probability of θ given x (i.e., after taking account of the value of x);
- $f(x|\theta)$ represents the likelihood function and it is the conditional probability of observing x given θ
- $f(x)$ represents the marginal probability of the data. It is obtained by integrating out the parameters from the joint probability. It does not depend on the uncertain parameter since it has been integrated out.

In general, numerical integration is required to obtain the normalisation constant, $f(x)$. However, in some cases, it can be obtained analytically (See Section 5.2.2). The normalisation constant is a constant that ensures the posterior density integrates equal to one [94], as it must be a valid probability density.

Therefore, it is not necessary to calculate $f(x)$ to evaluate properties of the posterior, and so Bayes' theorem in this context can be expressed simply as:

$$f(\theta|x) \propto f(x|\theta) \times f(\theta) \quad (5\text{-}7)$$

Where the proportionality is considered with relation to θ. Hence, Bayes theorem essentially states that:

$$Posterior \propto Likelihood \times Prior \quad (5\text{-}8)$$

In the Bayesian framework, the likelihood function and the prior distributions are the basis for parameter estimation and inference. The prior distribution, $f(\theta)$ expresses the previous knowledge about the uncertain parameter before new information is available. The likelihood function, $f(x|\theta)$ is defined to describe how likely is the data to happen for a given uncertain parameter [106]. The likelihood function describes how the data depends on the parameter values.

- **Likelihood Function**

  The likelihood function, $f(x|\theta)$ represents the contribution of the measured data in establishing the posterior distribution of the parameter of interest. It reflects how likely the measurements are observed from the model with a particular set of parameters. The likelihood function can be constructed given the class of probabilistic and physical models of the problem. If a large amount of measurements (data) is available, the likelihood function will be the dominant factor for the Bayesian inference.

- **Prior Distributions**

  The prior distribution indicates the prior information of the parameters of interest and it is based on previous knowledge or the user's judgement. The prior distribution plays an essential role in Bayesian analysis.

  Prior distributions are classified as either informative or non-informative (also known as reference or vague). The latter is intended for use in situations where there is not enough knowledge about the uncertain parameter. The term non-informative is misleading since all priors contain some information, so such priors are generally better referred to as vague or diffuse [107].

  A non-informative prior distribution contains little information about the parameter of interest [108]. When no expert opinion is available, i.e., knowledge about the parameter being estimated, it is recommended to use a non-informative prior

distribution [109]. It should be noted that this is rarely the case in practice, and usage of non-informative priors in such cases can lead to poor results [108]. However, it can be used when the analyst wants to use a prior that has little impact on the posterior. Non-informative priors, in general, are intended to let the data dominate the posterior distribution. Using a non-informative prior distribution causes the Bayesian inference to rely only on the likelihood of the data. The most common non-informative prior for a single parameter inference is the Jeffreys prior. The functional form Jeffreys prior depends on the likelihood function [108].

In some applications, when there is not enough knowledge about the parameter, the non-informative prior distribution is selected as a constant. However, this type of prior distribution does not satisfy the required property of the PDF (Probability Density Function), i.e., that its integral throughout the parametric space is unity. In general, a prior distribution that does not satisfy this property is referred to as an improper prior. For example, a uniform distribution over the whole real line will have an infinite integral. In many circumstances, this is not a problem, as an improper prior can still lead to a proper posterior distribution [107].

In contrast, the informative priors contain substantive information about the possible values of the model parameter. The informative prior distribution is used when there is enough information about the uncertain parameter before collecting data. The use of informative prior distributions includes a considered judgement concerning plausible values of the parameters based on external information [107]. Informative prior distributions can be based on pure judgement, a mixture of data and judgement, or data alone. Of course, even the selection of relevant data involves a substantial degree of judgement, therefore, the specification of an informative prior distribution is never an automatic procedure [107]. Derivation of the informative prior distribution is not a straightforward task due to some potential biases that have been identified. In reliability problems, informative prior distributions can be constructed using physical theory, computational analysis, and expert opinions (e.g., see [106] and [110]). In assessing probability distributions based on expert opinion, many potential biases must be minimised [106].

O'Hagan et al. emphasised that it is best to interview subjects face-to-face, with feedback and continual checking for biases, conducting sensitivity analysis to the consequence of the analysis, and avoiding verbal descriptions of uncertainty. They suggest using multiple experts and reporting a simple average, but it is also important to acknowledge imperfections in the process, and that even genuine expertise cannot guarantee the derivation of a suitable prior [111].

If there is no true prior, sensitivity analysis to alternative prior assumptions is vital and should be an integral part of Bayesian analysis. The phrase "community of priors" has been used in the clinical trial literature to express the idea that different priors may reflect different perspectives [101].

5.2.1.3 Different Uncertainties

When quantifying uncertainty for an unknown phenomenon or a complex system, it is helpful to consider such uncertainty as either epistemic or aleatory. Epistemic uncertainty is due to our lack of knowledge and could be reduced by extra information. On the other hand, the aleatory uncertainty is related to inherent chance variation in the system, and cannot be resolved except by direct observation. The distinction between aleatory and epistemic uncertainty is informal rather than precise, particularly within the view that all uncertainty stems from a lack of knowledge and understanding. Within the Bayesian formulation, the prior distribution can be considered to be an epistemic uncertainty whilst the likelihood function can be considered to be an aleatory uncertainty [112].

There are two main approaches for obtaining the posterior distribution of an uncertain parameter which are:

- Analytical Approach (Conjugate Priors)
- Numerical Approach

5.2.2 Analytical Approach (Conjugate Priors)

Within the Bayesian framework, the parameter θ is treated as a random quantity and the posterior distribution of the uncertain parameter is obtained via Bayes' theorem.

Based on Eq. (5-5), to obtain the posterior distribution, we need to compute $f(x)$ to normalise the posterior. For this purpose, the numerical integral in Eq. (5-6) must be computed which is integral with respect to the prior.

Based on Bayes' theorem, the posterior distribution is obtained by multiplying the likelihood function to the prior distribution up to a constant of proportionality.

In this section, the idea of a conjugate prior is introduced. The basic idea is, given a likelihood $f(x|\theta)$, a family of prior distributions can be chosen in a way that the integral in Eq. (5-6) can be solved analytically (closed-form).

A prior distribution is said to be conjugate to a class of likelihood function if the resulting posterior distribution is in the same probability distribution family as the prior distribution [113]. This family is chosen in a way that the updating yields a posterior that is also in the same family as the prior. Conjugate models are convenient because the exact distribution of the posterior is easily obtained, and it has an analytical solution. The use of conjugate priors allows all the results to be derived in closed form.

Conjugate priors have appealing computational properties and for this reason, they are often used in practice. Conjugate distributions are useful because the prior and posterior distributions have the same form so the contribution of the new data through the updating process can be easily quantified [94]. Since the posterior distributions are already known, the conjugate distributions provide tractable analytical results. Therefore, numerical integration to calculate Eq. (5-6) is not required. The use of conjugate priors allows obtaining the posterior distributions analytically. In the conjugate method, the posterior distribution can be easily updated when new data is available. Commonly used conjugate prior distributions are shown in Table 5.1 [114]. More discussions on the conjugate priors can be found in Appendix A.

Table 5.1 Common conjugate priors

Likelihood	Uncertain Parameter (θ)	Prior Distribution	Posterior Distribution
Binomial	Success probability (π)	Beta	Beta
Poisson	Rate (λ)	Gamma	Gamma
Normal	Mean (μ) [note: σ^2 known]	Normal	Normal
Normal	Variance (σ^2) [note: μ known]	Inverse Gamma	Inverse Gamma
Normal	Mean and Variance (μ, σ^2)	Normal Inverse Gamma	Normal Inverse Gamma
Exponential	Rate (λ)	Gamma	Gamma

It is noted that not every aleatory model will have an associated conjugate prior, and it is sometimes required to use a non-conjugate prior even when a conjugate prior is available [108]. Although for the complex models, the computational considerations are more common, there may be little choice to use conjugate priors. However, there are other reasons not to use conjugate priors.

It is important to note that conjugate priors involve making relatively strong assumptions. Indeed, conjugate priors minimise the impact of the data on the posterior. Therefore, it is important to perform sensitivity analysis to assess how strongly the posterior is influenced by the prior. If the posterior is not influenced strongly by the prior, then it can be used with more confidence. On the other hand, if the posterior is affected intensely by the prior, great care should be taken to assess whether an expert is comfortable with these priors. Otherwise, it is better to consider other kinds of priors or gather more data to lessen the effect of the prior. In practice, we rarely have conjugacy.

Since in the following section, the exponential distribution is chosen for the likelihood function of the fatigue crack size, the conjugate prior for this distribution is explained in Section 5.2.2.1. See Appendix A for other common conjugate priors.

5.2.2.1 Exponential Model with Unknown Rate

Suppose the likelihood of the data is exponentially distributed. The exponential distribution is defined as:

$$f(x|\lambda) = \lambda\, e^{-\lambda x} \tag{5-9}$$

Which the unknown parameter here is the rate parameter (λ). For an exponentially distributed variable, the expected value (mean value) is:

$$E[x] = \mu = \frac{1}{\lambda} \tag{5-10}$$

Based on Table 5.1, the conjugate prior distribution of uncertain parameter (λ) is Gamma distribution. The probability distribution function of Gamma distribution is:

$$f(\lambda) = \frac{\beta^{\alpha}}{\Gamma(\alpha)} \lambda^{\alpha-1} e^{-\beta\lambda} \tag{5-11}$$

Where α and β are shape and rate parameters, respectively. For a Gamma distribution, the expected value and variance of the parameter of interest is:

$$\begin{aligned} E[\lambda] &= \frac{\alpha}{\beta} \\ Var[\lambda] &= \frac{\alpha}{\beta^2} \end{aligned} \tag{5-12}$$

Now, let's assume new data is provided (which is shown by x). By using Eq. (5-8), the posterior distribution is proportional to:

$$\begin{aligned} f(\lambda|x) &\propto f(x|\lambda) \times f(\lambda) \\ f(\lambda|x) &\propto \left[\lambda e^{-\lambda x}\right] \times \left[\frac{\beta^{\alpha}}{\Gamma(\alpha)} \lambda^{\alpha-1} e^{-\beta\lambda}\right] \\ f(\lambda|x) &\propto \lambda^{(\alpha+1-1)} e^{-(\beta+x)\lambda} \end{aligned} \tag{5-13}$$

Which indicates:

$$Posterior \propto Gamma\,(\alpha + 1, \beta + x) \tag{5-14}$$

Based on the Bayes' rule, the posterior distribution is affected by both likelihood and prior. Therefore, it is important to find out the effect of these two distributions on the posterior distribution. Detailed sensitivity analysis for the considered application is explained in Section 5.5.

5.2.2.2 Quantity of Additional Data

Imagine N_{add} additional data is provided. The posterior distribution is obtained as:

$$f(\lambda|x) \propto f(x|\lambda) \times f(\lambda) \tag{5-15}$$

$$f(\lambda|x) \propto \left[\prod_{i=1}^{N_{add}} \lambda e^{-\lambda x_i}\right] \times \left[\frac{\beta^{\alpha}}{\Gamma(\alpha)}\ \lambda^{\alpha-1}\ e^{-\beta\lambda}\right]$$

$$\propto \left[\lambda^{N_{add}} e^{-\lambda(x_1+\cdots+x_{N_{add}})}\right] \times \left[\frac{\beta^{\alpha}}{\Gamma(\alpha)}\ \lambda^{\alpha-1}\ e^{-\beta\lambda}\right]$$

$$\propto\ \lambda^{(\alpha+N_{add}-1)}\ e^{-(\beta+\sum_{i=1}^{N_{add}} x_i)\lambda}$$

$$\propto\ \lambda^{(\alpha+N_{add}-1)}\ e^{-(\beta+N_{add}\times\bar{x})\lambda}$$

Which indicates:

$$Posterior\ \propto\ Gamma\ (\alpha + N_{add}, \beta + N_{add} \times \bar{x}) \tag{5-16}$$

Let's assume there is an exponential likelihood with an uncertain rate parameter and one estimation of the rate parameter which is known as λ_0. Prior values of α and β (which are shown by α_0 and β_0) are selected in a way that the expectation value becomes equal to λ_0:

$$\lambda \sim Gamma\ (\alpha_0, \beta_0 = \alpha_0 \times \mu_0)$$
$$(E[\lambda])_{prior} = \frac{\alpha_0}{\beta_0} = \frac{\alpha_0}{\alpha_0 \times \mu_0} = \frac{1}{\mu_0} = \lambda_0 \tag{5-17}$$

To demonstrate the effect of the number of additional data, it is assumed that:

$$\lambda_0 = 0.67\ (i.e.\ \mu_0\ = 1.5)$$

Now, consider the quantity N_{add} number of new additional data is provided. The posterior expected value for the uncertain parameter is obtained as:

$$(E[\lambda])_{postrior} = \frac{\alpha_{posterior}}{\beta_{posterior}} = \frac{\alpha_0 + N_{add}}{\beta_0 + N_{add} \times \bar{x}} = \frac{\alpha_0 + N_{add}}{\alpha_0\mu_0 + N_{add} \times \bar{x}} \tag{5-18}$$

The contribution of the mean value of the prior and data on the posterior mean can be understood from the denominator of Eq. (5-18). It can be seen that by increasing the quantity of new data, the mean value of the data ($\bar{x}$) has a bigger effect on the posterior mean value.

Figure 5.1 shows how the posterior distribution of the unknown parameter (λ) changes when new data is available. It is assumed that the mean value of these new results in all cases is equal to 1.0., i.e., $\bar{x} = 1$.

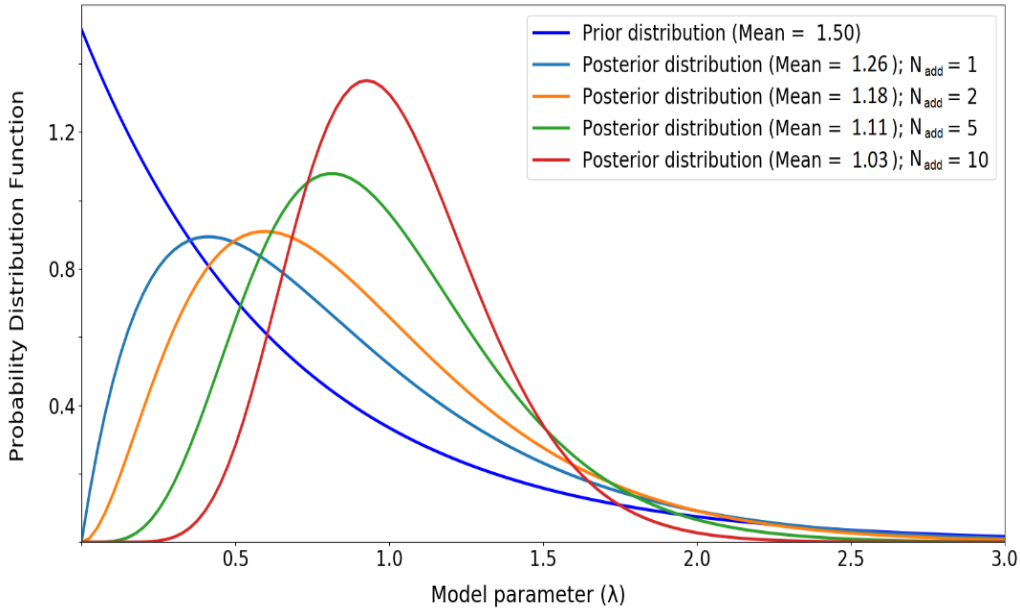

Figure 5.1. Effect of the number of additional data

As can be seen from Figure 5.1, the data has a great effect on the posterior. Data quickly dominates the prior as the quantity of additional data increases. Table 5.2 shows how the posterior mean values shift toward the data mean value with more additional data.

Table 5.2. Effect of No. of additional data on the posterior

Mean value of the prior	No. of additional data	Mean value of the new data	Mean value of the posterior
$\mu_0 = 1.5$	$N_{add} = 1$	$\bar{x} = 1$	$\mu_1 = 1.26$
	$N_{add} = 2$		$\mu_1 = 1.18$
	$N_{add} = 5$		$\mu_1 = 1.11$
	$N_{add} = 10$		$\mu_1 = 1.03$

Moreover, the posterior value of the variance of the gamma distribution is obtained as:

$$(Var[\lambda])_{posterior} = \frac{\alpha_{posterior}}{\beta_{posterior}^2} = \frac{\alpha_0 + N_{add}}{(\beta_0 + N_{add} \times \bar{x})^2} \quad (5\text{-}19)$$

Regarding the square power of the denominator, as the number of data (N_{add}) increases the variance of λ decreases. Therefore, by providing more new data, the uncertainty of the parameter of interest will be decreased (the posterior becomes narrower as N_{add} increases).

5.2.2.3 Effect of Prior Selection

In general, the prior estimation of an uncertain parameter relies on the expert's understanding of the problem. If there is not enough knowledge about the parameter of interest, the non-informative priors can be utilised. For using a non-informative prior for a gamma distribution, α_0 and β_0 should be chosen close to zero [112]. Figure 5.2 shows the posterior distribution for the non-informative and informative priors when two additional data are available. Figure 5.2 illustrates that the posterior distribution is sensitive to the prior selection.

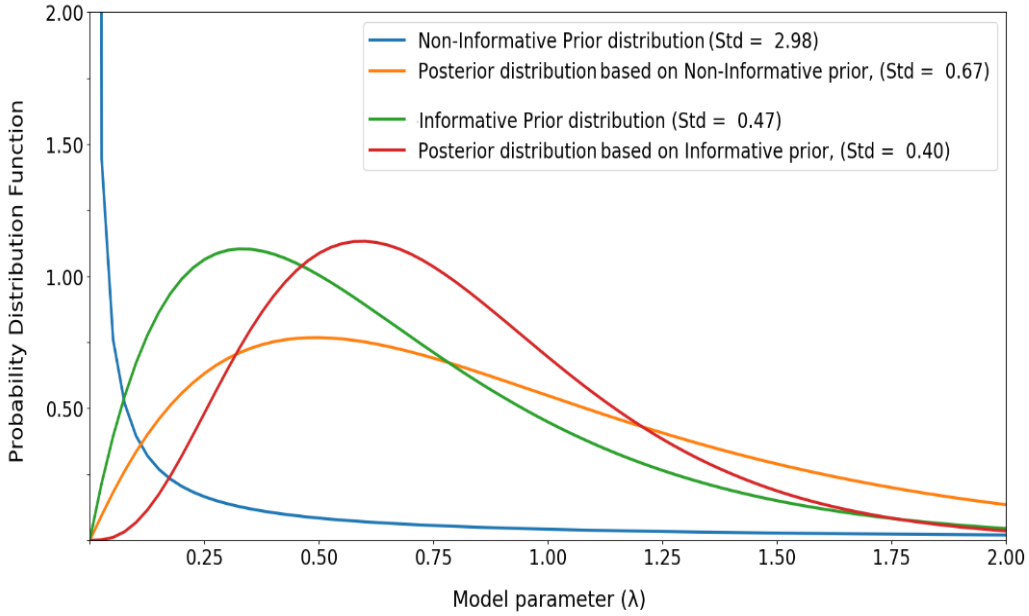

Figure 5.2. Effect of prior selection on the posterior (N_{add} = 2)

Figure 5.3 shows the posterior distributions in case of the availability of five additional data. This figure indicates that, although the selection of appropriate prior is important, if enough new data is available the posterior distribution is not very sensitive to the prior selection (posterior distributions converge).

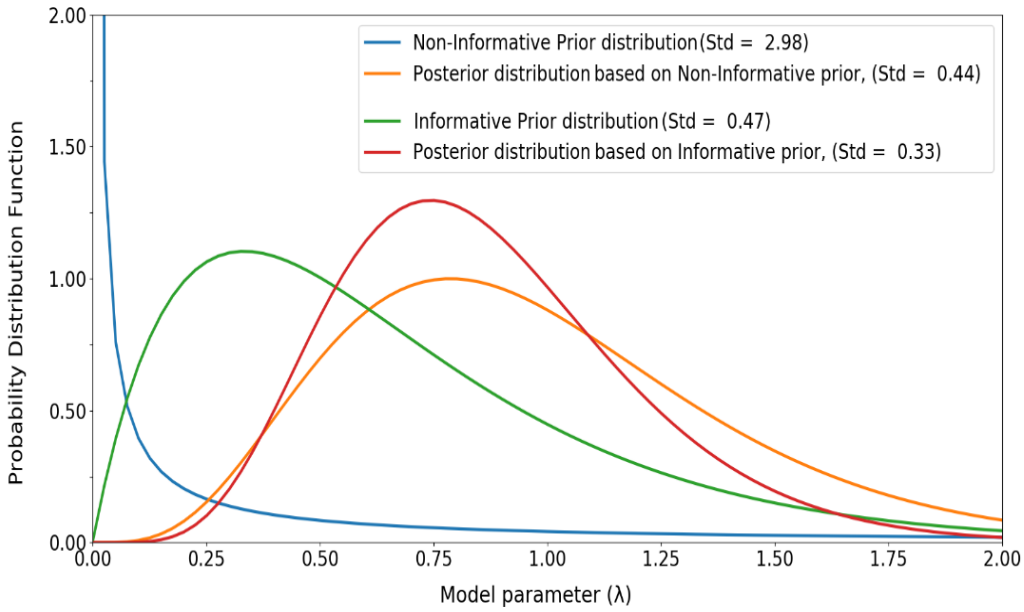

Figure 5.3. Effect of prior selection on the posterior (N_{add} = 5)

As it can be seen from Figure 5.2 and Figure 5.3, the posterior distribution has a bigger uncertainty (i.e. bigger standard deviation) in case a non-informative prior is selected which is reasonable.

5.2.2.4 Summary

Estimating the distribution of the uncertain parameter using Bayesian inference and conjugate priors is popular. The use of conjugate priors allows the results to be derived in closed form. The exact distribution of the posterior is already known. In the conjugate method, the posterior distributions are obtained without requiring numerical calculation to determine the normalisation constant. Different conjugate models were introduced in the literature. Based on the Bayes' rule, the posterior distribution is proportional to both prior distribution and new information. It was shown that, by increasing the quantity of available data, the posterior distribution shifts towards the new data. Moreover, uncertainty is reduced when more data is available.

5.2.3 Numerical Approach

The main shortcoming of the conjugate method is that in some cases, the uncertainty parameter does not have an associated conjugate prior. For example, generic databases often express uncertainty in terms of a lognormal distribution, which does not have a conjugate prior likelihood function [108]. To use conjugate methods, the likelihood

function and prior distribution must have specific standard distributions as presented in Table 5.1. In some cases, likelihood functions do not have known distributions. Therefore, using the conjugate method does not provide precise posterior distributions. Moreover, the conjugate approach contains assumptions that can influence the results. This influence is more predominant, especially when there is sparse data that conflicts with the prior distributions [108].

On the contrary, the numerical method provides a more general approach for predicting posterior distributions. The normalisation factor in Eq. (5-6) is calculated numerically. In numerical methods, prior and posterior distributions do not have to have the same functional forms. When the prior distribution is not conjugate, the posterior distribution cannot be presented in an analytical form (closed-form) [108]. Therefore, the posterior is not a standard distribution. Sampling from a non-standard distribution makes the updating procedure computationally more expensive.

However, due to not considering any assumption or simplification in performing the updating process, the obtained posterior distribution in the numerical method is usually expected to be more accurate.

5.2.4 Other Updating Approaches

For using probabilistic models in engineering applications, it is required to consider the relevant uncertainties in the analysis. The probabilistic models can be updated when new information becomes available. Bayesian methods have been identified as the most suitable for evaluating the probabilistic models required for structural integrity management problems.

However, there are some other approaches (non-Bayesian) for updating probabilistic models. Some of these approaches are:

- Maximum Likelihood Estimation (MLE):

  MLE is a method of estimating an uncertain parameter, given some observed data. It is achieved by maximising a likelihood function so that, under the assumed statistical model, the observed data is most probable. The point in the parameter space that maximises the likelihood function is called the maximum likelihood estimate [115].

However, this approach has some shortcomings. For instance, imagine an inspector claims to be able to detect the presence of sub-surface material flaws from an external visual inspection. If the inspector correctly identifies the presence of such flaws from the first 5 trials, what probability should be assigned to the inspector's claim? An MLE approach would identify a point estimate of 100% accuracy [116].

- Markov Chain Monte Carlo (MCMC):

  Bayesian inference problems can sometimes be very difficult to solve depending on the model settings (e.g., assumptions, and dimensionality). In large problems, exact solutions require, heavy computations that often become intractable and some approximation techniques must be used to overcome this issue and build fast and scalable systems [117].

  Based on the Bayes theorem, to obtain the posterior, three terms are required: a prior distribution, a likelihood function, and a normalisation factor. The first two can be expressed easily as they are part of the assumed model. However, the third term requires to be computed as:

$$f(x) = \int_{-\infty}^{\infty} f(x|\theta) \times f(\theta) \times d\theta \qquad (5\text{-}20)$$

  Although in low dimensions this integral can be computed without difficulties, it can become intractable in higher dimensions. In some cases, the exact computation of the posterior distribution is practically infeasible, and some approximation techniques must be used to get solutions [117].

  Markov Chain Monte Carlo (MCMC) approach is developed to overcome these numerical difficulties. MCMC approach is a sampling-based approach. MCMC methods create samples from a continuous random variable, with probability density proportional to a known function. These samples can be used to evaluate an integral over that variable, as its expected value or variance. Practically, an ensemble of chains is generally developed, starting from a set of points arbitrarily chosen and sufficiently distant from each other. These chains are stochastic processes of walkers which move around randomly according to an algorithm that looks for places with a

reasonably high contribution to the integral to move into next, assigning them higher probabilities.

Random walk Monte Carlo methods are a kind of random simulation or Monte Carlo method. However, whereas the random samples of the integrand used in a conventional Monte Carlo integration are statistically independent, those used in MCMC are autocorrelated. Correlations of samples introduce the need to use the Markov chain central limit theorem when estimating the error of mean values. These algorithms create Markov chains such that they have an equilibrium distribution that is proportional to the function given [117].

5.3 Previous Studies on Bayesian Updating Applications in Offshore Structures

It was explained that Bayesian inference is a method of statistical inference in which Bayes' theorem is used to update the probability for an uncertain parameter when new information becomes available.

Bayesian inference is used in many applications in medicine, insurance, finance, and engineering [118]. However, this section only introduces some of the previous studies on Bayesian updating applications in fatigue crack propagation in structures.

Fatigue is one of the important mechanisms of deterioration in structures subjected to repeated or cyclic load patterns. The design fatigue reliability is usually estimated by combining reliability analysis methods with fatigue life or fracture mechanics models. To maintain structural safety and monitor the fatigue risk, in-service inspections (e.g., non-destructive tests) are required at regular intervals. The data obtained from the inspection can be incorporated with the fatigue model to update the reliability estimate during the service life using Bayes' theorem.

Several studies have been performed to combine the information from inspection to update the fatigue reliability model. Madsen developed the idea of updating failure probability using the information from non-destructive inspection with the Bayesian approach [119].

Zhao and Haldar extended Madson's method. They proposed a linear elastic fracture mechanics-based reliability model which would incorporate uncertainties from many

different sources, including uncertainty in the results obtained from the non-destructive inspections. They investigated the effect of the uncertainties of detection on updating and used the updated reliability index for inspection schedule, maintenance, and repair decisions. The updated information on the reliability was used as a decision-making tool as to what to do next, in terms of whether to do nothing, reschedule the next inspection at an earlier date, or repair or replace the structure immediately [120].

Zhang and Mahadevan proposed a Bayesian procedure to quantify the modeling uncertainty, including the uncertainty in mechanical and statistical model selection and the uncertainty in distribution parameters. The procedure was developed using a simple example and then was applied to a fatigue reliability problem by considering the uncertainty in the statistical distribution parameters. The fatigue failure criterion for a structure was defined based on the crack size. The failure probability analysis was updated by incorporating the new information from nondestructive inspections performed on the structure [121].

Heredia-Zavoni and Montes-Iturrizaga [122] developed a Bayesian framework for updating the probability distributions of the uncertain parameters of a fracture mechanics model and crack size in tubular joints. The new information that they used was the information from inspection reports of a fixed offshore structure. They defined an error model, as the logarithmic difference between measured crack size during the inspection and crack size predicted by the fracture mechanics model. They assumed a normal distribution with a known mean and uncertain variance for the error model. Using conjugate models, the distribution of the error variance was modeled by an Inverse Gamma distribution. By considering these assumptions, they developed an analytical model for the updated distributions of the parameters of the fracture mechanics model and the crack size. They illustrated the capabilities of their model using examples using the fracture mechanics formulation for crack growth [122].

Peng et al. developed a general framework for probabilistic prognosis and uncertainty management under fatigue cyclic loading [123]. They considered several sources of uncertainties in the Bayesian updating framework. They also introduced an equivalent stress level model for the mechanism-based fatigue crack growth analysis, which

serves as the deterministic model for the lap joint fatigue life prognosis. Then, they designed an in-situ lap joint fatigue test with pre-installed piezoelectric sensors to collect experimental data. The proposed methodology was then demonstrated using the experimental data under both constant and variable amplitude loadings [123].

Garbatov and Guedes developed a Bayesian approach to update some of the uncertain parameters governing the reliability assessment of maintained floating structures [124]. They obtained the predicted fatigue crack size by expanding the Paris-Erdogan equation. They used a fatigue limit state based on the critical crack size. They considered material properties and inspection quality as the uncertain parameters in their study. Assuming different crack sizes as the results of the inspection, their approach was able to update the crack length [124].

Zarate et al. presented a framework to update and predict crack length as a function of the number of cycles in structural elements subjected to fatigue [125]. Their framework included two main sections: a model updating section to identify the probability density function of the fracture mechanics parameters, and a prognosis section to estimate the crack length of the specimen as a function of the number of cycles. The stress intensity factor range was assumed as an unknown parameter, and it was modelled as a polynomial equation function of the crack length. The polynomial coefficients were then treated as random variables and their joint probability distribution, together with the probability distribution of other fracture mechanics parameters are computed using Bayesian inference [125].

5.4 Application of Bayesian Updating

The purpose of this section is to apply the explained Bayesian methods (both analytical and numerical) to the tubular joints in a jacket platform and update the crack size distribution by incorporating the new information from the inspection results.

It is worth mentioning that the considered inspection results (i.e., crack measurements) in this research are artificial and are used to demonstrate the different Bayesian approaches. Nevertheless, the proposed methods can be applied for the real inspection results when they are available.

There is no need to consider further assumptions from the considered approach in case of accessibility to the real data. In this case, instead of using the hypothetical

distribution for the measured crack size, a distribution can be assigned to the real data. For instance, in Section 5.4.1.2, it is assumed that a normal distribution with a mean value of 2mm and a standard deviation of 0.2mm can be assigned to the inspection results. In case of accessibility to the real data, the real values for the mean and standard deviation will be used.

5.4.1 Crack Size Distribution in a Particular Tubular Joint

Fatigue damage accumulates during the structure's lifetime as the crack size increases. The accumulation of damage due to fatigue causes deterioration of the platform's structural capacity and increases the probability of failure. Therefore, offshore platforms are periodically inspected to assess the state of damage. Regarding fatigue damage, the information from inspection consists mainly of detection and measurement of crack sizes.

Regardless of the inspection outcome (detection or not detection of a crack), each inspection provides additional information which can be utilised to update the probability distribution of crack size in a joint. Using the updated distribution, it is also possible to update the estimation of joint reliability and consequently system reliability.

The main purpose of this section is to compare the conjugate and numerical methods for updating the crack size distribution in a specific tubular joint when new information is available. For this purpose, a particular tubular joint is considered and the crack size distribution is updated by using both conjugate and numerical methods.

5.4.1.1 Crack Size Distribution

The first step of updating the crack size distribution is to select an appropriate prior. The prior crack size distribution can be assumed based on theoretical considerations, experts' opinions, past experiences, or data reported in the literature [126]. Among all the parameters influencing the reliability of a structure, the crack size distribution plays a dominant role. In Chapter 3, the fatigue limit state was defined based on the crack size as:

$$g = a_c - a_t \tag{5-21}$$

where a_c is the critical crack size and a_t is the crack size at time t. The probability of failure is:

$$P[g \leq 0] = P[a_c \leq a_t] \tag{5-22}$$

A reliable estimate of the real crack size distribution is almost impossible and the calculated failure probability is very sensitive to the selection of this distribution. The failure probability is influenced by the right tail of the probability density function of the crack size. This tail depends on the type of distribution and is sensitive to minor changes within the data [127]. It can be shown that calculated probabilities of failure differ by several orders of magnitude depending on the crack size distribution assumed [128]. Figure 5.4 shows different crack size distributions and the critical crack size, schematically.

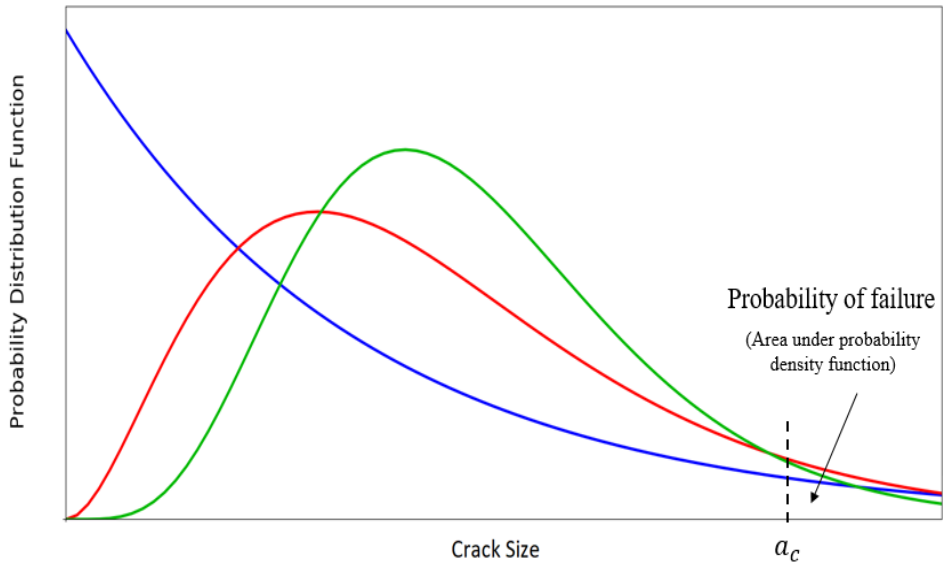

Figure 5.4. Different crack size distributions

There is no well-established rule for the selection of the crack size distribution. Difficulty in the selection of the crack size distribution comes from several reasons such as:

- Several sources of uncertainty in the fatigue phenomenon
- Lack of statistical data on crack size
- NDT devices cannot detect all cracks and they do not give the actual size of the cracks

Different distribution functions such as exponential (see [127] and [129]) or log-normal (see [130]) have been employed by experts based on the experimental results collected in laboratory tests. In this study, to resolve these difficulties in the selection of the crack size distribution, a sampling method is used. In the sampling method, both detected and undetected cracks are considered. It was shown in Chapter 3 that the fatigue crack size at a specific time is a function of uncertain parameters such as initial crack size, material parameter, geometry function, and the expected value of stress range:

$$a_t = \left\{ a_0^{1-\frac{m}{2}} + \left(1-\frac{m}{2}\right) \times Y^m \times \pi^{\frac{m}{2}} \times C \times (\varepsilon_s \times E[\Delta S^m]) \times N \right\}^{\frac{1}{1-\frac{m}{2}}} \qquad (5\text{-}23)$$

where:

- a_0: Initial crack size
- a_t: Crack size at time t
- m and C: Crack growth parameters
- Y: Geometry function
- $E[\Delta S^m]$: Expected value of the stress range
- ε_s: Uncertainties involved in the stress range
- N: Number of load (stress) cycles

Distributions of the uncertain parameters were explained in Chapter 3. Table 5.3 presents the distributions of the uncertain parameters.

Table 5.3. Statistical characteristics of random variables [N, mm]

Random Variable	Symbol	Type	Mean	COV
Initial crack size	a_0	Exponential	0.11	1.0
Crack growth parameters	C	Lognormal	8.1×10^{-12}	0.6
Uncertainties involved in the stress range	ε_s	Lognormal	1.0	0.2
Geometry function	Y	Lognormal	1.0	0.1

In the considered sampling method, a large number of simulations (N_{Sim}) is generated using random samples from the probability density function of each uncertain

parameter as provided in Table 5.3. A large number of simulations are used to include all relevant combinations of these uncertain parameters.

For each set of random samples (e.g. for the k[th] sample set: $a_{0k}, C_k, \varepsilon_{sk}$ and Y_k), the crack size (a_{tk}) is calculated based on Eq. (5-23). Here, the total number of simulations (N_{Sim}) is selected as 10^5. A Python code is used to generate samples from random variables and to obtain crack size distributions [131]. Figure 5.5 shows the flowchart of obtaining the prior crack size distribution and also updating the crack size distribution for both analytical and numerical methods.

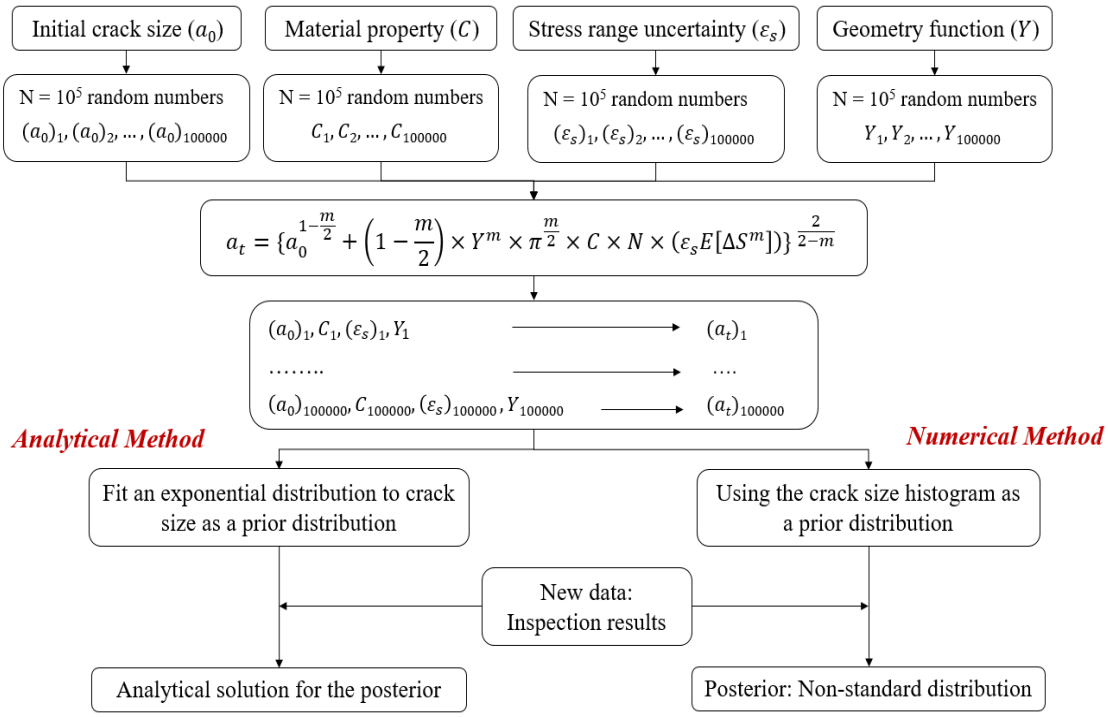

Figure 5.5. Flowchart for updating the crack size distribution

5.4.1.2 Analytical Method

After generating N_{sim} = 10^5 simulations for the crack size (a_t) based on Eq. (5-23), the crack size cumulative distribution function (CDF) can be obtained. Having obtained the CDF of crack size, the best distributions for crack size can be selected using fitting techniques (goodness of fit).

It is worth mentioning that 10^5 simulations of crack size are enough for assigning a distribution to the crack size. More numbers don't make significant changes in the result.

Figure 5.6 shows the results of the cumulative distribution function (CDF) for the simulated crack size, exponential, and lognormal distributions by using the Rt program [65]. Based on Figure 5.6, the exponential distribution is selected as appropriate prior for the crack size distribution.

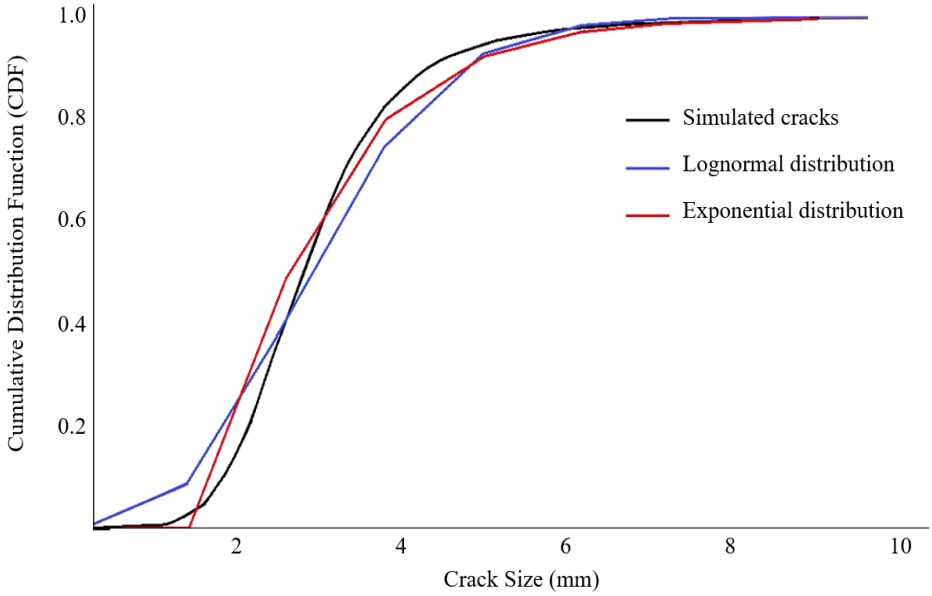

Figure 5.6. CDF for the simulated cracks, exponential and lognormal distributions

Figure 5.7 shows the histogram of simulated crack size distributions based on 10^5 simulations after five years and the fitted exponential distribution.

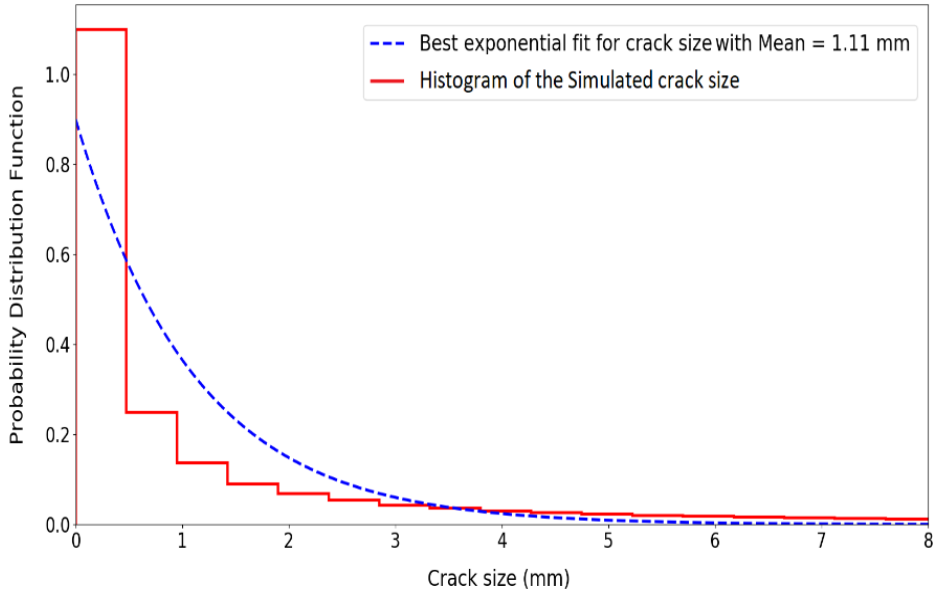

Figure 5.7. Histogram of the simulated cracks and fitted exponential distribution

As it can be seen from Figure 5.7, the fitted exponential distribution overestimates the probability of smaller cracks, whereas it underestimates the probability of bigger cracks. Therefore, the results of the analytical method include errors.

The fitted exponential distribution is used as an appropriate distribution for the crack size (before updating) with a probability density function as:

$$f(a_t|\lambda) = \lambda e^{-\lambda a_t} \tag{5-24}$$

Where λ is the rate parameter that is assumed as an uncertain parameter that will be updated when new information is available. Based on Figure 5.7, one point estimation of λ is obtained as:

$$\lambda_{fit} = \frac{1}{1.11} \tag{5-25}$$

It is noted that the value of λ_{fit} depends on the sample size.

In this study, the uncertain parameter is the rate of exponential distribution (λ), whereas the new information is the inspection results which contain the measurement of the crack size (a_m). Bayesian inference is employed to describe how the uncertainty in λ changes from the prior distribution to the posterior distribution by incorporating the new information. As can be seen from Table 5.1, for the exponential distribution with uncertain parameter (λ), the conjugate prior and posterior distributions for λ are Gamma distributions.

- **Prior Distribution**

  In this study, Jeffreys non-informative prior is used to describe the prior distribution [108]. The Jeffreys non-informative prior for the exponential likelihood is a gamma distribution. In Jeffreys non-informative prior for the exponential distribution, both shape (α_{prior}) and rate parameters (β_{prior}) are selected close to zero [108]. Moreover, these parameters are selected in a way that the expected value of λ becomes equal to λ_{fit}, i.e.:

$$\alpha_{prior} = 0.001 \qquad \beta_{prior} = \alpha_{prior} \times {}^{1}/_{\lambda_{fit}}$$
$$(E[\lambda])_{prior} = \frac{\alpha_{prior}}{\beta_{prior}} = \lambda_{fit} = \frac{1}{1.11} \tag{5-26}$$

- **New Information (Inspection Results)**

  It is assumed that ten inspection results ($N_{ins} = 10$) of crack sizes (i.e., $(a_m)_1, (a_m)_2, \dots, (a_m)_{10}$) are available. It is assumed that these inspections are independent of each other. A normal distribution with a mean value of 2mm and a standard deviation of 0.2mm is assigned to the inspection results.

- **Posterior Distribution**

  Having provided new information, the distribution of the uncertain parameter can be updated by using the Bayesian framework. The posterior distribution of the uncertain parameter is obtained by using Bayes' theorem.

  The parameters of the posterior distribution (which is a gamma distribution) are obtained by using Eq. (5-16) which are:

$$\alpha_{posterior} = \alpha_{prior} + N_{ins}\,; \qquad \beta_{posterior} = \beta_{prior} + \sum_{i=1}^{N_{ins}} (a_m)_i \tag{5-27}$$

  Figure 5.8 shows the prior and posterior distributions for the uncertain parameter (λ).

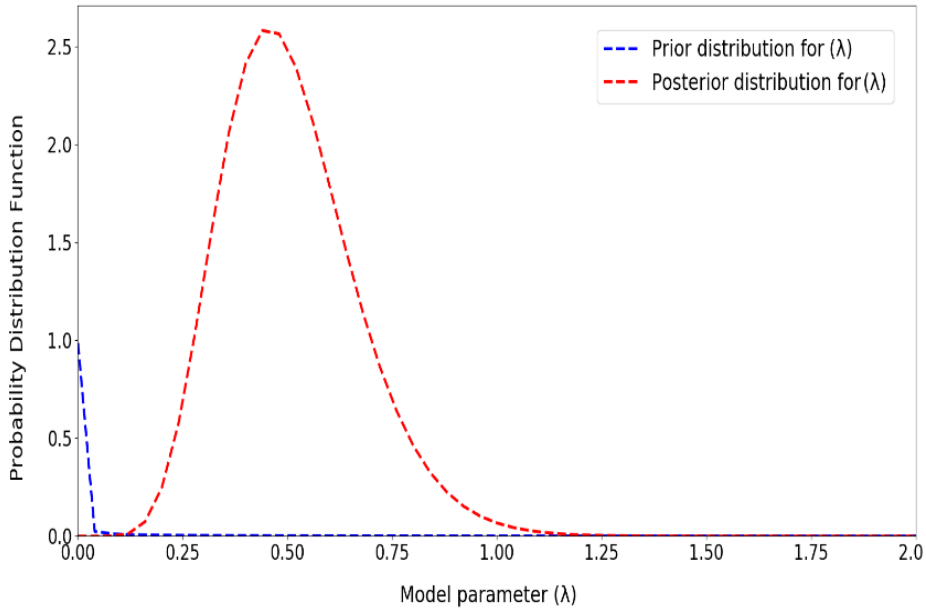

Figure 5.8. Prior and posterior distributions for the uncertain parameter

Based on Eq. (5-24), crack size distribution depends on the rate parameter. However, the rate parameter is an uncertain parameter with a distribution that depends on α and β. This is schematically shown in Figure 5.9.

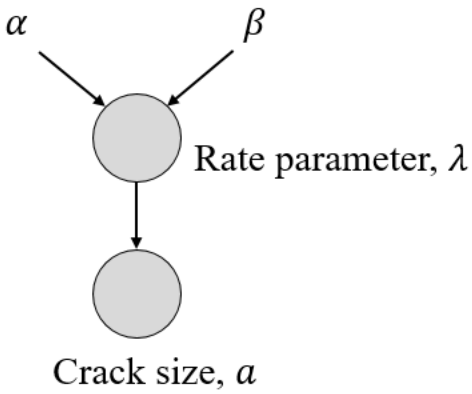

Figure 5.9. Dependency of the crack size on the distribution of the rate parameter

- **Predictive Distribution for Crack Size**

  After updating the uncertain parameter (λ), the crack size distribution can be updated based on a predictive distribution. The predictive distribution for the crack size can be obtained as [108]:

$$f(a_t) = \frac{\alpha_{posterior} \times \beta_{posterior}^{\alpha_{posterior}}}{(\beta_{posterior} + a_t)^{\alpha_{posterior}+1}} \quad (5\text{-}28)$$

  Figure 5.10 shows the crack size distributions before and after updating. As shown in the figure, the updated crack size distribution has a mean value of 1.97mm, which is close to the mean value of the observations (2mm).

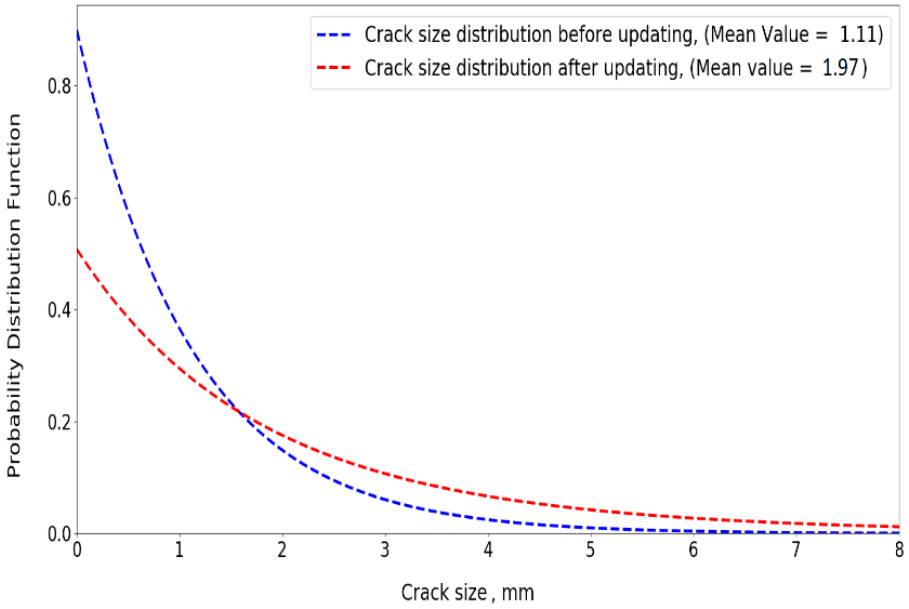

Figure 5.10. Crack size distributions before and after updating

Figure 5.11 summarises the conjugate method for updating the rate parameter (λ) and crack size distributions.

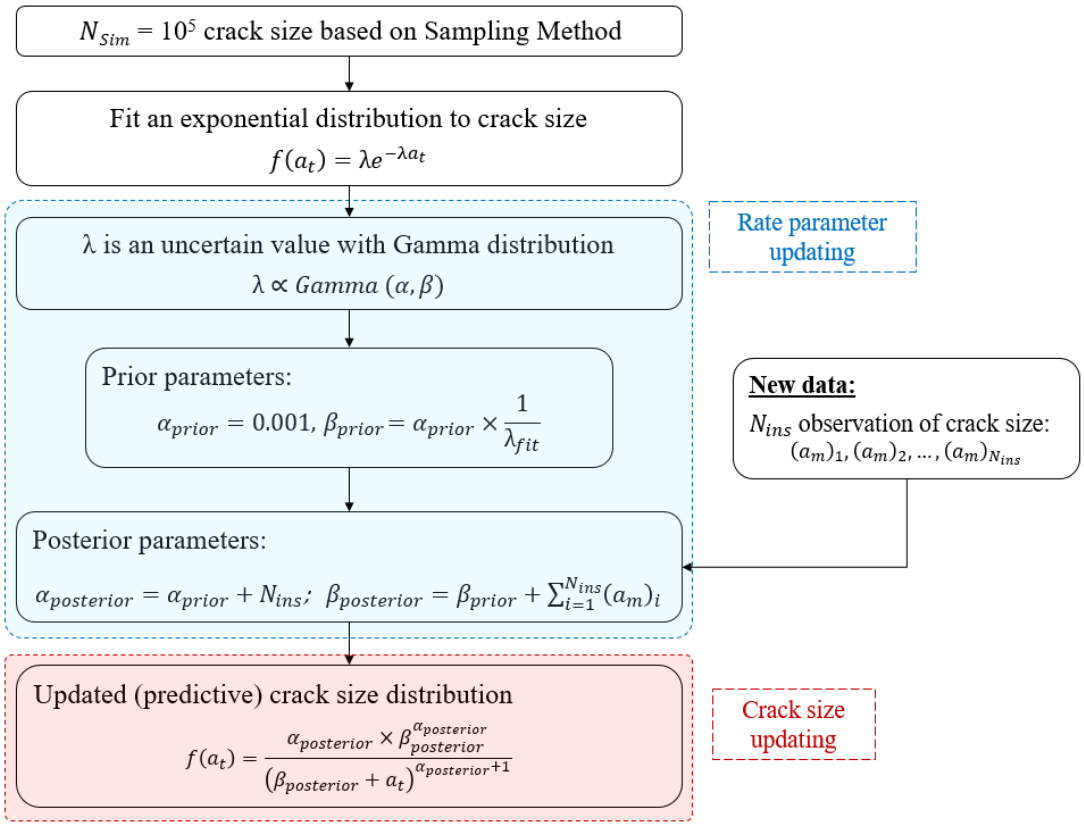

Figure 5.11. Updating the rate parameter and crack size distributions in the analytical method

5.4.1.3 Numerical Method

In the numerical method, the posterior is not a standard distribution and it cannot be presented in an analytical form. Therefore, the normalisation constant in Eq. (5-6) is calculated numerically. In this method, the posterior distribution is obtained by using Eq. (5-5).

- **Prior Distribution**

  As it was earlier mentioned, a large number of crack sizes (N_{Sim} =10^5) is generated by using random samples of uncertain parameters. In the numerical method, instead of fitting any distribution, the histogram of the simulated crack size is used as a prior distribution. Figure 5.12 shows the histogram of the simulated data which is used as a prior distribution for the crack size.

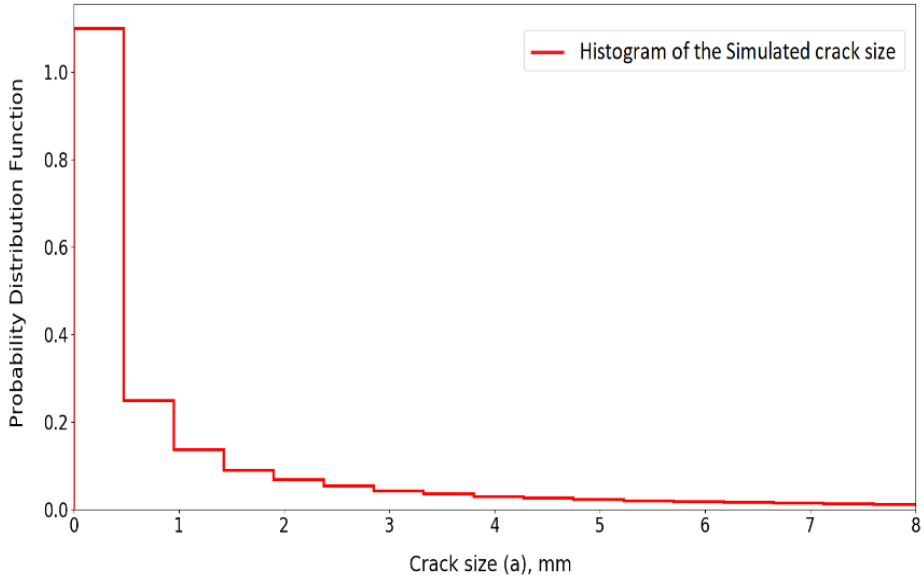

Figure 5.12. Prior crack size distribution in the numerical method

- **Likelihood Function**

Due to the uncertainties in the fatigue phenomenon and crack size measurements, the crack size is not a certain parameter. The uncertainties involved in the fatigue process and also in the crack size measurements can be assumed based on experts' beliefs. Therefore, the likelihood function is defined based on the expert's belief to take into account the involved uncertainties. The likelihood function can be represented as a non-normalised normal distribution as [126]:

$$L = \exp\left(-\frac{(a_t - a_m)^2}{2\sigma_L^2}\right) \tag{5-29}$$

Where a_m represents the measured crack size, a_t is the predicted crack size and σ_L is the assumed standard deviation of crack size (due to measurement and model uncertainty). For example, if the measured crack size is obtained equal to $a_m = 1.8\,mm$, it's very probable that the actual crack size is between 1.4 mm and 2.2 mm. In this case, it is unlikely that the actual crack size is greater than 3 mm.

The value of σ_L is estimated by the expert's judgements about uncertainty. In this study, two different values for σ_L are considered to check the effect of the likelihood function on the posterior results:

- Case (I): An accurate model for the predicted crack size and perfect measurement. In this case, it is assumed that the model can estimate the real crack size with reasonable accuracy. Moreover, the measurement is performed with a high-quality tool. Therefore, a small standard deviation ($\sigma_L = 0.5mm$) is considered for the likelihood function.
- Case (II): A less accurate model for the predicted crack size and inaccurate measurement. In this case, it is assumed that the model can predict the real crack size with less accuracy. Moreover, the measured crack sizes are not very reliable. Therefore, a bigger standard deviation ($\sigma_L = 1mm$) for the likelihood function is assumed.

Figure 5.13 shows the likelihood function for both cases when a crack is measured equal to $a_m = 2mm$. As it was mentioned, standard deviations of 0.5mm and 1mm are assumed for Case (I) and Case (II), respectively.

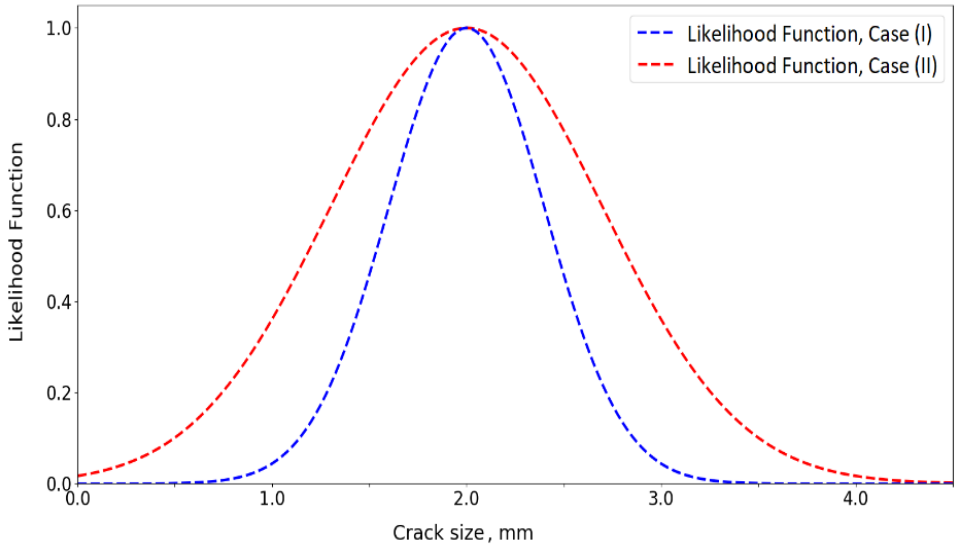

Figure 5.13. Likelihood functions for both accurate and inaccurate models

- **Posterior Distribution**

According to Bayes' theorem, the posterior distribution is proportional to the prior distribution and likelihood function as shown in Eq. (5-5). Note that, in the analytical method, the posterior distribution is updated only once by summing all the crack size information as shown in Eq. (5-27). However, in the numerical method, the posterior distribution needs to be updated for each observed crack size.

Therefore, the probability distribution function of crack size is updated N_{ins} times sequentially by using Eq. (5-5). Following steps should be performed to obtain the updated crack size distribution:

- Step 1: Use the crack size histogram as a prior distribution
- Step 2: Choose the measured crack size No. i (i = 1), $(a_m)_i$
- Step 3: Obtain likelihood function distribution by using Eq. (5-29)
- Step 4: Calculate the normalisation constant by using Eq. (5-6)
- Step 5: Obtain the posterior distribution by using Eq. (5-5)
- Step 6: Replace the prior with the obtained posterior and go to Step 2, (i = i +1)

The updating procedure for the numerical method is computationally more expensive than the analytical method. The obtained posterior is assumed as the prior distribution for the next updating process.

To demonstrate how the crack size distribution is updated in the numerical method, the same observations are considered (ten observations with a mean value of 2mm and a standard deviation of 0.2mm). Figure 5.14 and Figure 5.15 show the posterior crack size distributions after the updating process for both likelihood cases.

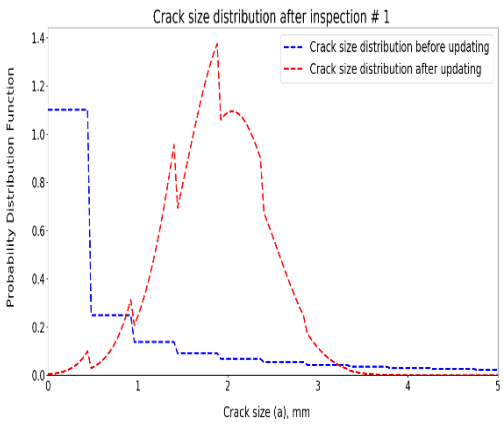

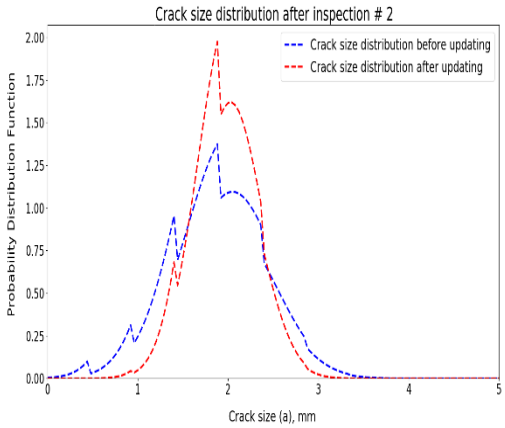

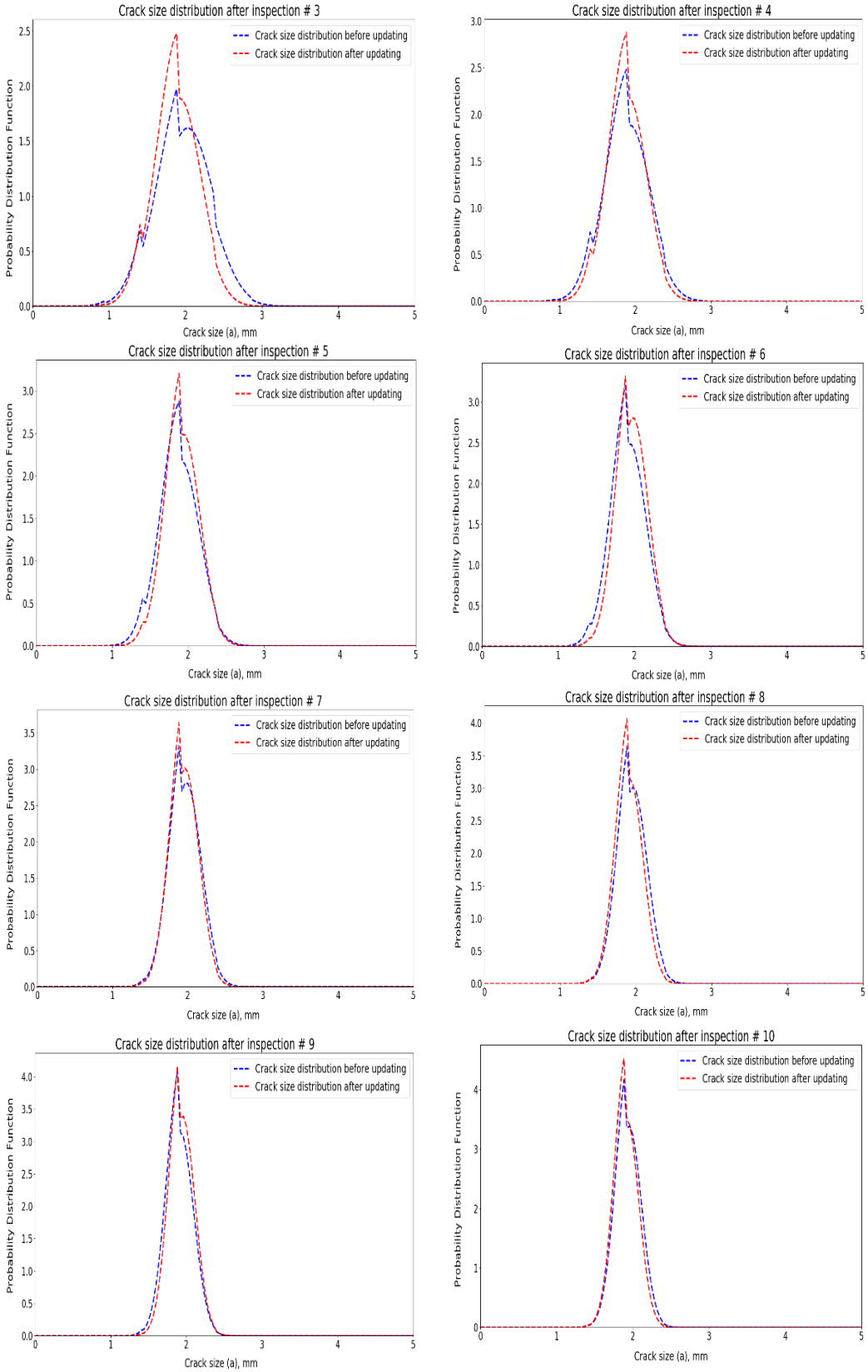

Figure 5.14. Sub sequentially updating of the crack size distributions for likelihood function, Case (I)

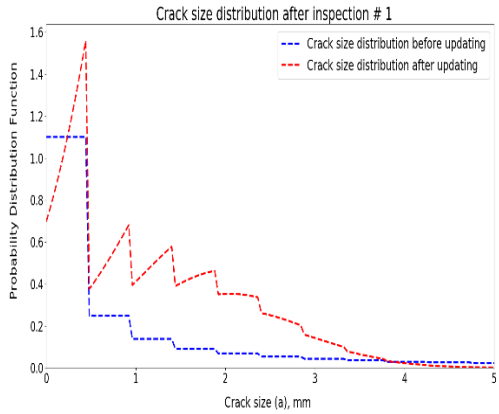
Crack size distribution after inspection # 1
Crack size distribution before updating
Crack size distribution after updating
Probability Distribution Function
Crack size (a), mm

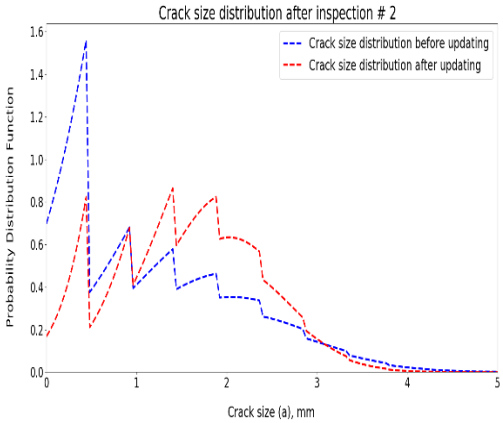
Crack size distribution after inspection # 2
Crack size distribution before updating
Crack size distribution after updating
Probability Distribution Function
Crack size (a), mm

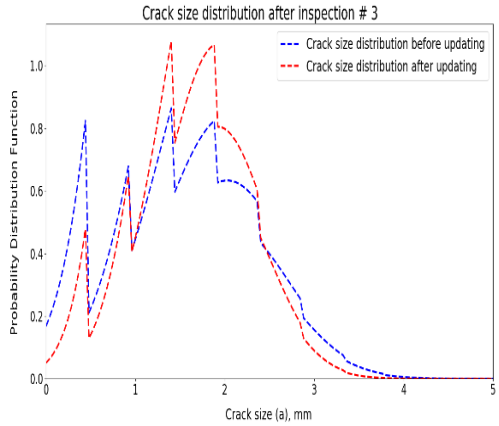
Crack size distribution after inspection # 3
Crack size distribution before updating
Crack size distribution after updating
Probability Distribution Function
Crack size (a), mm

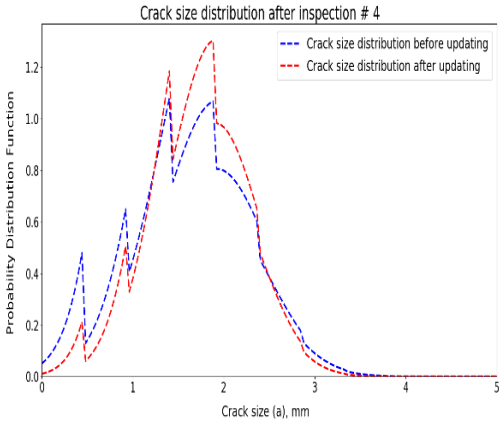
Crack size distribution after inspection # 4
Crack size distribution before updating
Crack size distribution after updating
Probability Distribution Function
Crack size (a), mm

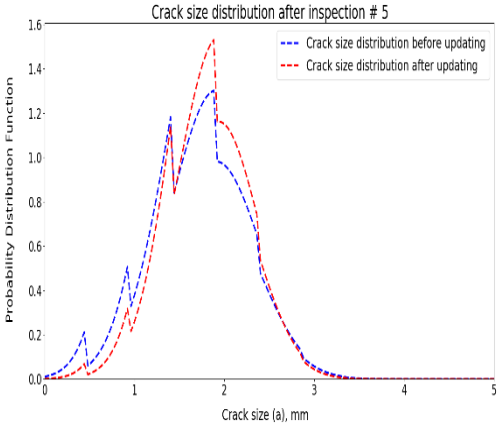
Crack size distribution after inspection # 5
Crack size distribution before updating
Crack size distribution after updating
Probability Distribution Function
Crack size (a), mm

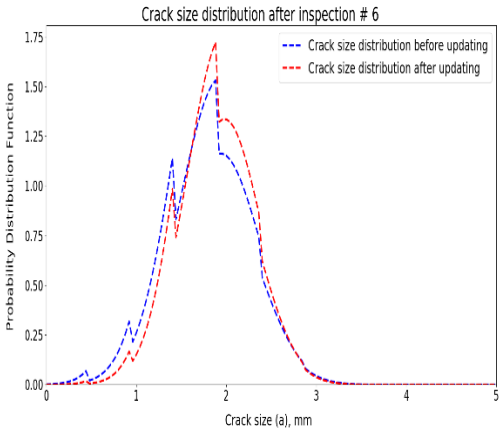
Crack size distribution after inspection # 6
Crack size distribution before updating
Crack size distribution after updating
Probability Distribution Function
Crack size (a), mm

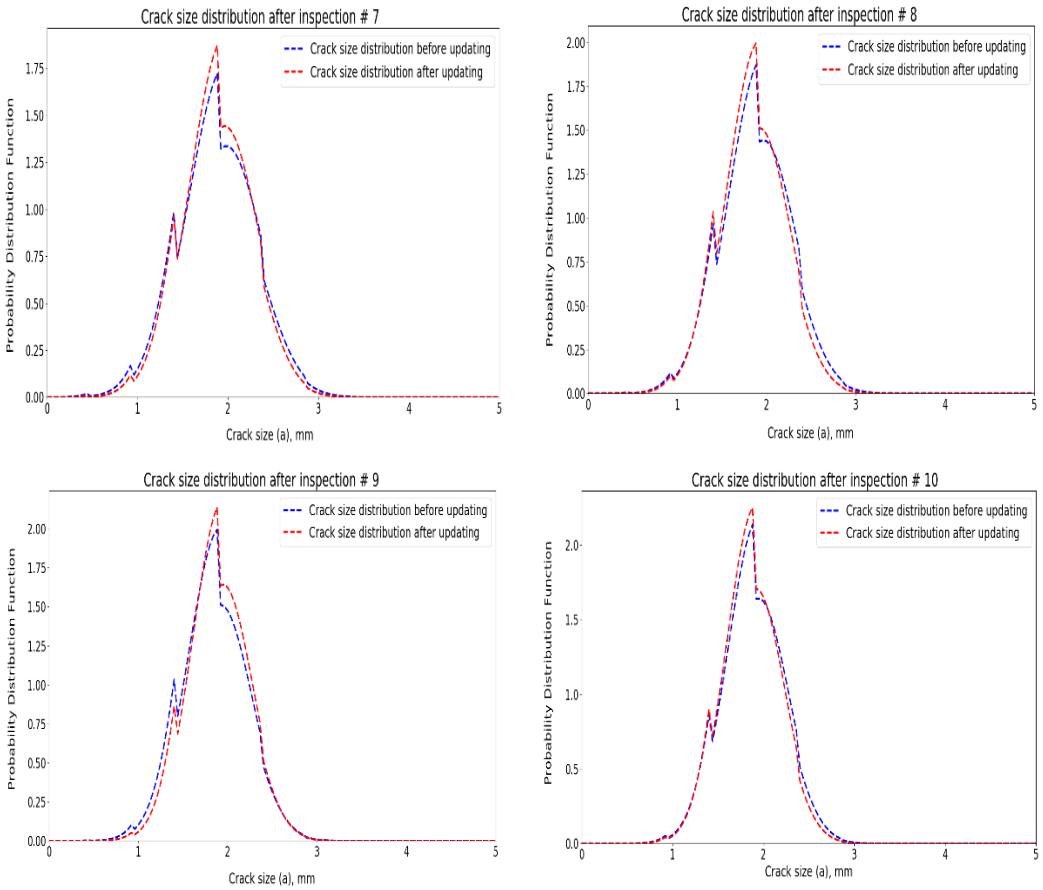

Figure 5.15. Sub sequentially updating of the crack size distributions for likelihood function, Case (II)

As it can be seen from Figure 5.14 and Figure 5.15, the posterior distributions shifted towards the observations, i.e. the observed data dominates the posterior distributions. Additionally, it is also observed that the expected value for the updated crack size is around 2.0 mm in both figures, which is close to the mean of the observed crack sizes.

Both figures show that after five observations, the posterior distribution approaches the observations. Therefore, if enough data is available, the posterior distribution is not sensitive to the prior selection. However, due to the high cost of underwater inspections, there may not be several inspections available for a specific joint. Most of the time, there is only one inspection result for each joint. As represented in Figure 5.14 and Figure 5.15, especially for the first and second updates, prior distribution has a great impact on the posterior distribution. Therefore, the prior distribution should be selected based on reasonable assumptions.

5.4.1.4 Comparing the Results of Two Methods

Figure 5.16 shows the posterior distributions of crack sizes for both analytical and numerical methods. Although the obtained mean values for the methods are not substantially different ($\mu_{Conjugate} = 1.97$, $\mu_{Numerical} = 1.88$ mm), the shape of the crack size distribution is different.

The reason is that the posterior distribution is restricted to a specific distribution shape in the conjugate method. This is an important disadvantage of using the conjugate methods since the prior distributions have a great impact on the posterior distributions.

Moreover, in the conjugate method, the simulated crack size is approximated with a fitted exponential distribution which is overestimating the probability of smaller cracks while underestimating the probability of bigger cracks. Therefore, when the prior distribution is not accurate, the posterior distribution may not be accurate.

Figure 5.16 also shows that the posterior distribution shapes in the numerical method are very similar to the likelihood functions given in Figure 5.13. In fact, in the numerical method, the observed data dominates the posterior distributions. The effect of the likelihood function on the posterior distribution can also be understood from Figure 5.16, i.e. the likelihood function for Case (II) which has a bigger uncertainty widens the posterior distribution. Using a larger uncertainty results in a bigger probability of failure. In reality, the actual value of σ_L in the likelihood function is unknown and it is estimated based on the engineering judgement.

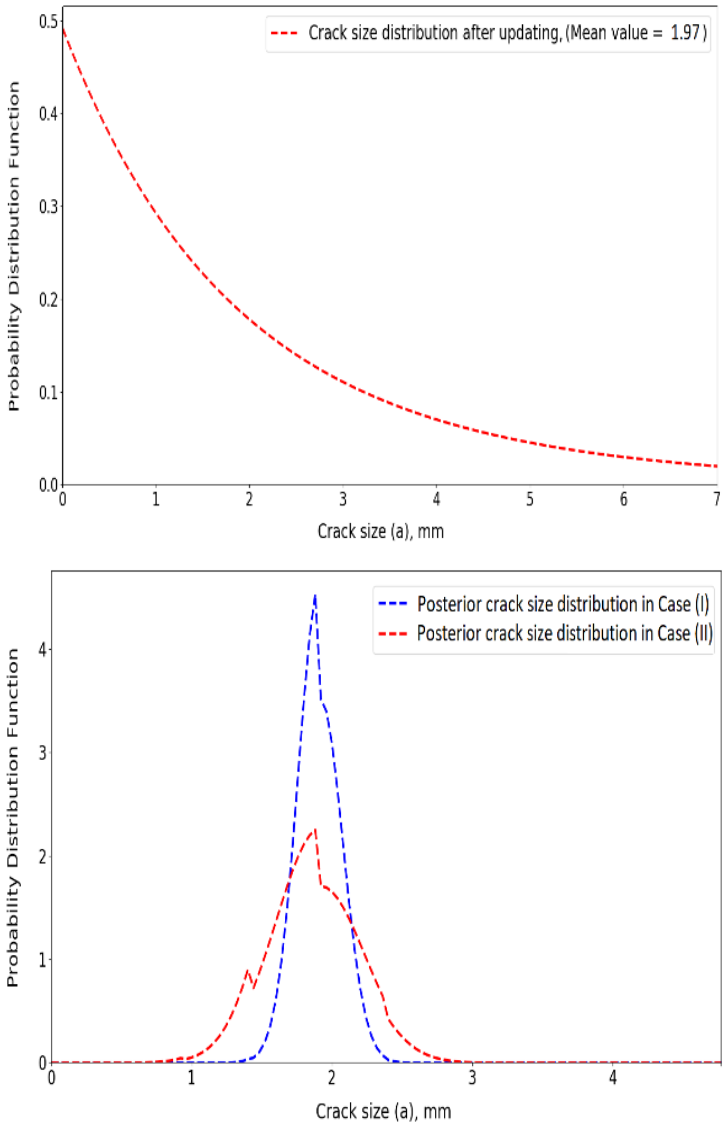

Figure 5.16. Posterior crack size distributions, analytical method (top), and numerical method (bottom)

In the numerical method, the observed data dominates the posterior distribution shape, whereas in conjugate methods, the prior distribution has a great effect on the posterior distribution shape and the effect of observed data is minimised. Since the numerical method allows us to incorporate the effect of the new data (inspection results) on the posterior distribution, the numerical methods are preferred. However, the numerical method is computationally more expensive especially when several inspection results are available.

5.4.2 Crack Size Distribution in Multiple Locations

In the previous section, the crack size distribution for a particular tubular joint was updated by using conjugate and numerical methods. In real situations, there are a few inspection results available for each tubular joint due to the expensive cost of the underwater inspection.

The purpose of this section is to update the crack size distribution for different locations that have almost the same conditions. It is assumed that these joints have identical configurations with the same material properties, and they are subjected to almost the same stress range. Therefore, a prior crack distribution can be assigned to these joints. When the inspection results for these similar joints are available, the posterior distribution can be obtained by using conjugate or numerical methods.

5.4.2.1 Prior Distribution

To assign a prior distribution for the crack size, a sampling method as explained in Section 5.4.1.1 is used. As provided in Eq. (5-29), the final crack size is a function of initial crack size, crack growth parameter, geometry function, and the expected value of stress range. Distributions of the uncertain parameters are presented in Table 5.3. However, since the stress range is not the same at different locations, a bigger coefficient of variation is assumed for the stress range parameter, i.e. $\varepsilon_S = 0.4$.

The histogram of the simulated crack sizes and the fitted exponential distribution are assumed as the prior distribution for numerical and conjugate methods, respectively. The prior distributions shown in Figure 5.17 are obtained based on N_{Sim} =10^5 simulations after five years.

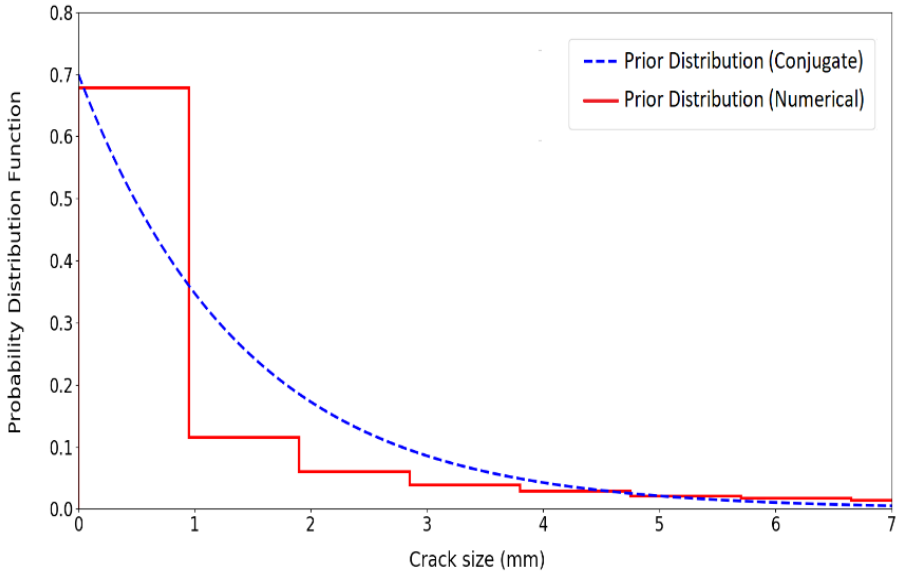

Figure 5.17. Prior crack size distributions for multiple locations in the conjugate and numerical methods

5.4.2.2 New Information (Inspection Results)

It is assumed that there are twenty tubular joints with similar conditions. To demonstrate the methodology, it is assumed that five independent inspection results are available for each tubular joint. Therefore, in total 100 inspection results ($N_{ins} = 100$) are available. A normal distribution with a coefficient of variation of 0.2 is assumed for these five inspection results. It is also assumed that the mean value of each tubular joint is different.

5.4.2.3 Posterior Distribution

- **Conjugate Method**

  As mentioned in Section 5.2.2.1, the prior and posterior distributions for the uncertain parameter (λ) are represented by the gamma distribution. The parameters, α and β for the prior and posterior are obtained from Eq. (5-26) and Eq. (5-27), respectively. After updating the distribution of the model parameter (λ), the crack size distribution is obtained by using Eq. (5-28). Figure 5.18 shows the crack size distributions before and after incorporating the inspection results.

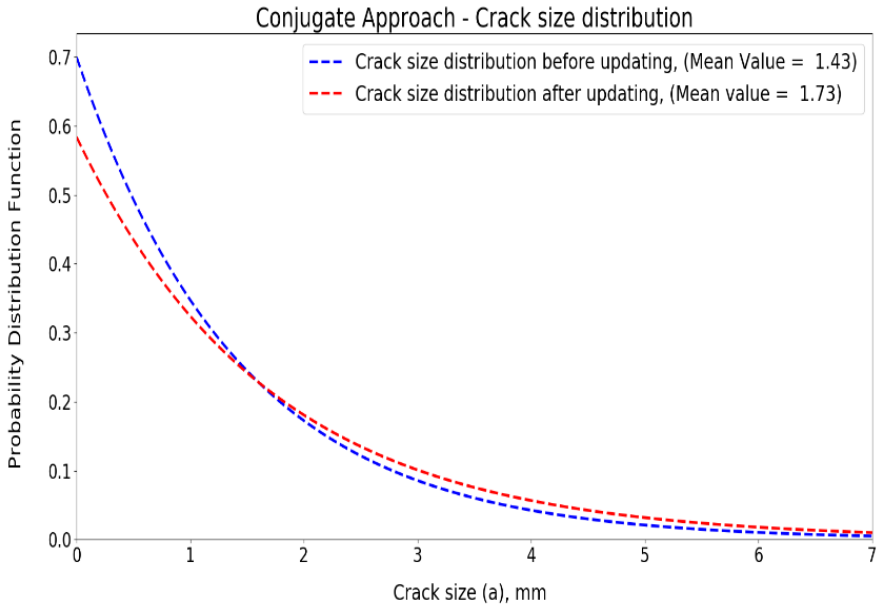

Figure 5.18. Crack size distributions for multiple locations in the conjugate method

- **Numerical Method**

  As it was mentioned in Section 5.4.1.3, the likelihood function is defined by Eq. (5-29). The standard deviation of crack size (due to measurement and model uncertainty) is assumed as σ_L = 0.8mm. Based on Bayes' theorem, the posterior distribution is obtained by using the prior distribution and likelihood function as presented in Eq. (5-5). It was assumed that the inspection results are available for twenty tubular joints.

  Updating of the crack size distribution for each tubular joint is carried out by using the numerical approach which was explained in Section 5.4.1.3. Figure 5.19 shows the crack size distributions for some joints before and after incorporating the inspection results (after incorporating all five inspections).

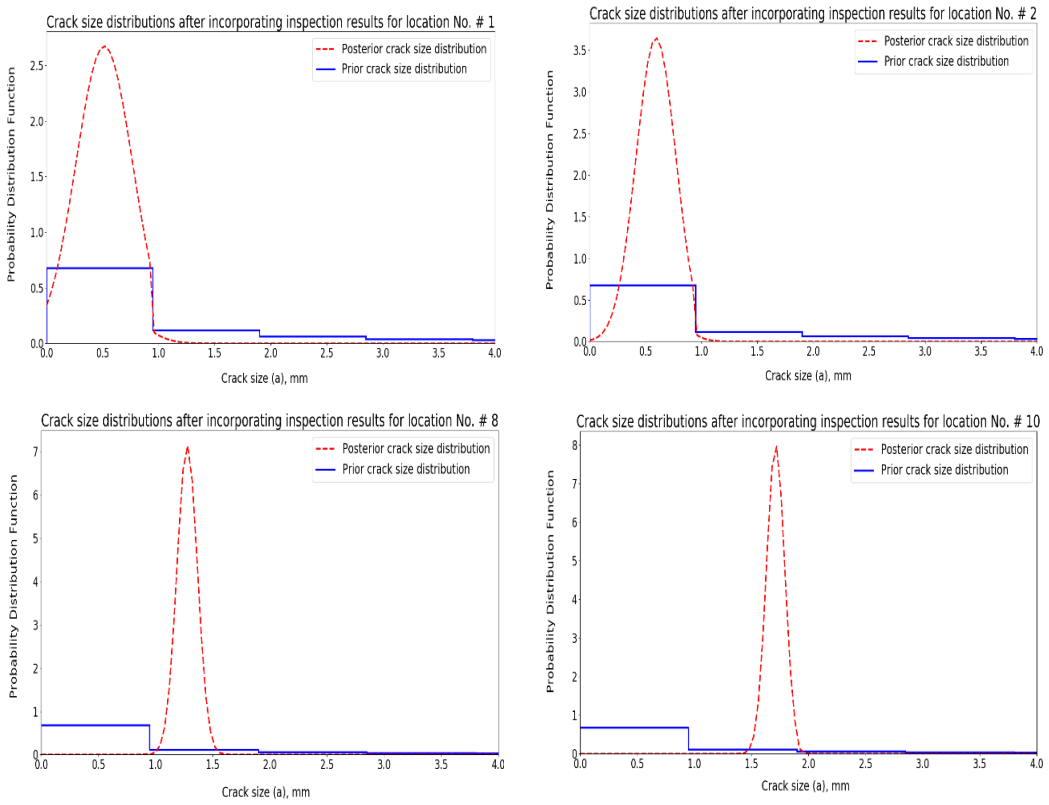

Figure 5.19. Crack size distributions for four different tubular joints

By combining all posterior distributions for each location and normalising the area below the combined distribution, a posterior distribution for all locations can be obtained. Figure 5.20 illustrates prior and posterior crack size distributions for all tubular joints.

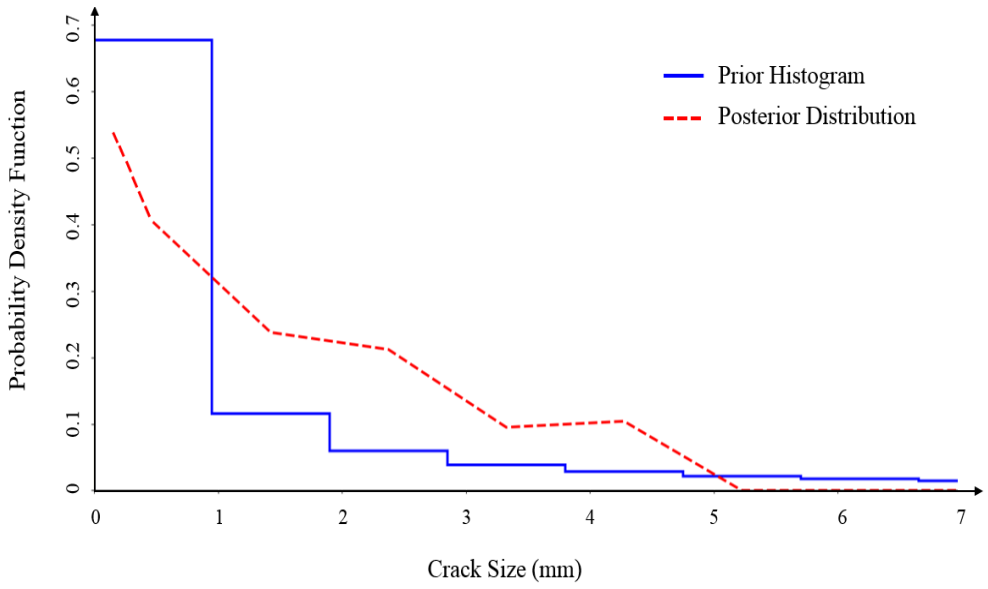

Figure 5.20. Crack size distributions for multiple locations in the numerical method

5.4.2.4 Comparing the Results of Two Methods

Figure 5.21 shows the posterior crack size distributions for a group of twenty similar joints based on the conjugate and numerical methods. It is observed that, if the results of several locations are combined, the posterior distribution in the numerical method approaches the conjugate posterior distribution. Note that the posterior distribution (in the numerical method) for each location is similar to a normal distribution. It is also found that both numerical and conjugate methods result in a similar distribution. Therefore, obtaining the posterior distribution by using the conjugate method might be preferred since it is much easier and less time-consuming for multiple locations.

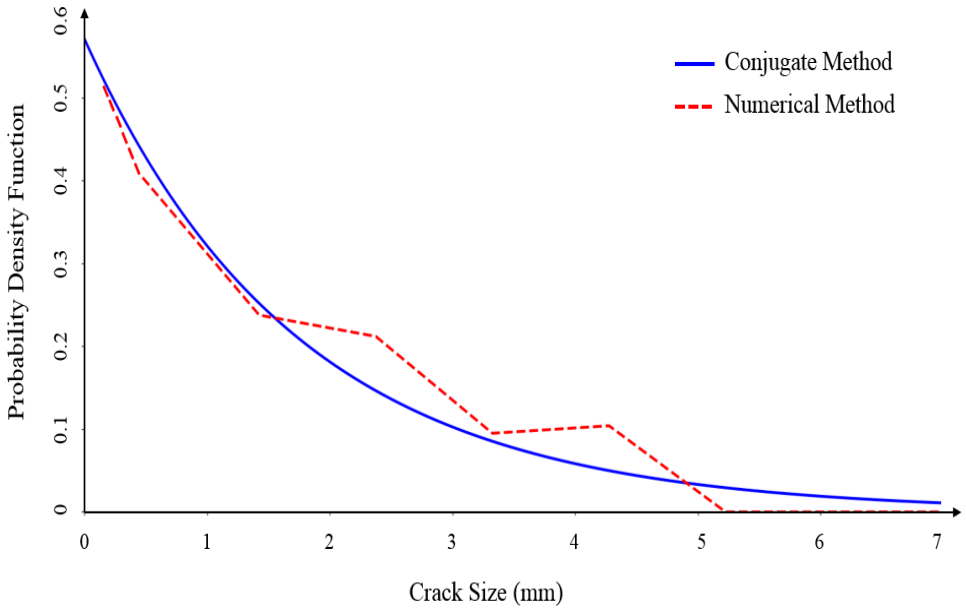

Figure 5.21. Posterior crack size distributions for multiple locations in both methods

5.4.3 Bayesian Updating Regarding Different Inspection Outcomes

5.4.3.1 Inspection Outcomes

Let's consider an inspection has been carried out for a specific tubular joint in a fixed offshore platform at the time t_j. Here, $I(j)$ denotes the outcome of the inspection. Two outcomes can be assumed as a result of the inspection:

- $I(j) = NC$: No crack is detected
- $I(j) = CM$: A crack is detected and measured

Regarding the inspection results, the uncertainties can be divided into two categories:

- Detectable crack size
- Accuracy of the measured crack (if detected)

In the first case (i.e. $I\ (j) = NC$), the uncertainty is related to the first category. This uncertainty can be taken into account by curves that estimate the probability of crack detection (POD). The POD curves depend on the quality (resolution) of the inspection methods and also on the existing crack size [122] (see Chapter 4).

The detectable crack size is related to a specified inspection method and it is usually modelled as a stochastic variable reflecting the actual probability of detection [132]. Among several formulations of POD available, the commonly used exponential distribution is [132]:

$$POD\ (a)\ =\ 1 -\ e^{-\frac{a}{a_{md}}} \tag{5-30}$$

where a is crack size and a_{md} is the mean detectable crack size for the specific inspection method. Figure 5.22 shows the POD curves for different mean detectable sizes.

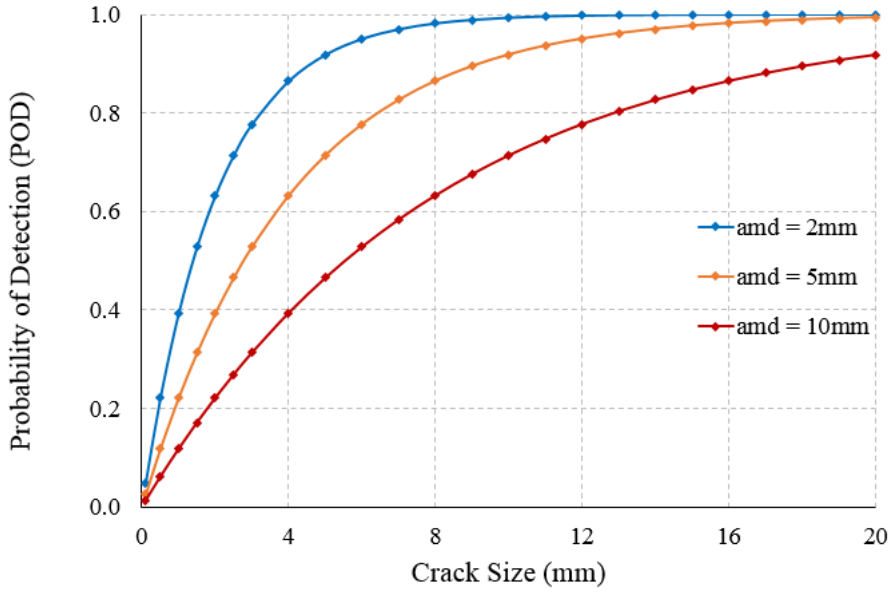

Figure 5.22. Probability of detection (POD) curves

In the second case (i.e. $I(j) = CM$), in addition to the uncertainties involved in the POD curves, another uncertainty is related to the measurement error which is also dependent

on the inspection quality. It is noted that this error is usually modelled as a normal random variable with a mean of zero and unknown variance ([122] and [132]).

Consider $A(j)$ denotes crack size at time t_j. It is noted that the crack size is an uncertain parameter. Posterior distribution of the crack size based on the results of an inspection is obtained according to Bayes theorem.

5.4.3.2 Posterior Distribution Expression

- **No Crack Detected**

  The probability of crack detection (POD) for a specific inspection tool, depends on the resolution of the inspection method and crack size at that time. Therefore, in this case, the likelihood, which is the probability of occurrence of a crack not detected, is presented as:

$$Likelihood = P[NC|a] = 1 - POD(a)$$
$$Likelihood = P[NC|a] = e^{-\frac{a}{a_{md}}} \quad (5\text{-}31)$$

  Therefore, the updated crack size distribution (given that no crack observed) is obtained based on Eq. (5-5) as:

$$Posterior = \frac{Likelihood \times Prior}{Normalisation}$$
$$f(a|NC) = \frac{f(NC|a) \times f(a)}{\int_0^\infty f(NC|a) \times f(a) da} \quad (5\text{-}32)$$
$$f(a|NC) = \frac{[1 - POD(a)] \times f(a)}{\int_0^\infty [1 - POD(a)] \times f(a)\, da}$$

  Therefore:

$$f(a|NC) \propto [1 - POD(a)] \times f(a) \quad (5\text{-}33)$$

  Eq. (5-33) shows that the posterior distribution depends on:

  - Inspection tool's quality, i.e. POD curve (a_{md})
  - The prior distribution of crack size, $f(a)$

- **Crack Detected and Measured**

Predicted crack size by the fatigue model (a_j) is obtained from Eq. (5-23). The predicted crack size is different from the measured crack size (a_m) at the same time. Therefore the associated error, ε which involves both measurement and model error can be defined as:

$$\varepsilon = ln\, a_j - ln\, a_m \tag{5-34}$$

The associated error is assumed as a normally distributed random variable with a known mean equal to zero and an uncertain variance, σ_ε^2 i.e.:

$$f_\varepsilon \sim Normal\,(0, \sigma_\varepsilon^2)$$

$$f_\varepsilon = \frac{1}{\sqrt{2\pi\sigma_\varepsilon^2}} exp\left(-\frac{(\varepsilon-\mu)^2}{2\sigma_\varepsilon^2}\right) = \frac{1}{\sqrt{2\pi\sigma_\varepsilon^2}} exp\left(-\frac{\varepsilon^2}{2\sigma_\varepsilon^2}\right) \tag{5-35}$$

Where f_ε is the probability distribution function for ε.

If the fatigue model is assumed unbiased to the mean value of model and measurement:

$$E\left[a_j\right] = E[a_m] \tag{5-36}$$

Therefore, ε has a known mean of zero:

$$E[\varepsilon] = E\left[\ln a_j\right] - E[\ln a_m] = 0 \tag{5-37}$$

However, the variance of the error is unknown which can be considered as an uncertain parameter.

If the predicted crack size by the fatigue model is denoted by a_j and the measured crack size denoted by a_m, one realisation of the error is obtained as:

$$e = ln\, a_j - ln\, a_m = ln\, (\frac{a_j}{a_m}) \tag{5-38}$$

Therefore, in this case, in addition to the crack size, error variance is also assumed as an uncertain parameter. In this case, the posterior distribution is proportional to:

$$f_{A_j,\sigma_\varepsilon^2|I(j)}(a, x|CM) \propto P[CM|a, x] \times f_{A_j,\sigma_\varepsilon^2}(a, x) \tag{5-39}$$

where:

- x is error variance
- $f_{A_j,\sigma_\varepsilon^2|I(j)}(a,x|CM)$ is the posterior joint PDF of crack size and error variance
- $P[CM|a,x]$ is the likelihood function
- $f_{A_j,\sigma_\varepsilon^2}(a,x)$ is the prior joint PDF of crack size and error variance

Likelihood Function:

Likelihood function can be written as:

$$P[CM|a,x] = P[a_m \mid \{(A(j)=a)\ \&\ (\sigma_\varepsilon^2 = x)\}] \times POD(a) \tag{5-40}$$

The event associated with measuring a_m is equivalent to event $\varepsilon = e$. Therefore, the likelihood function can be written as:

$$P[CM|a,\sigma_\varepsilon^2] = f_{\varepsilon|A_j,\sigma_\varepsilon^2}(e|a,x) \times POD(a) \tag{5-41}$$

Since ε is normally distributed:

$$f_{\varepsilon|A_j,\sigma_\varepsilon^2}(e|a,x) = \frac{1}{\sqrt{2\pi x}} exp\left(-\frac{e^2}{2x}\right) \tag{5-42}$$

Therefore, the likelihood function is obtained as:

$$P[CM|a,\sigma_\varepsilon^2] = \frac{1}{\sqrt{2\pi x}} exp\left(-\frac{e^2}{2x}\right) \times POD(a) \tag{5-43}$$

Prior Distribution:

By definition of conditional probability for the prior PDF:

$$f_{A_j,\sigma_\varepsilon^2}(a,x) = f_{A_j}(a) \times f_{\sigma_\varepsilon^2|A_j}(x|a) \tag{5-44}$$

Where $f_{\sigma_\varepsilon^2|A_j}(x|a)$ is the conditional PDF of error variance given that measurement is provided. This conditional PDF of error variance has a normal distribution with a mean equal to zero and unknown variance. The conjugate prior for this variable (variables with known mean and uncertain variance) is Inverse Gamma (see Table 5.1).

The inverse gamma distribution is a two-parameter distribution with shape parameter (α) and scale parameter (β). The PDF of this distribution is [112]:

$$f(\theta) = \frac{\beta^{\alpha}}{\Gamma(\alpha)} \times \theta^{-(\alpha+1)} \times exp\,(-\frac{\beta}{\theta}) \tag{5-45}$$

Therefore, the prior distribution of error variance can be written as:

$$f^{prior}_{\sigma^2_{\varepsilon}|A_j}(x|a) = \frac{{\beta_{prior}}^{\alpha_{prior}}}{\Gamma(\alpha_{prior})} x^{-(\alpha_{prior}+1)} exp\left(-\frac{\beta_{prior}}{x}\right) \tag{5-46}$$

To let the data dominate the posterior, a non-informative prior distribution is selected. For usage of non-informative prior for the inverse gamma, both parameters are selected close to zero [112], i.e.:

$$\alpha_{prior} = \beta_{prior} = 0.001 \tag{5-47}$$

When new data is available (a crack measured), using the conjugate approach, the posterior conditional distribution of the error variance is obtained as [112]:

$$\begin{aligned} \alpha_{post} &= \alpha_{prior} + \frac{1}{2} \\ \beta_{post} &= \beta_{prior} + \frac{(e-\mu)^2}{2} = \beta_{prior} + \frac{e^2}{2} \end{aligned} \tag{5-48}$$

where e is the realisation of the error (Eq. (5-38)). It can be seen that β_{post} is a function of realisation of the error (e) which is a function of crack size. The posterior conditional distribution of the error variance is obtained as:

$$f^{post}_{\sigma^2_{\varepsilon}|A_j}(x|a) = \frac{(\beta_{post})^{\alpha_{post}}}{\Gamma(\alpha_{post})} x^{-(\alpha_{post}+1)} exp\left(-\frac{\beta_{post}}{x}\right) \tag{5-49}$$

Substituting Eq. (5-49) into Eq. (5-44):

$$f_{A_j,\sigma^2_{\varepsilon}}(a,x) = f_{A_j}(a) \times \left[\frac{(\beta_{post})^{\alpha_{post}}}{\Gamma(\alpha_{post})} x^{-(\alpha_{post}+1)} exp\left(-\frac{\beta_{post}}{x}\right)\right] \tag{5-50}$$

Posterior Distribution:

Replacing likelihood function and the prior into Eq. (5-39), the posterior distribution is obtained as:

$$f_{A_j,\sigma^2_{\varepsilon}|I(j)}(a,x|CM) \propto$$

$$\left[POD(a) \times \frac{1}{\sqrt{2\pi x}} exp\left(-\frac{e^2}{2x}\right)\right] \times \left[f_{A_j}(a) \times \left[\frac{{\beta_{prior}}^{\alpha_{prior}}}{\Gamma(\alpha_{prior})} x^{-(\alpha_{prior}+1)} exp\left(-\frac{\beta_{prior}}{x}\right)\right]\right] \tag{5-51}$$

I.e.:

$$f_{A_j,\sigma_\varepsilon^2|I(j)}(a,x|CM) \propto$$

$$\frac{{\beta_{prior}}^{\alpha_{prior}}}{\Gamma(\alpha_{prior})\sqrt{2\pi}} x^{-(\alpha_{prior}+3/2)} exp\left(-\frac{\beta_{prior}+e^2/2}{x}\right) \times POD(a) \times f_{A_j}(a) \quad (5\text{-}52)$$

Therefore:

$$f_{A_j,\sigma_\varepsilon^2|I(j)}(a,x|CM) \propto$$

$$\left(\frac{{\beta_{prior}}^{\alpha_{prior}}}{\Gamma(\alpha_{prior})\sqrt{2\pi}}\right) \times \left[x^{-(\alpha_{post}+1)} exp\left(-\frac{\beta_{post}}{x}\right)\right] \times POD(a) \times f_{A_j}(a) \quad (5\text{-}53)$$

Based on Eq. (5-49):

$$x^{-(\alpha_{post}+1)} exp\left(-\frac{\beta_{post}}{x}\right) = \frac{\Gamma(\alpha_{post})}{(\beta_{post})^{\alpha_{post}}} \times f_{\sigma_\varepsilon^2|A_j}^{post}(x|a) \quad (5\text{-}54)$$

Therefore:

$$f_{A_j,\sigma_\varepsilon^2|I(j)}(a,x|CM) \propto$$

$$\left(\frac{{\beta_{prior}}^{\alpha_{prior}}}{\Gamma(\alpha_{prior})\sqrt{2\pi}}\right) \times \left[\frac{\Gamma(\alpha_{post})}{(\beta_{post})^{\alpha_{post}}} \times f_{\sigma_\varepsilon^2|A_j}^{post}(x|a)\right] \times POD(a) \times f_{A_j}(a) \quad (5\text{-}55)$$

I.e.:

$$f_{A_j,\sigma_\varepsilon^2|I(j)}(a,x|CM) \propto$$

$$\frac{({\beta_{prior}}^{\alpha_{prior}}) \times \Gamma(\alpha_{post})}{({\beta_{post}}^{\alpha_{post}}) \times \Gamma(\alpha_{prior})} \times f_{\sigma_\varepsilon^2|A_j}^{post}(x|a) \times POD(a) \times f_{A_j}(a) \quad (5\text{-}56)$$

Eq. (5-55) shows that the posterior joint distribution of the crack size and error variance.

The marginal crack size distribution is then obtained by integrating the above equation over all of the possible values of σ_ε^2. It is noted that $a, \alpha_{prior}, \alpha_{post}, \beta_{prior}, \beta_{post}$ do not depend on the value of x, therefore:

$$f_{A_j|I(j)}(a|CM) \propto$$

$$\left(\frac{{\beta_{prior}}^{\alpha_{prior}}}{{\beta_{post}}^{\alpha_{post}}} \times \frac{\Gamma(\alpha_{post})}{\Gamma(\alpha_{prior})}\right) \times POD(a) \times f_{A_j}(a) \times \int_0^\infty f_{\sigma_\varepsilon^2|A_j}^{post}(x|a)dx \quad (5\text{-}57)$$

The area under probability distribution function is equal to one, i.e:

$$\int_0^{\infty} f_{\sigma_\varepsilon^2|A_j}^{post}(x|a)dx = 1 \tag{5-58}$$

Therefore:

$$f_{A_j|I(j)}(a|CM) \propto \left(\frac{{\beta_{prior}}^{\alpha_{prior}}}{{\beta_{post}}^{\alpha_{post}}} \times \frac{\Gamma(\alpha_{post})}{\Gamma(\alpha_{prior})}\right) \times POD(a) \times f_{A_j}(a) \tag{5-59}$$

Eq. (5-59) presented an analytical expression for the updated density function of crack size when a crack is detected and measured. Based on the equation, the updated distribution is proportional to:

- Prior distribution
- Probability of detection
- A function that depends on the prior and posterior parameters of the density function of the error variance

5.4.3.3 Updating the Crack Size Distribution in a Tubular Joint

To demonstrate the application it is assumed that a tubular joint is subjected to the stress ranges which are modelled by a lognormal distribution with a mean of 300MPa and coefficient of variation of 0.2. It is assumed that at the time of reference, the prior distribution of the uncertain crack depth (a), is a lognormal distribution with a mean value of 5 mm and a coefficient of variation of 0.3.

Imagine the inspection result is now available. Three different cases for the inspection result are considered to investigate the effect of the new data on the posterior distribution. These three cases are:

- No crack detected
- A crack is detected and measured equal to 6mm
- A crack is detected and measured equal to 10mm

Figure 5.23 shows the updated distributions for the crack size at the time of reference, for these three different results during the inspection activity. For obtaining the posterior distributions, Eq. (5-33) and Eq. (5-59) are used for the no crack detected and the crack detected cases, respectively.

Figure 5.23 shows that in case of no crack detected, the posterior distribution of crack size shifts to the left and has a smaller mean value than the prior mean value. On the other hand, when a crack is measured, the posterior distribution shifts to the right-hand side. Moreover, the mean value in the updated distribution becomes greater as the measured crack size increases.

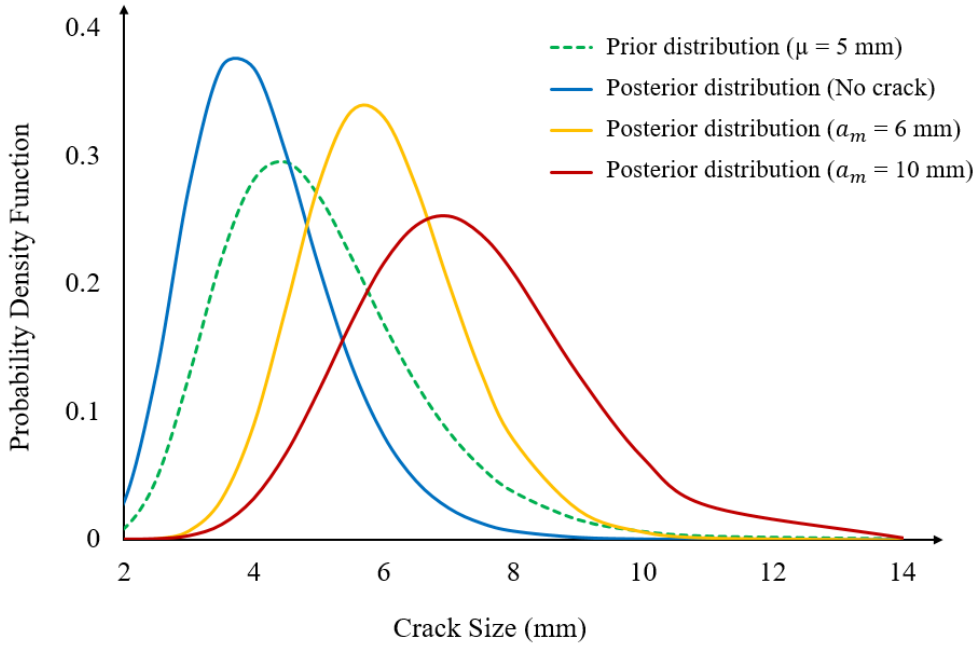

Figure 5.23. The updated probability density functions of the crack depth based on the inspection result

As it can be seen from Figure 5.23, if the fatigue model is an accurate model for prediction (i.e. the measured crack size is close to the mean value of the prior distribution), the posterior distribution includes less uncertainty (narrower distribution), whereas if the model cannot predict fatigue crack size precisely (e.g. $a_m = 10mm$), the posterior distribution is wider than the prior. In fact, in this case, the updated distribution involves more uncertainty.

5.4.4 Planning for Inspection

Due to the existence of several uncertainties in the fatigue process, the predicted fatigue crack size might not represent the real crack size. Therefore, offshore platforms are periodically inspected throughout their lifetime to find out the level of degradation and to assure that existing defects in the structure do not exceed the critical size.

Regarding fatigue damage, the inspection results involve the detection and measurement of fatigue cracks. The inspection results can be used to improve the estimation of the crack size. A Bayesian procedure is utilised to update the fatigue crack size distribution in light of inspection results (See section 5.4).

In Chapter 4, it was explained that two approaches exist for inspection planning. The first approach, which is called the time-based inspection approach, is to set the inspection interval to a fixed time, e.g. every five years. The other approach, which is called the reliability-based inspection approach, is to set the annual failure probability threshold to be a fixed value, and the inspection is carried out when the failure probability is more than the threshold. Figure 5.24 shows the reliability-based inspection plan for a tubular joint in case of no crack is detected during the inspection activity.

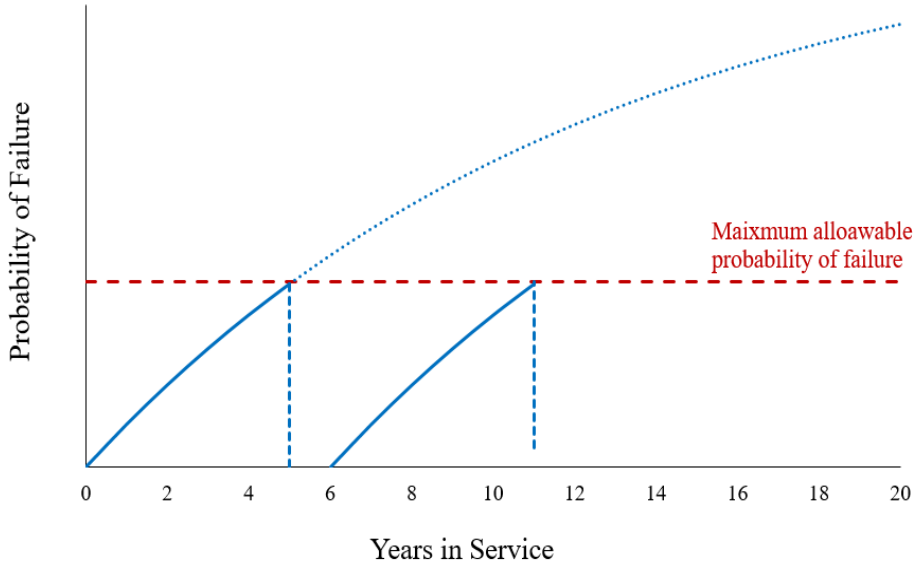

Figure 5.24. Reliability-based inspection plan for a specific joint assuming no crack is found

5.4.4.1 Reliability-Based Inspection

After updating the crack size distribution, the component probability of failure (reliability) can be updated using the fatigue limit state (Eq. (5-21)) and Monte Carlo simulations. Failure happens when the crack size reaches a critical size (a_c), which is assumed equal to the thickness of the joint.

Consider a_k as the crack size at time k and $f(a_k)$ as the corresponding distribution. If $f_0(a_k)$ indicates the crack size distribution before updating and $f_1(a_k)$ indicates the distribution after updating, the probability of failure before updating is estimated by:

$$P_{f_0} = P[a_k \geq a_c] = 1 - \int_0^{a_c} f_0(a_k) \times da \tag{5-60}$$

And the probability of failure after updating is:

$$P_{f_1} = P[a_k \geq a_c] = 1 - \int_0^{a_c} f_1(a_k) \times da \tag{5-61}$$

Figure 5.25 shows the probability of failure before and after updating, schematically.

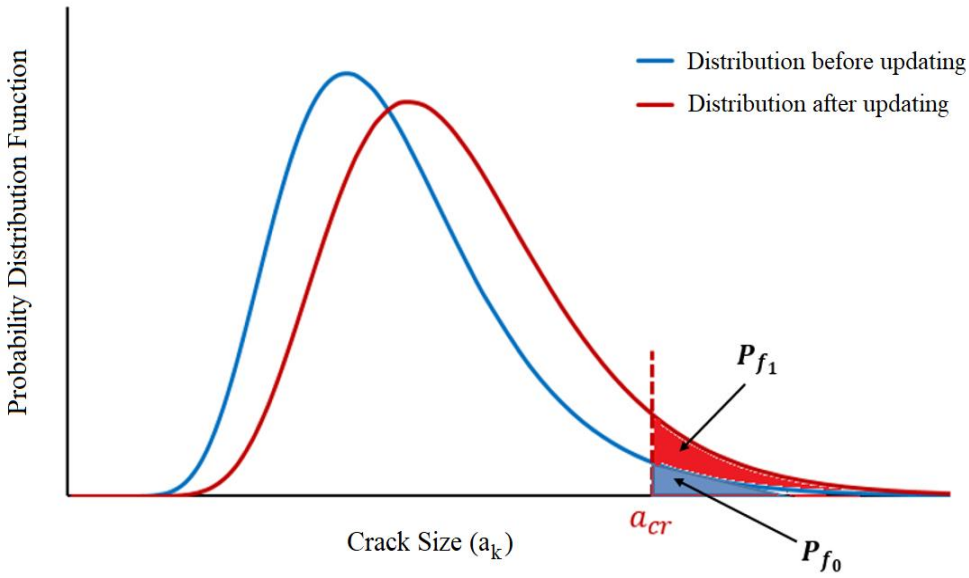

Figure 5.25. Probability of failure before and after updating

After updating the probability of failure of the considered joint, the updated probability will be used for obtaining the next inspection time. Based on the crack size findings in the inspection activity, the next inspection activity will be performed:

- In a shorter period of time than expected if the measured crack size is bigger than the predicted crack size
- In a longer period of time than expected if no crack is found or the measured crack size is smaller than the predicted crack size

Therefore, the results of each inspection activity have a crucial effect on the time interval for the next inspection activity.

5.4.4.2 Tubular Joint Reliability Updating – Application of the Inspection Planning

To calculate the probability of failure during the time, the fatigue proposed model based on the Paris law is used. By using Eq. (5-23) and the sampling method, the crack size distribution at each year can be obtained. Let's assume an inspection activity is performed after five years (t_{insp}=5). For simplicity, it is assumed that the predicted crack size distribution at inspection time (t_{insp}=5) is a lognormal distribution with a mean value of 3mm and a standard deviation of 0.3mm.

Two possible results are no crack is detected and a crack is detected and measured. To demonstrate the application, the following cases are considered for the inspection results:

(I) No crack is detected at inspection time

(II) A crack of 5mm is measured at inspection time

Having provided new data (inspection results), the updated crack size distribution in case (I) and (II), is obtained by using Eq. (5-33) and Eq. (5-59), respectively. By using the updated distribution of the crack size at the time of inspection (t_{insp}=5), the joint reliability during the time is estimated.

Figure 5.26 and Figure 5.27 show the variation of the joint probability and joint reliability as a function of time using the updated distributions at t_{insp}=5 years.

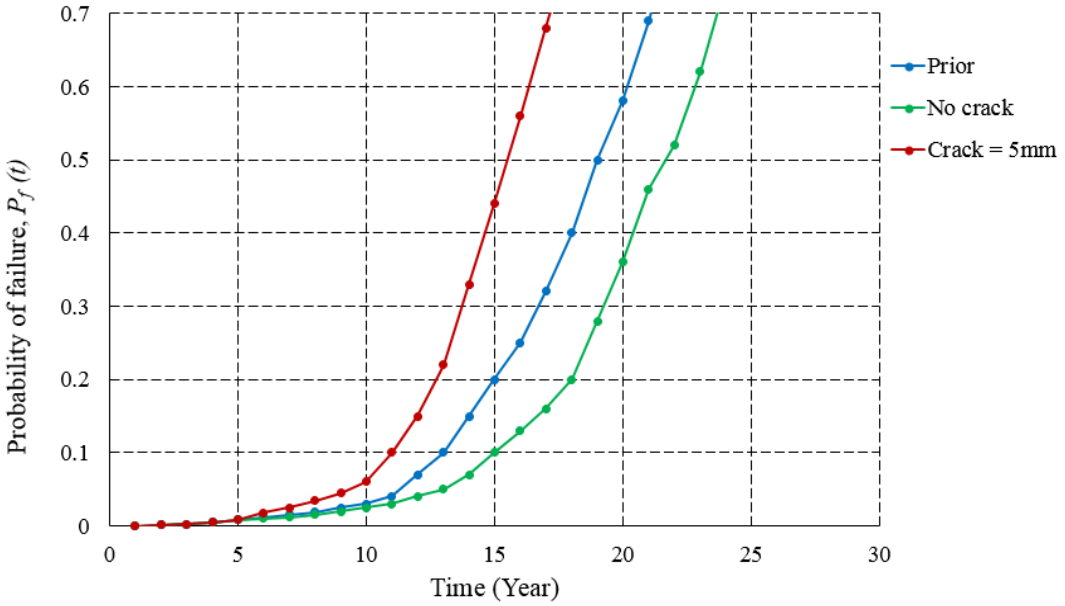

Figure 5.26. Joint probability of failure over time (t_{insp}=5)

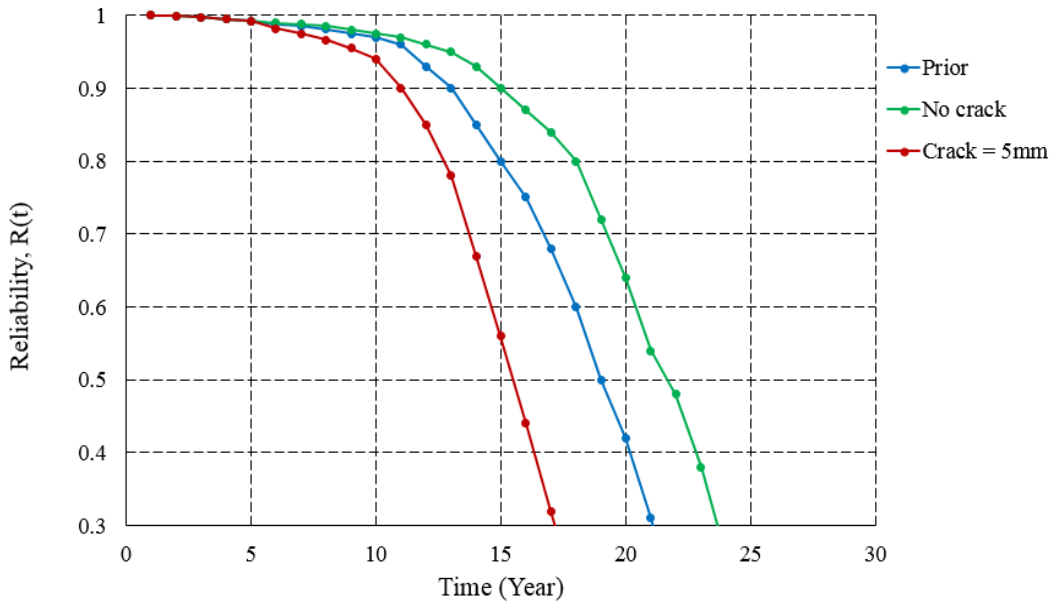

Figure 5.27. Joint reliability over time (t_{insp}=5)

If case (I) happens as the result of the inspection, the green line in Figure 5.26 will be used for the next inspection activity and the time interval for the next inspection activity is increased. Whereas for case (II), the red line will be considered for the next inspection, and the time interval between inspection activities will be reduced.

Depending on the inspection findings at inspection time (t_{insp}=5), the following decisions are made for the next inspection activity as:

- In case of no crack is detected at inspection time (Case (I)):
  - The time interval is greater than the time-based inspection interval (which is assumed 5 years). Therefore, the next inspection will be performed at a later time, for instance at year 12 instead of year 10 (the inspection time will be based on the maximum acceptable probability of failure).
  - For the next updating process (when the inspection is performed at year 12), the green line in Figure 5.26 will be used as the prior at the inspection time (t_{insp}=12).
- In case of a crack of 5mm is measured at inspection time (Case (II)):
  - The time interval is smaller than the time-based inspection interval. Therefore, the next inspection will be performed at an earlier time, for instance at year 8

instead of year 10 (the inspection time will be based on the maximum acceptable probability of failure).

- For the next updating process (when the inspection is performed at year 8), the red line in Figure 5.26 will be used as the prior at the inspection time (t_{insp}=8).

Figure 5.28 shows the prior probability of failure that will be used for the next inspection activity depending on the inspection findings at year 5.

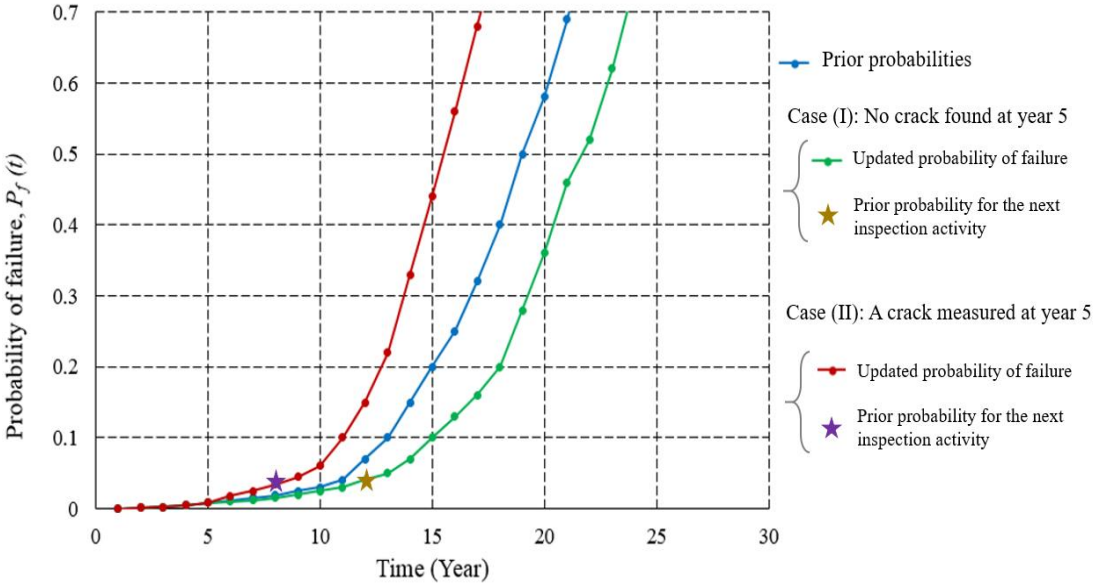

Figure 5.28. The prior probability of failure curves for the next inspection activity

5.5 Sensitivity of the Bayesian Updating to the Input Parameters

The Bayesian approach is explained in Section 5.2. Based on Bayes' theorem, the posterior is proportional to the prior and likelihood. Therefore, the credibility of the posterior distribution depends on the credibility of the inputs. If the inputs are not reliable, the results of the Bayesian updating methods are not valid.

Sensitivity analysis can be performed to find out which parameters have the greatest effect on the posterior distribution. Having found the important parameters, the user can focus on those parameters to obtain more data.

When new information (inspection results) is available for the fixed offshore platforms, the posterior distribution of crack size for tubular joints can be updated by using a Bayesian approach. In this section, an expression for the posterior distribution based on the input parameters (e.g. prior distribution, likelihood function, POD curves,

etc.) is derived. After obtaining the expression, the sensitivity of the posterior to the inputs is developed.

5.5.1 Sensitivity of the Bayesian Updating to the Inputs - No Crack Detected

Based on Eq. (5-33), in case of no crack detection, the posterior distribution depends on two parameters:

1) The prior distribution of crack size
2) Inspection tool's quality, i.e. POD curve

Therefore, in this section, the sensitivity of the posterior distribution (Bayesian updating) to these two inputs is investigated.

5.5.1.1 Sensitivity to the Prior Selection

The prior distribution indicates the prior information of the parameter of interest and it is based on previous knowledge or the user's judgement. When there is not enough knowledge about the parameter, the non-informative prior distribution is recommended.

The prior crack size distribution can be assumed based on theoretical considerations, experts' opinions, past experiences, or data reported in the literature. Different distributions such as exponential, normal, and lognormal are considered for the crack size in the literature [126].

The following priors are considered to perform sensitivity analysis. In all cases, it is assumed that the expected value of the crack size is equal to 5mm.

a) Normal distribution: $f(a) \sim Normal(5, 1.5)$
b) Lognormal distribution: $f(a) \sim Lognormal(5, 1.5)$
c) Exponential distribution: $f(a) \sim Exponential\ (5)$
d) Uniform distribution: $f(a) \sim Uniform(0.4, 9.6)$
e) Sampling method: The numerical approach presented in Section 5.4.1.3

Figure 5.29 shows the selected prior distributions for the crack size.

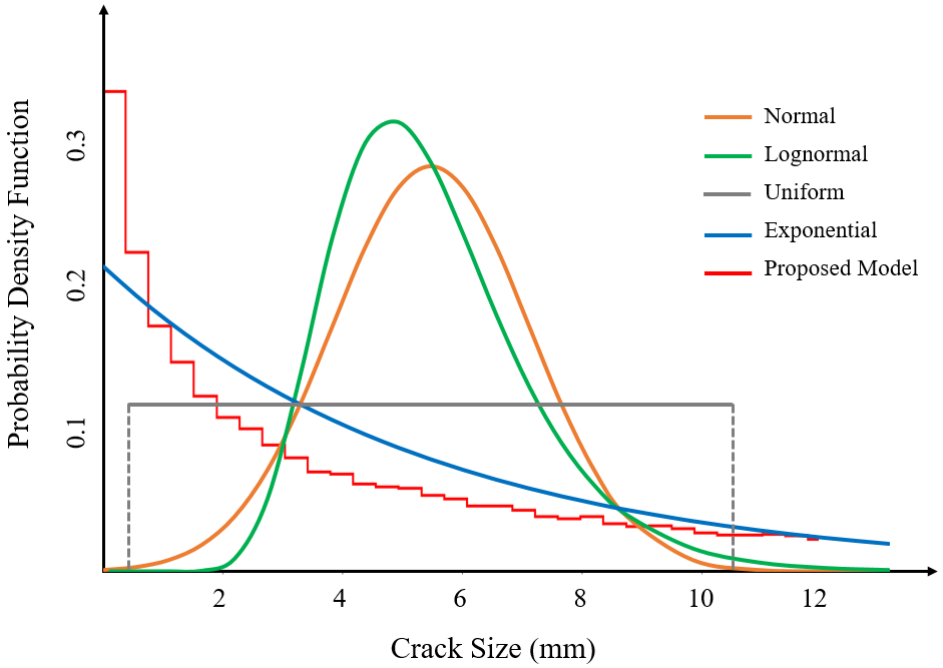

Figure 5.29. Selected prior distributions for the crack size

Figure 5.30 shows the posterior distribution for each prior when no crack is detected during the inspection activity.

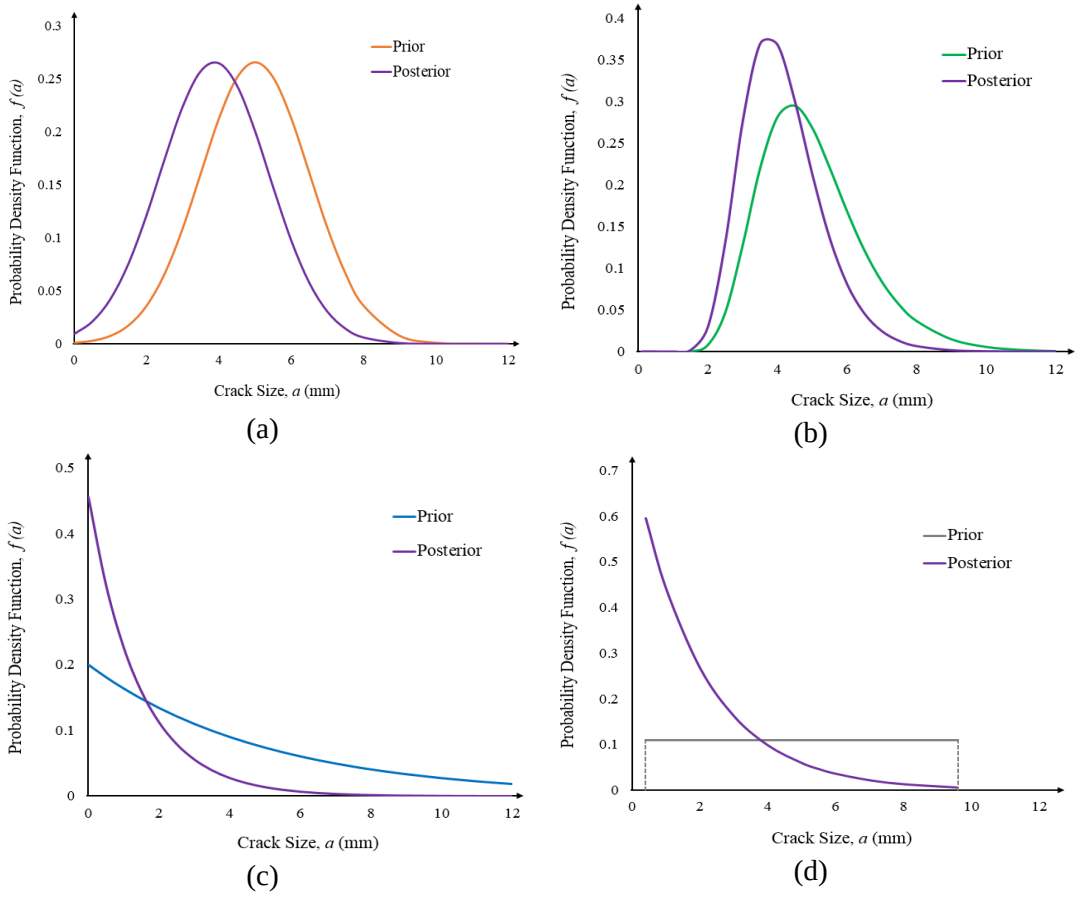

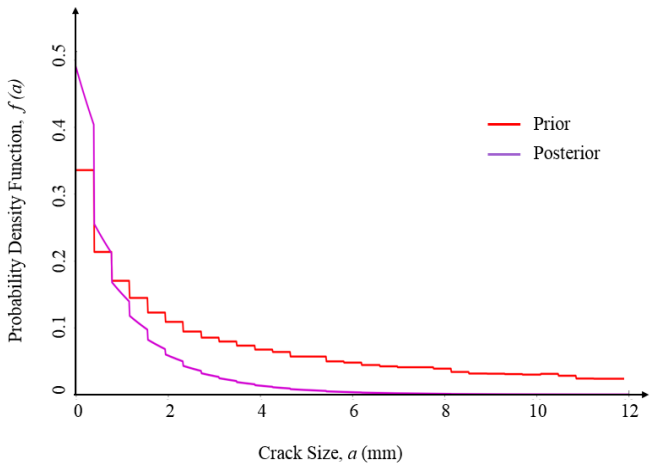

(e)

Figure 5.30. Posterior distributions of crack size for the different priors, (a) normal, (b) lognormal, (c) exponential, (d) uniform and (e) proposed model

The above figures indicate that, regardless of the prior distribution, the posterior distributions shift to the left if no crack is detected. Therefore, the updated probability of failure, in this case, will be reduced which is reasonable.

Figure 5.31 shows the posterior distributions of the crack size for different prior distributions.

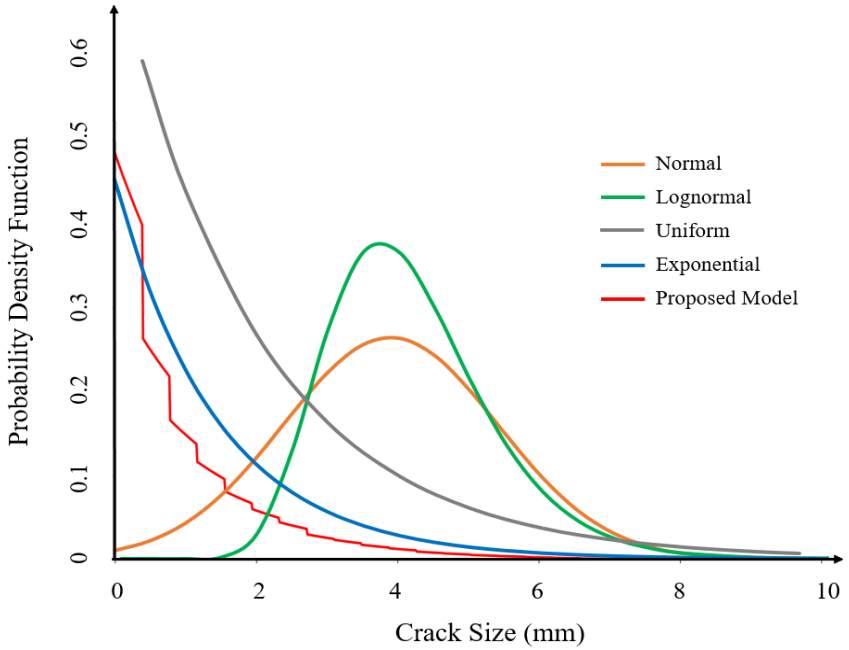

Figure 5.31. Posterior distributions of the crack size for the different priors (No crack detected)

Figure 5.31 illustrates that if the selected prior is either a normal or lognormal distribution, the posterior distributions still have a long tail (right tail), whereas, for the exponential and the proposed model distribution, the posterior distribution has a much smaller tail. Table 5.4 shows the probability of a crack being greater than 8mm before and after updating for each prior distribution.

Table 5.4. Probability of a crack being greater than 8mm for different prior distributions

Selected distribution	Prior probability	Posterior probability	$P_{posterior}/P_{prior}$ (%)
Normal	$P_{prior}(a \geq 8) = 0.0447$	$P_{posterior}(a \geq 8) = 0.0069$	$0.0069/0.0447$ (= 15%)
Lognormal	$P_{prior}(a \geq 8) = 0.0609$	$P_{posterior}(a \geq 8) = 0.0086$	$0.0086/0.0609$ (= 14%)
Uniform	$P_{prior}(a \geq 8) = 0.1744$	$P_{posterior}(a \geq 8) = 0.0117$	$0.0117/0.1744$ (= 7%)
Exponential	$P_{prior}(a \geq 8) = 0.1408$	$P_{posterior}(a \geq 8) = 0.0033$	$0.0033/0.1408$ (= 2%)
Proposed Model	$P_{prior}(a \geq 8) = 0.1982$	$P_{posterior}(a \geq 8) = 0.0011$	$0.0011/0.1982$ (= 0.6%)

The last column in Table 5.4 indicates that if the prior distribution is assumed either exponential or based on the proposed model, the posterior distribution significantly will be affected in this case, e.g. the probability of a crack being greater than 8mm is sharply reduced. Therefore, in the not detection case, the posterior distribution is strongly affected by prior selection. Hence, the prior distribution should be selected based on reasonable assumptions.

5.5.1.2 Sensitivity to the POD Curves

The posterior distribution is also being affected by the inspection tool's quality, i.e. POD curve (a_{md}). Three different cases are considered for the POD curve:

- High quality inspection method: $a_{md} = 2mm$
- Medium quality inspection method: $a_{md} = 5mm$
- Low quality inspection method: $a_{md} = 10mm$

Figure 5.32 shows the posterior distributions for different inspection methods when different distributions are selected as a prior distribution.

(a)

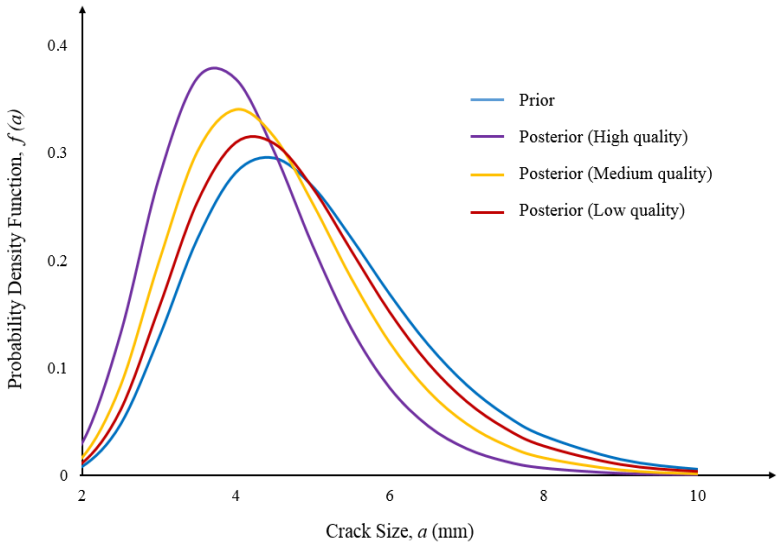

(b)

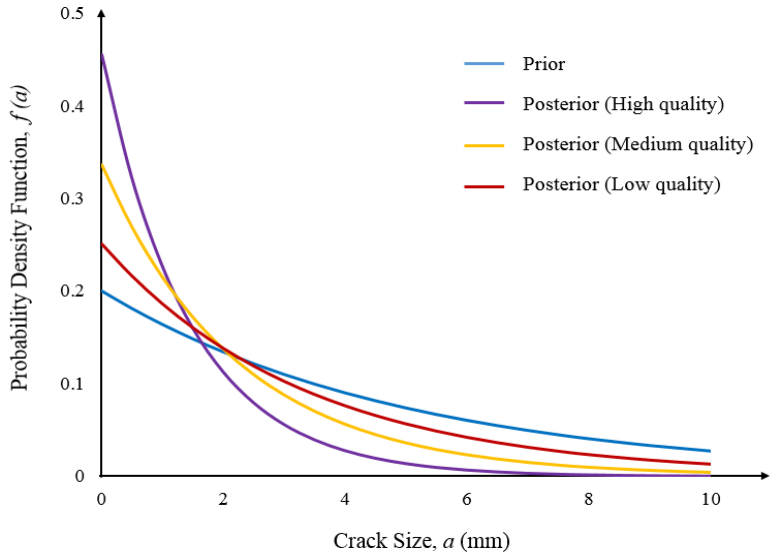

(c)

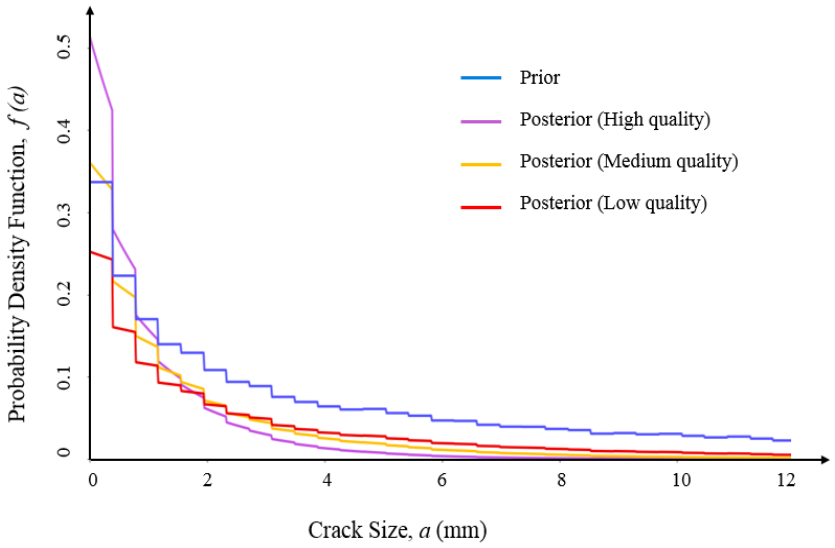

Figure 5.32. Posterior distributions for different inspection resolutions, (a) lognormal prior, (b) exponential prior, and (c) proposed model for prior

Results show that regardless of the resolution of the inspection technique, the posterior distributions shift to the left in case of no detection. However, when the low-quality inspection tool is used, the posterior is close to the prior. In fact, in this case, the prior dominates the posterior result. On the other hand, if the inspection tool has acceptable performance (high quality), data has a bigger effect on the posterior results.

5.5.2 Sensitivity of the Bayesian Updating to the Inputs- Crack Measured

In Section 5.4.3.2, an analytical expression was presented to update the density function of crack size when a crack is detected and measured. Based on Eq. (5-59), the posterior (updated) distribution is proportional to:

1) Prior distribution
2) Probability of detection
3) A function that depends on the prior and posterior parameters of the error variance distribution

5.5.2.1 Sensitivity to Prior Selection

The same priors as those introduced in Section 5.5.1 are considered to perform sensitivity analysis. Again, it is assumed that the expected value of the crack size is equal to 5mm. However, in this section, it is assumed that a crack of 6mm is measured during the inspection activities.

Figure 5.33 shows the posterior distribution for each prior when a crack of 6mm is measured during the inspection activity.

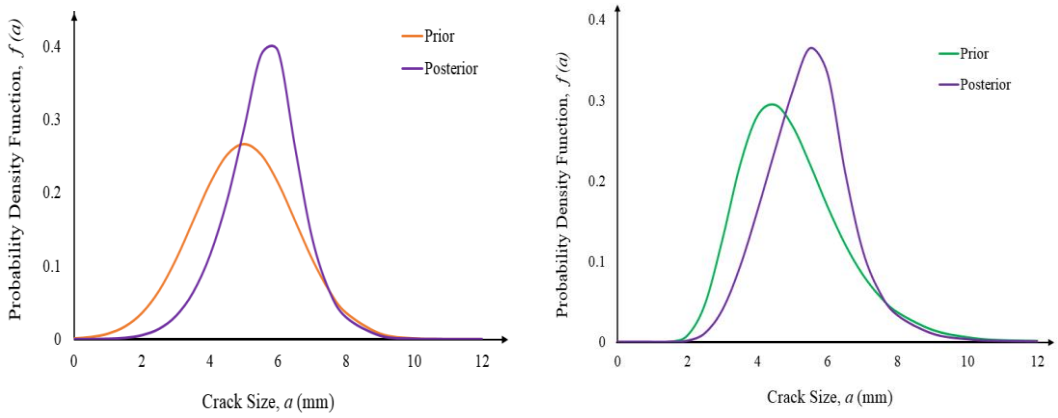

(a) (b)

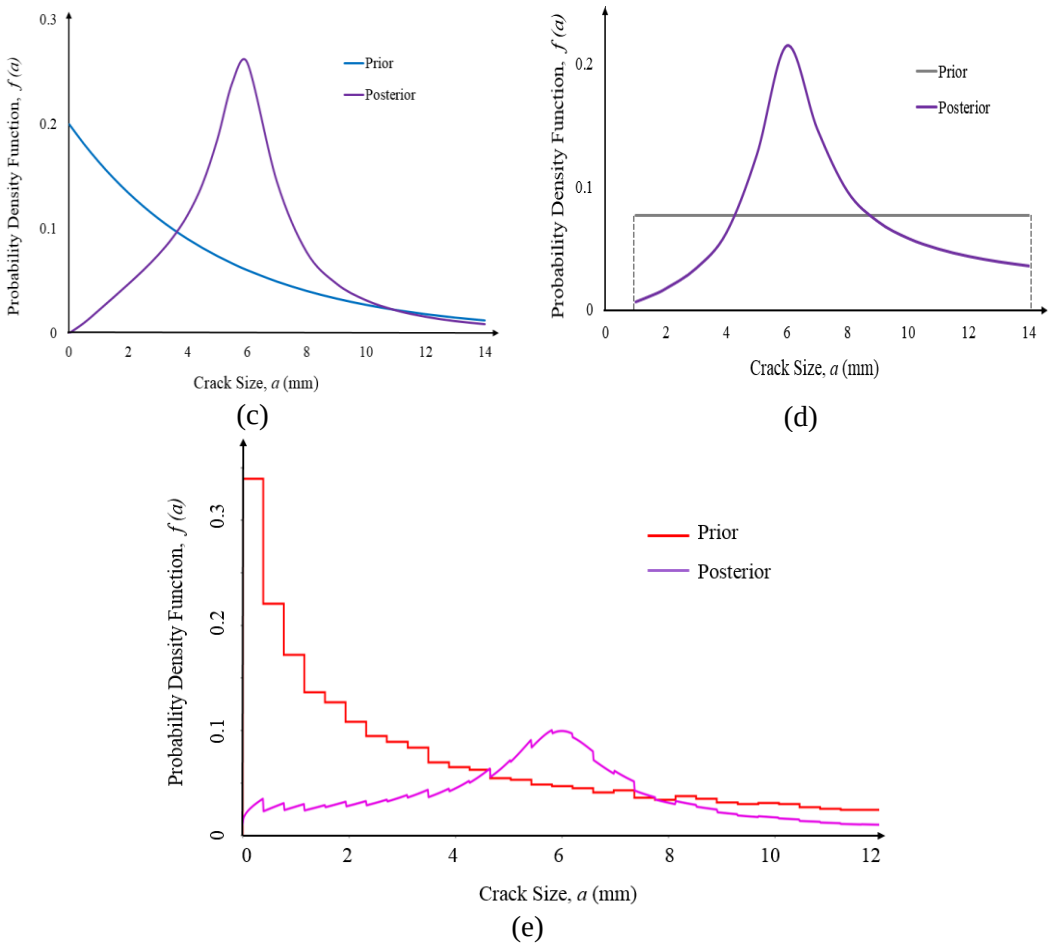

Figure 5.33. Posterior distributions of crack size for the different priors, (a) normal, (b) lognormal, (c) exponential, (d) uniform and (e) proposed model

Figure 5.33 shows that regardless of the prior distribution, the posterior distribution is influenced by the observed crack size which is 6mm crack.

Figure 5.34 shows the posterior distributions of the crack size for different prior distributions in the case of a 6mm crack being measured. As it can be seen from Figure 5.34, if the prior is selected either exponential distribution or based on the proposed model, the posterior distributions have a long tail (right tail), whereas, for the normal and lognormal distributions, the posterior distribution only has a small tail.

This is completely opposite of the results obtained in the 'No crack detected' case. It was shown in Section 5.5.1 that in the 'No crack detected' case if the prior is selected as either normal or lognormal distributions, the posterior distributions have a long tail.

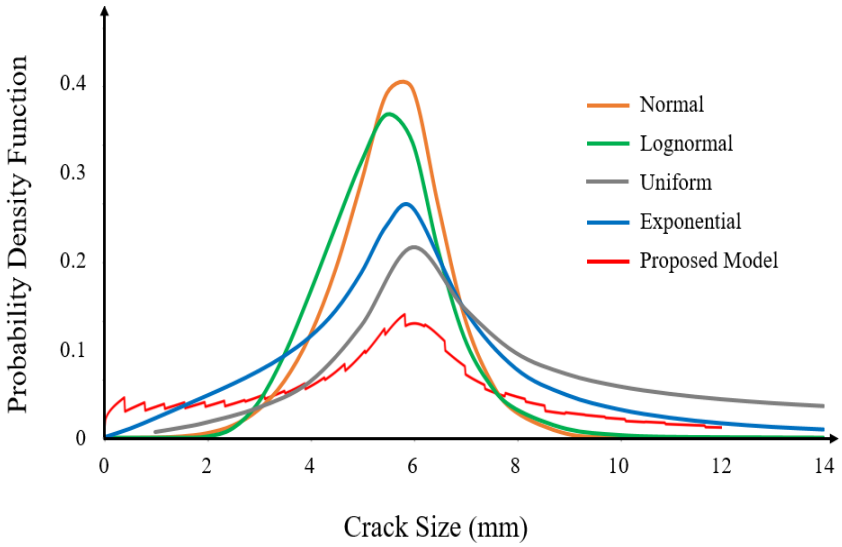

Figure 5.34. Posterior distributions of crack size for different prior distributions

5.5.2.2 Sensitivity to POD Curves

Based on Eq. (5-59), the posterior distribution is also being affected by the inspection tool's quality, i.e. POD curve (a_{md}). Three different cases (as explained in Section 5.5.1) are considered for the POD curve.

Figure 5.35 shows the posterior distributions for different inspection methods when a lognormal distribution is selected as a prior distribution. It can be seen that, in this case, the posterior distribution is not sensitive to the quality of the inspection method. It is a reasonable result because given that a crack has been detected, the quality of the inspection method does not have a significant effect on the posterior.

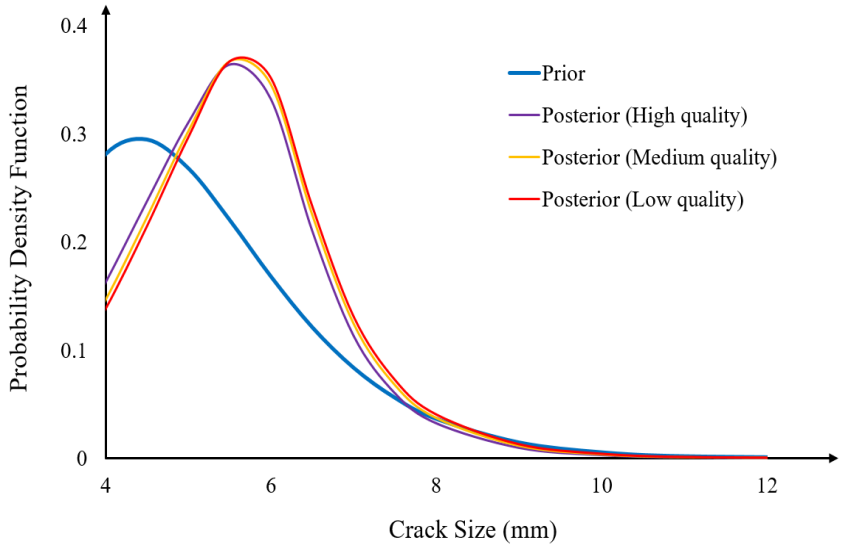

Figure 5.35. Prior and posterior distributions for different inspection resolutions

5.5.2.3 Sensitivity to the Error Model

The associated error (ε) which involves both measurement and model error was explained in Section 5.4.3.2. A normal distribution with a mean value equal to zero and an uncertain variance (σ^2) is assumed for the associated error. The conjugate prior and posterior distributions for the variance of error (ε) are inverse gamma distribution. Two different priors are considered for the distribution of variance:

- Non-informative prior: If the values of α and β are selected close to zero (e.g. 0.01), then these values yield a non-informative prior for the variance distribution.
- Informative prior: Expert's knowledge is required for the selection of an informative prior for the error variance distribution. The informative prior can be selected based on the expert's opinion about how the predicted fatigue model represents reality. Here, for the informative prior of the variance of the error, the values α and β are taken equal to 3 and 2, respectively.

Figure 5.36 shows the informative and non-informative priors for the parameter of interest (error variance).

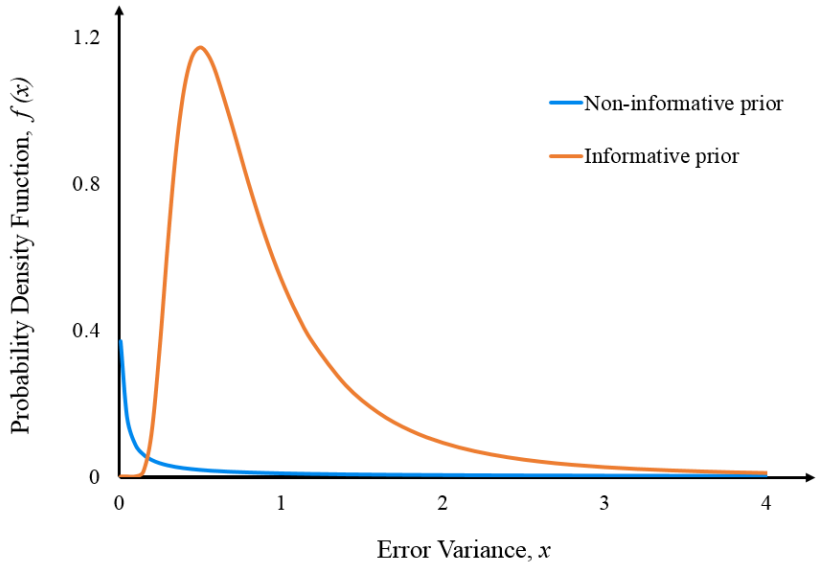

Figure 5.36. Informative and non-informative prior distributions for error variance

When a new inspection result is available, α_{post} and β_{post} can be obtained by using Eq. (5-48). Figure 5.37 shows the posterior distribution for error variance when a crack of 6mm is measured.

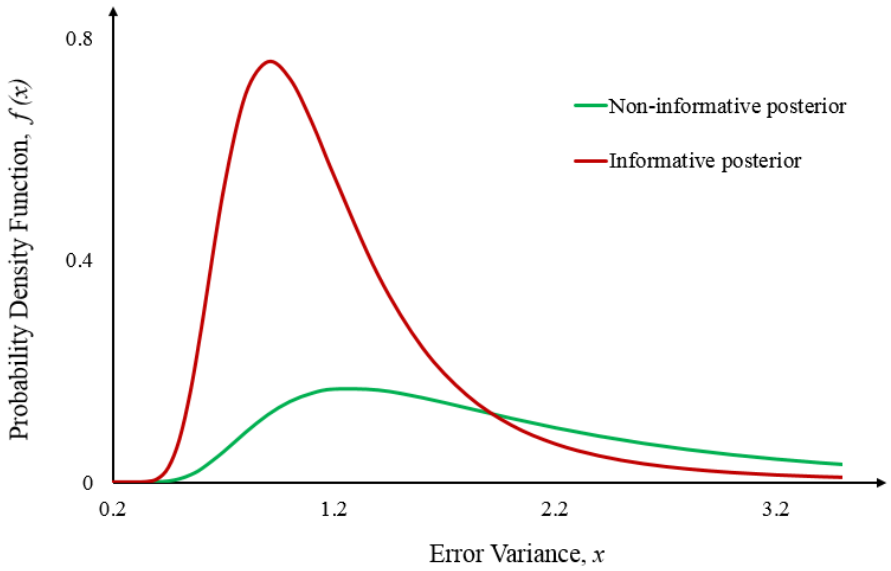

Figure 5.37. Posterior distributions for informative and non-informative priors

Figure 5.38 shows the sensitivity of the posterior distribution of the crack size to the error variance model when three different prior distributions are considered for crack size (a crack of 6mm is measured).

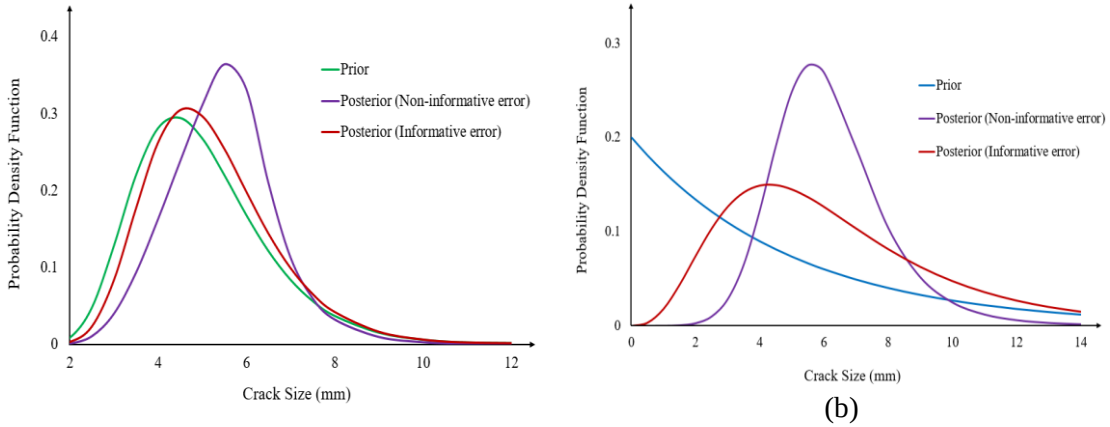

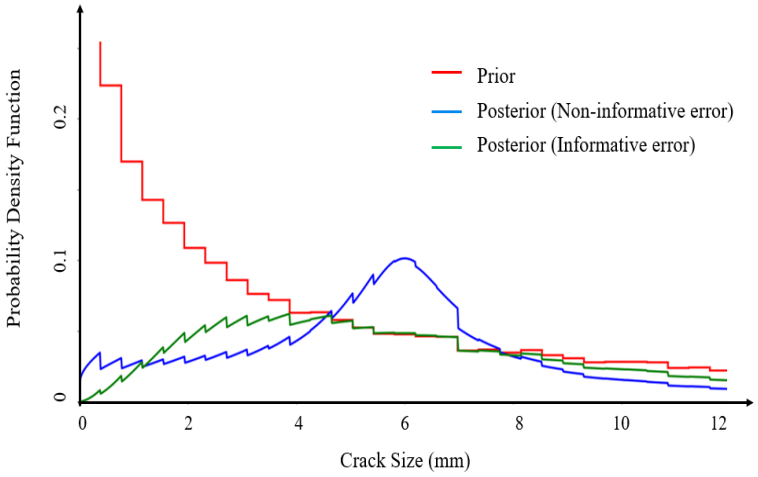

(c)

Figure 5.38. Effect of error variance on the posterior distributions of crack size for (a) lognormal prior, (b) exponential prior, and (c) proposed model prior when a 6mm crack is measured

Figure 5.38 demonstrates that if a non-informative prior for the error variance is chosen, the posterior distribution of the crack size is dominated by data, whereas if an informative prior is selected for the error variance, the posterior is much affected by the prior distribution of crack size.

5.5.3 Sensitivity of the Bayesian Updating to the No. of Inspections

Regardless of the employed NDT technique (i.e. a_{md} value), the chance of finding the defects increases if the inspections are independently repeated. If k independent inspections are implemented, the probability of finding a crack is obtained as:

$$\begin{aligned} P(Crack\ detection) &= P(E_1 \cup E_2 \cup \ldots \cup E_k) \\ &= 1 - P(\overline{E_1 \cup E_2 \cup \ldots \cup E_k}) \\ &= 1 - P(\overline{E_1} \cap \overline{E_2} \cap \ldots \cap \overline{E_k}) \end{aligned} \tag{5-62}$$

Where E_i an event in which a crack is detected in the i[th] inspection. Moreover, $\overline{E_i}$ the complement of the event E_i , i.e. the probability of not detection of a crack in inspection No. i.

Assuming inspection events are statistically independent events:

$$P(Crack\ detection) = 1 - [P(\overline{E_1}) \times P(\overline{E_2}) \times \ldots \times P(\overline{E_k})] \tag{5-63}$$

Using Eq. (5-30):

$$P(Crack\ detection) = 1 - \left[e^{-\frac{a}{a_{md}}} \times e^{-\frac{a}{a_{md}}} \times \ldots \times e^{-\frac{a}{a_{md}}}\right] = 1 - e^{-k\times\frac{a}{a_{md}}} \quad (5\text{-}64)$$

Eq. (5-64) indicates that even with a poor inspection technique, a reasonable success can be expected if the inspection can be repeated several times. The equation is valid if the inspections are independent. In practice, it is hard to achieve by the same inspectors since the results probably are influenced in each inspection by what the inspectors had found during the earlier inspections [132]. Moreover, in reality, several inspections are not carried out for a particular joint at a specific time.

5.5.3.1 Not Detected Case

Figure 5.39 shows the effect of the repeated inspections on the posterior for different prior distributions of crack size.

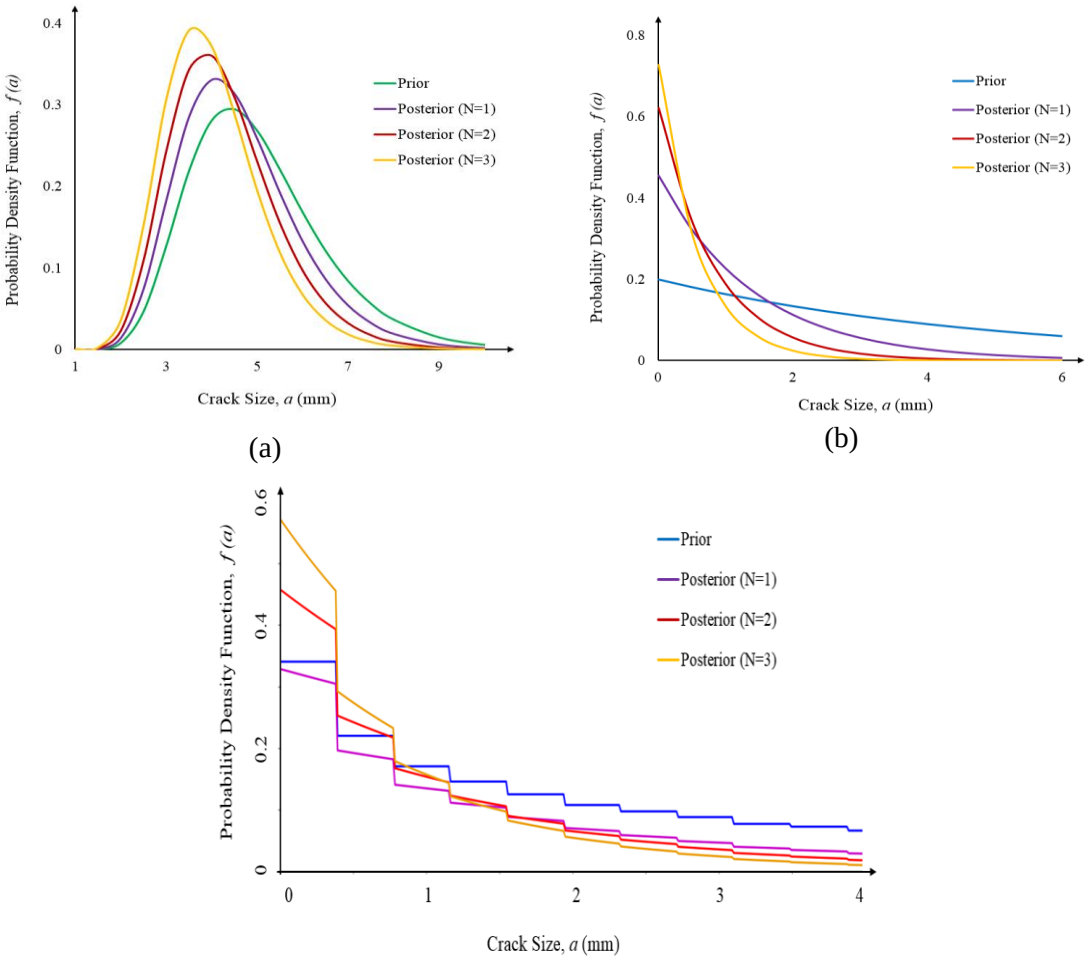

Figure 5.39. Effect of repeated inspections on the posterior distributions, (a) lognormal prior, (b) exponential prior, and (c) proposed model prior (no crack is detected)

The results show that even a low-quality inspection method is employed, if the repeated inspection results (at a particular location) reveal that no crack is detected, the uncertainty in the posterior distribution will be reduced. It was mentioned that the inspections should be independent.

However, the prior distribution still has a great effect on the posterior. If the prior is selected based on the proposed model, performing several inspections (more than two inspections) does not change the posterior distribution significantly (right tail), whereas, if the prior is a lognormal distribution, performing several inspections is valuable because the uncertainty in the posterior will be reduced considerably.

5.5.3.2 Crack Measured Case

Figure 5.40 shows the effect of the repeated inspections on the posterior distributions in the case of crack measurement. Here, the prior distribution is assumed lognormal with a mean value of 5mm. Three different situations are considered based on the number of repeated inspections:

- One inspection: $a_m = 6$
- Two inspections: $(a_m)_1 = 5, \quad (a_m)_2 = 7$
- Three inspections: $(a_m)_1 = 5, \quad (a_m)_2 = 6, \quad (a_m)_3 = 7$

It is noted that the mean value of the measured crack size is assumed equal to 6mm in each situation. Figure 5.40 illustrates that by increasing the number of repeated inspections, the posterior distribution shifts to the inspection results. Moreover, the uncertainty of the posterior distribution will be reduced.

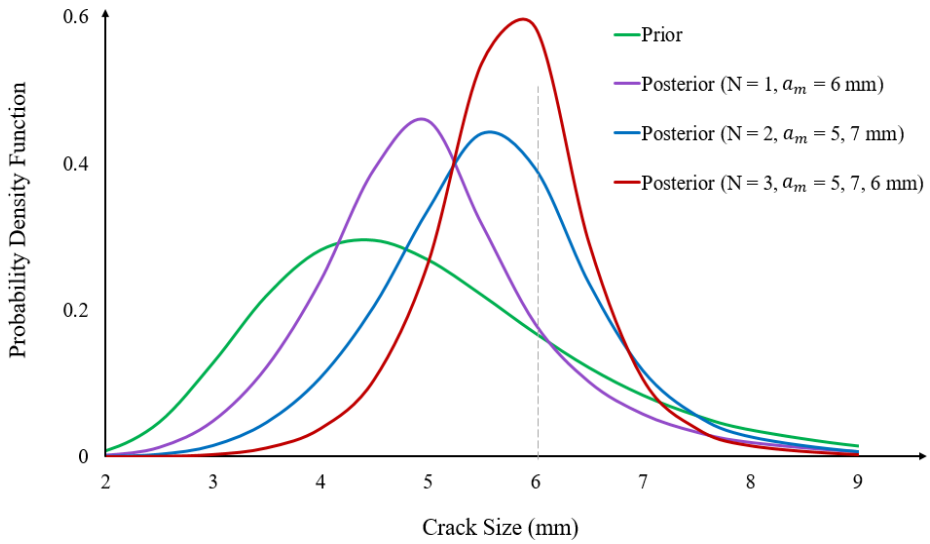

Figure 5.40. Effect of repeated inspections on the posterior distributions (prior: lognormal)

It should be noted that if there are $n_1 + n_2$ inspections in which the first n_1 inspections do not detect any cracks and in each of the following n_2 a crack is detected and measured, the probability distribution of the crack size can be updated by applying consecutively n_1 times Eq. (5-32) and then n_2 times Eq. (5-59).

5.5.4 Sensitivity of the Bayesian Updating to the Prior-Data Conflict

One important issue in the Bayesian inference is that the posterior has a strong dependence on the prior. In particular, when data is limited or unreliable, the actual estimate obtained by Bayesian techniques relies heavily on prior knowledge, expressed as a prior distribution. Consider a situation in which there is a prior-data conflict, i.e. the observed data is unexpected under the prior. Moreover, the sample size is not large enough to eliminate the influence of the prior [133].

In this section, the sensitivity of the posterior on potential prior-data conflict is considered. Here, it is assumed that the sample size is not sufficiently large to discard the possibly invalid prior knowledge and thus to rely on data only.

It will be expected that the posterior distribution has a bigger variance (uncertainty) in the situation of prior-data conflict. However, it can be shown that depending on the prior selection, the posterior variance will be reduced even in the prior-data confliction. This case occurs, in particular when adopting conjugate priors. This is another disadvantage of the conjugate methods. As a simple demonstration that conjugate

models might not react to prior-data conflict reasonably, a normal model with an unknown mean and a known variance is described.

To illustrate the results, it is assumed that the data is normal with an unknown mean μ and a known variance σ^2. Based on Table 5.1, the distribution of the parameter of interest (which is μ) is normal distribution as:

$$\mu \sim N\left(\mu_0, \tau_0^2\right) \tag{5-65}$$

The posterior expectation is obtained as (See Appendix A):

$$\mu_1 = \left(\frac{1/\tau_0^2}{1/\tau_0^2 + N}\right) \times \mu_0 + \left(\frac{N}{1/\tau_0^2 + N}\right) \times \bar{x} \tag{5-66}$$

The posterior expectation is a simple weighted average of the prior mean (μ_0) and the mean value of the new data ($\bar{x}$) with weights $1/\tau_0^2$ and N, respectively.

The posterior variance is (See Appendix A):

$$\frac{1}{\tau_1^2} = \frac{1}{\tau_0^2} + N \tag{5-67}$$

Eq.(5-67) illustrates that the variance of the posterior distribution is getting smaller automatically by providing any new information.

Now, imagine that the data is rare but we are very confident about the prior information. Therefore, a small value for τ_0^2 is chosen. A small value for τ_0^2 is resulting in high weight for the prior mean (μ_0) in the calculation of the posterior mean (Eq. (5-66)). The posterior distribution will be located somewhere around a mean between μ_0 and $\bar{x}$, and it will be even more pointed as the prior, because τ_1^2 is smaller than τ_0^2 (Eq. (5-67)). The posterior indicates that we can be quite sure that the mean is around μ_1, regardless if μ_0 and $\bar{x}$ are near to each other or not (i.e. prior-data conflict).

On the other hand, the posterior variance does not depend on prior-data conflict; therefore, the variance distribution is insensitive to prior-data conflict. Even if one is not confident about the prior knowledge (i.e. assigning a relatively large variance to the prior), the posterior mean is less influenced by the prior mean, but the posterior variance still is getting smaller no matter if the data support the prior information or not.

In performing the Bayesian updating process, great care should be considered in case of prior-data conflict. Results of the Bayesian updating will be inaccurate if the updating is performed regardless of the prior-data conflict, even in the case of reduction in the posterior uncertainty. For example, assume normal observation for data with an unknown mean and known variance σ^2 equal to one (i.e. $x \sim N(\mu, 1)$) which μ is the parameter of interest with the following distribution:

$$\mu \sim N\ (\mu_0 = 0, \tau_0^2 = 1) \tag{5-68}$$

Now, let's assume there is an observation of $x = 10$ which conflicts with the considered prior (Eq. (5-68)). The Bayesian updating process will lead to:

$$\mu_1 = \left(\frac{1/\tau_0^2}{1/\tau_0^2 + N}\right) \times \mu_0 + \left(\frac{N}{1/\tau_0^2 + N}\right) \times \bar{x} = \left(\frac{1}{1+1}\right) \times 0 + \left(\frac{1}{1+1}\right) \times 10 = 5$$
$$\frac{1}{\tau_1^2} = \frac{1}{\tau_0^2} + N = \frac{1}{1} + 1 = 2 \rightarrow \tau_1^2 = 0.5 \tag{5-69}$$

Although the variance is reduced from $\tau_0^2 = 1$ to $\tau_1^2 = 0.5$, but the expected value is located around $\mu = 5$, a value supported neither by prior nor data. Figure 5.41 shows the prior and posterior distributions for this sample.

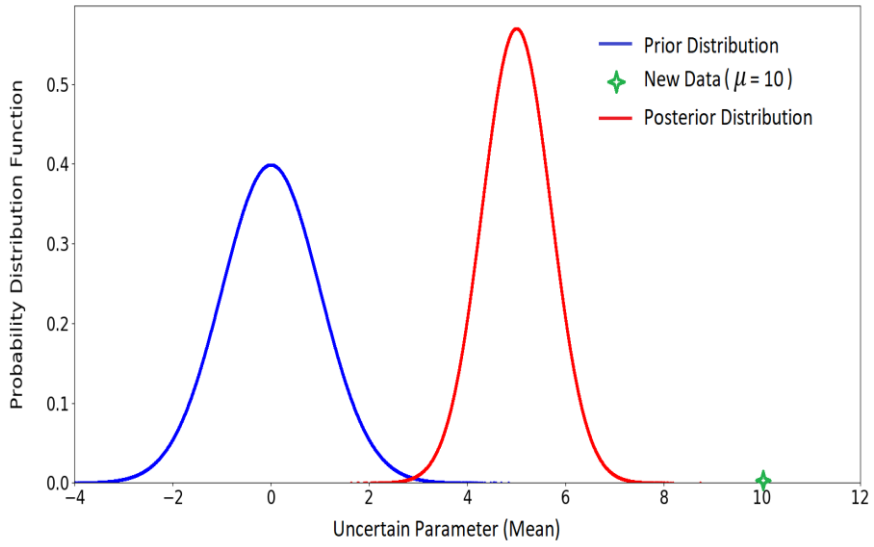

Figure 5.41. Prior and posterior distributions

As a general practice, in the case of prior-data conflict, the data is usually given priority and it is the prior distribution that is called into question and rejected if necessary

[133]. A more sophisticated and detailed model will be needed in each case of prior-data conflict.

5.6 Summary

In this chapter, the Bayesian inference for updating the uncertainties is explained. Two different approaches for updating the crack size distribution are introduced; the analytical method (conjugate) and the numerical method. The main advantage of using the conjugate method is having known posterior distributions. The posterior can be easily obtained when new information is available. However, conjugate priors contain substantial assumptions. In fact, in the conjugate method, priors have a strong influence on the posterior compared to the influence of the data. A numerical method is a general approach for Bayesian updating which is used to obtain the posterior by multiplying likelihood function and prior distribution directly. By using the numerical method, data dominates the posterior distribution. However, the numerical method is computationally expensive.

When the inspection data is available for a particular tubular joint, it is reasonable to use the numerical method due to several assumptions included in the conjugate method. However, when the inspection data is available for several joints (with similar conditions), the conjugate method might be preferred.

In this chapter, the effect of different parameters and inputs on the updated distribution of crack size is investigated. In general, the outcome of the inspection results is either no crack detected or a crack is detected and measured. Therefore, two different expressions for the posterior probability distribution of the crack size are obtained. If the result of the inspection indicates no crack detection, the posterior is dependent on two parameters; the prior distribution and POD curve.

In the case when a crack is measured, an uncertain error is defined as the logarithmic difference between measured crack size during the inspection and crack size predicted by the fracture mechanics model. The uncertain error is assumed to have a normal distribution with a known mean and uncertain variance. Therefore, a conjugate distribution for the variance of the uncertain error can be considered. In this case, the posterior distribution depends on the POD curve, the prior distribution, and also the variance of the error.

After obtaining the posterior expression in each case, the sensitivity of the posterior distribution to the inputs is taken into account and the results are explained. Some important results are:

- Regardless of the inspection outcome, the selected prior distribution has a great effect on the posterior distribution. The posterior distribution of the crack size is very sensitive to the prior distribution. Therefore, the prior distribution should be chosen based on reasonable assumptions and the expert's knowledge.
- The quality of the inspection methods is an important input to the posterior distribution in the 'not detected' case, whereas the posterior distribution is not sensitive to the POD curve in the 'crack measured' case.
- The posterior distribution in the 'crack measured' case is also sensitive to the error between predicted and measured crack size. A lognormal distribution is assigned to the error and the variance of the error is assumed as an uncertain parameter. Results show that if a non-informative prior is selected for the error variance, the posterior distribution of the crack size is dominated by data, whereas if an informative prior is selected, the posterior is moved into the prior distribution of crack size.
- By repeating the inspection activity for a tubular joint, the uncertainty in the posterior distribution will be reduced.

Finally, time-varying reliability is assessed based on the updated distributions of the crack size. The results indicate that in the 'not detected' case, the corresponding reliability is increased in comparison to the prior reliability. On the other hand, when a crack is measured, depending on the results of inspections, updated reliabilities may be higher or lower than the original values. If the measured crack is bigger than the mean value of the prior distribution, the reliability is reduced. Depending on the inspection findings at inspection time:

- The time interval for the next inspection activity is greater than the time-based inspection interval (in case of no crack is detected).
- The time interval for the next inspection activity is smaller than the time-based inspection interval (in case of a crack is measured).

6 . UPDATING THE DISTRIBUTIONS OF ALL UNCERTAIN PARAMETERS

6.1 Introduction

Fatigue damage accumulates during a structure's lifetime as crack sizes increase. The accumulation of damage causes deterioration of the component capacity and increases the probability of failure. To assess the state of damage, offshore platforms are periodically inspected. After an inspection of a structure, the perception of the structure's condition can be improved. A Bayesian framework can be used to update the probability distributions of the uncertainties such as parameters of fracture mechanics and crack size in tubular joints using information from inspection reports.

It was explained in Chapter 5 how to incorporate inspection results to update the probability distribution of crack size in a tubular joint using different Bayesian methods. After updating the distribution of the crack size, it is possible to update the estimation of joint reliability and system reliability.

The main purpose of this chapter is to present and investigate a novel methodology to update the probability distributions of all uncertain parameters (including the crack size) when new information becomes available. Three different categories of uncertainties will be updated using this methodology:

- Fatigue crack size (a);
- POD curve (a_{md});
- Uncertainties involved in the predicted fatigue crack size (are also called "input variables"):
  - Initial crack size (a_0)
  - Crack growth parameter (C)
  - Stress range (S)
  - Uncertainty in estimation of the geometry function (ε_Y)

As it was explained in Chapter 5, the posterior distribution of an uncertain parameter is dependent on both prior distribution and new information. In this chapter:

Section 6.2 introduces the proposed approach for updating the distributions of all uncertain parameters involved in the fatigue model. Based on the provided flowchart, two sets of estimations are required for obtaining the updated distributions. These two sets are called “simulated reality” estimations and “prior” estimations.

Section 6.3 explains how to obtain the posterior (updated) distributions of the uncertain parameters. To obtain the posterior distributions, two sets of estimations are required: Simulated reality estimations and Prior estimations.

The credibility of the updating process is the main concern in any updating application. The reliability of the proposed approach is investigated in Section 6.4 to Section 6.7:

- Section 6.4 investigates the sensitivity of the posterior distributions to the inputs. The posterior distributions are affected by both prior and simulated reality distributions. Therefore, sensitivity analysis is performed to find out the influence of each input on the posterior distribution.
- In the proposed approach in Section 6.3 for obtaining the posterior distributions, it is assumed that several inspection results (observations) are available. Section 6.5 explains the modification of the proposed approach when only one inspection result is available.
- Section 6.6 investigates the reliability of the proposed approach in case of inappropriate prior selection. This section is provided to find out when the proposed approach might lead to poor results.
- The proposed approach can update all uncertain parameters including crack size. However, the crack size distribution can be also updated by using the conventional Bayesian methods (i.e., analytical, or numerical) that were introduced in Chapter 5. Since the crack size distribution can be updated by both approaches (Chapter 5 and Chapter 6), Section 6.7 compares the results of these two methods and provides some useful suggestions for platforms’ operators/owners.

To help users to implement the proposed approach in practice, Section 6.8 provides guidance for using the proposed approach by explaining the framework, advantages,

and limitations. Finally, Section 6.9 summarises the proposed approach and some important results.

6.2 Proposed Approach for Updating All Uncertain Parameters - Overview

To obtain the updated distributions for the uncertain parameters, like any Bayesian approach, two sets of estimations are required:

- The previous knowledge about the uncertain parameters (i.e., prior estimation)
- New information from the inspection activities

Figure 6.1 shows the flowchart of the proposed approach.

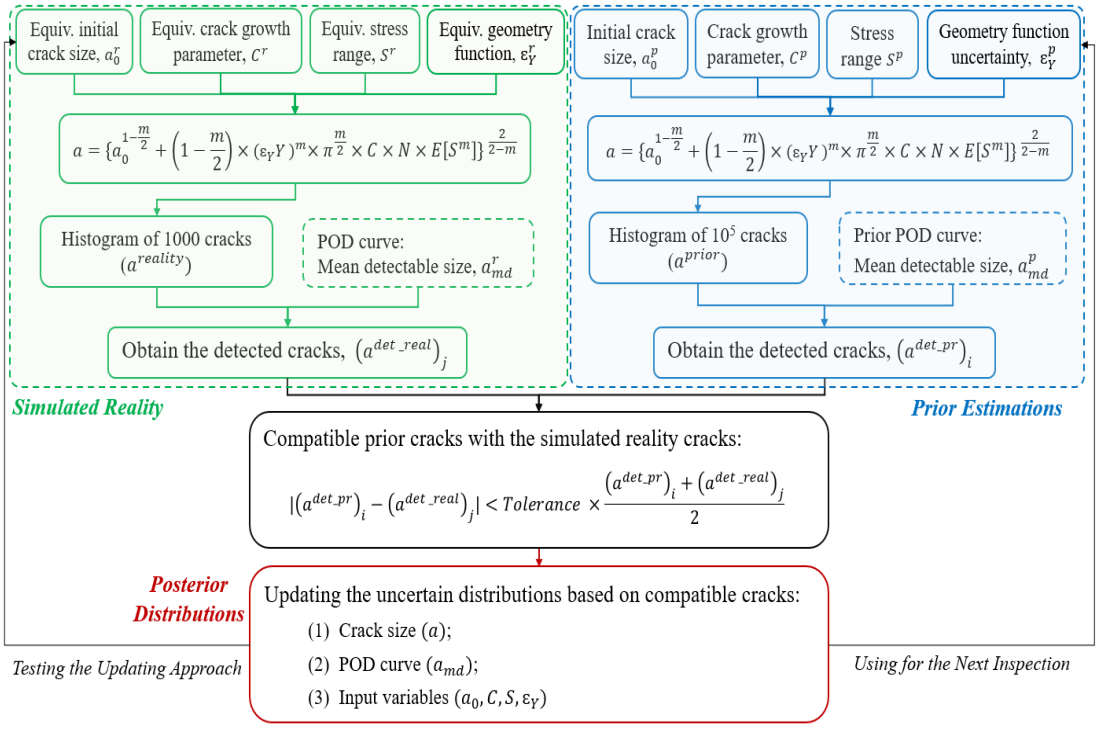

Figure 6.1. Flowchart of the proposed approach for updating the distributions of all uncertain parameters

As can be seen from Figure 6.1, the proposed approach for updating the distributions of uncertain parameters consists of three main estimations:

(I). Statistics of the simulated reality (green box)

(II). Prior estimations of uncertain parameters (blue box)

(III). Posterior estimates based on the application of the proposed method to update (II) by using (I), (red box)

The simulated reality distributions are useful for this research because, in reality, we do not have a full understanding of the Real-World statistics and a few inspection results (e.g., crack measurements) are the only information from the real world. Moreover, the updating methodology is tested using the simulated reality distributions to determine the effectiveness of the proposed Bayesian method and the limits beyond which the proposed approach results in poorer posterior estimates. The quality of the updating is determined in terms of how the posterior estimates become closer to (or possibly further away from) the simulated reality estimates.

Within the updating methodology, the prior cracks (a^{prior}) obtained by sampling the prior distributions are compared with the simulated reality cracks ($a^{reality}$). The samples from the prior distributions that result in compatible cracks with the simulated reality cracks are used to update the prior distributions of the uncertain parameters. These updated distributions (which are also called posterior distributions) are then compared with the simulated reality distributions so that the effectiveness of the proposed Bayesian method can be determined.

The proposed methodology results in all the prior distributions being updated. It would seem that the updating approach could work well but could also, depending on the prior estimates, find the posterior distributions that do not correspond well to the simulated reality. For instance, if the prior distribution of the crack growth parameter is underestimated (a very low mean value for the crack growth parameter) and the prior POD is overestimated (a very high resolution), then this over and underestimate may continue into the posterior distribution of the crack size. Therefore, for reliability analysis, this posterior distribution of crack size would result in an unsafe assessment of the considered joint. Therefore, this chapter also includes an investigation of poor prior estimates that may lead to these undesirable results.

One of the main advantages of the proposed approach is future inspection planning and reliability analysis of the inspected platforms. Although updating crack size estimates is useful for a known critical location, the ability to improve estimates of other uncertain parameters (i.e., initial crack size, crack growth parameter, POD, etc.) is much more valuable. The updated distributions of the other uncertain parameters

can be used as the prior distributions for the next updating process (next inspection results).

Note that although the proposed approach updates the uncertain parameters at one location, the method can be also applied to multiple locations at the same time where the stress range is the same.

6.3 Proposed Approach for Updating All Uncertain Parameters

6.3.1 Simulated Reality Distributions

6.3.1.1 Crack Size Function

In the Fracture Mechanics approach, the relationship between crack growth during a load cycle and a global parameter can be developed using the Paris law. By expanding the Paris law the relation between crack size and the number of cycles for the propagation of a crack can be obtained (for more detail see Chapter 3). The crack size at time t is obtained as follows:

$$a_t = \left\{ a_0^{1-\frac{m}{2}} + \left(1-\frac{m}{2}\right) \times (\varepsilon_Y Y)^m \times \pi^{\frac{m}{2}} \times C \times N \times E[S^m] \right\}^{\frac{1}{1-\frac{m}{2}}} \qquad (6\text{-}1)$$

It can be seen that the crack size at a specific time t is a function of uncertain parameters (input variables) such as:

- Initial crack size, a_0
- Crack growth parameter, C
- Stress range term, $E[S^m]$ (hereafter is shown by S)
- Uncertainty in estimation of the geometry function (ε_Y)

When the crack size exceeds the critical crack size, it is assumed that the failure happens (See Section 3.8.3), i.e. the fatigue limit state function is defined as:

$$g = a_c - a_t \qquad (6\text{-}2)$$

where a_c is the critical crack size (which is considered equal to the wall thickness) and a_t is the crack size at time t. The wall thickness for the considered tubular joint is 0.875 inches (22.22 mm).

Different guidelines (e.g., DNV [19], BS [47], JCSS [134]) introduce various distributions for the uncertain parameters. Since these distributions are obtained based on the experimental tests, they are not representative of the real distributions. For example, the crack growth parameter is estimated by fitting fatigue test data measured under controlled, laboratory-environment conditions which are different from the real conditions for offshore platforms [126].

The purpose of this section is to find out the simulated reality distributions for these uncertain parameters (input variables).

6.3.1.2 Previous Studies: Equivalent Initial Flaw Size

The concept of equivalent initial flaw size (EIFS) was introduced by Gray and Rudd [135], and developed by Yang and Manning [136] in probabilistic risk analysis of aircraft structures. In the reliability analysis of aircraft structures, the distribution of the crack size at any given time in a joint is a highly influential parameter. In particular, the distribution of crack sizes at time zero (EIFS distribution) plays a critical role as it determines the subsequent distribution of crack sizes [135].

The EIFS is usually obtained by back extrapolating the observed crack sizes, together with the related life, to its corresponding size at time zero. This involves fitting a crack growth model to the crack size, hence, the EIFS is an artificial crack size. Therefore, for an observed crack size, the EIFS is not unique, i.e. for the same observed crack size, different EIFS values can be achieved by using different crack growth models [135]. Despite this shortcoming, the concept of the EIFS has been used by scientists to quantify the initial crack size distribution, due to its consistency with the crack growth to calculate the crack size at a given time.

Torregosa and Hu developed a method to improve the accuracy of the probabilistic risk analysis of aircraft structures by updating the distribution of the initial flaw sizes based on the observations [137]. They used the flight hours of an aircraft to update the distribution of the initial flaw sizes, by using Bayesian methods. They proposed two Bayesian updating methods, the first one was using the flight hours of the particular aircraft and the second one was using the flight histories of similar aircraft in the fleet. In fact, in the second method, they improved the risk analysis result by utilising the flight histories of all aircraft in a fleet. They proposed an inexpensive method of

updating the PoF of a fleet of aircraft using the Bayesian approach without the use of NDT techniques [137].

Cross et al. [138] developed a Bayesian technique to improve the simultaneous estimation of the equivalent initial flaw size (EIFS) and crack growth rate distributions in fracture mechanics based on the inspection data. In their article, the crack growth rate parameters were sampled using the Markov chain Monte Carlo simulation method.

Li et al. [139] used a Bayesian approach to jointly estimate the probability of detection (POD) and the crack size distribution at a given time. In their method, a 'crack found' signal during the inspection is used to update the POD estimate and the crack length distribution at a given time.

Macheret and Teichman [140] used a Bayesian updating process to improve the estimate of the equivalent pre-crack size distribution. They were able to show that the probability of failure can be updated using only the successful flight hours of an aircraft, without using the inspection results themselves.

In the EIFS approach, for a given set of crack sizes (for a particular joint at different years) with the corresponding crack growth curves, the EIFS distribution may be derived as follows:

1) A specific crack size is defined as a baseline crack size (a_{BCS})
2) For a given set of crack sizes, the crack sizes that are bigger than the baseline crack size are regressed using the crack growth curve
3) For a given set of crack sizes, the crack sizes that are smaller than the baseline crack size are grown using the crack growth curve
4) A time distribution for the baseline crack size is modelled by a suitable probability distribution
5) A cumulative probability, $F_T(t)$, at the baseline crack size is transferred to an initial crack size with a cumulative probability of $1-F_T(t)$
6) An appropriate distribution for the EIFS is obtained.

In fact, in this method, the time distribution for a specific crack size (baseline) is transferred to the initial crack size (EIFS) distribution. Figure 6.2 illustrates how EIFS distribution is obtained.

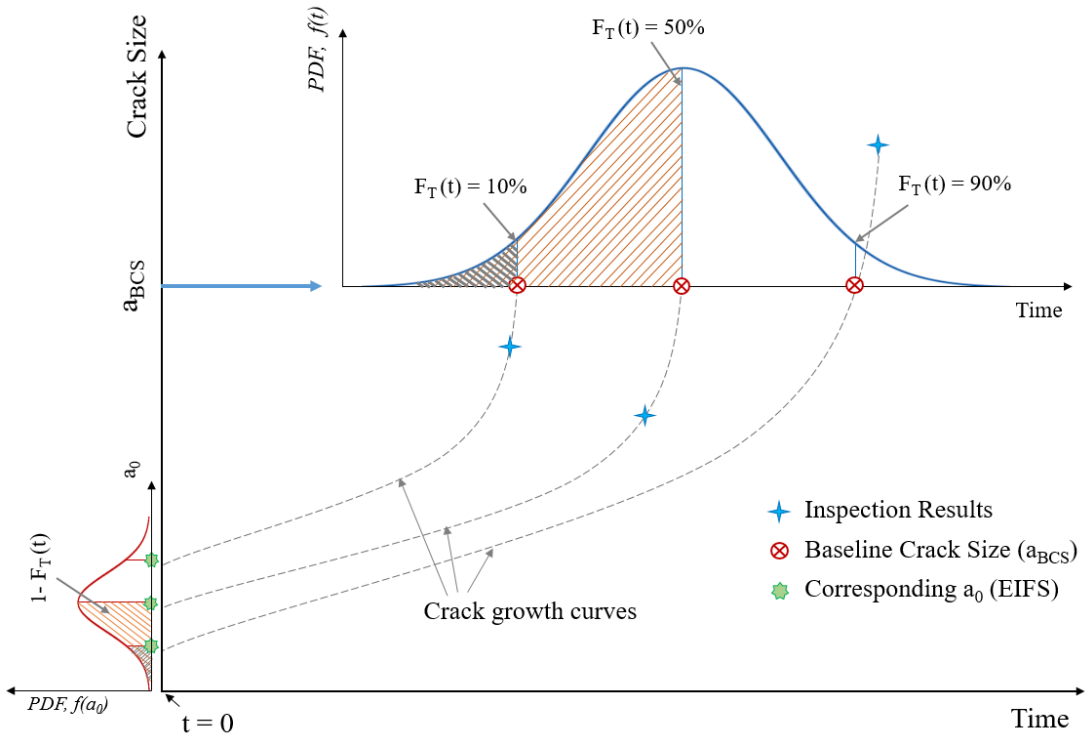

Figure 6.2. Obtaining the equivalent initial flaw size (EIFS) distribution

The EIFS distribution is determined by regressing the observed crack sizes from teardown inspections back to the beginning of its fatigue life or time zero [137]. However, to obtain a suitable distribution, sufficient data points are required, although the teardown inspection data are very limited and expensive to obtain. Therefore, obtaining an appropriate EIFS distribution is hard to achieve [137]. Since the EIFS distribution is derived based on the time distribution for baseline crack size, the quality of the EIFS distribution strongly depends on the number of available inspection results.

For obtaining the EIFS distribution, it is assumed that the crack growth parameters are constant. After generating the EIFS distribution, the crack size distribution at any given time is achieved by growing the EIFS distribution using a crack growth law, as schematically illustrated in Figure 6.3. In this figure, $f(a_0)$ represents the EIFS distribution.

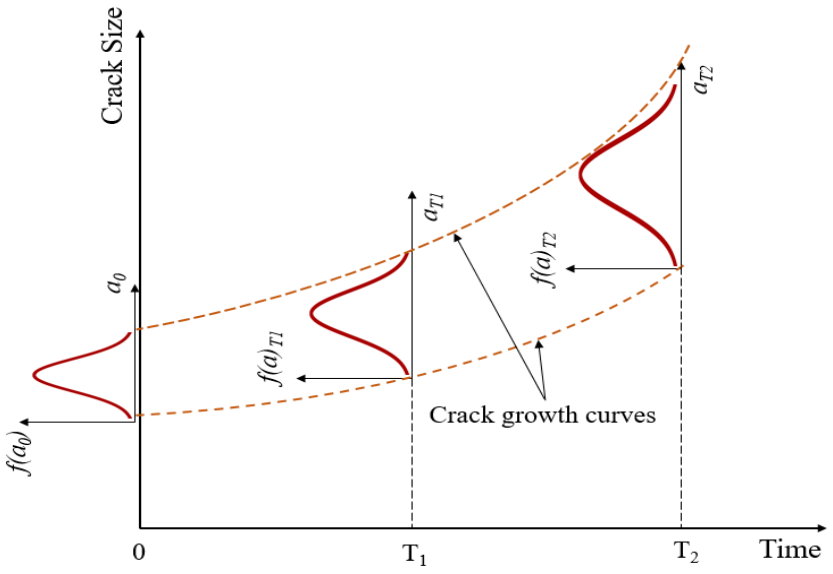

Figure 6.3. Development of the crack size distribution using the crack growth curves

6.3.1.3 Derivation of Simulated Reality Distributions by Using EIFS Concept

The concept of EIFS was explained in Section 6.3.1.2. However, this approach is used for the probabilistic analysis of aircraft, and it is only considered for obtaining the initial crack size distribution.

In reliability analysis of the jacket platforms, the distribution of the crack size in a tubular joint (at any given time) is dependent on several uncertain parameters. Based on Eq.(6-1), the crack size is a function of initial crack size, crack growth parameter, stress range, and geometry function. Therefore, in this section, it is tried to obtain the equivalent distributions for these uncertain parameters by using the concept of EIFS. The obtained equivalent distributions for the uncertain parameters are hereafter called simulated reality distributions.

For this purpose, it is assumed that several inspection results (let say five inspections) are available for a particular tubular joint at a specific time (e.g. after five years). It is noted that in real situations, due to the expensive cost of the underwater inspection, there are few inspection results available (usually one inspection) for each tubular joint. However, the method could be extended to results for one inspection at different locations that have almost the same conditions (i.e. joints that have identical configurations with the same material properties and are subjected to the same stress range).

For the purpose of illustration, for a particular tubular joint at a specific time (e.g. after five years) the observed cracks are assumed as:

$$a^{observed} = \{2\ mm, 3mm, 4.2mm, 5.7mm, 6.7mm\} \tag{6-3}$$

It is assumed that these inspections are independent of each other (e.g. inspections are carried out by different inspectors).

The first step is to assign a distribution to the inspection results (observed cracks). The mean value and the standard deviation of the observed cracks are obtained as:

$$\begin{aligned} \left(a^{observed}\right)_{mean} &= \frac{1}{n}\sum_{i=1}^{n}\left(a^{observed}\right)_i = \frac{1}{5}\sum_{i=1}^{5}\left(a^{observed}\right)_i = 4.3mm \\ \left(a^{observed}\right)_{std} &= \sqrt{\frac{1}{n-1}\sum_{i=1}^{n}[(a^{observed})_i - (a^{observed})_{mean}]^2} = 1.92mm \end{aligned} \tag{6-4}$$

In this study, a lognormal distribution with a mean value of 4mm and a standard deviation of 2mm is assigned to the observed cracks. This distribution is shown as:

$$a_{BCS} \sim LN(4mm,\ COV = 0.5) \tag{6-5}$$

To find out the equivalent distribution (simulated reality distribution) of each uncertain parameter, the same approach as explained in Section 6.3.1.2 (EIFS distribution) is utilised.

- ***Simulated Reality Distribution of the Initial Crack Size (a_0^r)***

  To obtain the simulated reality distribution for the initial crack size, the approach described in Section 6.3.1.2 is implemented. For this purpose, the mean values of the crack growth parameter, stress range, and geometry function are selected.

  Here, to derive the simulated reality distribution of the initial crack size, the sampling method is used. A large number of artificial cracks is generated based on the assigned distribution of the observed cracks (a_{BCS}). For each randomly generated crack, the corresponding initial crack size (a_0) is obtained by the calculation of Eq.(6-1).

  Figure 6.4 shows how the simulated reality distribution of the initial crack size is obtained by using the proposed approach, schematically. As it was mentioned, a

large number of cracks are generated based on the assumed distribution, however, only three randomly generated cracks are shown in Figure 6.4.

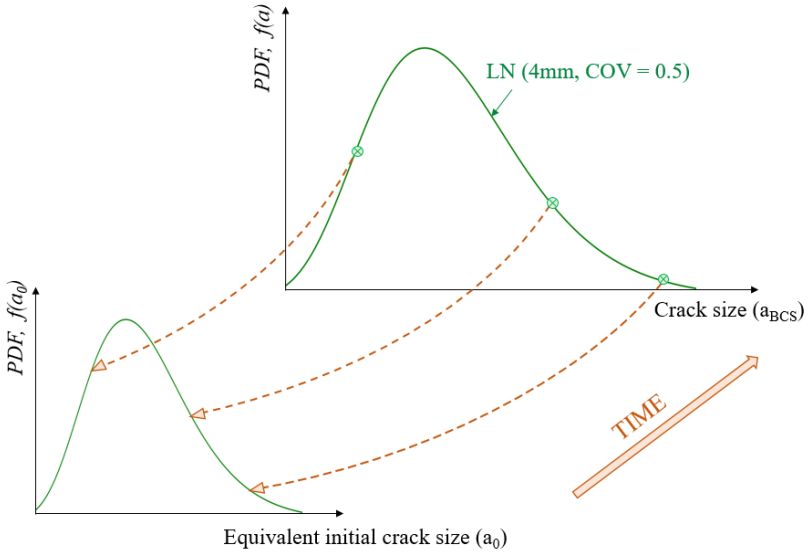

Figure 6.4. Obtaining the simulated reality (equivalent) distribution of the initial crack size

Having obtained the initial crack size for each sample, the best distribution is fitted for the equivalent initial crack size histogram. Figure 6.5 shows the simulated reality distribution of the initial crack size based on the observed cracks.

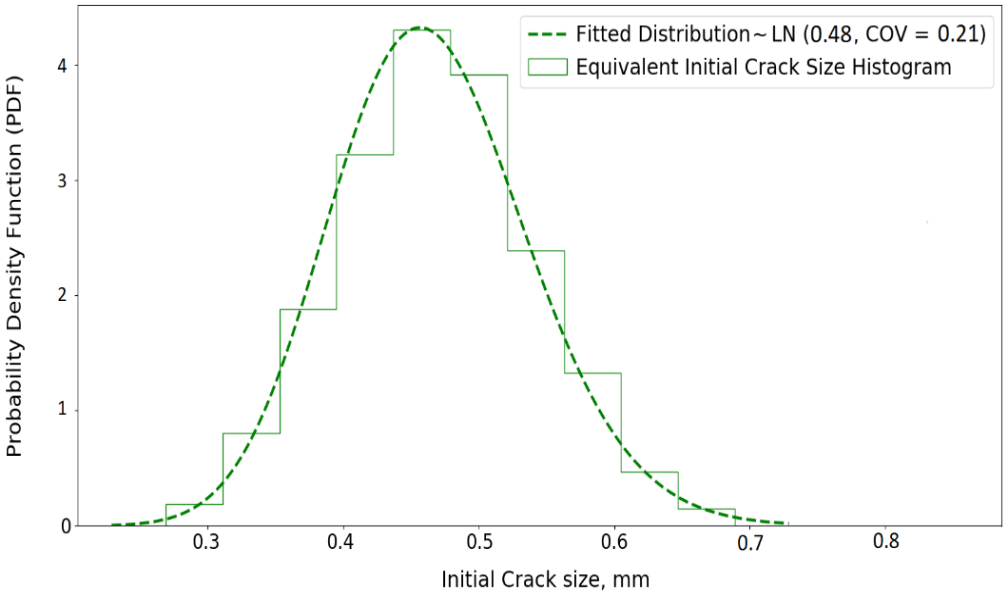

Figure 6.5. Obtained simulated reality (equivalent) distribution of the initial crack size

- ***Simulated Reality Distribution of the Crack Growth Parameter (C^r)***

The next step is to find out the equivalent distribution of the crack growth parameter based on the observed crack. As it was mentioned, a lognormal distribution is assigned to the observed cracks (Eq. (6-5)).

The same approach as described in Section □ is utilised to derive the simulated reality distribution of the crack growth parameter. For this purpose, the mean value of the initial crack size and other uncertain parameters are used.

By using the sampling method, the simulated reality distribution of the crack growth parameter is derived. Again, a large number of artificial cracks is generated based on the assigned distribution of the observed cracks (a_{BCS}).

For each randomly generated crack, the corresponding crack growth parameter is obtained by the calculation of Eq.(6-1). Figure 6.6 shows how the simulated reality distribution of the crack growth parameter is obtained by using the proposed approach, schematically. As it was mentioned a large number of cracks are generated based on the distribution, however, only four cracks are shown in Figure 6.6.

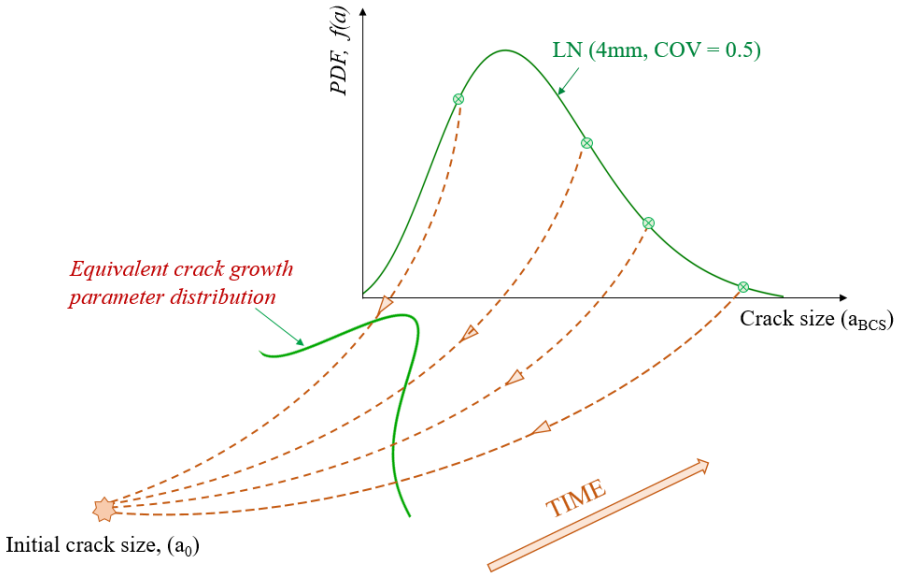

Figure 6.6. Obtaining the simulated reality (equivalent) distribution of the crack growth parameter

Having obtained the crack growth parameter value for each sample, the best distribution is fitted for the equivalent crack growth parameter distribution.

Figure 6.7 shows the simulated reality distribution of the crack growth parameter based on the observed cracks.

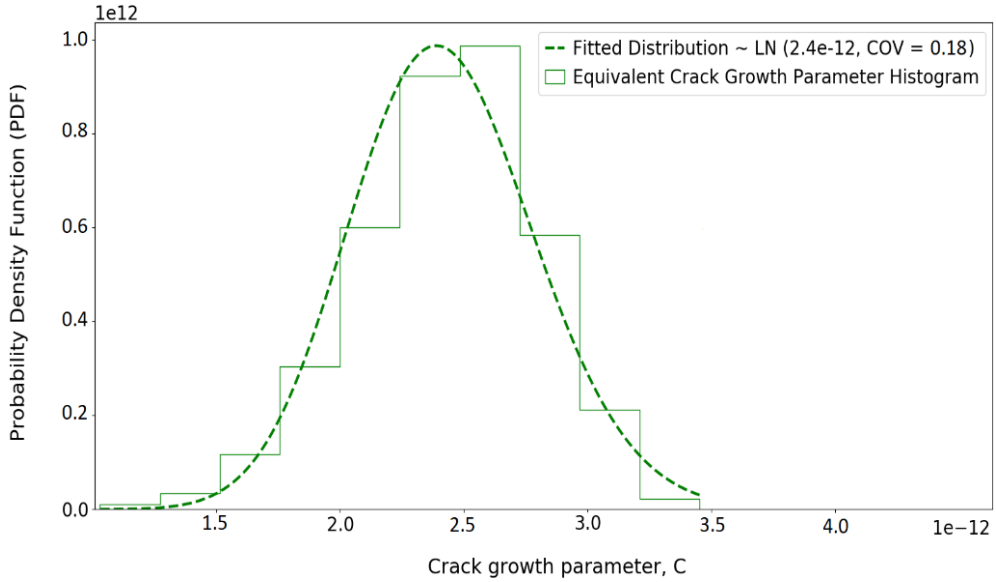

Figure 6.7. Obtained simulated reality (equivalent) distribution of the crack growth parameter

- ***Simulated Reality Distribution of the Stress Range (S^r)***

The same approach as described in Section □ is utilised to derive the simulated reality distribution of the stress range. For this purpose, the mean values of other uncertain parameters are used. Figure 6.8 shows the simulated reality distribution of the stress range based on the observed cracks.

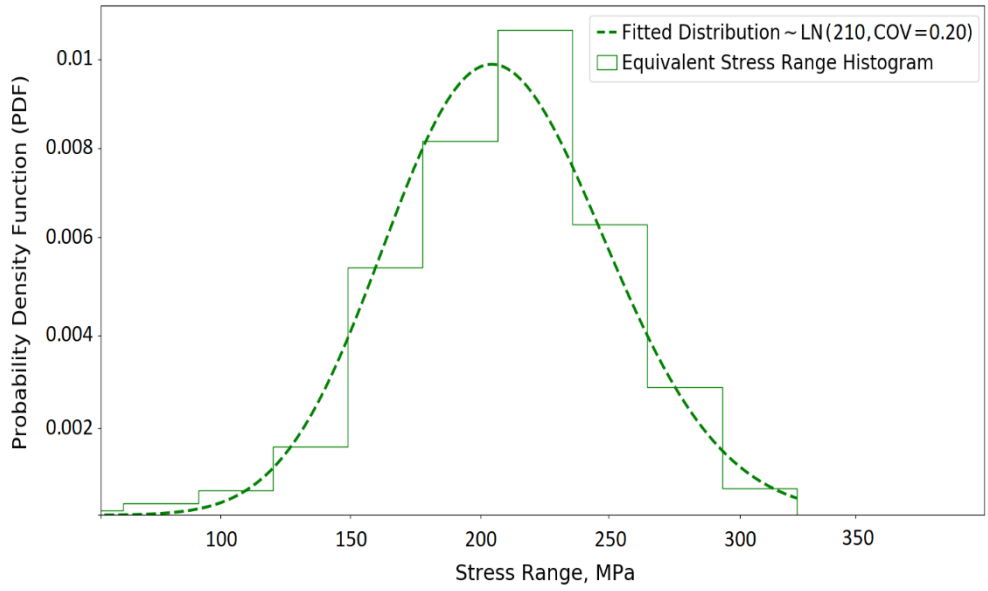

Figure 6.8. Obtained simulated reality (equivalent) distribution of the stress range

- ***Simulated Reality Distribution of the Geometry Function (ε_Y^r)***

  The same approach as described in Section □ is utilised to derive the simulated reality distribution of the uncertainty in the geometry function. To obtain the simulated reality distribution of the uncertainty in the geometry function, the mean values of other uncertain parameters are used. Figure 6.9 shows the simulated reality distribution of the uncertainty in geometry function based on the observed cracks.

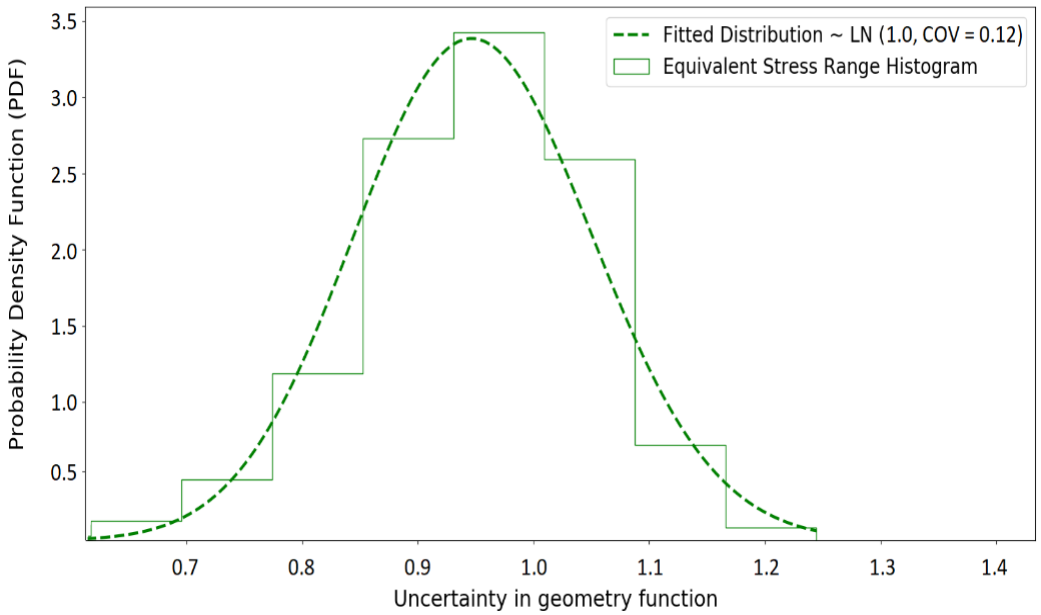

Figure 6.9. Obtained simulated reality (equivalent) distribution of the uncertainty in geometry function

Table 6.1 summarises the simulated reality distributions of the uncertain parameters.

Table 6.1. Uncertain parameter statistics in the simulated reality case [N, mm]

Uncertain Parameter	Type	Mean [2]	COV [2]
Initial crack size, a_0^r [1]	Lognormal	0.48	0.21
Crack growth parameter, C^r [1]	Lognormal	2.4 x 10^{-12}	0.18
Stress range, S^r [1]	Lognormal	210	0.20
Uncertainty in estimation of geometry function, ε_Y^r [1]	Lognormal	1.0	0.12

Note:

[1] Superscript r indicates the simulated reality distribution

[2] Mean and COV of the uncertain parameters are shown in Figure 6.5, Figure 6.7, Figure 6.8, Figure 6.9

After obtaining the simulated reality distributions for the input variables, the next step is to find out the simulated reality distribution of the crack size.

6.3.1.4 Simulated Reality Distribution of the Crack Size

Having obtained the simulated reality distributions for the input variables, the simulated reality distribution of crack size can be achieved.

Although a lognormal distribution is assigned to the observed cracks (Eq. (6-5)), a sampling method is used to obtain the simulated reality distribution of the crack size. The reason for using the sampling method is that the observations are limited to a few inspections. Therefore, assigning a distribution to the limited numbers of data points includes some inaccuracies (the assigned distribution in Eq. (6-5) is based on only five inspections).

In the sampling method, N^r =1000 random numbers are generated for each uncertain parameter based on their distributions introduced in Table 6.1. For each set of samples (e.g. for the kth sample set: a_{0k}^r, C_k^r, S_k^r and ε_{Yk}^r), the crack size ($a_k^{reality}$) is calculated based on Eq.(6-1). Although the real number of inspections may be low, using a large number of samples for this part of the research enables the way in which, the updating method deals with multiple variables to be better understood.

A code has been written in Python to generate random samples for the uncertain parameters and to obtain the crack size distribution [131].

Figure 6.10 shows the normalised histogram of the simulated reality cracks. The normalised histogram is then used as a simulated reality distribution for the crack size. As can be seen from Figure 6.10, the obtained histogram of the crack size by using the sampling method has an acceptable shape since it is almost similar to the assigned distribution of the observed cracks. In the other words, the obtained simulated reality cracks ($a^{reality}$) is consistent with the observations (a_{BCS}).

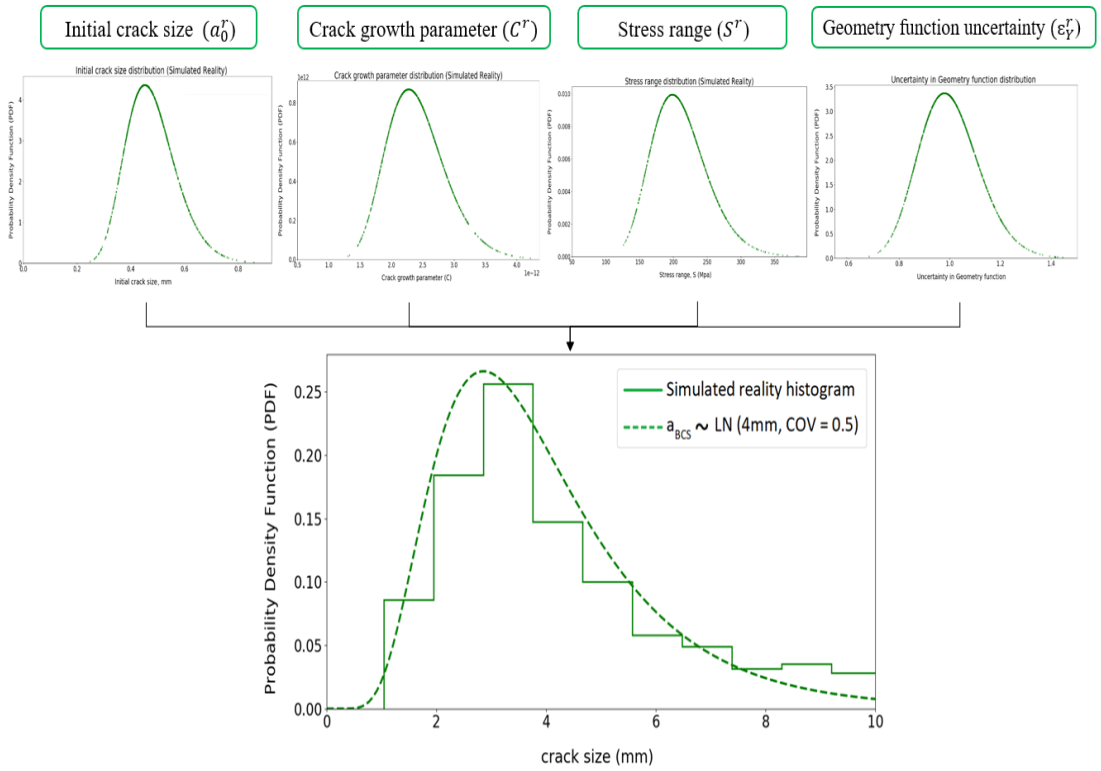

Figure 6.10. Obtaining the simulated reality distribution of the crack size using the sampling method

6.3.1.5 Estimation of POD Curve

Several fatigue cracks usually exist in a welded connection such as a tubular joint in the offshore platforms. Not all of these existing cracks can be detectable. The probability of detection of a crack depends on the resolution of the inspection technique. There is a wide variety of NDT techniques for finding a crack. The probability of detection, POD, varies with crack size and the inspection technique employed. The probability of detection of a crack is usually given by [82]:

$$POD\ (a)\ =\ 1 -\ e^{-\frac{a}{a_{md}}} \tag{6-6}$$

where a_{md} is the mean detectable size (mm) and it depends on the resolution of the inspection technique. It is noted that in general a_{md} is an uncertain value, hence, a distribution can be assigned to it.

It is assumed that the inspection activity is carried out with a specific device and the device manufacturer provides the resolution of the device. To demonstrate the approach, a lognormal distribution with a mean value equal to 2mm and a coefficient

of variation (COV) equal to 0.2 is assumed for the simulated reality distribution of the mean detectable size, i.e.:

$$a_{md}^{r} \sim LN(2mm,\ COV = 0.2) \tag{6-7}$$

To find out which simulated reality crack can be detected, N^r =1000 random numbers for a_{md}^{r} are selected based on its distribution.

6.3.1.6 Obtain the Detected Cracks

In Section 6.3.1.4 and Section 6.3.1.5, a number of 1000 crack sizes ($a^{reality}$) and 1000 mean detectable size (a_{md}^{r}) were generated, respectively. Therefore, for each crack size, a corresponding value of mean detectable size is available.

In general, tiny cracks cannot be detected by using any NDT techniques. A criterion should be defined to show which crack size (with the corresponding a_{md}^{r}) is detectable and which one is missed. The proposed criterion is described below:

1) For each set of $(a^{reality}, a_{md}^{r})_j$, $j = 1, 2, \dots, 1000$; $(POD^r)_j$ is calculated using Eq.(6-6) which is between zero and one.

2) N^r = 1000 random numbers are generated from a uniform distribution between [0,1], i.e.:

$$(Chance^r)_j = Random\ number,\quad j = 1,2, \dots, 1000$$

3) A simulated reality crack is assumed as a detected crack; $\left(a^{det\_real}\right)_j$, if:

$$(Chance^r)_j \le (POD^r)_j,\quad j = 1,2, \dots,1000$$

4) Otherwise, the simulated reality crack is assumed as a missed one.

Figure 6.11 shows the PODs for both detected and missed cracks.

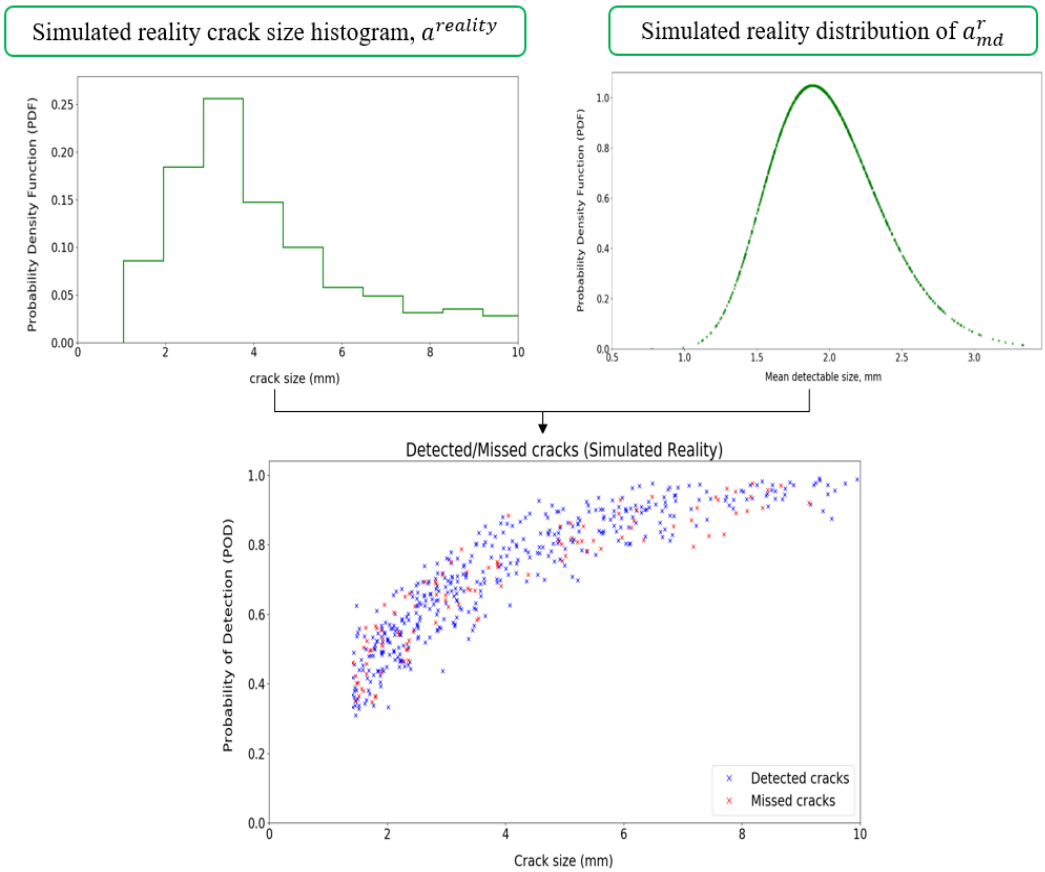

Figure 6.11. PODs for both detected/missed defects

Figure 6.12 summarises the proposed approach for obtaining the detected cracks in the simulated reality case by using the sampling method.

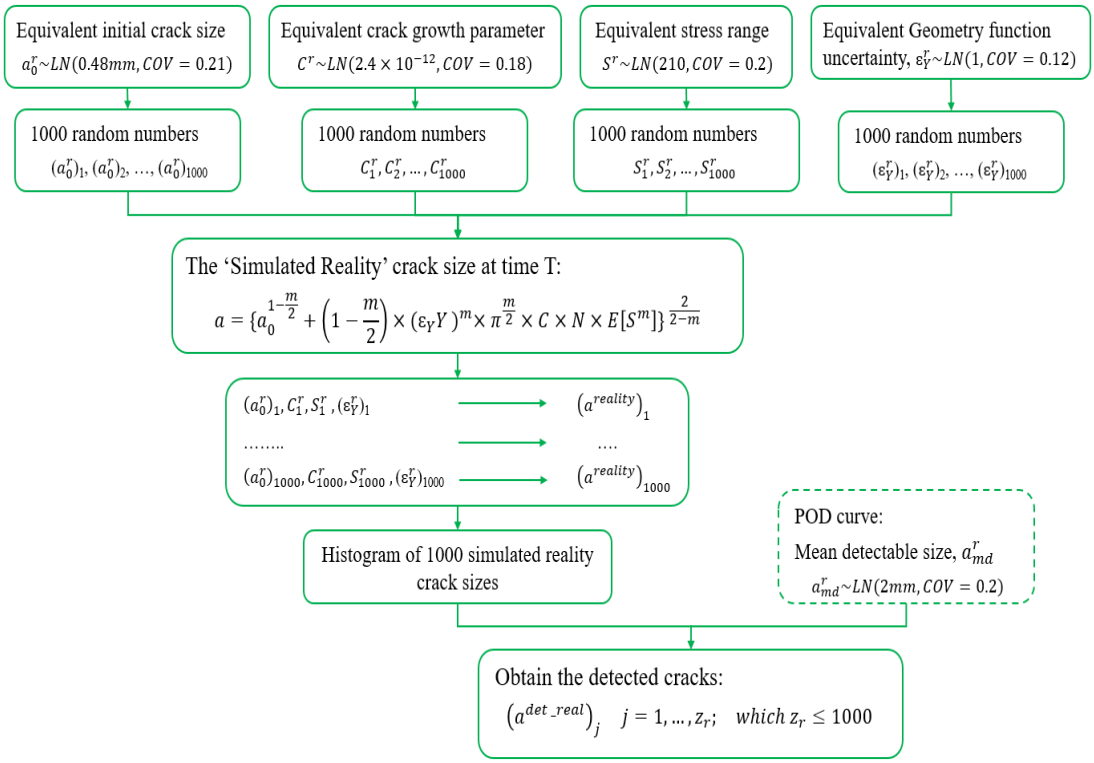

Figure 6.12. The proposed approach for obtaining the detected cracks (simulated reality estimations)

6.3.2 Prior Estimations

6.3.2.1 Estimation of the Involved Uncertainties

As it was shown in Eq. (6-1) the crack size at any time is a function of uncertain parameters (i.e., initial crack size, crack growth parameter, stress range term, and uncertainty in the estimation of the geometry function).

The assumed distributions of these uncertain parameters have a great impact on the reliability analysis results. Therefore, it is crucial to choose the distributions for these parameters reasonably. In fact, the accuracy of the reliability analysis results depends on the assumed distributions.

The prior distributions for the uncertain parameters can be assumed based on theoretical considerations, expert opinions, past experiences, or test results. Different distributions have been introduced in the literature.

In the previous studies, for the initial crack size distribution, both exponential (e.g., [52], [82]) and lognormal (e.g., [1], [15]) distributions were utilised whereas for the other uncertain lognormal distributions were used.

Table 6.2 shows the considered prior distributions for the uncertain parameters. These distributions are selected to illustrate the application of the proposed approach. Section 6.4.1 investigates the sensitivity of the proposed approach to the different prior distributions.

Table 6.2. Statistics of the uncertainties [N, mm]

Uncertain Parameter	Type	Mean	COV(1)
Initial crack size, a_0^p (2)	Lognormal	0.4	0.35
Crack growth parameter, C^p (2)	Lognormal	2.1 x 10^{-12}	0.35
Stress range, S^p (2)	Lognormal	180 (3)	0.35
Uncertainty in estimation of the geometry function, ε_Y^p (2)	Lognormal	1	0.2

Note:

(1) Coefficient of variation

(2) Superscript p indicates the estimation of the prior distribution

(3) Calculated for the critical component in fatigue analysis (SESAM software)

6.3.2.2 Prior Distribution for Crack Size

The prior distribution of crack size can be assumed based on theoretical considerations, expert opinions, past experiences, or data reported in the literature.

To generate the prior distribution of the crack size, the sampling method that is explained in Section 6.3.1.4 is used. A large number of random numbers (e.g. N^p=10^5) for each input variable (introduced in Table 6.2) is selected based on their distributions. For each set of samples (e.g. for the kth sample set, a_{0k}^p, C_k^p, S_k^p and ε_{Yk}^p), the prior crack size (a_k^{prior}) is calculated based on Eq.(6-1). A large value of N^p improves the probability that all relevant combinations of these uncertain parameters are included. Here, the number of samples is considered equal to 10^5. Therefore, 10^5 cracks are calculated by using Eq. (6-1). A code has been written in Python to generate random samples for the uncertain parameters and to obtain the prior distribution of the crack size [131].

Figure 6.13 shows the histogram of the prior cracks after five years. The normalised histogram is then used as the prior distribution of the crack size.

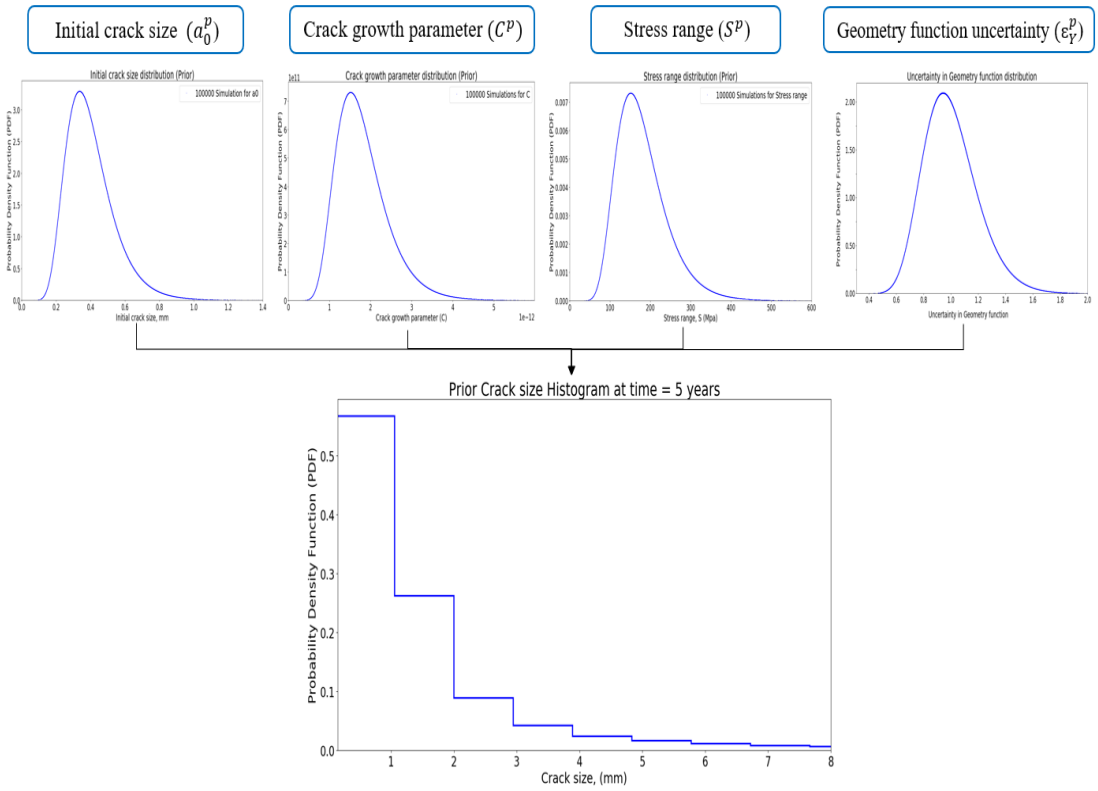

Figure 6.13. Prior crack size distribution obtained by using the sampling method

6.3.2.3 Estimation of POD Curves

It was mentioned that the probability of detection of a crack depends on the resolution of the inspection technique. The probability of detection, POD, varies with crack size and the inspection technique employed. The probability of detection of a crack is obtained by using Eq. (6-6).

For the prior estimation of the mean detectable size, a lognormal distribution with a mean value equal to 3mm and a coefficient of variation (COV) equal to 0.5 is assumed:

$$a_{md}^{p} \sim LN(3mm,\ COV = 0.5) \tag{6-8}$$

Here, a large COV is considered for a_{md} to have the prior estimation as non-informative as possible. Non-informative priors are intended to let the data (observations) dominate the posterior distribution.

To find out which prior crack can be detected, N^p =10^5 random numbers for a_{md}^p is selected based on the defined distribution.

6.3.2.4 Obtain the Detected Cracks

In Section 6.3.2.2 and Section 6.3.2.3, N^p =10^5 simulations were generated for the crack size (a^{prior}) and the mean detectable size (a_{md}^p), respectively. Therefore, for each crack size, a corresponding value of mean detectable size is available.

The same criterion as introduced in Section 6.3.1.6 is considered to decide which crack size (with the corresponding a_{md}^p) is detectable and which one is missed:

1) For each set of $\left(a^{prior}, a_{md}^p\right)_j, j = 1, 2, \dots, 10^5$; $(POD^p)_j$ is calculated using Eq.(6-6) which is between zero and one.

2) N^p = 10^5 random numbers are chosen from a uniform distribution between [0,1], i.e.:

$$(Chance^p)_j = Random\ number, \quad j = 1,2, \dots, 10^5$$

3) A prior crack is assumed as a detected crack $\left(a^{det\ \_pr}\right)_j$ if:

$$(Chance^p)_j \leq (POD^p)_j, \quad j = 1,2, \dots, 10^5$$

4) Otherwise, the simulated prior crack size is assumed as a missed one.

Figure 6.14 shows the PODs for both detected and missed cracks. As the figure shows, the majority of the missed cracks are tiny defects, which are quite impossible to detect using the specified NDT techniques.

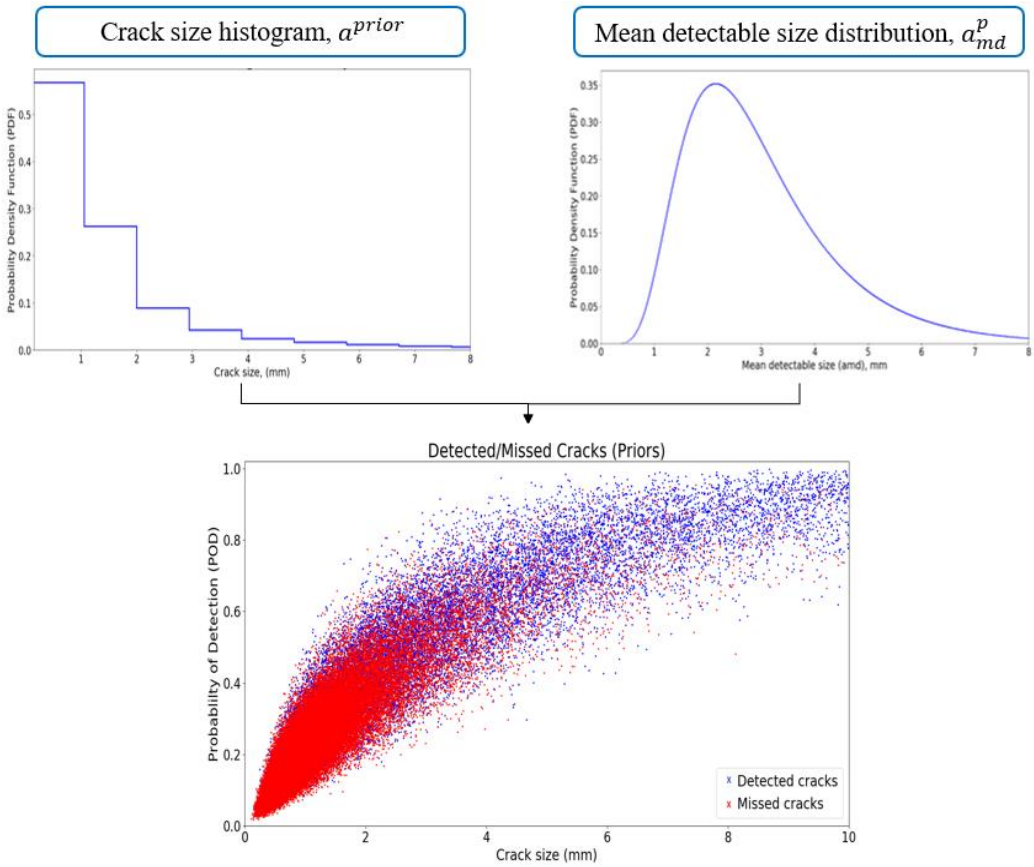

Figure 6.14. PODs for both detected/missed defects

Figure 6.15 summarises the proposed approach to obtain the prior distribution of the crack size by using the sampling method.

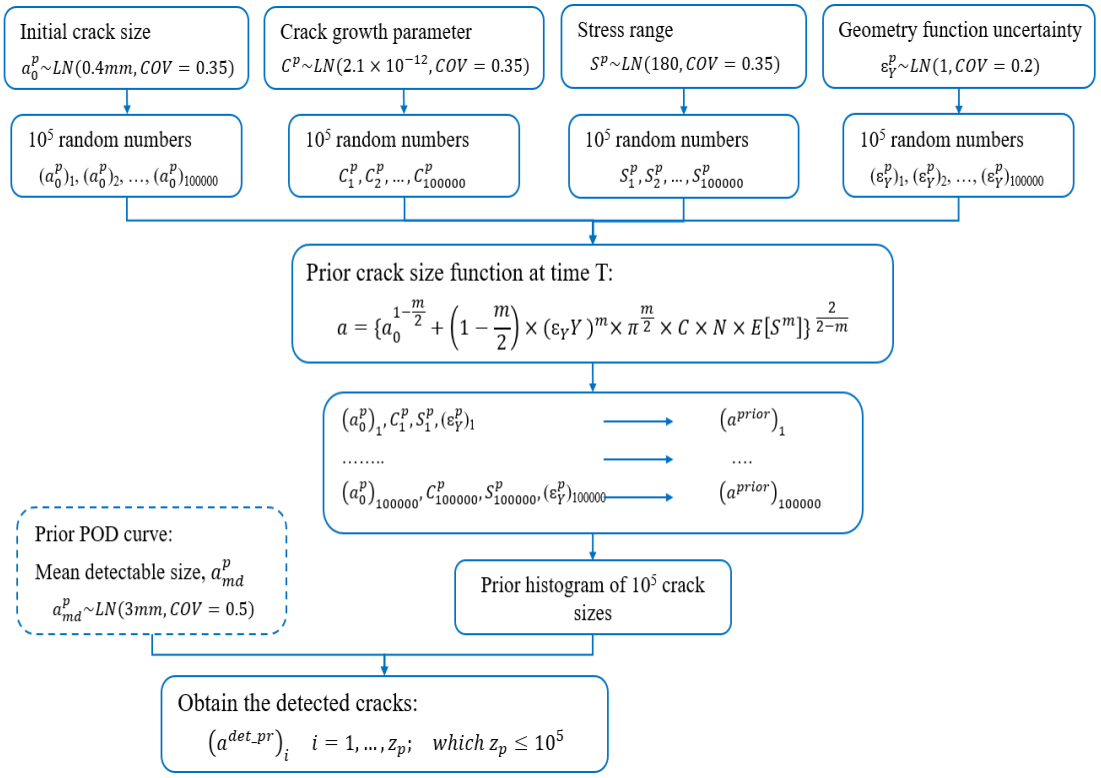

Figure 6.15. The proposed approach for obtaining the detected prior cracks

6.3.3 Posterior (Updated) Distributions of the Uncertain Parameters

Bayes' theorem states that the updated distribution of an uncertain parameter depends on two sets of information, the previous knowledge about the uncertain parameter (prior distribution), and the new information that is provided. Bayesian inference is a statistical inference in which Bayes' theorem is employed to update the distribution of an uncertain parameter when new information becomes available.

For the proposed approach in this Chapter, two sets of cracks are available. The detected prior cracks (previous knowledge) and detected cracks in the simulated reality case (new information which is obtained from the inspection results).

To obtain the posterior distributions of the uncertain parameters, the concept of "Compatibility" is introduced. This is based on an idea mentioned in [141].

In this approach for obtaining the posterior distributions of the uncertain parameters, the following steps are taken:

(I). Selection of the compatible prior cracks

The first step is to find out which prior estimations of cracks are compatible with the simulated reality cracks. For this purpose, each detected prior crack is compared with each simulated reality crack to determine whether it is compatible or not. If a prior crack is close to the simulated reality crack, that prior is accepted otherwise it is assumed as an unacceptable simulation.

A prior estimation is defined as a compatible estimation if:

$$\left|\left(a^{det\_pr}\right)_i - \left(a^{det\_real}\right)_j\right| < Tolerance \times \frac{\left(a^{det\_pr}\right)_i + \left(a^{det\_real}\right)_j}{2} \qquad (6\text{-}9)$$

Where:

- $\left(a^{det\_pr}\right)_i$: Detected prior crack, $i = 1,2,\dots,z_p$
- $\left(a^{det\_real}\right)_j$: Detected crack in the simulated reality case, $j = 1,2,\dots,z_r$
- z_p: Number of detected prior cracks (is less than 10^5)
- z_r: Number of detected cracks in the simulated reality case (is less than 1000)
- $Tolerance$: is assumed equal to 0.2

Based on the compatibility definition, many prior cracks will not match any simulated reality crack. On the other hand, some prior cracks may match several simulated reality cracks. The number of possible matched simulations is:

$$N_{possible} = z_p \times z_r \qquad (6\text{-}10)$$

The number of compatible simulations is obtained from the code which has been written in Python [131].

(II). Removing the incompatible prior estimates

The concept of compatibility is defined by using the provided criterion introduced in Eq.(6-9). By using this criterion the prior cracks are divided into two categories:

- Compatible prior simulations
- Incompatible prior simulations

In this approach, for obtaining the posterior distributions of the uncertain parameters, the incompatible prior simulations are removed and the distributions of the compatible prior estimations are considered as the posterior distributions.

By implementing this approach, the new data (which is the observed cracks) is used to obtain the simulated reality cracks (See Section 6.3). The simulated reality cracks are then utilised to update the prior distribution of the cracks (Section 6.3.3.1), the prior distribution of the uncertain parameters involved in the fatigue crack model (Section 6.3.3.2), and the prior POD curve (Section 6.3.3.3).

6.3.3.1 Posterior Distribution of the Crack Size

Figure 6.16 illustrates how to obtain the posterior cracks by using the compatible priors.

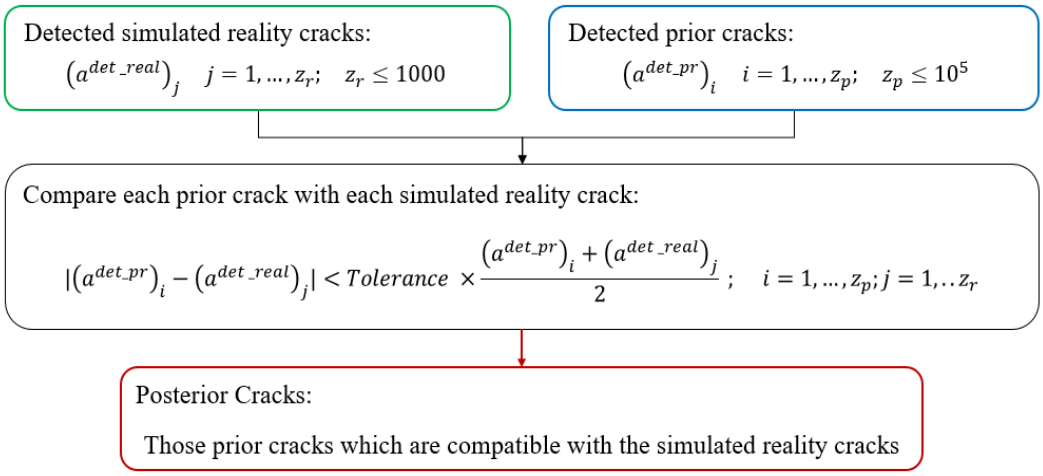

Figure 6.16. Obtaining the posterior cracks

The assigned distribution to the compatible prior cracks is considered as the posterior distribution of the crack size. Figure 6.17 shows the posterior distribution of crack size based on the compatible prior cracks. Although both prior cracks and simulated reality cracks have a great effect on the posterior distribution, it can be seen that the posterior distribution moves towards the simulated reality distribution.

Moreover, as can be seen from Figure 6.17, the variance of the posterior distribution is reduced in comparison with the prior distribution (i.e. the posterior distribution is narrower than the prior distribution). Therefore, by implementing the new information

from the inspection results (i.e. observed cracks), the updated distribution of the crack size is less uncertain than the prior knowledge.

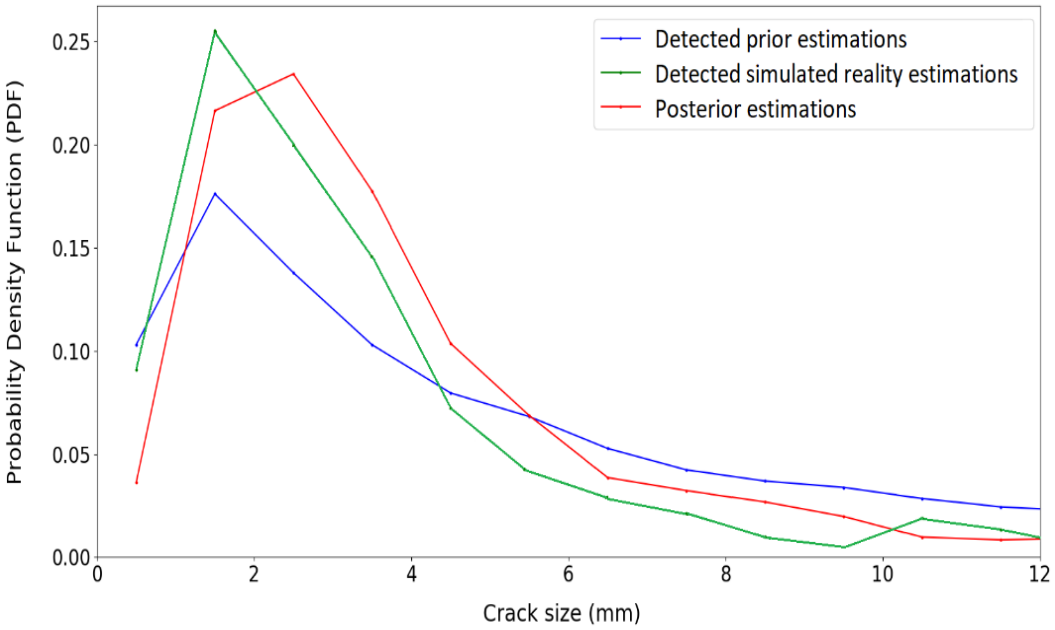

Figure 6.17. Posterior distribution of the crack size

6.3.3.2 Posterior Distributions of the Uncertain Parameters Involved in the Fatigue Crack Model

This section describes how to update the distributions of the uncertainties involved in the fatigue crack size. Based on Eq. (6-1), the fatigue crack size is a function of the following uncertain parameters:

- Initial crack size (a_0)
- Crack growth parameter (C)
- Stress range (S)
- Uncertainty in estimation of geometry function (ε_Y)

Therefore, each detected prior crack corresponds to a set of the above-mentioned parameters. For example, the k[th] detected prior crack ($a_k^{det\_pr}$) corresponds to a_{0k}^p, C_k^p, S_k^p and ε_{Yk}^p.

Let's assume a specific prior crack (e.g. $a_j^{det\_pr}$) is an incompatible prior crack, i.e., it doesn't satisfy the Eq.(6-9). Therefore, the combination of the corresponding input

variables ($a_{0j}^{p}, C_j^{p}, S_j^{p}$ and ε_{Yj}^{p}) are not acceptable due to resulting in an invalid crack size (incompatible prior crack). Hence, these values are removed from the initial set of simulations. On the other hand, if a prior crack is compatible with the simulated reality crack, the corresponding input variables are appropriate values because of the result in a valid crack size.

As it was mentioned, all detected prior cracks are compared to all simulated reality cracks. For those prior cracks that are compatible with the simulated reality, the corresponding input variables are considered as appropriate values and are kept to use for the posterior distributions.

The following figures show the posterior distributions for the uncertain parameters. It can be seen from the figures that the posterior distributions of the uncertain parameters, move towards the simulated reality distributions. This can be seen clearly in Figure 6.19. In this figure, in point "A" the posterior distribution is ascending, although the prior distribution is descending. This illustrates that the posterior distribution tends to shift to the simulated reality distribution.

Moreover, in all figures, the most probable amount of the uncertain parameter (i.e. Mode values) shifts towards the Mode value of the simulated reality distribution, although the posterior distribution shape is affected by both prior and simulated reality shapes.

Another important outcome of these figures is that although the posterior distribution shifts to the simulated reality case, the uncertainty of the posterior distributions mainly increases due to the involved uncertainties in both prior and simulated reality cases. However, the uncertainty of the posterior distribution of the crack size decreases (Section 6.3.3.1). That is because the inspection results include information about the crack size (i.e. observed cracks). The inspection results do not provide any information about the other uncertain parameters such as initial crack size, etc.

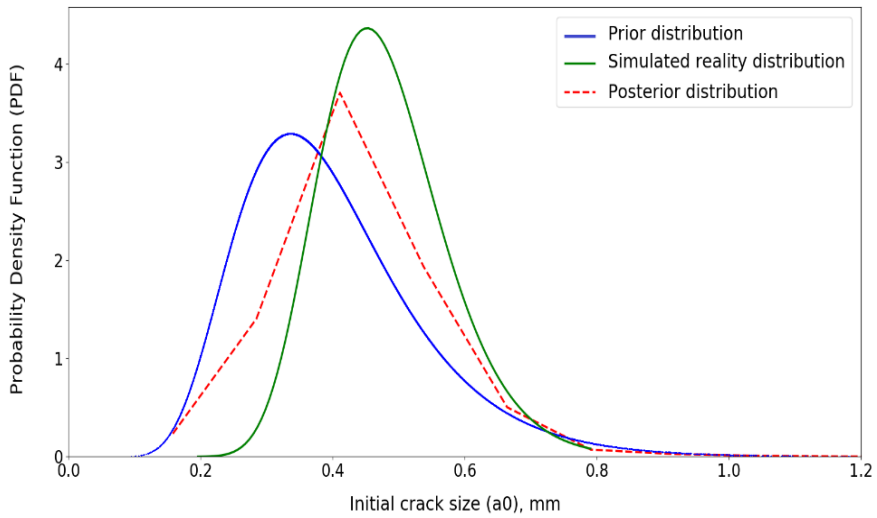

Figure 6.18. Posterior distribution of the initial crack size (a_0)

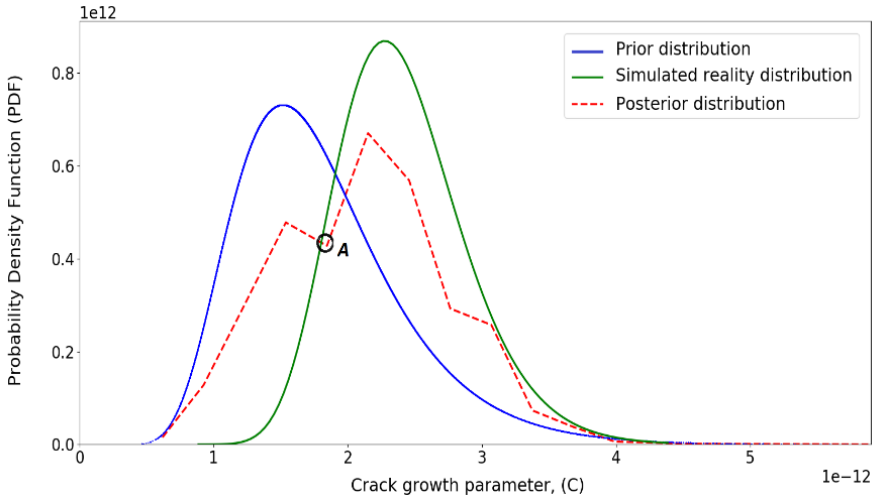

Figure 6.19. Posterior distribution of the crack growth parameter (C)

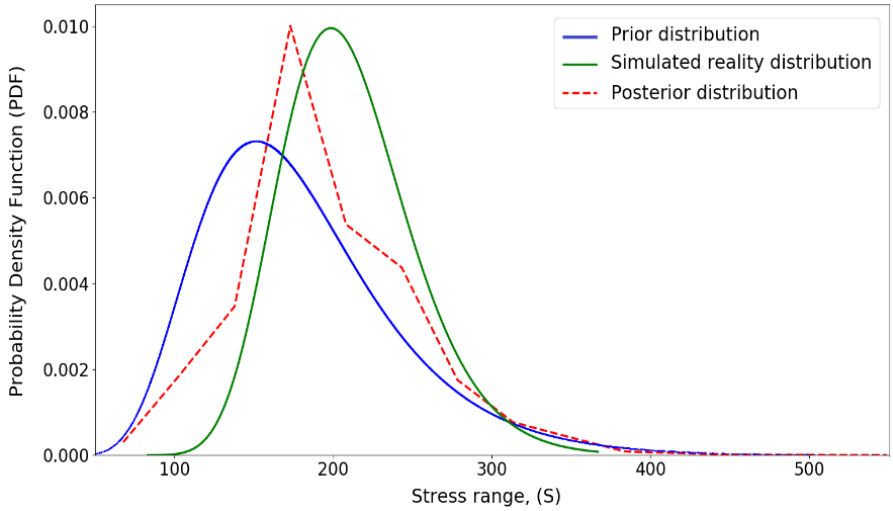

Figure 6.20. Posterior distribution of the stress range (S)

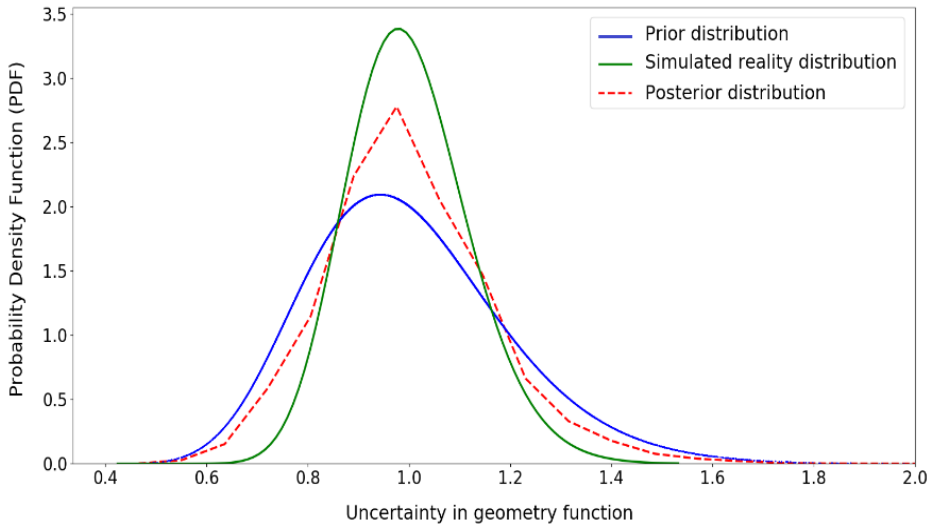

Figure 6.21. Posterior distribution of the uncertainty in the estimation of geometry function (ε_Y)

After obtaining the posterior distributions of the uncertain parameter (i.e. initial crack size, crack growth parameter, stress range, and geometry function), these distributions can be used as the prior distributions for the next updating process when new inspection results become available (Figure 6.1).

6.3.3.3 Updated POD Curve

The same approach as described in Section 6.3.3.2 is utilised to update the POD curve. Figure 6.22 shows the best fit for the POD curve based on the compatible prior simulations. It can be seen that the updated POD curve moves towards the simulated reality curve.

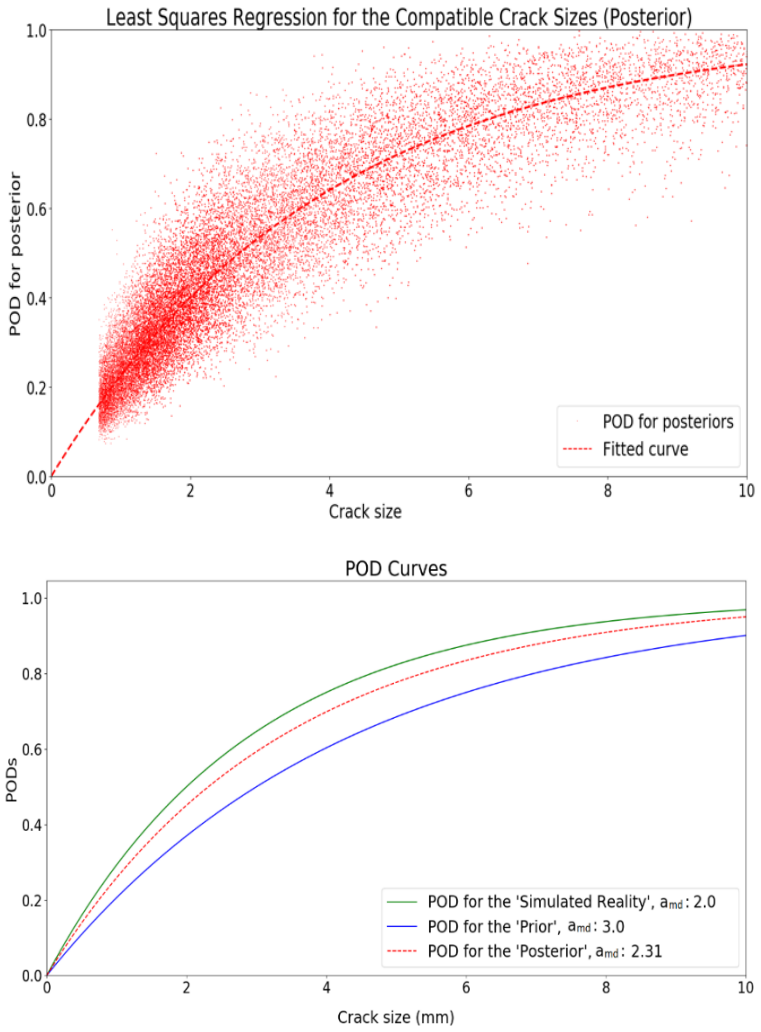

Figure 6.22. Updated POD curve

6.4 Reliability of the Proposed Approach: Sensitivity to the Inputs

It was shown that the posterior distributions of the uncertain parameters are affected by both prior distributions and the simulated reality distributions (which are obtained from the new information, i.e., inspection results). The sensitivity of the updating process is a crucial part of any updating approach. The sensitivity analysis is performed to find out which inputs have great influences on the posterior distribution. Knowing the important parameters, the user (owner) can focus on gathering more data on these crucial parameters.

6.4.1 Sensitivity of the Posterior Distributions to the Prior Distributions

The prior distributions for the uncertain parameters can be assumed based on theoretical considerations, expert opinions, past experiences, or test results. Different

distributions have been introduced by recommendation guidelines. Table 6.3 shows the statistics of the initial crack size and crack growth parameter which have been proposed by different guidelines.

Table 6.3. Statistics of the uncertain parameters [N, mm]

Variable	DNV 95-3204 [19]	BS 7910 [47]	JCSS [134]
Initial crack size, a_0^p	Exp (0.11, COV = 1)	---	LN (0.15, 0.66)
Crack growth parameter, C^p	LN ($1.27\text{x}10^{-13}$, 0.55)	LN ($5.16\text{x}10^{-12}$, 0.78)	LN ($5.86\text{x}10^{-13}$, 0.60)

To find out the effect of the prior distributions on the posterior, different distributions with different COVs (in comparison with those introduced in Section 6.3.2.1) are considered. Table 6.4 shows the statistics of the prior distributions for performing the sensitivity analysis.

Table 6.4. Statistics of the different prior distributions for input variables [N, mm]

Variable	Case (I) (Introduced in Section 6.3.2.1)	Case (II) (New Prior Distributions)
Initial crack size, a_0^p	LN (0.4, COV = 0.35)	Exp (0.4, COV = 1)
Crack growth parameter, C^p	LN (2.1×10^{-12}, COV = 0.35)	LN (1.5×10^{-12}, COV = 0.5)
Stress range, S^p	LN (180, COV = 0.35)	LN (210, COV = 0.5)
Uncertainty in estimation of geometry function, ε_Y^p	LN (1.0, COV = 0.2)	LN (1.1, COV = 0.4)

6.4.1.1 Sensitivity to the Prior Distribution of Initial Crack Size (a_0^p)

To take into account the effect of the selection of different prior distributions for the initial crack size (a_0^p) on the posterior distributions of all uncertain parameters, an exponential distribution, and a lognormal distribution (as introduced in Table 6.4) are considered. Figure 6.23 shows these two distributions.

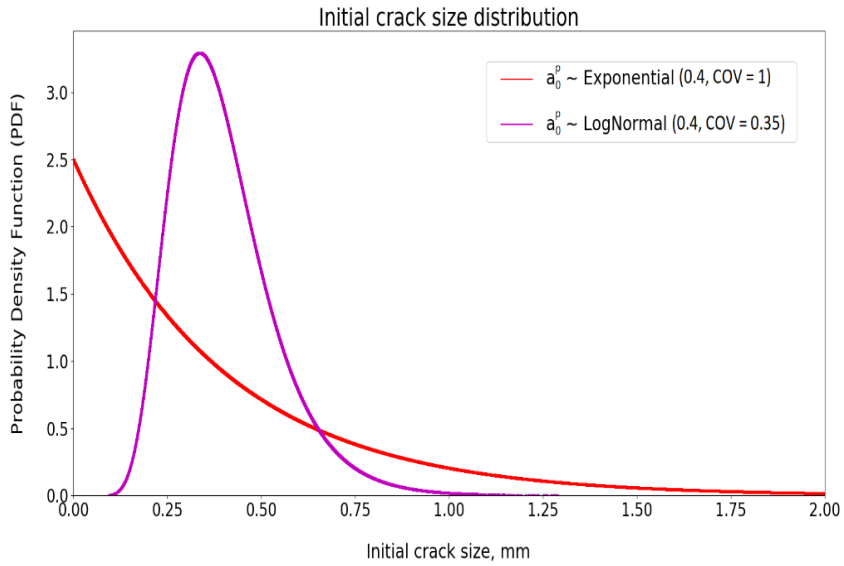

Figure 6.23. Different prior distributions of the initial crack size

- Sensitivity of the posterior distribution of the crack size to a_0^p

  Figure 6.24 shows the posterior distributions of the crack size for both prior distributions of the initial crack size (by using the proposed approach). Although both prior distributions of the initial crack size have the same mean value (0.4 mm), the prior distribution of the initial crack size affects the posterior distribution of the crack size, especially in small crack sizes.

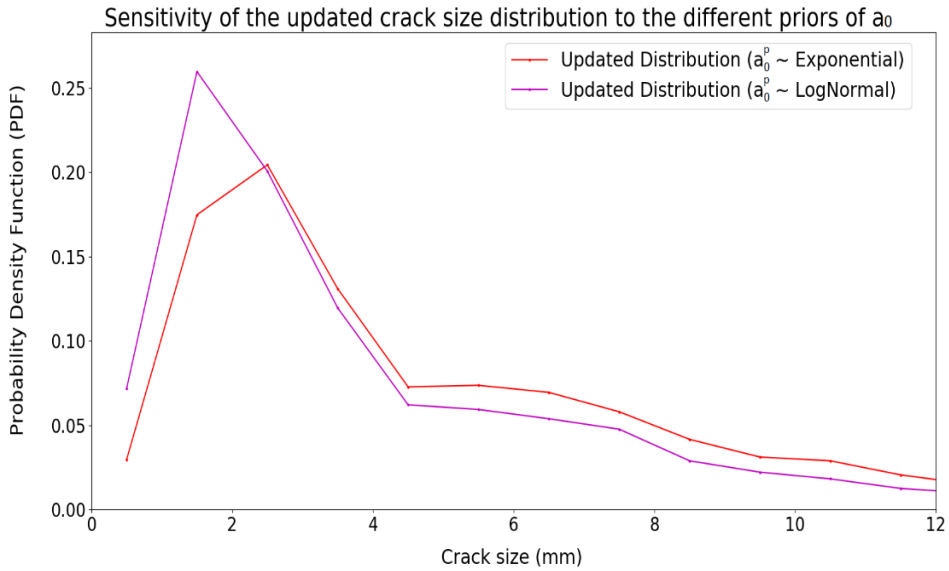

Figure 6.24. Posterior distributions of the crack size for different prior distributions of the initial crack size

Nevertheless, the shape of the posterior distributions for the larger crack sizes (which are important for the probability of failure calculation, see Eq. (6-2)) is similar.

Since the COV of the initial crack size in the exponential distribution is greater than COV in the lognormal distribution, the probability of bigger initial cracks in the exponential distribution is greater than the lognormal distribution (Figure 6.23). Bigger initial cracks result in bigger cracks. Therefore, the probability of bigger cracks (and consequently the probability of failure) in the case of the exponential distribution is larger than the lognormal case.

Table 6.5 shows the probability of failure in the case of the selection of different prior distributions for the initial crack size. The probability of failure in each case is calculated by using the fatigue limit state defined in Eq. (6-2) and by performing the Monte-Carlo simulation. Table 6.5 shows that the probability of failure in Case (II) is around 2.5 times bigger than the probability of failure in Case (I).

Table 6.5. Probability of failure for different prior distributions of the initial crack size

Prior Distribution of Initial Crack Size (a_0^p)	Probability of Failure (Reliability Index)	Change in Probability of Failure (%)
Case (I): LN (0.4, COV = 0.35)	0.00068 (3.20)	262%
Case (II): Exp (0.4, COV = 1)	0.00178 (2.92)	

In conclusion, the posterior distribution of the crack size is very sensitive to the selected COV of the prior distribution of the initial crack size, whereas distribution shape is mostly affecting the updated probability of small crack sizes. Therefore, for the calculation of the probability of failure, the COV of the prior distribution of the initial crack size is important.

- Sensitivity of the posterior distributions of the other uncertain parameters to a_0^p

Figure 6.25 illustrates the posterior distributions of the initial crack size for different prior distributions. Although the posterior distributions of the initial crack size are affected by the prior distributions, regardless of the prior shape

(even for the exponential distribution), the posterior distributions move towards the simulated reality distribution.

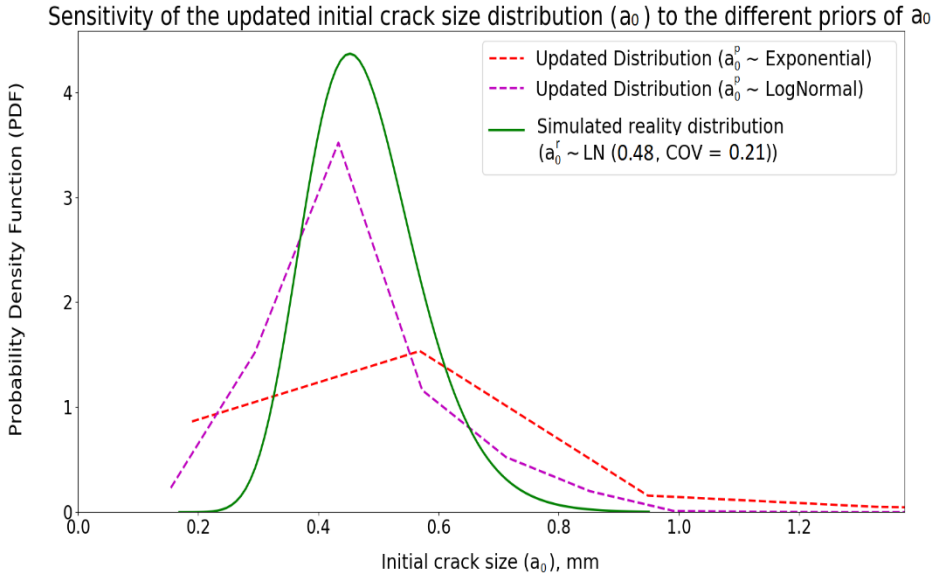

Figure 6.25. Posterior distributions of the initial crack size for different prior distributions of initial crack size

Figure 6.26 shows the effect of different prior distributions of the initial crack size on the posterior distributions of other uncertain parameters (i.e. crack growth parameter, stress range, and uncertainty in the estimation of geometry function). As it can be seen, the posterior distributions of other uncertain parameters are not sensitive to the prior distribution of the initial crack size which seems reasonable.

The initial crack size generally depends on the quality of the welding procedure, whereas the crack growth parameter is a material property and the stress range is dependent on the loading conditions. This is probably why the posterior distributions of these parameters are less sensitive to the initial crack size distributions.

(a)

(b)

(c)

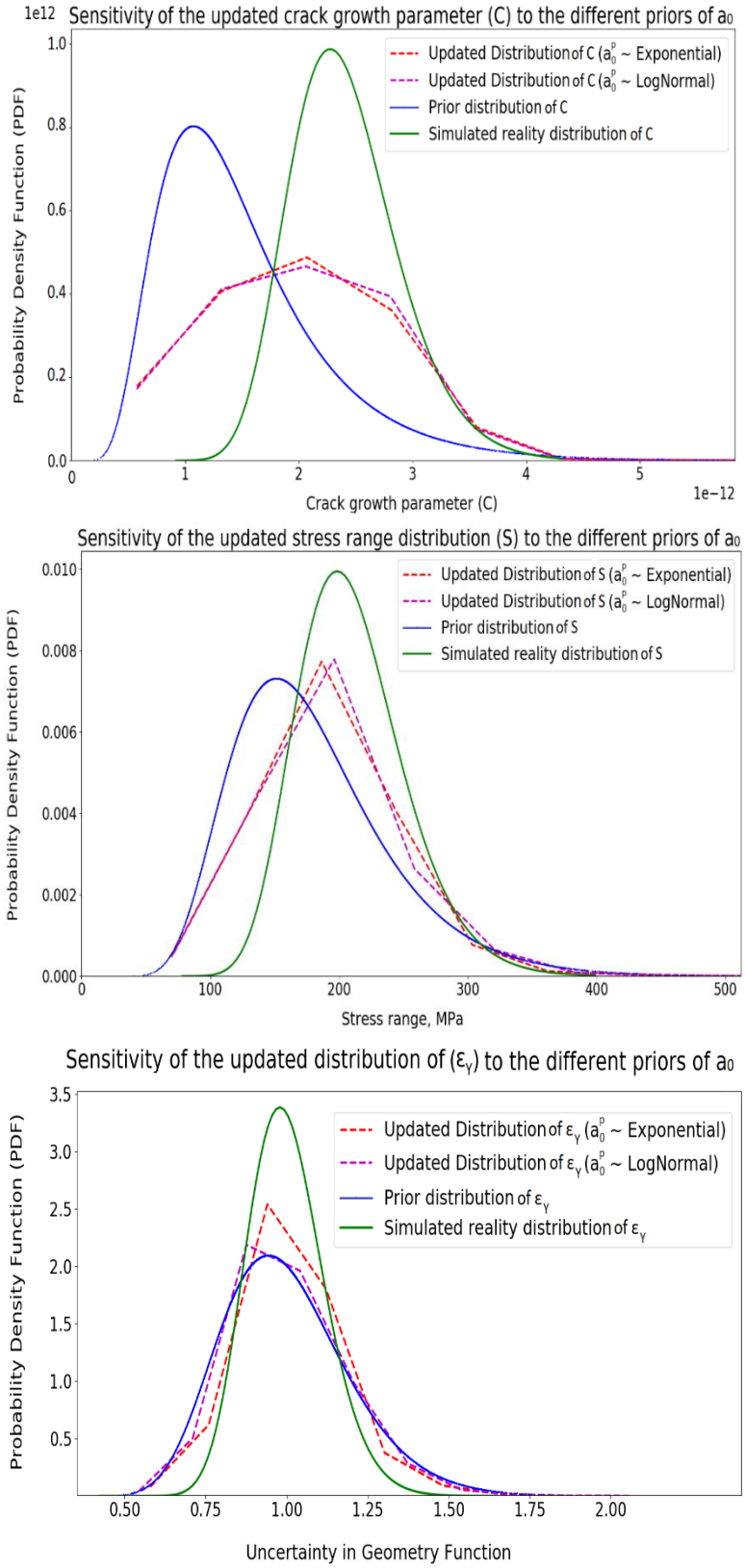

Figure 6.26. Effect of different prior distributions of the initial crack size on the other uncertain parameter distributions (a: Crack growth parameter, b: Stress range, and c: Uncertainty in the estimation of geometry function)

6.4.1.2 Sensitivity to the Prior Distribution of Crack Growth Parameter (C^p)

To take into account the effect of the selection of different prior distributions for the crack growth parameter (C^p) on the posterior distributions of all uncertain parameters, two lognormal distributions (introduced Table 6.4) are considered. Figure 6.27 shows these two distributions.

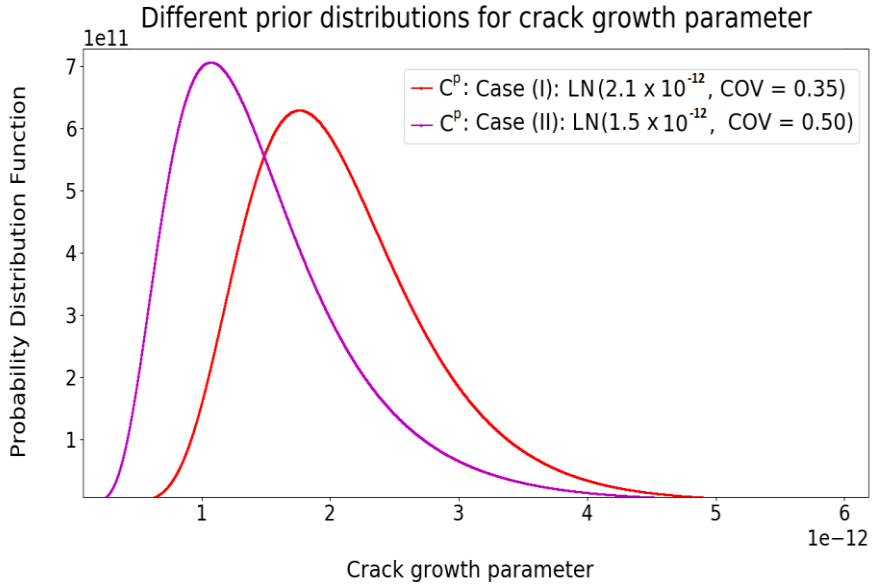

Figure 6.27. Different prior distributions of the crack growth parameter

- Sensitivity of the posterior distribution of the crack size to C^p

  Figure 6.28 shows the posterior distributions of the crack size for both prior distributions of the crack growth parameter. Since the mean value of the crack growth parameter in Case (II) is smaller than Case (I), the updated probability of smaller cracks, in this case, is larger than the probability of smaller cracks in Case (I) which is sensible. However, for the larger crack sizes, the posterior distributions are less sensitive to the prior distributions of the crack growth parameter.

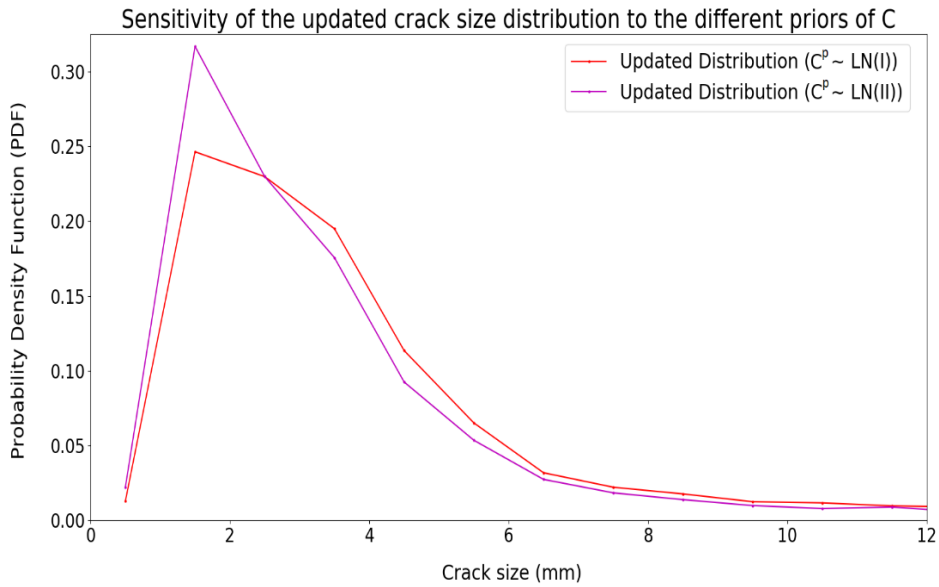

Figure 6.28. Posterior distributions of the crack size for different priors of the crack growth parameter

Table 6.6 shows the probability of failure in the case of the selection of different prior distributions for the crack growth parameter. The probability of failure in each case is calculated by using the fatigue limit state defined in Eq. (6-2) and by performing the Monte-Carlo simulation.

Table 6.6. Probability of failure for different prior distributions of crack growth parameter

Distribution of Crack Growth Parameter (C^p)	Probability of Failure (Reliability Index)	Change in Probability of Failure (%)
Case (I): LN (2.1×10^{-12}, COV = 0.35)	0.00068 (3.20)	12%
Case (II): LN (1.5×10^{-12}, COV = 0.5)	0.00076 (3.17)	

- Sensitivity of the posterior distributions of the other uncertain parameters to C^p

Figure 6.29 shows the posterior distributions of the crack growth parameter for different prior distributions. The posterior distributions shift towards the simulated reality distribution although their shapes are affected by the prior distributions. Since the prior COV in Case (II) is bigger than Case (I), the posterior distribution, in this case, has a bigger uncertainty (i.e. is wider).

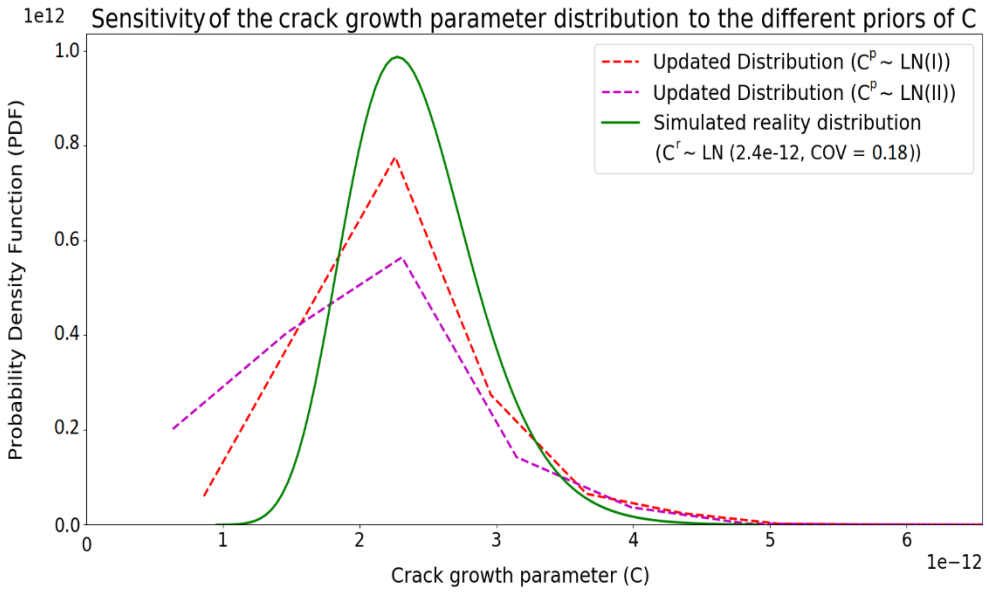

Figure 6.29. Posterior distributions of the crack growth parameter for different priors of the crack growth parameter

Figure 6.30 shows the effect of different prior distributions of the crack growth parameter on the posterior distributions of other uncertain parameters (i.e. initial crack size, stress range, and the uncertainty in the estimation of geometry function).

The crack growth parameter is a material property, whereas the initial crack size generally depends on the quality of the welding procedure, and the stress range is dependent on the loading conditions. Therefore, the posterior distributions of other uncertain parameters are less sensitive to the prior distribution of the crack growth parameter.

(a)

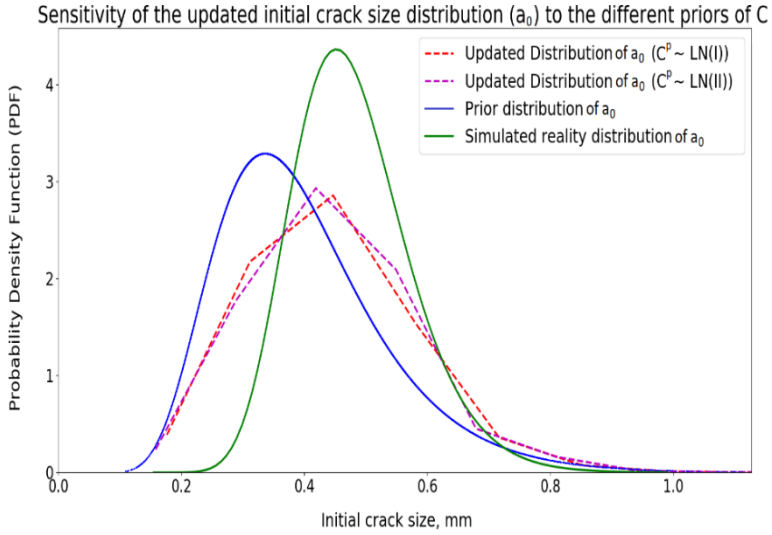

(b)

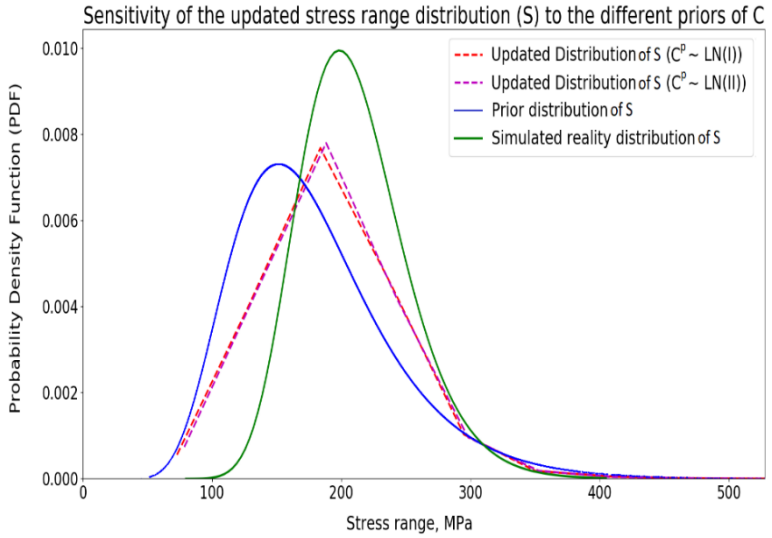

(c)

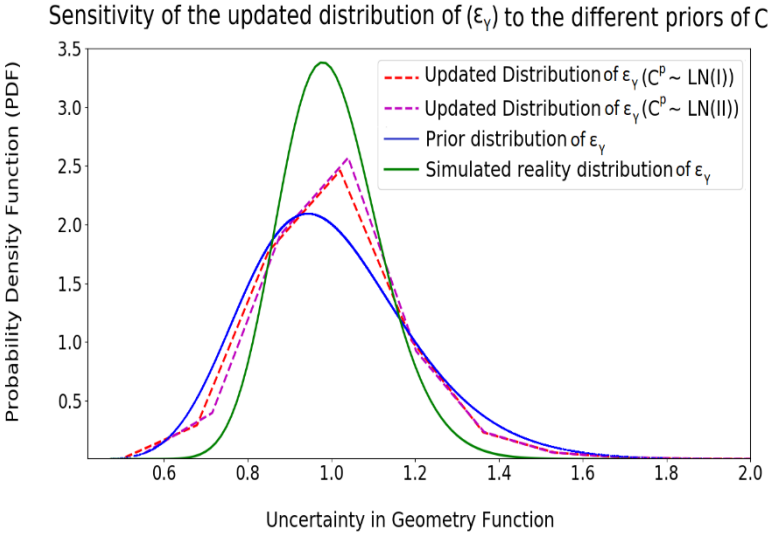

Figure 6.30. Effect of different prior distributions of the crack growth parameter on the posterior distributions of other uncertain parameters (a: Initial crack size, b: Stress range, and c: Uncertainty in the estimation of geometry function)

6.4.1.3 Sensitivity to the Prior Distribution of Stress Range (S^p)

Two lognormal distributions are introduced in Table 6.4 to take into account the effect of the selection of different prior distributions of the stress range (S^p) on the posterior distributions of all uncertain parameters. These two distributions are shown in Figure 6.31.

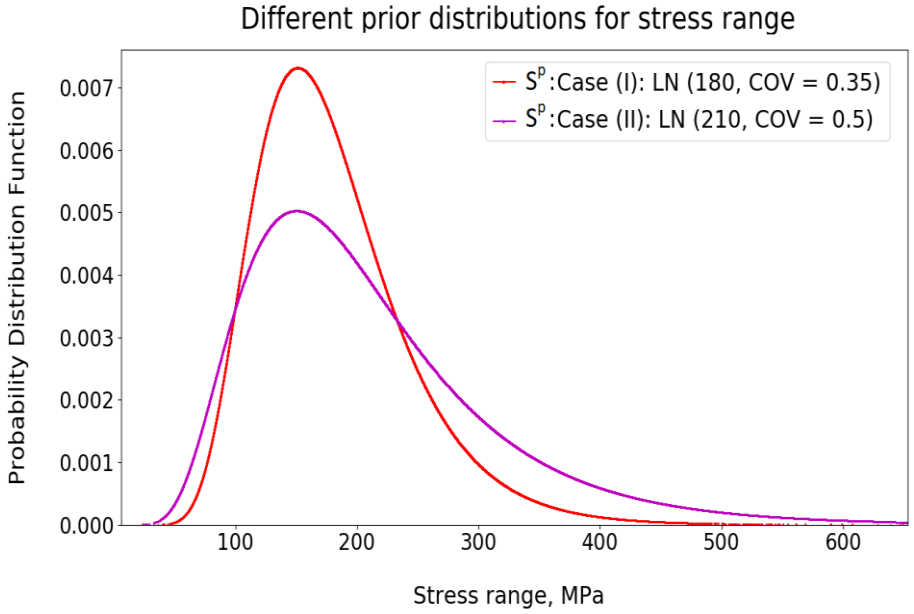

Figure 6.31. Different prior distributions of the stress range

- Sensitivity of the posterior distribution of the crack size to S^p

  Figure 6.32 illustrates that the posterior distributions of the crack size are sensitive to the prior distributions of the stress range (S^p). Since the stress range distribution in Case (II) has a bigger mean value in comparison with Case (I), the probability of occurrence of larger cracks is greater than the other case which is sensible. Moreover, it can be seen that the shape of the posterior distribution of the crack size is not sensitive to the COV of the stress range.

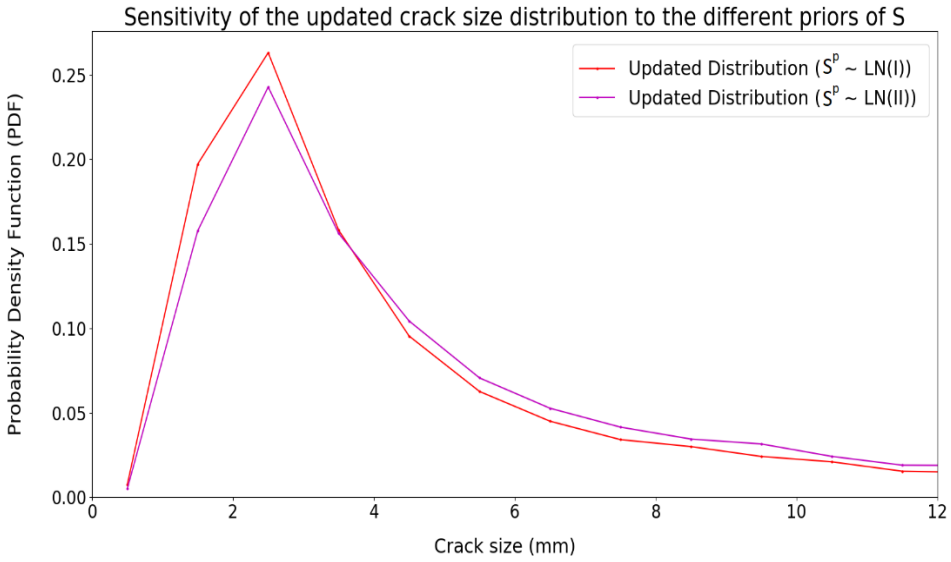

Figure 6.32. Posterior distributions of the crack size for different prior distributions of the stress range

Table 6.7 shows the probability of failure for different prior distributions of the stress range. The probability of failure in each case is calculated by using the fatigue limit state defined in Eq. (6-2) and by performing the Monte-Carlo simulation.

Table 6.7. Probability of failure for different prior distributions of stress range

Distribution of Stress Range (S^p)	Probability of Failure (Reliability Index)	Change in Probability of Failure (%)
Case (I): LN (180, COV = 0.35)	0.00068 (3.20)	57%
Case (II): LN (210, COV = 0.5)	0.00107 (3.07)	

- Sensitivity of the posterior distributions of the other uncertain parameters to S^p

Figure 6.33 shows the posterior distributions of the stress range for different prior distributions. The posterior distributions shift towards the simulated reality distribution in both cases. Since the prior COV in Case (II) is bigger than Case (I), the posterior distribution, in this case, has a bigger uncertainty.

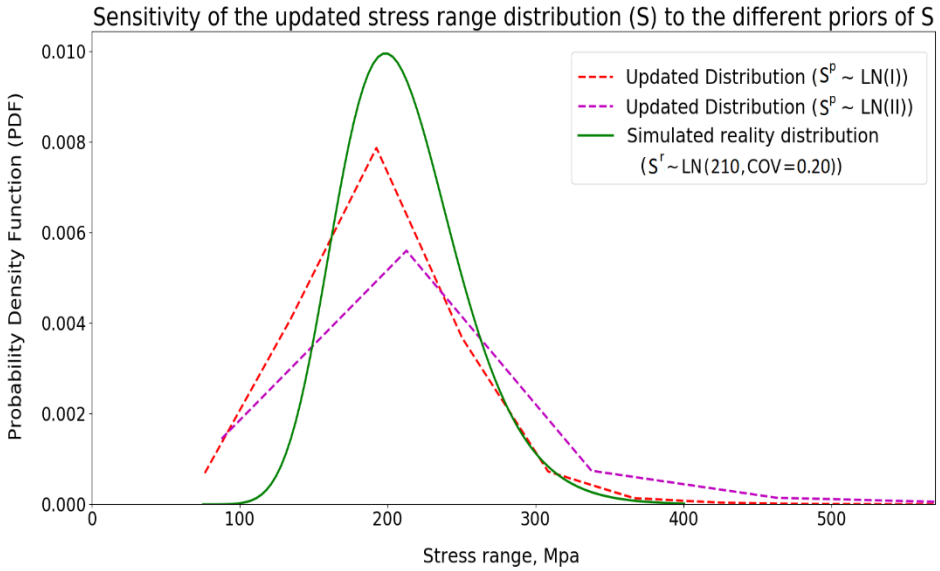

Figure 6.33. Posterior distributions of the stress range for different prior distributions

Figure 6.34 shows the effect of different prior distributions of the stress range on the posterior distributions of other uncertain parameters. As it can be seen, the posterior distributions are insensitive to the prior distribution of the stress range.

(a)

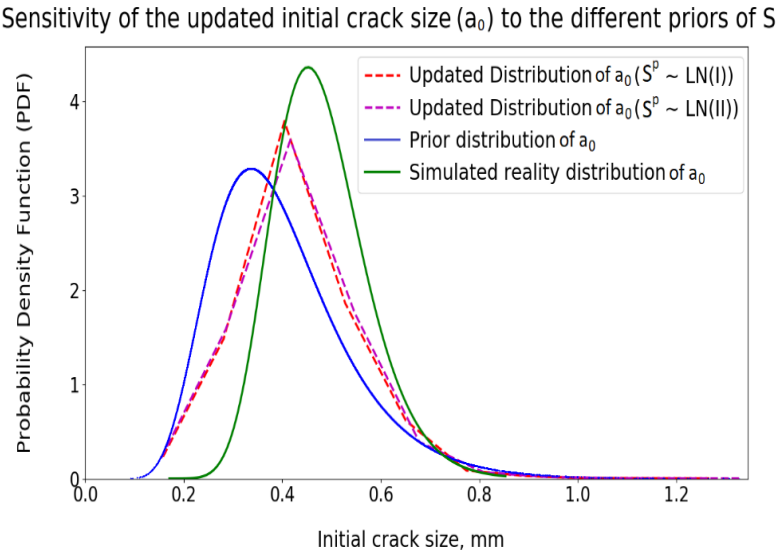

(b)

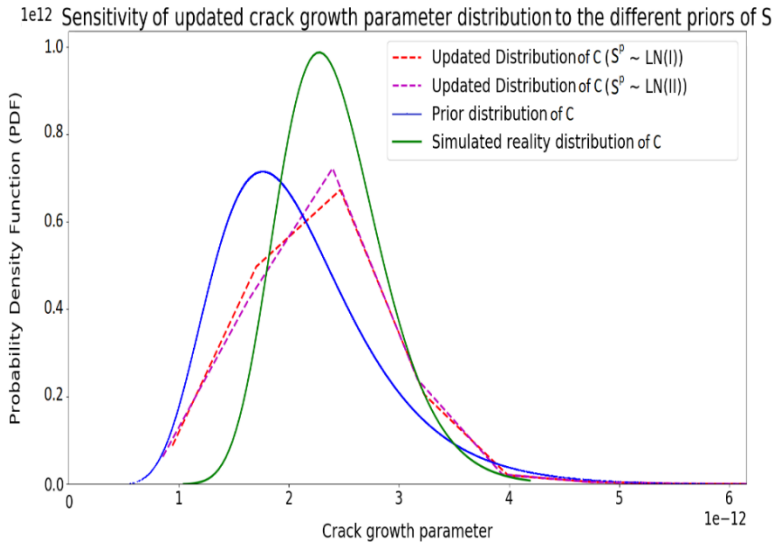

(c)

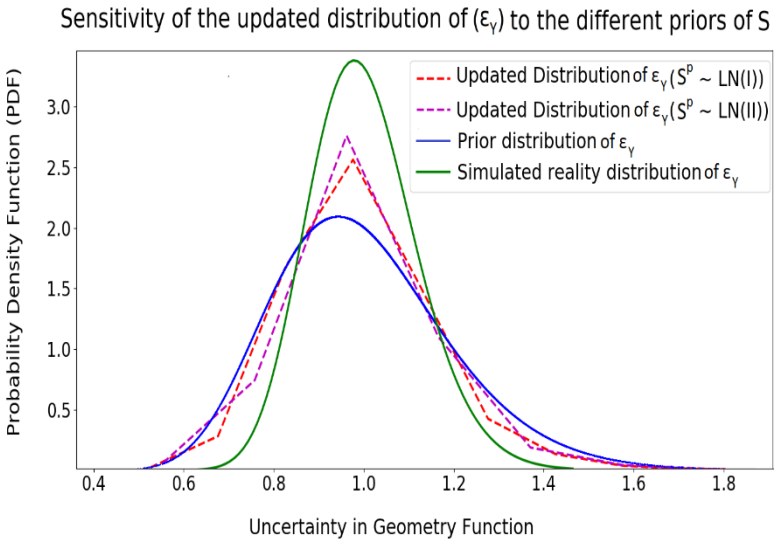

Figure 6.34. Effect of different stress range priors on the posterior distributions of other parameters (a: Initial crack size, b: Crack growth parameter, and c: Uncertainty in the estimation of geometry function)

6.4.1.4 Sensitivity to the Prior Distribution of Uncertainty in Geometry Function (ε_Y^p)

Two lognormal distributions for ε_Y^p are considered (Table 6.4) to investigate the effect of selection of different prior distributions of the ε_Y^p on the posterior distributions of all uncertain parameters. Figure 6.35 shows these two distributions.

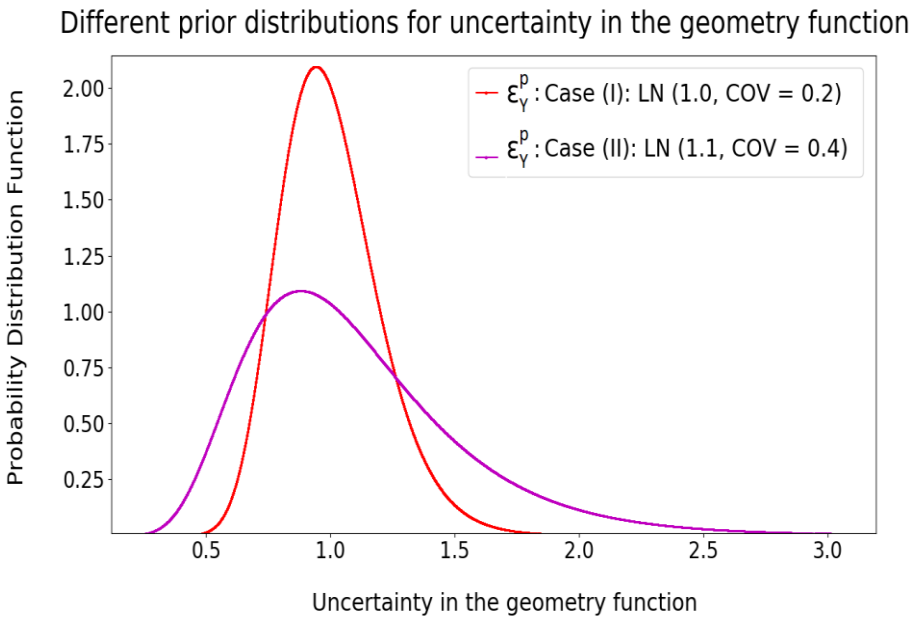

Figure 6.35. Different prior distributions for uncertainty in geometry function

- <u>Sensitivity of the posterior distribution of the crack size to ε_Y^p</u>

  Figure 6.36 shows that the posterior distributions of the crack size have a similar shape. However, the probability of occurrence of larger cracks in Case (II) is slightly bigger than the probability of occurrence in Case (I) due to the bigger mean value in Case (II). Moreover, it can be seen that the posterior distribution of the crack size is insensitive to the COV of ε_Y.

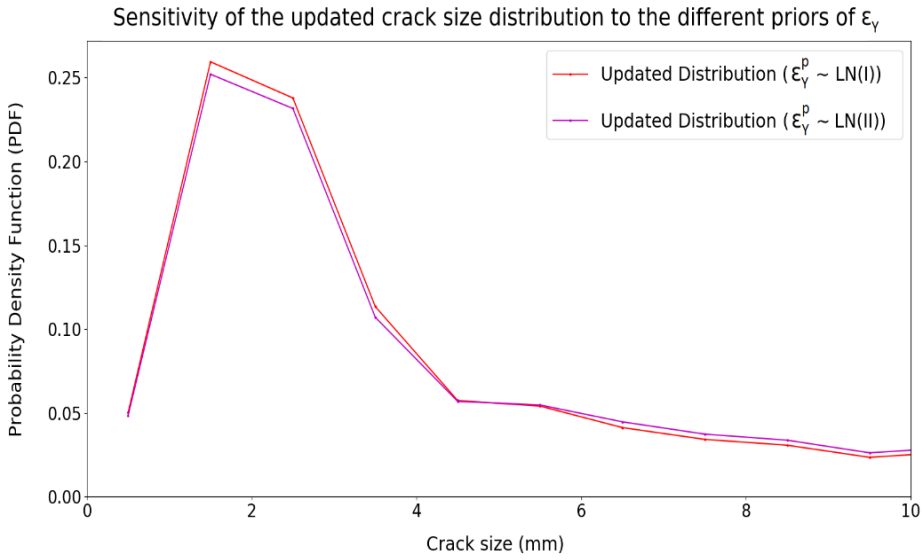

Figure 6.36. Updated crack size distributions for different priors of ε_Y

Table 6.8 shows the probability of failure for different prior distributions of the uncertainty in the geometry function.

Table 6.8. Probability of failure for different prior distributions of geometry function

Distribution of the Uncertainty in the Geometry Function (ε_Y^p)	Probability of Failure (Reliability Index)	Change in Probability of Failure (%)
Case (I): LN (1.0, COV = 0.2)	0.00068 (3.20)	28%
Case (II): LN (1.1, COV = 0.4)	0.00087 (3.13)	

- Sensitivity of the posterior distributions of the other uncertain parameters to ε_Y^p

Figure 6.37 shows the posterior distributions of ε_Y for different prior ditributions. The posterior distributions shift towards the simulated reality distribution. Since the prior COV in Case (II) is bigger than Case (I), the posterior distribution, in this case, is broader than the posterior distribution in Case (I).

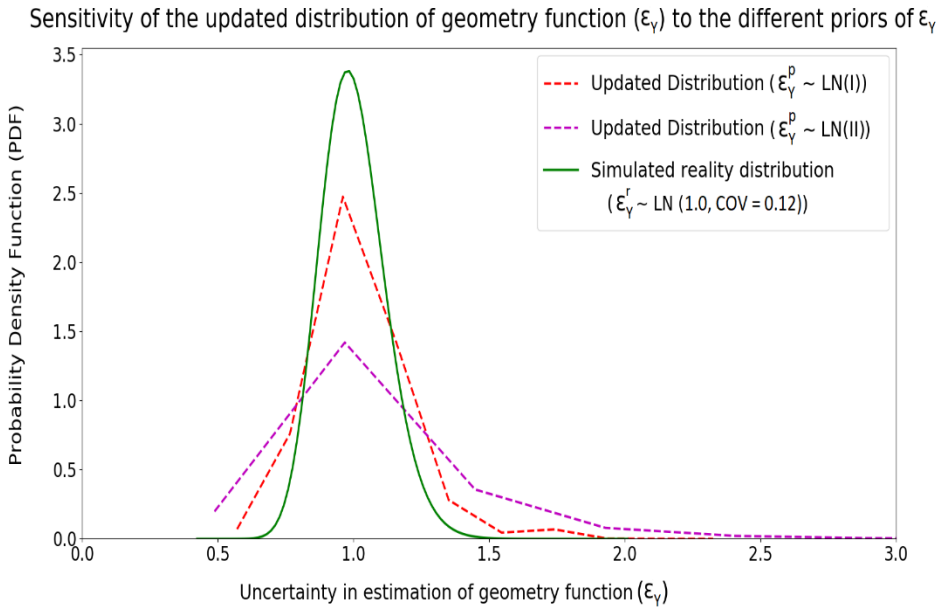

Figure 6.37. Posterior distributions of the uncertainty in the estimation of geometry function

Figure 6.38 shows the effect of different priors of ε_Y on the updated distributions of other uncertain parameters. As it can be seen, the updated distributions of other distributions (i.e. a_0, C, and S) are not sensitive to the prior distribution of ε_Y.

(a)

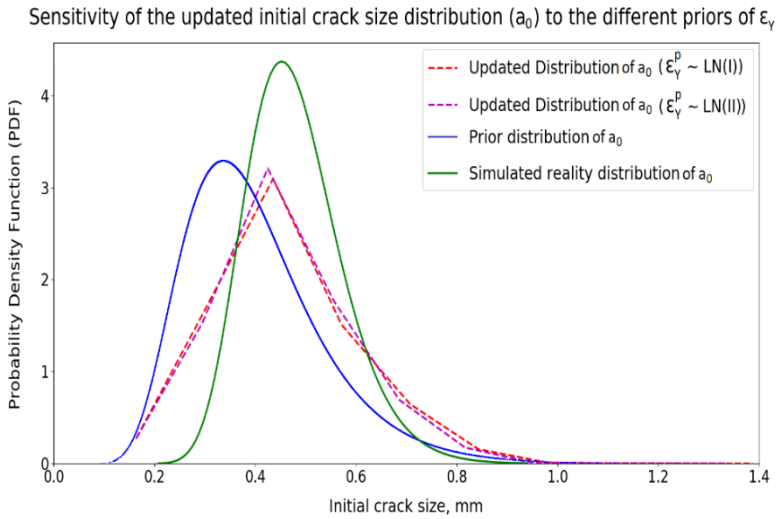

(b)

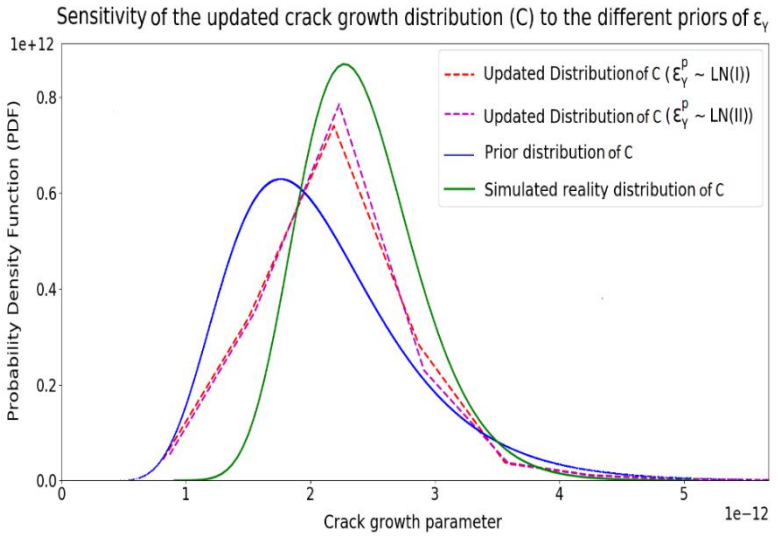

(c)

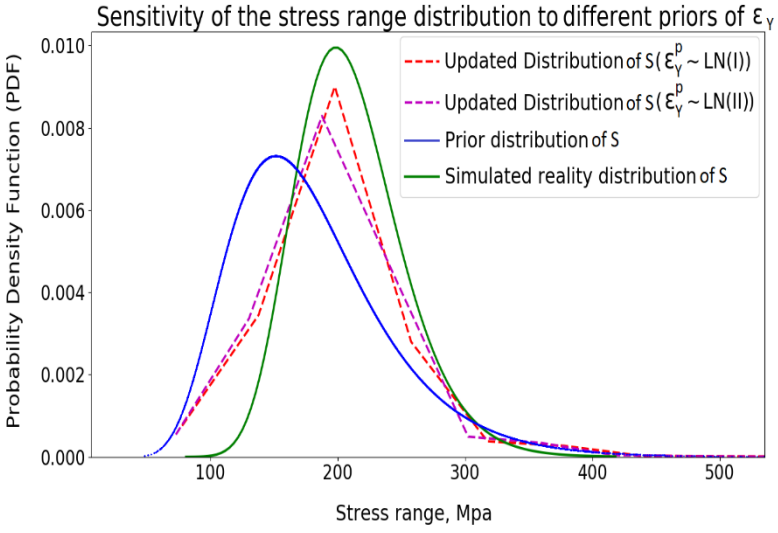

Figure 6.38. Effect of different prior distributions of ε_Y on the posterior distributions of other parameters (a: Initial crack size, b: Crack growth parameter, and c: Stress range)

6.4.1.5 Conclusion

In Section 6.4.1, the sensitivity of the posterior distributions of all uncertain parameters (including crack size and other input variables) to the prior distributions is investigated. For each input variable (i.e. initial crack size, crack growth parameter, stress range, and uncertainty in the estimation of geometry function), two different prior distributions are introduced in Table 6.4. The main results of these analyses are:

- The probability of big crack sizes (and subsequently the probability of failure) is very sensitive to the prior distributions of the initial crack size and the stress range whereas, it is not sensitive to the prior distributions of the other input variables (i.e. crack growth parameter and the uncertainty in the geometry function). Therefore, the prior distributions for the initial crack size and stress range should be assigned as accurately as possible.
- The prior distribution of each input variable has a great effect on the posterior distribution of itself. Based on the Bayes' theorem, the posterior distribution is a function of the prior distribution.
- Since the source of uncertainty of these input variables is almost independent of each other, the prior distribution of each input variable does not have a considerable effect on the posterior distributions of the other variables.

6.4.2 Sensitivity of the Posterior Distribution to the POD Curves

Based on the proposed approach, the probability of detection is employed to determine whether a crack is detected or missed (Figure 6.1). By using POD curves, the prior cracks (and also the simulated reality cracks) are divided into two categories; detected cracks and missed cracks. In the proposed approach for updating the crack size distribution, only detected cracks are used (see Section 6.3.3). Therefore, the sensitivity of the posterior distribution of the crack size to the POD curves should be considered. Based on Eq.(6-6), the probability of detection is a function of a_{md} (mean detectable size) which depends on the resolution of the inspection technique. A lognormal distribution was assigned to the prior distribution of the mean detectable size (Section 6.3.2.3).

To find out the effect of the prior distribution of the mean detectable size on the posterior distribution of the crack size, three different prior distributions are considered. Table 6.9 shows these three cases.

Table 6.9. Statistics of the mean detectable size for sensitivity analysis

Case	Prior distribution for a_{md}^{p}	Simulated reality distribution for a_{md}^{r}	Obtained value for $a_{md}^{posterior}$
Case (I): High-resolution technique	$LN(2\ mm,\ COV = 0.5)$	$LN(2\ mm, COV = 0.2)$	1.58
Case (II): Mid-resolution technique	$LN(4\ mm,\ COV = 0.5)$		3.02
Case (III): Low-resolution technique	$LN(6\ mm,\ COV = 0.5)$		4.55

Figure 6.39 shows the effect of the prior distributions of the mean detectable size on the posterior distribution of the crack size. The figure shows that the posterior distribution of the crack size is very sensitive to the value of the mean detectable size. It was explained that the probability of failure is dependent on the crack size distribution since the fatigue limit state is a function of crack size (Eq. (6-2)). Therefore, the estimated probability of failure is strongly sensitive to the prior distribution of the mean detectable size.

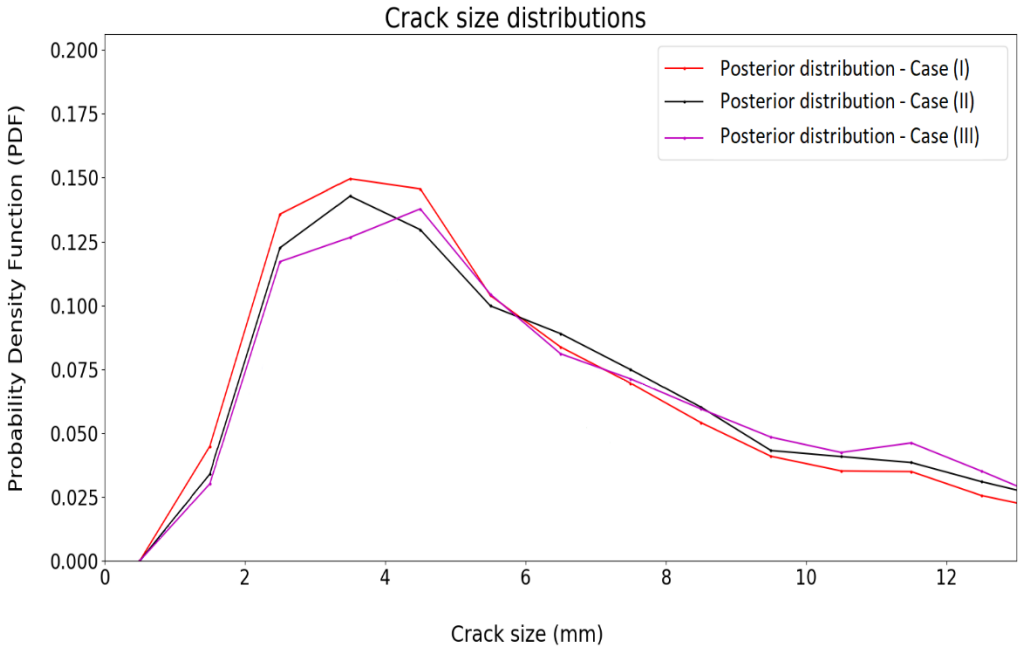

Figure 6.39. Posterior distributions of the crack size for different prior distributions of the mean detectable size (a_{md}^{p})

Figure 6.39 also indicates that the probability of the large cracks (e.g. bigger than 12mm) in Case (I) which is a high-resolution technique is less than the probability of the large cracks in Case (II) which is a mid-resolution technique.

To explain the reason, it is assumed that there are "n" and "m" cracks that are bigger and smaller than 12mm, respectively. Both considered NDT techniques (i.e. Case (I) and Case (II)) are likely to find cracks that are bigger than 12mm. The probability of detection of a 12mm crack is obtained by using Eq.(6-6) as:

$$\begin{aligned} &\text{Case (I):} \quad POD\ (a) = 1 - e^{-\frac{a}{a_{md}}} = 1 - e^{-\frac{12}{2}} = 0.99 \\ &\text{Case (II):} \quad POD\ (a) = 1 - e^{-\frac{a}{a_{md}}} = 1 - e^{-\frac{12}{4}} = 0.95 \end{aligned} \tag{6-11}$$

Therefore, it can be assumed that both cases can detect "n" cracks. Whereas, for the smaller cracks, Case (I) can detect more cracks in comparison with Case (II). Now, it is assumed that Case (I) can detect 60% of small cracks ($0.6 \times m$) while in Case (II) this percentage is reduced for example to 50% (i.e. $0.5 \times m$). Since only detected cracks are considered in this approach, the updated probability of big cracks (e.g. bigger than 12mm) in Case (I) is less than the updated probability of big cracks in Case (II), i.e.:

$$\begin{aligned} &\text{Case (I):} \quad P\ (a > 12) = \frac{number\ of\ cracks > 12mm}{all\ detected\ cracks} = \frac{n}{n + 0.6m} \\ &\text{Case (II):} \quad P\ (a > 12) = \frac{number\ of\ cracks > 12mm}{all\ detected\ cracks} = \frac{n}{n + 0.5m} \end{aligned} \tag{6-12}$$

6.4.3 Sensitivity to the Considering All Cracks (Detected/Missed)

In the proposed approach for obtaining the posterior distribution of the crack size, detected prior cracks are compared with the detected cracks in the simulated reality case. In fact, in the definition of compatibility, the not detected (missed) cracks are removed from the initial list of cracks. The purpose of this section is to include all cracks whether they are detected or missed. In other words, all prior cracks are compared with all simulated reality cracks. Figure 6.40 shows the updated crack size distributions in two cases:

- Case (I): Considering only detected cracks (which is the base case)
- Case (II): Considering all cracks (both detected and missed cracks)

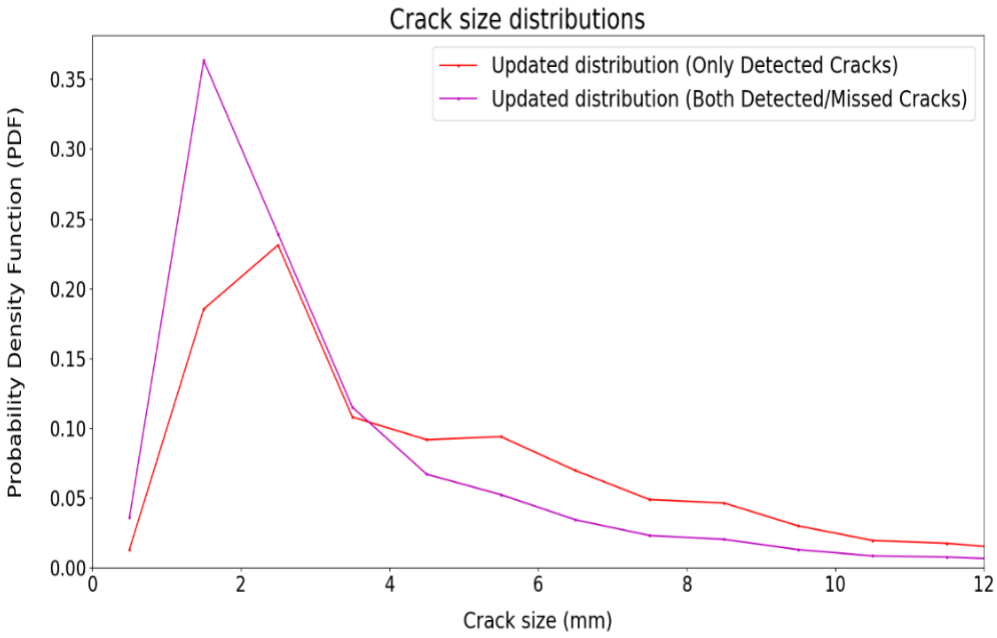

Figure 6.40. Posterior distribution of the crack size for detected/missed cracks

Figure 6.40 shows that the probability of big cracks (e.g. bigger than 12mm), and consequently the probability of failure, in case of considering all cracks is less than the probability of big cracks in the only detected cracks case.

The same explanation as Section 6.4.2 can be provided here. Case (II) can be assumed as a case with an extremely high resolution of crack detection (e.g. $a_{md} = 0.001$) that can detect all tiny cracks. Therefore, as it can be seen from Figure 6.39, the probability of big cracks for a high-resolution NDT technique is less than the mid-resolution technique (Section 6.4.2).

6.4.4 Sensitivity of the Posterior Distribution to the Value of 'Tolerance'

In the definition of the compatible prior cracks in Section 6.3.3, it was mentioned that a prior crack is a compatible crack if its size is 'close' to the simulated reality crack size. To quantify the word 'close', the parameter of tolerance is used. If a small value is selected for this value, it means that the difference between the prior crack and the simulated reality crack should be small, whereas the bigger value for tolerance allows

the bigger difference between the prior and the simulated reality cracks. Figure 6.41 shows the acceptable range for a prior crack for two different amounts of tolerance.

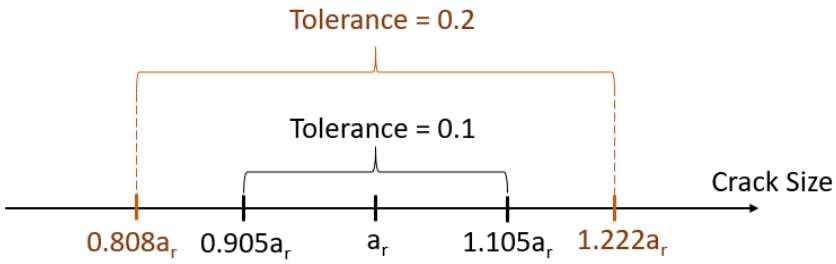

Figure 6.41. The acceptable range for a prior crack for different amounts of tolerance

To consider the effect of the selected tolerance on the posterior distribution of the crack size, two different amounts for tolerance are considered. These values are assumed equal to 0.1 and 0.3. Figure 6.42 illustrates the posterior distributions for both cases. When a smaller tolerance is selected, the posterior distribution shape is very similar to the simulated reality distribution. In fact, when a small tolerance is chosen, only those prior cracks are acceptable that are very close to the simulated reality cracks. Therefore, the posterior distribution shifts towards the simulated reality distribution (this can be seen clearly for the big crack sizes). On the other hand, for a bigger tolerance, further prior cracks are compatible, hence, the posterior distribution shape is affected by the prior distribution.

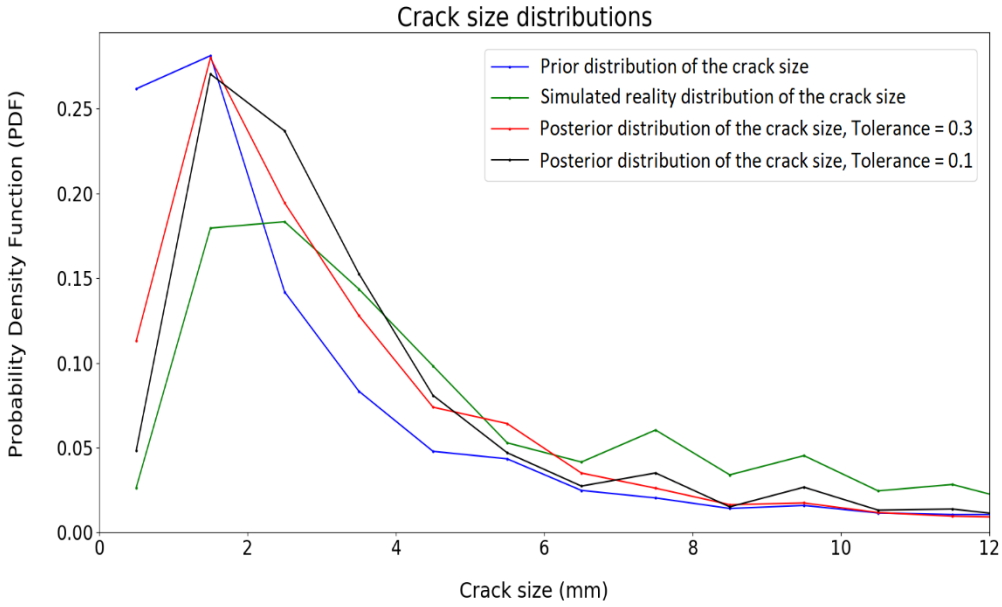

Figure 6.42. Posterior distribution of the crack size for different amounts of Tolerance

As it can be seen from Figure 6.42, the posterior distribution of the crack size is sensitive to the selected amount of tolerance. A suitable value for the tolerance should be selected based on the engineering judgment and the user's beliefs about the compatibility definition.

6.5 Reliability of the Proposed Approach: A Limited Number of Inspection Results (Observations)

In Section 6.3.1.3, it was assumed that there are several numbers of inspection results (observations) for a particular joint. Based on this assumption, a lognormal distribution was assigned to the crack observation (Eq.(6-5)). The proposed methodology (in Section 6.3.1.3) for obtaining the simulated reality distributions of the input variables (i.e. a_0^r, C^r, S^r and ε_Y^r) relies on the assigned distribution of the observed cracks.

In reality, inspection results are usually limited to one inspection for each tubular joint (at a given time, e.g. after five years) due to the significant costs of underwater inspections. When only one inspection result is available for a specific joint, it is not logical to assign a distribution to the measured crack size. Therefore, the proposed method in Section 6.3.1.3 cannot be employed to obtain the simulated reality distributions of the input variables (i.e. a_0^r, C^r, S^r and ε_Y^r).

Therefore, in case of the availability of only one inspection result, another method is considered to obtain the simulated reality distributions of the input variables. Let's assume there is only one inspection result for a specific tubular joint at the given time (after five years). The observed crack size has been measured equal to a_m.

To find out the simulated reality distributions of the input variables, a sampling method is used. It was shown in Section 6.4.1 that the posterior distribution of the crack size is more sensitive to the initial crack size and the stress range distributions. Therefore, it is tried to obtain the simulated reality distributions of these two random variables separately.

6.5.1 Simulated Reality Distributions of a_0 and C

To find out the simulated reality distributions of the initial crack size and crack growth parameter, a large number of random samples (let say 10^4 samples) are generated.

These random numbers are uniformly distributed:

- Between 0 and 4mm for the initial crack size
- Between 10^{-11} and 10^{-14} for the crack growth parameter

The reason for choosing the uniform distribution is that we don't have any information about the real distribution of the uncertain parameters. Therefore, a non-informative distribution (i.e. uniform distribution) is selected.

For each combination of initial crack size and crack growth parameter (a_{0j}^r, C_k^r ; $j,k = 1,2,..,10^4$) the predicted crack size is calculated based on Eq.(6-1). It is noted that the mean value of the other two input variables (S, ε_Y) are considered in calculation of the predicted crack size. The calculated crack size for this combination is denoted as $(a_{cal})_{k,j}$. It is noted that the total number of combinations is equal to $10^4 \times 10^4 = 10^8$. Table 6.10 shows the combinations of the initial crack size and the crack growth parameter.

Table 6.10. Generated samples for a_0^r, C^r and the corresponding crack sizes

		Random numbers for initial crack size			
		$(a_0^r)_1$	$(a_0^r)_2$	...	$(a_0^r)_{10000}$
Random numbers for crack growth parameter	$(C^r)_1$	$(a_{cal})_{1,1}$	$(a_{cal})_{1,2}$	...	$(a_{cal})_{1,10000}$
	$(C^r)_2$	$(a_{cal})_{2,1}$	$(a_{cal})_{2,2}$	...	$(a_{cal})_{2,10000}$
	…	…	...	...	...
	$(C^r)_{10000}$	$(a_{cal})_{10000,1}$	$(a_{cal})_{10000,2}$	...	$(a_{cal})_{10000,10000}$

Now, the calculated crack sizes can be divided into three categories:

1) Cracks that are much larger than the observed crack size,
2) Cracks that are much smaller than the observed crack size,
3) Cracks that are approximately equal to the observed crack size.

The ratio of the calculated crack size to the observed crack size is then computed for each combination as:

$$e_{k,j} = \frac{(a_{cal})_{k,j}}{a_m}; \quad k,j = 1,2,..,10^4 \tag{6-13}$$

If the calculated crack size is close enough to the observed crack size, that combination of initial crack size and crack growth parameter (a_{0j}^r and C_k^r) is kept, otherwise, it is removed from the samples. The acceptable combinations are those combinations that:

$$0.8 \leq e_{k,j} \leq 1.2 \tag{6-14}$$

By using Eq. (6-14), each calculated crack size is compared with the measured crack size to determine whether it matches within a specified tolerance. If the calculated crack size satisfies Eq.(6-14), the corresponding cell in Table 6.10 is replaced with one, whereas it is replaced with zero if it is an unacceptable crack size.

Figure 6.43 shows the proposed method to obtain the marginal histogram of the uncertain parameters (i.e. initial crack size and crack growth parameter).

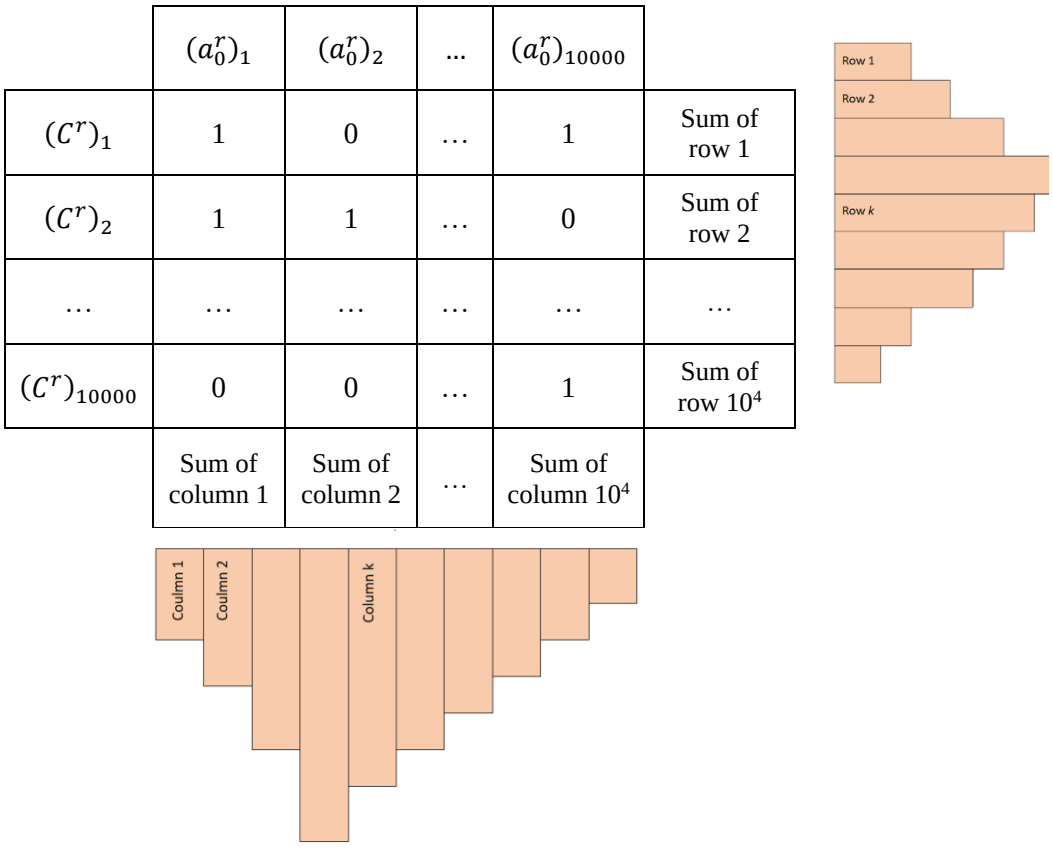

Figure 6.43. The proposed method for obtaining the marginal histogram of the input variables (a_0^r and C^r)

Having obtained the frequency of each row and column, the histogram of the simulated reality distribution for the initial crack size and the crack growth parameter is generated. By normalising the obtained histogram and fitting an appropriate

distribution for each uncertain parameter, the marginal PDFs of these variables are achieved.

6.5.2 Simulated Reality Distributions of S and ε_Y

The same approach as explained in Section 6.5.1 is considered to find out the simulated reality distributions for the stress range and geometry function. Again, a large number of random samples (10^4 samples) are generated. These random numbers are uniformly distributed:

- Between 50 and 500 MPa for the stress range
- Between 0.5 and 2 for the uncertainty in the estimation of the geometry function

For each combination of stress range and uncertainty in the geometry function ($\varepsilon_{Ym}^r, S_n^r$; $m,n = 1,2,..,10^4$) the predicted crack size is calculated based on Eq.(6-1). This time, the mean value of C, a_0 are considered in calculation of the predicted crack size. The calculated crack size for this combination is denoted as $(a_{cal})_{m,n}$.

Table 6.11 shows the generated samples for the considered uncertain parameters.

Table 6.11. Random samples for ε_Y^r, S^r and the corresponding crack sizes

		Random numbers for uncertainty in geometry function			
		$(\varepsilon_Y^r)_1$	$(\varepsilon_Y^r)_2$	…	$(\varepsilon_Y^r)_{10000}$
Random numbers for stress range	$(S^r)_1$	$(a_{cal})_{1,1}$	$(a_{cal})_{1,2}$	…	$(a_{cal})_{1,10000}$
	$(S^r)_2$	$(a_{cal})_{2,1}$	$(a_{cal})_{2,2}$	…	$(a_{cal})_{2,10000}$
	…	…	…	…	…
	$(S^r)_{10000}$	$(a_{cal})_{10000,1}$	$(a_{cal})_{10000,2}$	…	$(a_{cal})_{10000,10000}$

Again, if the calculated crack size satisfies Eq.(6-14), the corresponding cell in Table 6.11 is replaced with one, otherwise, it is replaced with zero.

Figure 6.44 shows the proposed method to obtain the marginal histogram of the uncertain parameters (i.e. stress range and uncertainty in the geometry function).

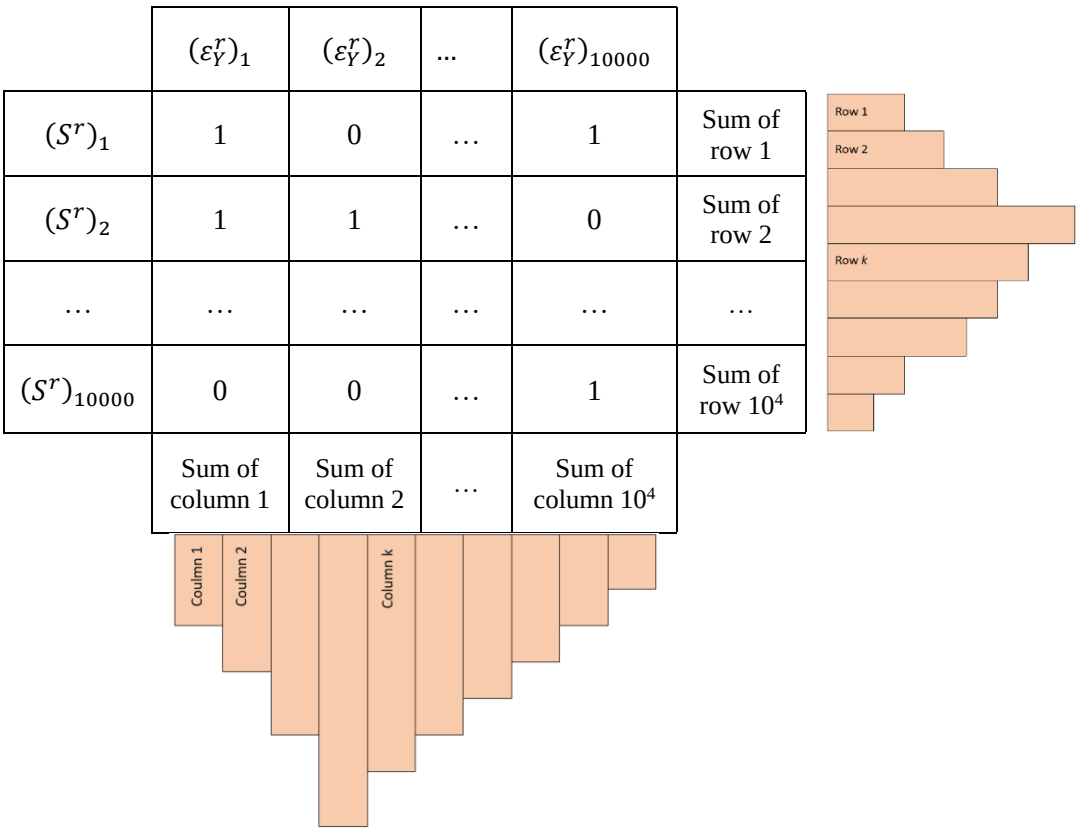

Figure 6.44. The proposed method for obtaining the marginal histogram of the input variables (S^r and ε_Y^r)

6.5.3 Modification of the Proposed Method - Application

To demonstrate the modification of the proposed method, it is assumed that there is only one inspection result with the measured crack equal to $a_m = 4mm$. By applying the method, the acceptable combinations of (a_0^r, C^r) and (S^r, ε_Y^r) are achieved. Figure 6.45 shows the histograms and the fitted distributions of the input variables in the simulated reality case.

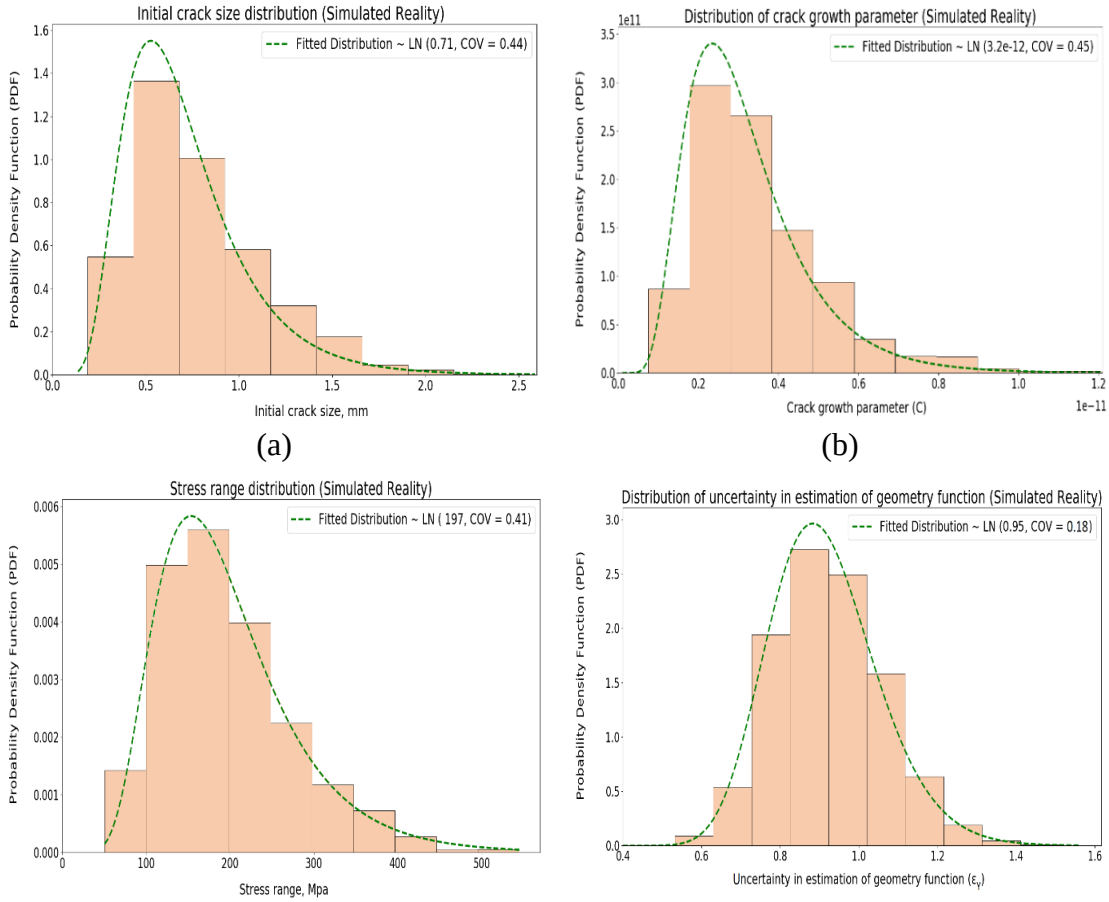

Figure 6.45. Histogram and the best fit distribution for (a) a_0^r, (b) C^r, (c) S^r and (d) ε_Y^r

Table 6.12 compares the simulated reality distributions of the input variables in case of the availability of one inspection result or several inspection results (Section 6.3.1.3).

Table 6.12. Effect of the number of inspections on the simulated reality distributions

Input Variable	One Inspection $a_m = 4mm$	Several Inspections $a_m \sim LN\ (4mm, COV = 0.5)$
Initial crack size, a_0^r	$LN\ (0.71mm, COV = 0.44)$	$LN\ (0.48mm, COV = 0.21)$
Crack growth parameter, C^r	$LN\ (3.2 \times 10^{-12}, COV = 0.45)$	$LN\ (2.4 \times 10^{-12}, COV = 0.18)$
Stress range, S^r	$LN\ (197, COV = 0.41)$	$LN\ (210, COV = 0.20)$
Uncertainty in estimation of geometry function, ε_Y^r	$LN\ (0.95, COV = 0.18)$	$LN\ (1.0, COV = 0.12)$

Table 6.12 indicates that when only one inspection result is available, the simulated reality distributions include bigger uncertainty (bigger COV). In fact, only one inspection result cannot provide enough information about the uncertain input

parameters. Therefore, distributions of these input variables include bigger uncertainties. When inspections are independently repeated for the considered joint, the uncertainty of the input variables is reduced.

Having obtained the simulated reality distributions for the input variables in both cases (one inspection and several inspections), the simulated reality distributions for the crack size are obtained by using the method described in Section 6.3.1.4. Then, the posterior distributions of the crack size are obtained regarding Section 6.3.3.1.

Figure 6.46 shows the posterior distributions of the crack size in the case of one or several inspection results.

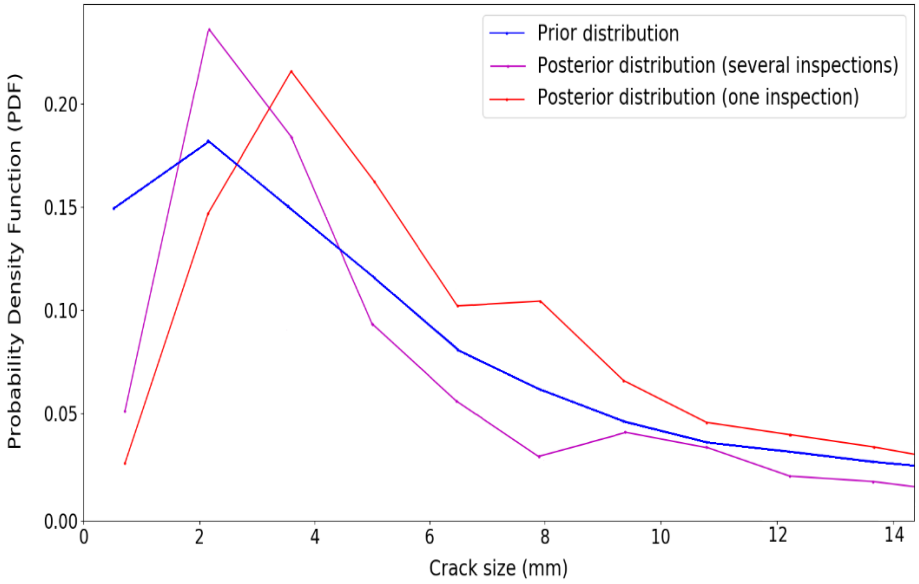

Figure 6.46. Posterior distributions of the crack size in case of availability of one or several inspections

Figure 6.46 illustrates that the number of inspection results has a great effect on the posterior distribution of the crack size. When only one inspection ($a_m = 4mm$) is available, the posterior distribution has a Mode value around 4mm.

Moreover, in this case, the posterior crack size has a broader distribution (bigger uncertainty) which seems reasonable. By providing more inspection results, the uncertainty of the posterior distribution of the crack size is reduced. Therefore, the posterior distribution of the crack size (and the probability of failure) is very sensitive to the number of available inspection results.

When several inspection results are available, the owner (user) is more confident about the simulated reality distribution of the crack size. Whereas only one inspection result includes more uncertainty.

Figure 6.46 also shows that when one inspection result is available, the probability of big crack size (and consequently, probability of failure) is bigger than when several inspection results exist. Therefore, the proposed method results in more conservative results when one inspection result exists which is rational.

6.6 Reliability of the Proposed Methodology: Inappropriate Prior Selection

The proposed methodology in this chapter (Section 6.3) can:

- Obtain the posterior distribution of the crack size
- Obtain the posterior distributions of the involved uncertainties in the fatigue crack model (i.e., initial crack size, crack growth parameter, stress range, and the uncertainty in the geometry function)
- Update the POD curves

Moreover, the sensitivity of the proposed methodology to the different inputs is discussed in Section 6.4.

Table 6.13 summarises the considered distributions in the proposed methodology. The prior distributions are defined based on the previous knowledge (Section 6.3.2) and the simulated reality distributions are obtained by using the described approach in Section 6.3.

Table 6.13. Considered distributions in the proposed approach

Uncertain Parameter	Prior Distribution	Simulated Reality Distribution
Initial crack size, a_0	a_0^p ~ LN (0.4, 0.35)	a_0^r ~ LN (0.48, 0.21)
Crack growth parameter, C	C^p ~ LN (2.1 x 10^{-12}, 0.35)	C^r ~ LN (2.4 x 10^{-12}, 0.18)
Stress range, S	S^p ~ LN (180, 0.35)	S^r ~ LN (210, 0.2)
Uncertainty in estimation of the geometry function,	ε_Y^p ~ LN (1, 0.2)	ε_Y^r ~ LN (1, 0.12)
POD	a_{md}^p ~ LN (3, 0.5)	a_{md}^r ~ LN (2, 0.2)

Table 6.13 shows the prior distributions were chosen rationally because the mean values of these distributions are close enough to the mean values of the simulated reality distributions. In this situation, the methodology works properly, as shown in Section 6.3.3.

This section is provided to find out how reliable the methodology is under some extreme conditions, for instance, when a too low (or high) mean value is selected for a prior distribution of an uncertain parameter.

6.6.1 Effect of Considering a Very Low Mean Value for Prior Distribution

Here, two extreme cases for the prior distributions of the uncertain parameters are considered to find out how the proposed methodology works:

- **Case (1):** Assuming a very low mean value for the prior distribution of the initial crack size, for instance:

$$a_0^p \sim \text{LN}\ (0.1,\ 0.2)$$

The considered mean value for the initial crack size is 0.1mm which is much lower than the mean value of the simulated reality (0.48 mm). Distributions of the other uncertainties are the same as those introduced in Table 6.13. The proposed methodology is applied for Case (1) and the results of the updated distributions are shown in Figure 6.47.

(i)

Crack size distribution

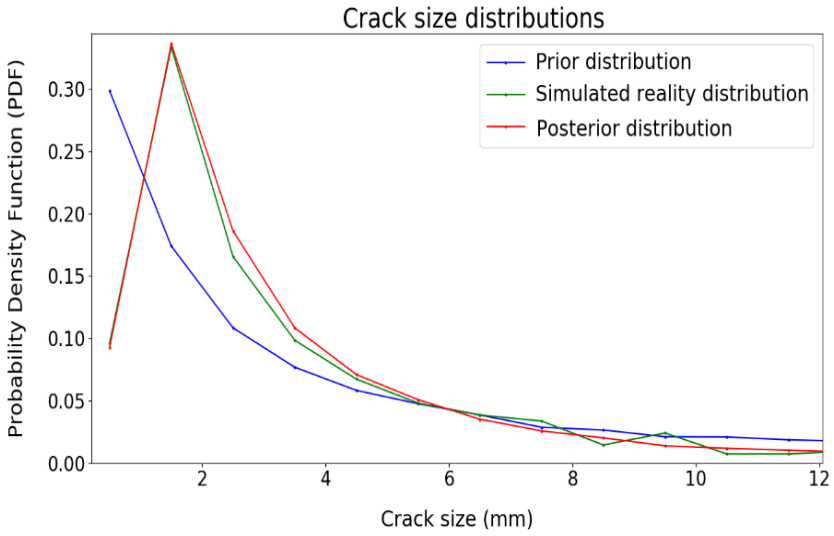

(ii)

Initial crack size distribution

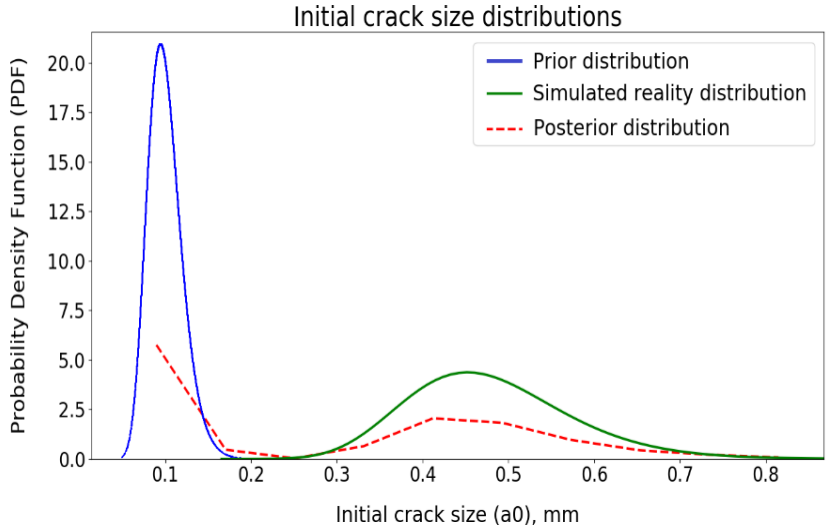

(iii)

Crack growth parameter distribution

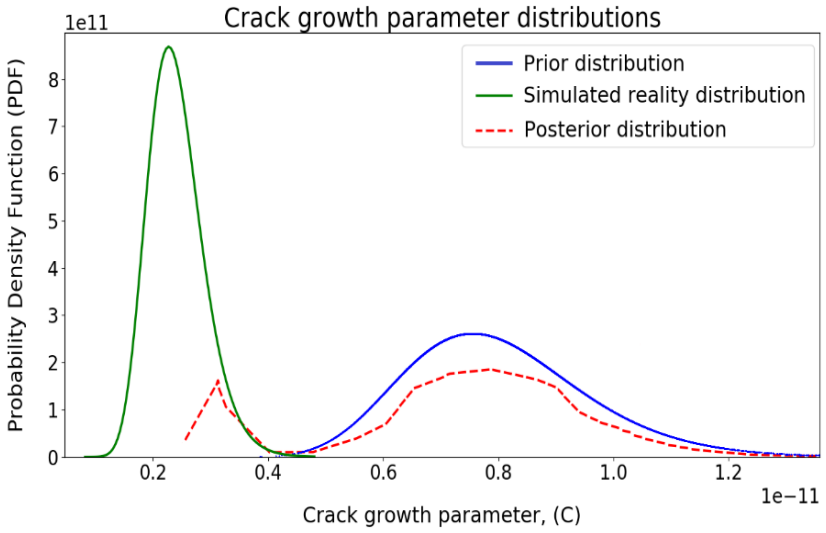

(iv)

Stress range distribution

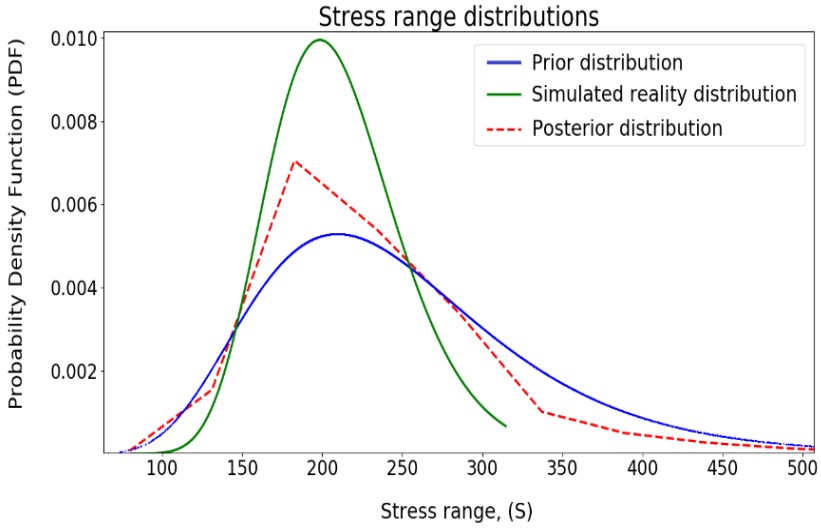

Figure 6.47. Posterior distributions in Case (1); (i) Crack size, (ii) Initial crack size, (iii) Crack growth parameter, (iv) Stress range

As it can be seen from Figure 6.47:

- For the crack size distribution (i):

  The posterior distribution of the crack size shifts toward the simulated reality distribution even in the case of selecting a very low mean value for the initial crack size distribution.

- For the initial crack size distribution (ii):

  The posterior distribution of the initial crack size shifts toward the simulated reality distribution even in the case of selecting an inappropriate prior distribution, although it is still affected by the inappropriate prior.

- For the crack growth parameter distribution (iii):

  Selection of a low value for a_0^p, causes a higher value for crack growth parameter (C^p) or stress range (S^p) to obtain the compatible crack size with the simulated reality crack ($^{da}/_{dN} = C(\Delta K)^m$).

  It can be seen that the mean value of C^p is bigger than the mean value of C^r (whereas the mean value of a_0^p is smaller than a_0^r).

  The posterior distribution of the crack growth parameter cannot shift substantially towards the simulated reality distribution. It can be seen that in this case (a very low value for the prior initial crack size), the posterior distribution of the crack growth parameter is stuck to the prior distribution instead of moving towards the simulated reality distribution.

- For the stress range distribution (iv):

  Selection of a low value for a_0^p, causes a higher value for the stress range (S^p) to obtain the compatible crack size with the simulated reality.

  The posterior distribution of the stress range shifts towards the simulated reality distribution, although it is still affected by the prior distribution.

- **Case (2):** Assuming a very low mean value for the prior distribution of the crack growth parameter, for instance:

$$C^p \sim \text{LN}\ (6 \times 10^{-13},\ 0.2)$$

The considered mean value for the crack growth parameter is 6×10^{-13} which is a quarter of the mean value of the simulated reality (2.4×10^{-12}). Distributions of the other uncertainties are the same as those introduced in Table 6.13. The proposed methodology is applied for Case (2) and the results of the posterior distributions are shown in Figure 6.48.

(i) Crack size distributions

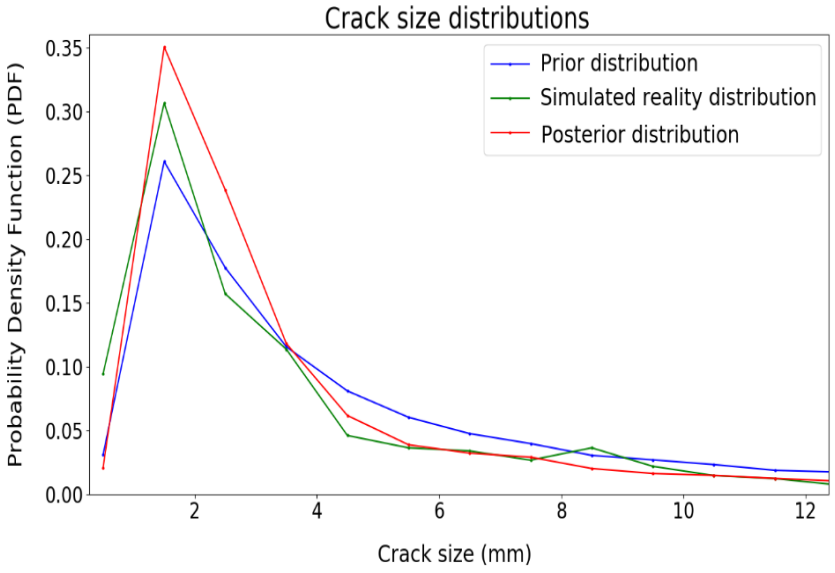

(ii) Initial crack size distributions

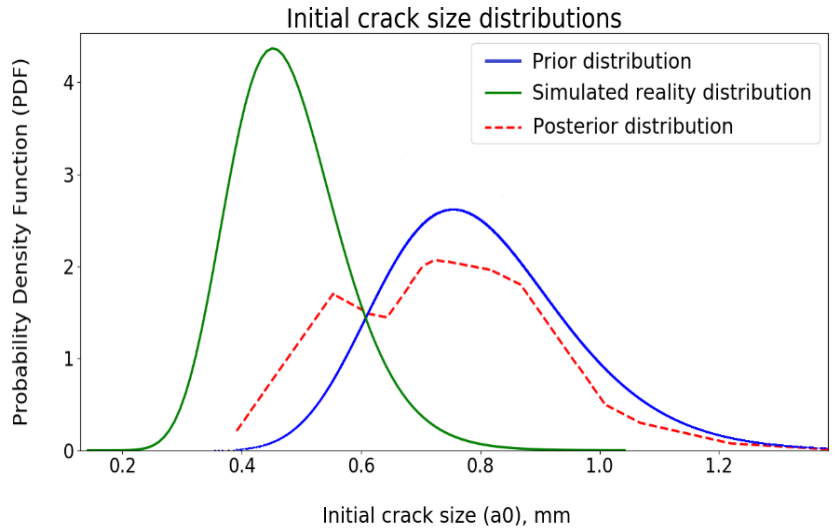

(iii)
Crack growth parameter distributions

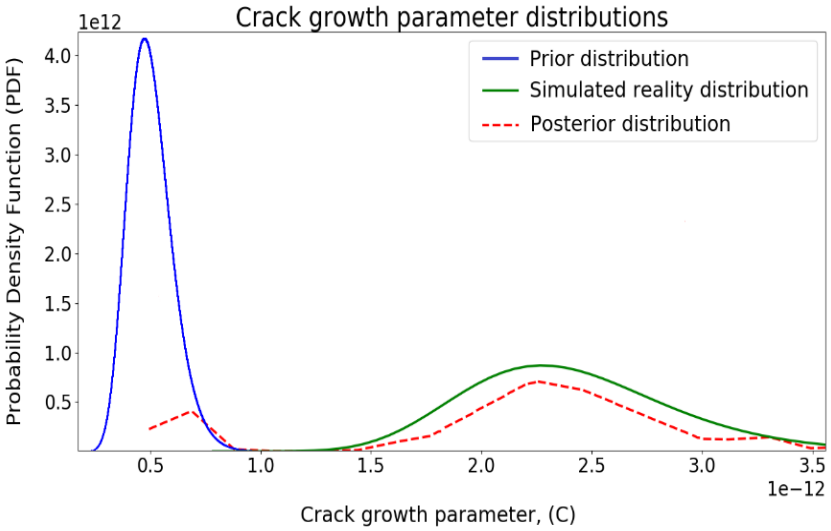

(iv)

Stress range distributions

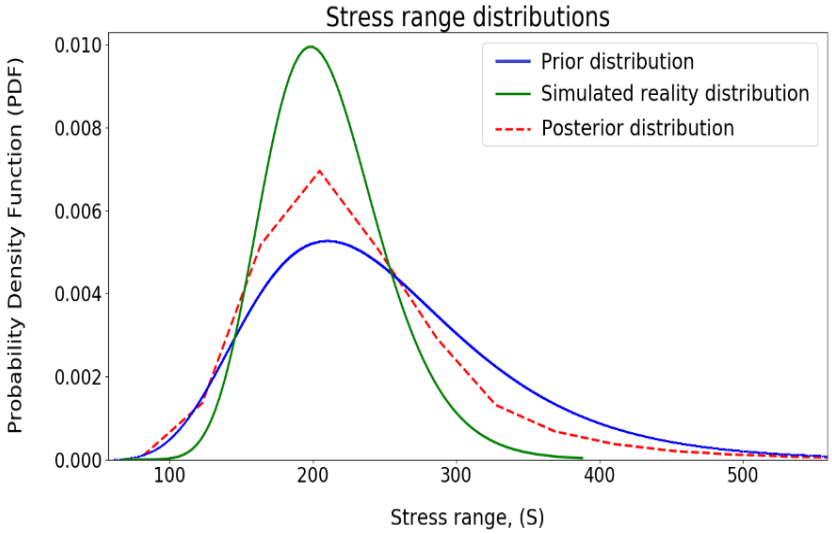

Figure 6.48. Posterior distributions in Case (2); (i) Crack size, (ii) Initial crack size, (iii) Crack growth parameter, (iv) Stress range

As it can be seen from Figure 6.48:

- For the crack size distribution (i):

  The posterior distribution of the crack size for the big cracks shifts towards the simulated reality distribution even in the case of selecting a very low value for the crack growth parameter.

  The posterior distribution obtained by this methodology doesn't provide acceptable results for the small crack sizes. The probability of small cracks in the posterior distribution is larger than both probabilities in the prior and the simulated reality distributions.

- For the initial crack size distribution (ii):

  Selection of a low value for C^p, causes a higher value for initial crack size (a_0^p) to obtain the compatible crack sizes with the simulated reality.

  The mean value of a_0^p is bigger than the mean value of a_0^r (whereas C^p is smaller than C^r).

  The posterior distribution of the initial crack size cannot shift substantially towards the simulated reality distribution. It can be seen that in this case (a very low mean value for the prior distribution of the crack growth parameter), the posterior distribution of the initial crack size is stuck to the prior distribution instead of moving towards the simulated reality distribution.

- For the distribution of the crack growth parameter (iii):

  The posterior distribution of the crack growth parameter shifts towards the simulated reality distribution even in the case of selecting an inappropriate prior distribution.

- For the stress range distribution (iv):

  The posterior distribution of the stress range shifts towards the simulated reality distribution, although it is still affected by the prior distribution.

In general, the following considerations need to be taken in case of considering an inappropriate prior distribution for an uncertain parameter:

- The posterior distribution of the crack size shifts towards the simulated reality distribution for big cracks even in the case of selecting an inappropriate (very low/very high) prior distribution for an uncertain parameter. However, the posterior distribution for the small cracks is not acceptable (in some cases). It was mentioned that in this research, the probability of failure (POF) is defined as the probability of a crack being bigger than wall thickness (see Eq. (6-2)). i.e.:

$$POF = P(g \leq 0) = P(a_c - a_t \leq 0) = P(a_c \leq a_t) \qquad (6\text{-}15)$$

  where a_c is the critical crack size and a_t is the crack size at time t. The critical crack size in this research is considered equal to the plate thickness which is

0.875 inches (22.22 mm) for the considered tubular joint. Hence, Eq. (6-15) is written as:

$$POF = P(a_t \geq 22.22\, mm) \tag{6-16}$$

Therefore, the proposed methodology can properly update the probability of failure, even, in the case of an inappropriate prior distribution.

- If an inappropriate prior distribution is selected for an uncertain parameter, the posterior distribution for that parameter doesn't move substantially towards the simulated reality distribution.

6.6.2 Effect of Considering an Optimistic Prior Distribution for POD Curve

Three different cases as shown in Table 6.14 are considered to find out the effect of POD curves on the posterior distributions.

Table 6.14. Considered POD distributions in the proposed approach

Uncertain Parameter		Prior Distribution	Simulated Reality Distribution
a_{md}	Base Case	a_{md}^{p}~ LN (3, 0.5)	a_{md}^{r}~ LN (2, 0.2)
	Case (3)	a_{md}^{p}~ LN (3, 0.1)	
	Case (4)	a_{md}^{p}~ LN (1, 0.1)	

Figure 6.49 shows the effect of the selection of different prior distributions for the mean detectable size on the posterior distribution of the crack size. The graphs show that the posterior distributions of the crack size are less sensitive to the prior distributions of the POD curves.

(i) Base case

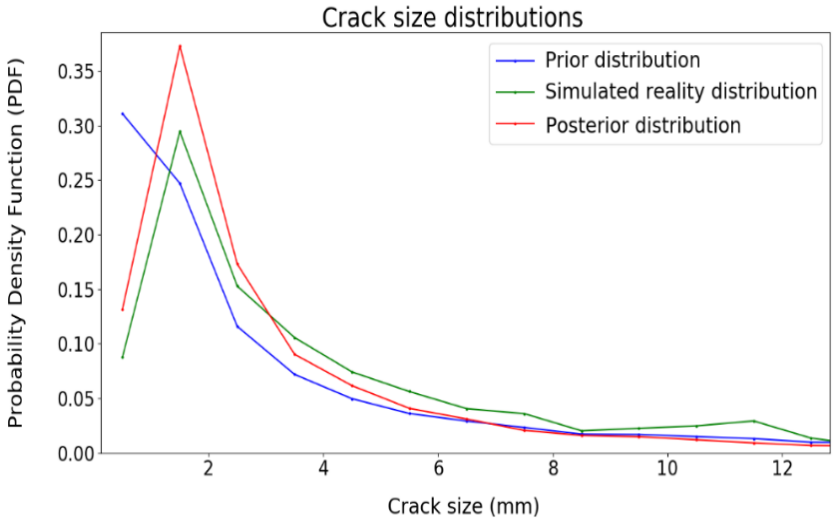

(ii) Case (3)

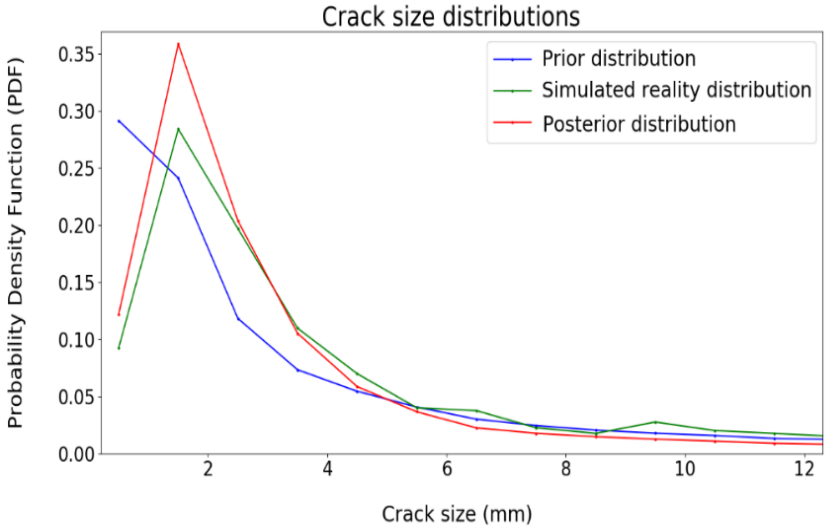

(iii) Case (4)

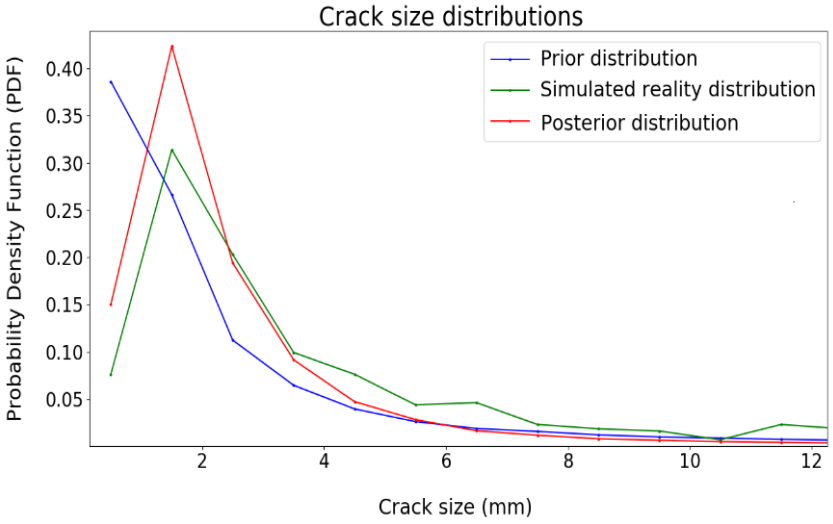

Figure 6.49. Posterior distributions of the crack size for different prior distributions of the POD curve; (i) Base case, (ii) Case (3), and (iii) Case (4)

Figure 6.50 shows the posterior POD curves for the considered cases.

(i) Base case

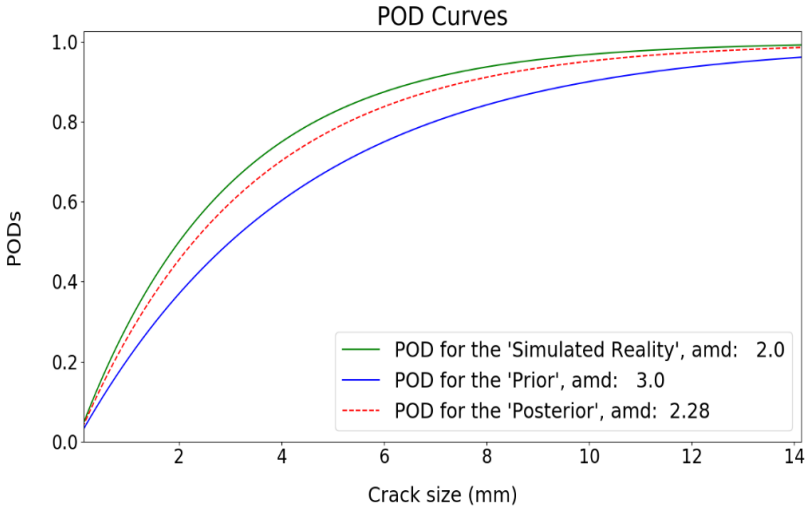

(ii) Case (3)

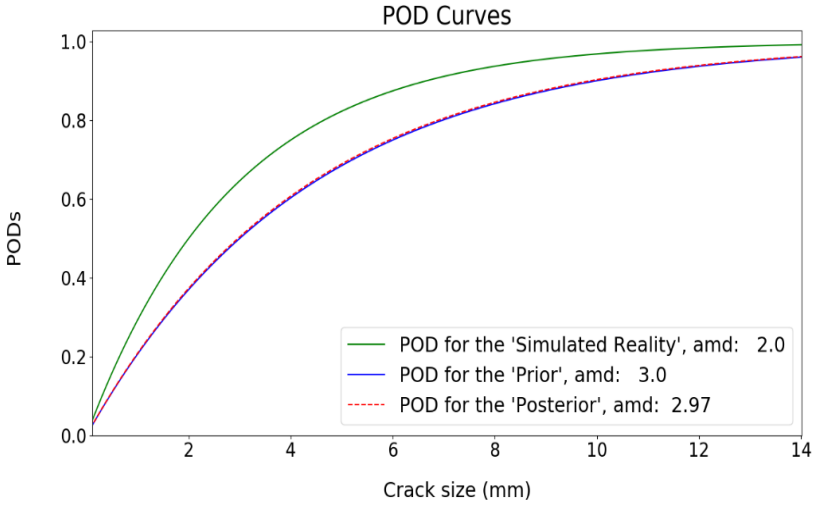

(iii) Case (4)

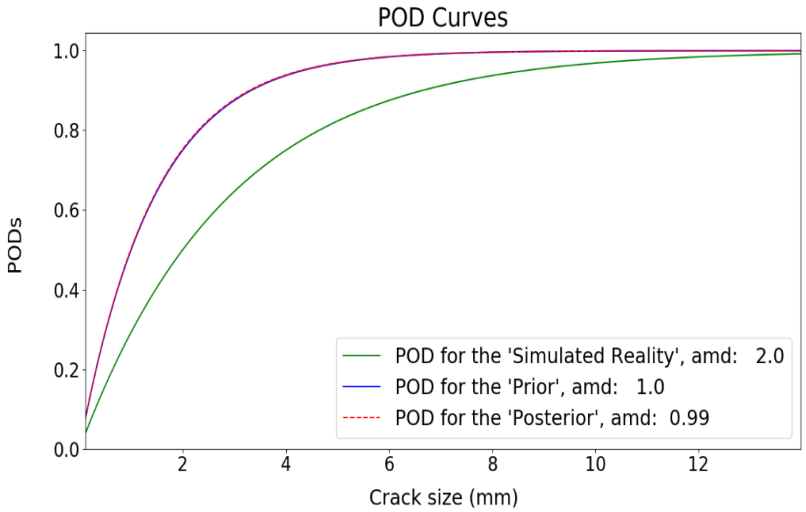

Figure 6.50. Updated POD curves for different POD prior distributions; (i) Base case, (ii) Case (3), and (iii) Case (4)

Figure 6.50 shows that, when a very low value of COV is selected for the prior distribution of the mean detectable size (Case (3) and Case (4)), the proposed methodology cannot update the POD curve correctly and the posterior distribution is completely affected by the prior distribution.

On the other hand, when the COV of the prior distribution of the mean detectable size is greater than the COV in the simulated reality distribution, the posterior POD distribution shifts towards the simulated reality distribution (Base case).

6.6.3 Considering a Very Low Mean Value for Two Uncertain Parameters

In the previous cases (Section 6.6.1 and Section 6.6.2), the effect of selecting a very low mean value (or a very low COV) for the prior distribution of one uncertain parameter is considered. The purpose of this section is to find out how the methodology works when poor prior distributions are selected for more than one uncertain parameter.

- **Case (5):** Assuming a very low mean value for the prior distribution of the crack growth parameter in addition to considering an optimistic prior distribution for the POD curve, for instance:

$$C^p \sim \text{LN}\ (6 \times 10^{-13},\ 0.2)$$

$$a_{md}^p \sim \text{LN}\ (1,\ 0.1)$$

  Distributions of the other uncertainties are the same as those introduced in Table 6.13. The proposed methodology is applied for Case (5) and the results of the posterior distributions are shown in Figure 6.51.

(i) Crack size distribution

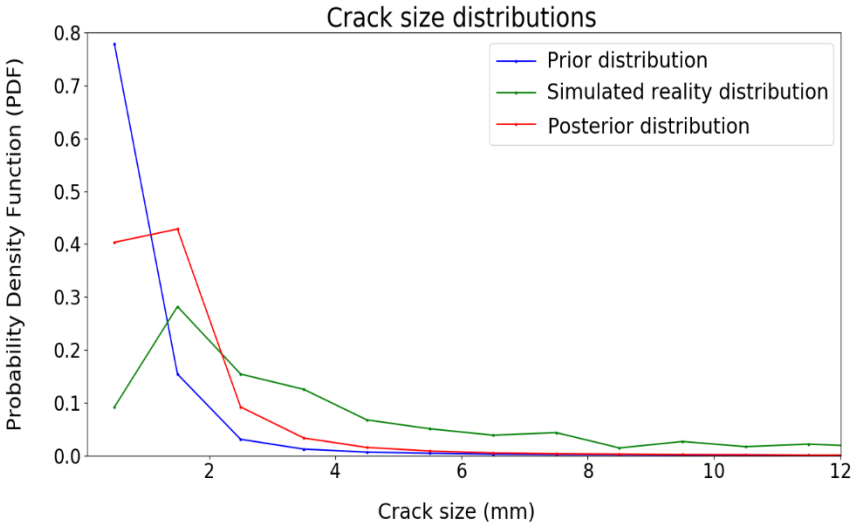

(ii) Initial crack size distribution

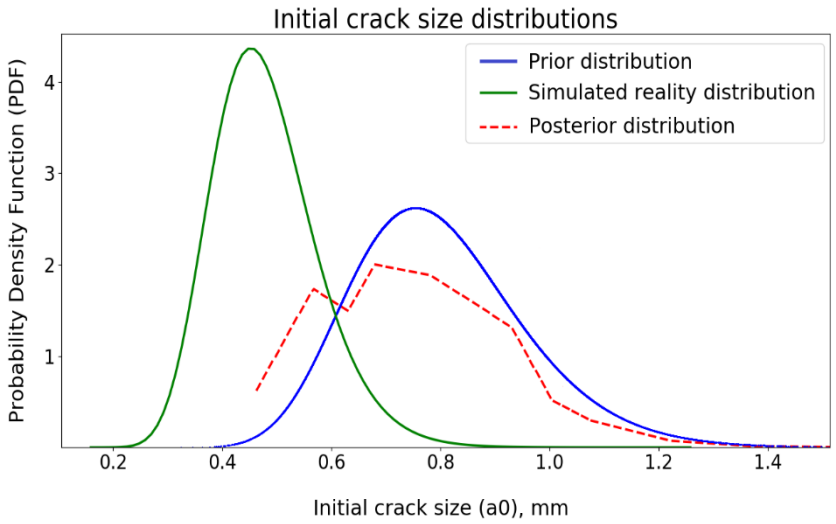

(iii) Crack growth parameter distribution

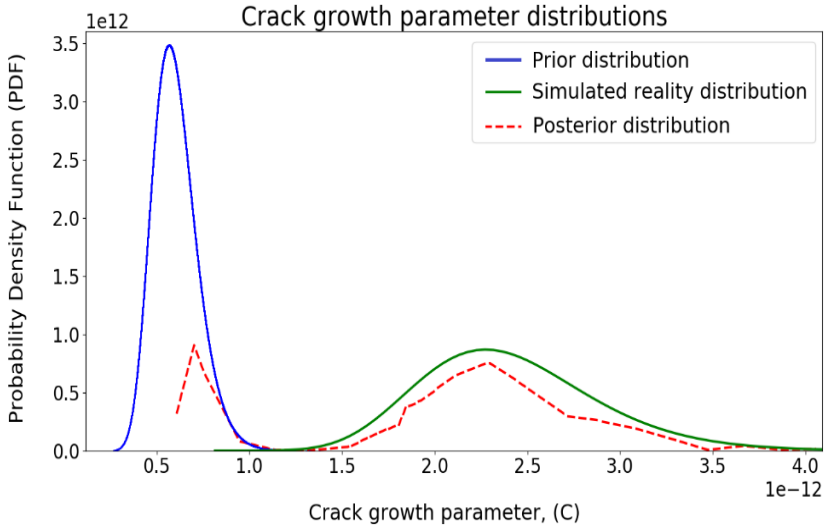

(iv) POD curves

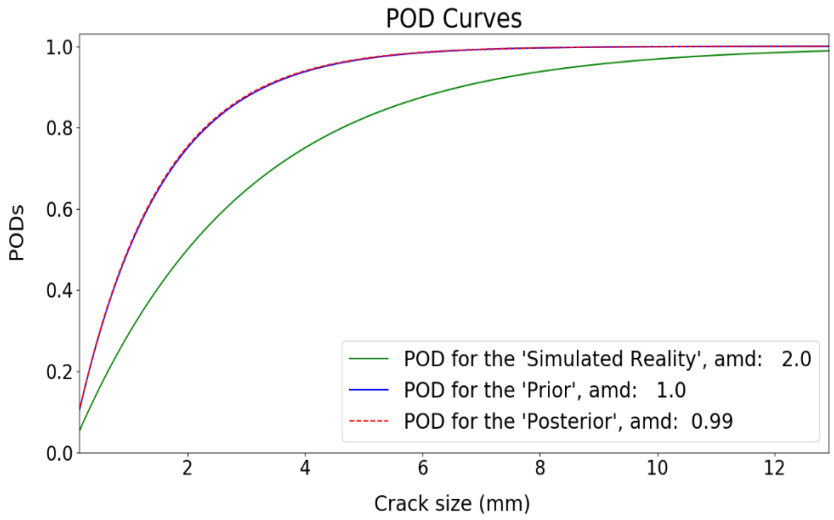

Figure 6.51. Posterior distributions in Case (5); (i) Crack size, (ii) Initial crack size, (iii) Crack growth parameter, (iv) POD curves

As it can be seen from Figure 6.51:

- For the crack size distribution (i):

  The posterior distribution of the crack size cannot shift towards the simulated reality distribution for big cracks in the case of selecting a very low value for the crack growth parameter and an optimistic POD curve. It seems that the posterior distribution of the crack size is stuck to the prior distribution instead of moving towards the simulated reality distribution.

- For the initial crack size distribution (ii):

  The posterior distribution of the initial crack size cannot shift towards the simulated reality distribution (similar to the results of Case (2)).

- For the distribution of the crack growth parameter (iii):

  The posterior distribution of the crack growth parameter shifts towards the simulated reality distribution even in the case of selecting an inappropriate prior distribution (similar to the results of Case (2)).

- For the POD curves (iv):

  The proposed methodology cannot update the POD curve correctly and the posterior distribution is completely affected by the prior distribution (similar to the results of Case (4) and Case (5)).

As a result, the posterior distribution of the crack size obtained by using this methodology in Case (5) is not acceptable. The posterior distribution of the crack size, in this case, is affected by prior distribution for the big crack sizes and cannot shift towards the simulated reality distribution.

6.7 Reliability of the Proposed Approach: Comparison of Results

The main purpose of Chapter 5 and Chapter 6 is to update the distributions of the uncertain parameters when inspection results are available. In Chapter 5, only crack size is assumed as an uncertain parameter and the updated (posterior) distribution is obtained by different conventional Bayesian methods (i.e. analytical and numerical methods). In Chapter 6, the proposed approach is capable to update all uncertain parameters including crack size, POD curves, and uncertainties involved in the fatigue crack model (Eq.(6-1)).

Since both methods in these two chapters can update the crack size distribution, the purpose of this section is to compare the results of these approaches. To compare the posterior distribution of the crack size, two cases are considered:

6.7.1 Availability of One Inspection Result

To compare the posterior distributions of the crack size, it is assumed that there is one inspection result with a measured crack size equal to 4mm (i.e. $a_m = 4mm$). The crack size distribution is updated using the approaches introduced in Chapter 5 (numerical method, Section 5.4.1.3) and Chapter 6 (Section 6.5.3).

Figure 6.52 shows the posterior distributions of the crack size for both approaches when there is only one inspection result available. The figure illustrates a big difference between the two approaches.

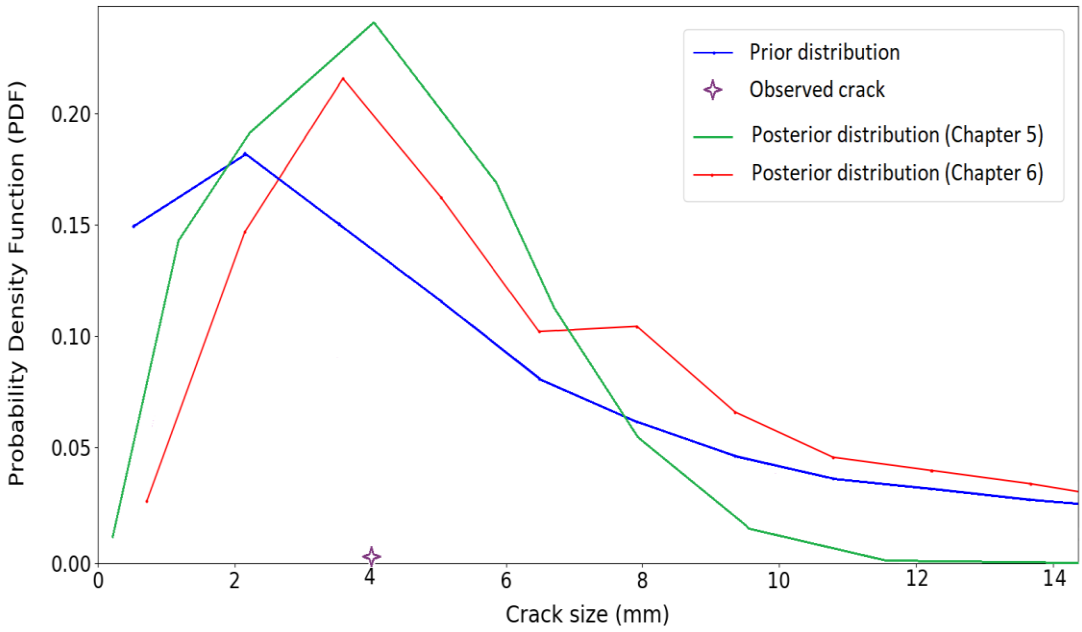

Figure 6.52. Posterior distributions of the crack size (one inspection result)

Figure 6.52 shows that when a typical Bayesian method is implemented (green line, Chapter 5), the probability of big cracks is sharply reduced. It was explained that in the Bayesian updating method, the posterior distribution is proportional to the likelihood function and prior distribution, i.e.:

$$Posterior \propto Likelihood \times Prior \tag{6-17}$$

The likelihood function in case of a crack detection is obtained in Chapter 5 (see Eq. (5-59)) as:

$$Likelihood \propto \left[\frac{{\beta_{prior}}^{\alpha_{prior}}}{{\beta_{post}}^{\alpha_{post}}}\right] \times \left[\frac{\Gamma(\alpha_{post})}{\Gamma(\alpha_{prior})}\right] \tag{6-18}$$

A non-informative prior is selected for the error variance as:

$$\alpha_{prior} = \beta_{prior} = 0.001 \tag{6-19}$$

The posterior parameters for the error variance are then obtained as (see Eq. (5-48)):

$$\begin{aligned} \alpha_{post} &= \alpha_{prior} + \frac{1}{2} = 0.5 \\ \beta_{post} &= \beta_{prior} + \frac{e^2}{2} = \frac{e^2}{2} \end{aligned} \tag{6-20}$$

Where parameter e was defined equal to (see Eq. (5-38)):

$$e = ln\, a - ln\, a_m = ln\, (\frac{a}{a_m}) \tag{6-21}$$

By implementing the above equations in Eq.(6-18), the likelihood function is obtained proportional to:

$$Likelihood \propto \frac{1}{\beta_{post}{}^{0.5}} = \frac{1}{\sqrt{\frac{e^2}{2}}} = \frac{\sqrt{2}}{e} \tag{6-22}$$

Table 6.15 shows the value of the likelihood function for three different crack sizes.

Table 6.15. Value of the likelihood function for different crack sizes

Real crack size (a)	Measured crack size (a_m)	Likelihood ($\sim \sqrt{2}/_e$)
2 mm	4 mm	2.0
4.1 mm		57.3
10 mm		1.5

Table 6.15 shows that the likelihood function value for bigger cracks is sharply reduced. Therefore, as can be seen from Figure 6.52, the probability of big cracks in the posterior distribution in this case (green line) is very low.

On the other hand, the posterior distribution which is obtained by using the proposed approach in Section 6.5.3 (red line, Chapter 6), has a broader shape and the probability of big cracks are higher than the previous case. This is mainly because, in the proposed approach in Chapter 6, the measured crack size is used to obtain the simulated reality distributions of the uncertainties involved in the fatigue crack model (i.e. a_0^r, C^r, S^r and ε_Y^r). As it was mentioned in Section 6.5.3, more uncertainty exists in this approach to find out the simulated reality distributions of the input variables. Therefore, the posterior distribution in this case (red line) is wider and lower.

The obtained probability of failure (Eq. (6-16)) by using the proposed approach in Chapter 6, is higher than the other approach (green line). Therefore, the proposed approach in Chapter 6 is recommended, especially when we are not sure how reliable the inspection result is.

6.7.2 Availability of Several Inspection Results

Now, assume several inspection results are available for a specific tubular joint. Here, the same observations as introduced in Section 6.3.1.3 are considered and a lognormal distribution with the following properties is assigned to the crack measurements:

$$a_m \sim LN(4mm, COV = 0.5)$$

Figure 6.53 shows the posterior distributions of the crack size for both approaches (Chapter 5 and Chapter 6) when several inspection results exist.

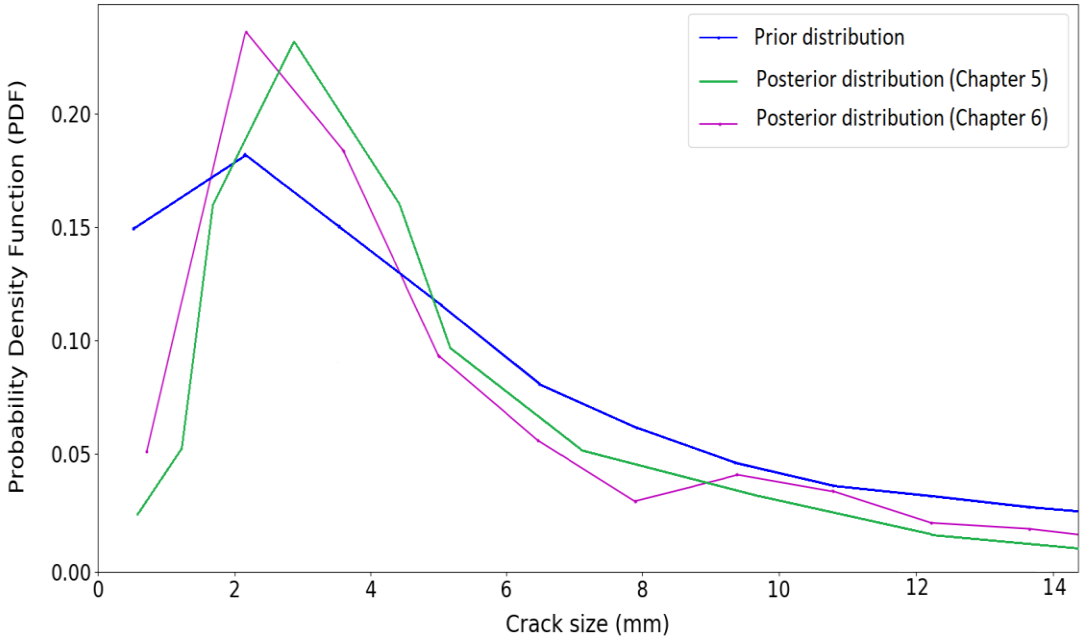

Figure 6.53. Posterior distributions of the crack size (several inspection results)

Figure 6.53 illustrates that the posterior distributions in both approaches are not substantially different. Although there are some differences in small cracks, in big cracks both approaches come close to each other. Therefore, both approaches result in a similar probability of failure (Eq. (6-16)).

Hence, when several inspection results are available, both approaches can be utilised to obtain the posterior distribution of the crack size. Moreover, the similar shape of the posterior distributions indicates that the proposed approach in Chapter 6 can be confidently used for updating the crack size distribution.

6.7.3 Benefits of the Proposed Approach

Fatigue is an important failure mode in offshore jacket structures. To evaluate the fatigue damage, these structures are periodically inspected. Regarding fatigue damage, the information from inspection consists of crack measurement. The new information obtained from the inspection activity is then used to improve the previous estimate of the uncertain parameter which is crack size.

However, for future inspection planning and reliability analysis of inspected and other platforms, updated estimates of other uncertain parameters (i.e. initial crack size, crack growth parameter, POD, etc.) are really useful. Just updating crack size estimates at one location is sometimes useful for a known critical location, but the ability to improve estimates of reliability and to plan better future inspections is much more valuable.

Most of the previous studies implemented the conventional Bayesian methods for updating the crack size distribution which were explained in Chapter 5. In these studies:

- A prior distribution was assigned for the crack size
- A likelihood function was considered based on the author's opinion
- A posterior distribution was obtained by using the Bayesian methods (i.e. by using Eq. (6-17))

However, the credibility of the Bayesian methods has not been considered in these studies. The integrity of any Bayesian updating method depends on how reliable the inputs (e.g. inspection results) are.

Figure 6.54 shows how a Bayesian updating method works.

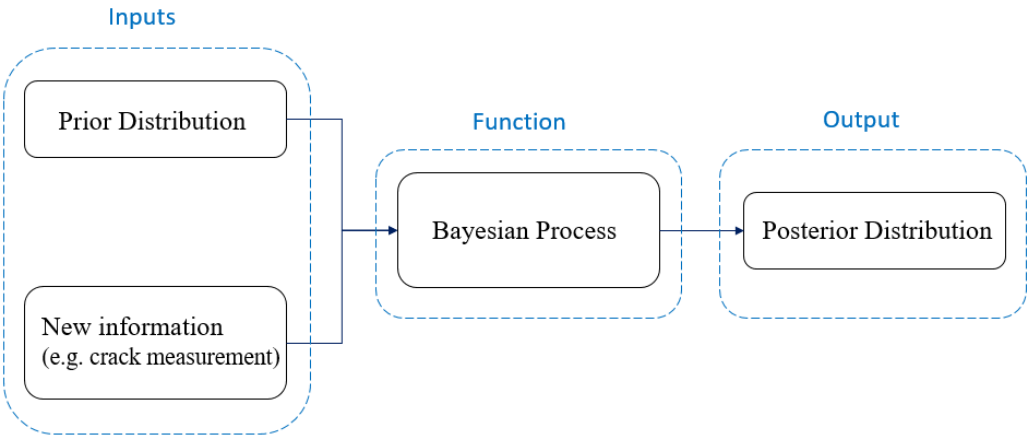

Figure 6.54. Inputs and output for a Bayesian updating process

As can be seen from Figure 6.54, a Bayesian method is a function that processes the inputs and generates the output based on the provided inputs. Therefore, if the inputs are inaccurate, the updated results may be poor and can even lead to the wrong decisions for the next inspection activity.

Therefore, the reliability of the updating process is the main concern for the platforms' owners. Due to the high cost of underwater inspection activities, in practical applications, the inspection result for each joint is usually limited to one inspection. Therefore, the reliability of the Bayesian updating is completely sensitive to the reliability of the measured crack size that depends on several factors such as:

- Resolution of the inspection technique
- Competence of the inspection technician (both technical, personal, etc.)

Let's consider the value of likelihood for the considered example again (Table 6.15). Two cases are assumed here:

1) An accurate inspection technique and a competent inspector:

   If the crack size is measured equal to 4mm, and the real crack size is 4.1mm, then the posterior distribution is completely reliable. The likelihood value for this case is proportional to 57.3.

2) An inaccurate inspection technique and/or an incompetent inspector:

Now, assume the inspection technique is not accurate and detects a crack of 4mm, whereas the real crack size is 6mm. The likelihood value for this case is obtained proportional to 3.5 which is 16 times less than the real value (i.e. 57.3).

As can be seen from Figure 6.52, for the conventional Bayesian method (green line), the posterior distribution is sharply reduced for big cracks. Therefore, if the real crack size is 6mm, the updated probability of failure (Eq. (6-16)) is underestimated which leads to the wrong decisions (because the probability of failure is estimated less than the real value).

It was mentioned that several studies have been performed by using the common Bayesian methods which were explained in Chapter 5. Therefore, the credibility of the posterior distribution in these studies depends on the user's confidence in the inspection results.

To overcome the issue of reliability (credibility) of the typical Bayesian methods, the presented approach in Chapter 6 can be employed when the inspection result is not reliable. Although this approach results in a broader distribution (bigger uncertainty), the reliability results are conservative which is acceptable in case of employing an inaccurate inspection technique.

6.8 Guidance for Using the Proposed Approach

The main objective of Chapter 6 is to propose a novel methodology for updating the probability distributions of the parameters in a fracture mechanics model and also crack size in tubular joints using information from the inspections. The explained methodology in Section 6.3 to Section 6.3.3 can update the distribution of the crack size, distributions of the involved uncertainties in the fatigue crack model (i.e. initial crack size, crack growth parameter, stress range, and the uncertainty in the geometry function), and the POD curves. The reliability of the proposed approach was discussed in Section 6.6, in detail. Moreover, the benefits of the proposed approach were explained in Section 6.7.

This section is presented to provide guidance for the user in practice, including:

(I) How to use the methodology to get the best results

(II) When the methodology works best

(III) What are the advantages of the proposed approach

(IV) What are the limitations of the proposed approach

6.8.1 How to Use the Methodology to Get the Best Results

The proposed methodology for obtaining the posterior distributions of the uncertain parameters is explained in Section 6.3 to Section 6.3.3, in detail. For getting the best results, the following steps need to be taken:

1) Select the prior distributions of the uncertain parameters involved in the fatigue crack model based on the previous knowledge, beliefs, and the suggested distributions in the recommended practices, for instance:
   - Use the suggested distributions in the recommended practices (e.g. DNV 95-3204 [19], BS 7910 [47], JCSS [134], etc.) for initial crack size (a_0^p), and crack growth parameter (C^p).
   - For the stress range distribution (S^p), the mean value is obtained from the global fatigue analysis results (SESAM software) for the considered tubular joint. Select the coefficient of variation (COV) based on the experts' beliefs regarding the uncertainties in the global analysis (or use e.g. DNV recommendations).
   - For the uncertainty in the estimation of the geometry function (ε_Y^p), select the prior distribution based on the available literature review. Most of the previous studies suggest a mean value of 1 and a COV of 0.1-0.2 for the uncertainty in the estimation of the geometry function.
2) Obtain the prior distribution of the crack size by using the sampling method as described in Section 6.3.2.2.
3) Select a prior distribution for the POD curve based on previous knowledge and obtain the detected crack size as explained in Section 6.3.2.4.
4) Use the explained method in Section 6.3.1.3 for obtaining the simulated reality distributions of the uncertain parameters involved in the fatigue crack model (i.e. $a_0^r, C^r, S^r, \varepsilon_Y^r$).

- **Note:** if the obtained COV value of any of the uncertain parameters in the simulated reality distribution is bigger than the considered COV in the prior distribution, go to step 1 and increase the COV for the uncertain parameter in the prior distribution.

5) Obtain the simulated reality distribution of the crack size by using the sampling method as described in Section 6.3.1.4.

   - **Note:** Make sure the obtained histogram for the simulated reality cracks in the sampling method is similar to the real observation distribution.

6) Select a simulated reality distribution of the POD curve based on the available information for the inspection device (provided by the device manufacturer). Then obtain the detected simulated cracks as explained in Section 6.3.1.6.

7) Obtain the posterior distributions of the uncertain parameters, including crack size; uncertainties in the fatigue crack model; and the POD curves as explained in Section 6.3.3.

6.8.2 When the Methodology Works Best

Based on the considered cases in Section 6.6, the proposed methodology works properly when:

- The mean values of the considered prior distributions for the uncertain parameters (i.e. $a_0^p, C^p, S^p, \varepsilon_Y^p$) are close enough to the mean values of the simulated reality distributions (i.e. $a_0^r, C^r, S^r, \varepsilon_Y^r$).
- The coefficient of variation of the above-mentioned parameters (as well as the POD curve) in prior distribution is bigger than the coefficient of variation in the simulated reality distribution.

The proposed methodology can be led to poor results if:

- A very low mean value is selected for a prior distribution of the initial crack size (a_0^p) or the crack growth parameter (C^p) in comparison to the simulated reality distributions. A mean value for the prior is considered as a very low mean value if:

$$\frac{(Mean\ Value)_{prior}}{(Mean\ Value)_{simulated\ reality}} \leq 0.25$$

- The coefficient of variation of the POD curve in prior distribution is smaller than the coefficient of variation of the POD curve in the simulated reality distribution.

6.8.3 Advantages of the Proposed Approach

The proposed methodology has several advantages, including:

- It maximises the benefits of the inspection results. This approach is capable of updating several uncertain parameters, including uncertainties involved in the predicted fatigue crack size, POD curves besides fatigue crack size:
  - Although updating crack size estimates for a known critical location is useful, but the ability to improve estimates of reliability and to plan better future inspections is much more useful.
  - For future inspection planning and reliability analysis of the inspected platform (and other similar platforms), the updated estimates of other uncertain parameters (i.e. initial crack size, crack growth parameter, POD, etc.) are valuable.
- It is a more reliable method when only one inspection result is available and there is concern about the credibility of the inspection result (see Section 6.7.1).
- It can be used to find out the importance of each uncertain parameter on the posterior distribution of the crack size (based on the sensitivity analysis performed in Section 6.4).

6.8.4 Limitations of the Approach

Some important limitations of this approach are:

- The prior distributions for the uncertain parameters need to be selected reasonably regarding the obtained simulated reality distributions.
- The proposed methodology might be led to poor results if a very low mean value is selected for a prior distribution of an uncertain parameter.

- The proposed methodology cannot work properly when inappropriate prior distributions are selected for two uncertain parameters (e.g. crack growth parameter and POD curve), simultaneously.

6.9 Summary

In this chapter, a novel methodology is presented to update the probability distributions of the uncertain parameters (involved in the fatigue analysis) when new information becomes available. The considered uncertainties in this chapter are fatigue crack size, POD curve, and input variables involved in the predicted model of the fatigue crack size (initial crack size, crack growth parameter, stress range, and uncertainty in the estimation of the geometry function).

Note that whilst the proposed approach considers a specific location, the method can be applied to multiple locations at the same time by suitably non-dimensionalising the variables.

To obtain the simulated reality distributions of the input variables, the concept of equivalent initial flaw size distribution is utilised. These distributions are obtained by back extrapolating the observed cracks.

A sampling method is used to generate the prior distribution of the crack size. A large number of random samples for each input variable is generated based on their distributions and the crack size is calculated for each set of randomly generated numbers.

For obtaining the posterior distributions, the concept of compatibility is defined. For this purpose, each detected prior crack is compared with each simulated reality crack. If the prior crack is close enough to the simulated reality crack, that prior is assumed as a compatible prior otherwise it is called an incompatible prior. The posterior distributions are then achieved by removing the incompatible priors and fitting the best distributions to the compatible priors.

The results of the proposed approach show that for reasonable prior estimates, the posterior distributions of the uncertain parameters will shift towards the simulated reality distributions. It is shown that the uncertainty of the posterior distribution of the crack size decreases whereas the uncertainty of the posterior distribution for the input

variables increases. That is because the inspection results include only information about the crack size and do not provide any information about the input variables such as initial crack size.

To find out which parameters have great influences on the posterior distributions, sensitivity analyses are performed. The main results of the sensitivity analyses are:

- The probability of failure is very sensitive to the initial crack size and stress range distributions.
- The posterior distribution of the crack size is sensitive to the resolution of the NDT technique.

Moreover, the results of the proposed approach for updating the crack size distribution are compared with the results of the conventional Bayesian methods (explained in Chapter 5). When several inspection results are available, both approaches (Chapter 5 and Chapter 6) can be utilised to obtain the posterior distribution of the crack size. However, when few inspection results are available, there is a big difference between the two approaches. Since the posterior distribution is sensitive to the measured crack size in the common Bayesian methods, the credibility of the posterior distribution depends on the user's confidence in the inspection results. On the other hand, although the proposed approach (in Chapter 6) results in a broader distribution (bigger uncertainty), it can be employed when the inspection result is not reliable.

Finally, the reliability of the proposed methodology is assessed when an inappropriate distribution is chosen for the prior distribution of an uncertain parameter. The advantages and limitations of the proposed methodology are described and guidance for using this approach is provided.

7 . CONCLUSION

In this PhD thesis, a comprehensive approach for improving the reliability assessment of offshore jacket platforms is presented. Starting from the fatigue reliability analysis at the component level, continuing the reliability analysis at the system level, updating the reliability analysis by using the Bayesian approach when the inspection results are provided, and finally ending with proposing a new updating approach for updating all uncertain parameters involved in the analysis.

The summary of the PhD research thesis and the novelty of the research are briefly provided in Section 7.1 and 7.2, respectively. The contributions to research, and industry, are explained in Section 7.3. The future work and some final concluding remarks are elaborated in Sections 7.4 and 7.5, respectively.

7.1 Summary of the Chapters

The thesis commences in Chapter 1 with an introduction to the research work. The background and motivations of this research are presented. The existing problems in the offshore structures are briefly described and the main aim and objectives of the thesis are defined. The considered approach to solving the described problems and the structure of the thesis is outlined and the publications regarding the thesis are listed.

Chapter 2 reviews the basic concepts of probability theory, random variables, and commonly used probability distributions. Fundamental concepts of the reliability analysis including different approaches to structural safety, uncertainties related to loading and capacity, limit state functions, probability of failure, and reliability index are introduced. Different methods for estimation of the reliability, including First-Order Reliability Method (FORM), Second-Order Reliability Method (SORM), and Monte-Carlo simulation are explained. The advantages and disadvantages of each method are described. Finally, the sensitivity measures for the selection of important basic variables are introduced.

Fatigue reliability analysis at the component level for tubular joints is explained in Chapter 3. Jacket platforms are one of the most common types of offshore structures. They are usually constructed as truss frameworks in which tubular members are the structural elements. These tubular members are welded together to create a steel frame,

to transfer the gravitational and lateral loads to the pile foundations. Fatigue is an important failure mechanism in jacket structures. Fatigue damage occurs due to the cyclic nature of wave loading on the structure. This wave loading creates stress ranges at the hot spot regions and results in crack initiation. The crack initiation is followed by crack propagation through the thickness of the tubular wall which is assumed as the end of fatigue life of the tubular joints.

In Chapter 3, at first, the concept of the fatigue process, and fatigue analysis is explained. The Chapter also describes how to model the wave loading in the sea environment, and how to obtain the response of the structure due to environmental loads by introducing the transfer function concept. Different types of tubular joints are introduced and the concept of hot spot stress (HSS) and stress concentration factor (SCF) is presented. Concerning the fatigue analysis, two approaches are introduced; the S-N curve approach and the fracture mechanics (FM) approach, and the reason for selecting the FM approach in this research is described.

After explaining the fatigue process, fatigue reliability analysis, and different sources of uncertainties in fatigue analysis are addressed. To carry out the fatigue reliability analysis, an appropriate probabilistic model is developed and the limit state function is introduced. In this thesis, for the component reliability analysis, the crack size is considered as the failure criterion which is acceptable for low toughness material. Several uncertainties are considered in the limit state function and the probability of failure for the tubular joints is obtained by using FORM and Monte-Carlo simulation. Sensitivity analyses are carried out to find out the effect of each uncertain parameter on the fatigue reliability results.

Finally, the application of the fatigue reliability analysis to a jacket platform is provided in Chapter 3. A three-dimensional structural model of the considered platform is generated using SESAM software. A global fatigue analysis is performed by SESAM software and the generated stress results are used in the probabilistic crack size model which is developed based on the FM approach. This model predicts the fatigue crack size at any given time for the tubular joints in the considered jacket platform. The crack size is considered as the failure criterion and failure occurs when the crack size is bigger than a critical value. By performing the FORM and Monte-

Carlo simulation, the fatigue probability of failure and the corresponding reliability for any tubular joint are estimated. Sensitivity studies are also performed to find out the influence of uncertain parameters on the probability of failure.

In Chapter 3 of this research work, only one failure mode for a specific component is considered. Nevertheless, jacket structures in the real situation are redundant structures. Therefore, failure of a few structural components doesn't necessarily lead to structural failure or collapse, since the load can be redistributed among undamaged members. Due to the high redundancy of jacket platforms, the probability of failure of the whole system is more applicable than the component probability of failure.

Chapter 4 introduces the fundamental of the structural systems and the reliability calculation for each system. In this chapter, a system reliability approach is presented to estimate the probability of failure of a jacket platform by considering fatigue and extreme wave loads.

In this approach, at first, the fatigue probability of failure of each component is obtained by using the Monte-Carlo simulation. Then, important failure paths are identified by using a searching process in which, components with the maximum change in the accumulated damage are considered as the candidate joints in the path. By removing the candidate joint, which is assumed to fail in fatigue, the probability of failure of the structure under extreme wave loading increases. System failure criterion is evaluated by comparing the platform strength and loading distributions in terms of base shear. Nonlinear pushover analysis is also carried out to determine the capacity of the platform and the annual probability of failure under an extreme wave is calculated. When the probability of failure exceeds the maximum acceptable probability, the platform is assumed to fail.

To demonstrate the application of the proposed approach in Chapter 4, a jacket platform is considered and the three-dimensional structural model of the considered platform is generated using SESAM software. Nonlinear pushover analysis is carried out by using USFOS software to determine the capacity of the platform.

At first, it is assumed that no failure happened and all components are in safe conditions and Monte-Carlo simulation is employed to calculate the probability of failure under extreme load in the intact case. Spectral fatigue analysis for the jacket

platform is performed using SESAM software and by obtaining the stress range for each component, the probability of failure of each joint is obtained. In the next step, the component that has the highest probability of failure is selected as the first component in the failure path and the platform is modified by removing this component. By removing the candidate joint, the probability of failure of the structure under extreme wave loading increases. This probability of failure under an extreme wave is calculated and compared to the maximum probability of failure. The process of removing the critical components continues till the annual probability of failure exceeds the maximum acceptable probability which is assumed as the failure of the structure.

Chapter 4 also describes the inspection plan for a jacket platform. Inspection activities are performed to find out the level of degradation of each component. Underwater inspection is an expensive activity and the cost of the inspection is proportional to the number of inspections. Therefore, an inspection strategy can be proposed based on the effect of each component on the system reliability. This is an alternative inspection plan in comparison with the regular inspection plan. In this plan, the inspections are prioritised on the critical joints in the failure path that have a great effect on the system reliability.

Offshore platforms are regularly inspected during the operational lifetime to make sure they comply with the structural integrity requirements and to assess the state of damage. Fatigue damage accumulates during the structure's lifetime as the crack size increases. The accumulation of fatigue damage causes deterioration of the tubular joint capacity and increases the probability of failure. Regardless of the inspection outcome (detection or not detection of a crack), inspection activities provide additional information which can be utilised to update the probability distribution of crack size in a tubular joint.

Chapter 5 shows how the inspection results can be incorporated for updating the crack size distribution in a tubular joint. A Bayesian framework is typically used for updating the probability distributions of an uncertain parameter when new information becomes available. Bayesian inference provides a formal method of belief updating when new

information becomes available. The purpose of updating is to incorporate any available inspection history into an improved estimate of the parameters.

Moreover, in Chapter 5, the Bayesian framework and the terminology in this context are introduced. There are two main approaches for updating the distribution of an uncertain parameter; the analytical approach and the numerical approach. These two approaches and their advantages and disadvantages are explained. In this chapter, the application of Bayesian inference for updating the crack size distribution is demonstrated. The updating process is carried out by using both analytical and numerical approaches and the results of the two approaches are compared. Moreover, in the numerical method, depending on the results of inspections, an expression for the updated crack size is obtained. Additionally, the effect of different parameters and inputs on the updated distribution of the crack size is investigated. After updating the crack size distribution, the probability of failure for each component is updated. Depending on the results of inspections, the updated probability of failure may be higher or lower than the original value.

In Chapter 6, a new methodology is proposed to update the probability distribution of all uncertain parameters involved in the fatigue crack model when new information becomes available. Three different categories of uncertainties are updated using the proposed methodology; Fatigue crack size, POD curve, and Uncertainties involved in the predicted fatigue crack size (i.e. initial crack size, crack growth parameter, stress range, and uncertainty in the estimation of the geometry function).

According to the proposed methodology in Chapter 6 two sets of estimations are used; prior estimations of the uncertain parameters, and statistics of the simulated reality. Two sets of cracks are compared and the posterior estimates of the crack size are obtained by introducing the concept of compatibility. The proposed methodology is tested using the simulated reality distributions to determine the effectiveness of the Bayesian method and also the limits beyond which the method results in poorer posterior estimates. To verify the proposed methodology, the posterior distribution of the crack size obtained by this approach is compared with the updated crack size that is achieved by the conventional Bayesian methods (Chapter 5). Results show that the proposed methodology in Chapter 6 can be used for updating the crack size distribution

confidently. Moreover, sensitivity analyses are performed to find out the influence of different parameters on the posterior distribution.

The proposed methodology has several advantages, for instance, it maximises the benefits of the inspection results. This approach is capable of updating several uncertain parameters, including uncertainties involved in the predicted fatigue crack size, POD curves besides fatigue crack size. Moreover, in Chapter 6, guidance on how to implement the proposed methodology in practice is provided by explaining the framework, advantages, and limitations.

The developed and applied approaches are disseminated through several paper publications in scientific journals, along with oral and poster presentations at international conferences, as listed in Section 1.6.

7.2 Novelty of the Research

The biggest novelty of the research in this thesis lies in developing a methodology to update all uncertainties involved in the fatigue crack model when new information (inspection results) is available. Moreover, investigating the credibility of the proposed approach is an important part of this research work.

Most of the previous studies for updating the crack size distribution implemented conventional Bayesian methods (e.g., the numerical method). In these studies, a prior distribution was assumed for the crack size, and a likelihood function was considered based on the author's opinion. The posterior distribution was then obtained by using the Bayesian methods and the updated results were presented.

However, the credibility of the Bayesian methods was not considered in these studies. The reliability of the Bayesian updating depends on how reliable the inputs (e.g. inspection results) are. A Bayesian process is a mathematical function that processes the inputs and generates the output based on the provided inputs. Therefore, if the inputs are inaccurate, the updated results may be poor and can even lead to wrong decisions.

Unlike previous studies, the proposed approach in Chapter 6 investigates the reliability of the updating method since the credibility of the Bayesian updating is an important issue in any engineering application including offshore structures.

Moreover, guidance notes are presented for the user in practice that explains how to use the methodology to get the best results, when the methodology works best, the advantages, and the limitations of the approach.

7.3 Thesis Contributions to the Research and Industry

The biggest contribution of this study to the research lies in expanding the application of the reliability analysis to an offshore jacket structure. The research includes a comprehensive study, starting from the reliability analysis at the component level for an important failure mechanism in jacket structures (i.e., fatigue failure), continuing to the reliability analysis at the system level, and updating the probability of failures when new information (inspection results) is available.

To achieve the research aim, six main objectives are introduced in Section 1.3 which are:

1) Developing a probabilistic fatigue model to obtain the component probability of failure
2) Developing a methodology to obtain the system probability of failure
3) Prioritising the inspection locations
4) Using conventional Bayesian methods to update the crack size distribution
5) Proposing a novel Bayesian approach for updating the distributions of all uncertain parameters involved in the fatigue analysis
6) Investigating the credibility of the proposed approach

The main contributions to the research achieved in this thesis are:

- *Component reliability analysis (Objective #1):*

  A probabilistic model for fatigue crack based on the fracture mechanics approach is developed. The proposed model predicts the fatigue crack size as a function of several uncertain parameters. The crack size is considered as the failure criterion, i.e., failure occurs, as soon as the crack size is bigger than a critical value.

  A specific jacket platform is considered and the probability of failure of the tubular joints is calculated based on the introduced limit state function. To obtain

the probability of failure, appropriate distribution is assigned to each uncertainty, and the probability of failure is obtained by using both FORM and Monte-Carlo simulation approaches.

- *System reliability analysis (Objective #2):*

  Jacket platforms are redundant structures. For redundant structures, reliability at the system level is more applicable. Therefore, the reliability model is expanded to the system level by considering both fatigue and extreme environmental loading.

  Due to the considerable degree of redundancy, there are several possible combinations of element failures that can result in the failure of the whole structure. Therefore, a searching process is developed to identify important failure sequences, and the system failure event is then approximated as the union of these identified important sequences.

  The same jacket structure is considered, and the system probability of failure is estimated. The initial failures occur by fatigue at the critical joints, and the weakened structure collapses under the extreme wave loading.

- *Prioritising the inspection locations (Objective #3):*

  Underwater inspection is an expensive activity. The cost of the inspection is directly proportional to the number of inspections carried out. Therefore, it is required to concentrate only on the critical locations in the structures. At the system level, critical components are those that have a big effect on system reliability.

  The identified failure paths are suggested as a database for the inspection plan. By identifying the dominant failure paths, the critical joints that have a greater effect on the system probability of failure are selected and therefore inspection can be focused on these joints.

- *Bayesian updating methods (Objective #4):*

  Different Bayesian methods are introduced for updating the distribution of any uncertain parameter, in general. Analytical and numerical methods are explained, and the advantages and disadvantages of each method are provided.

The explained methods are then applied to the considered jacket platform. To demonstrate the Bayesian methods, a tubular joint is considered and the distribution of the crack size is updated by using both analytical and numerical methods. A comparison of the results for both methods is provided.

- *Proposing a novel Bayesian approach (Objective #5):*

  In the previous studies, the conventional Bayesian methods were used to incorporate inspection results (i.e., crack measurements) to update the probability distribution of crack size. I.e., both observation and the uncertain parameter are crack sizes. The previous studies didn't provide any updates about the other uncertain parameters which are involved in the estimation of the fatigue behaviour of the tubular joints.

  A novel methodology is proposed to update the probability distributions of all uncertain parameters (including the crack size) when new information becomes available. Three different categories of uncertainties are updated using this methodology: Fatigue crack size; POD curve; and Uncertainties involved in the predicted fatigue crack size (i.e., initial crack size, crack growth parameter, stress range, and uncertainty in the estimation of the geometry function). Therefore, this approach maximises the benefits of the inspection activities by updating all uncertain parameters involved in the fatigue crack model.

- *Investigating the credibility of the proposed approach (Objective #6):*

  The credibility of the updating process is the main concern in any updating application. However, the credibility of the conventional Bayesian methods was not considered in the previous studies. The reliability of any Bayesian updating method depends on how reliable the inputs (e.g., inspection results) are. A Bayesian process is a mathematical function that processes the inputs and generates the output based on the provided inputs. Therefore, if the inputs are inaccurate, the updated results may be poor and can even lead to wrong decisions. Unlike previous studies, in this research, the reliability of the proposed approach is investigated to find out when the proposed approach might lead to poor results.

The main contribution of this research to the industry is:

- *Proposing and applying a methodology for a reliable Bayesian updating process in offshore structures:*

  The reliability of the updating process is the main concern of the platforms' owners. Due to the high cost of underwater inspection, in practical applications, the inspection result for each joint is usually limited to one inspection. Therefore, the reliability of the Bayesian updating is sensitive to the reliability of the measured crack size that depends on several factors such as the resolution of the inspection technique, and the competence of the inspector technician (both technical, personal, etc.).

- *Future inspection planning:*

  Another contribution of this research to the industry is future inspection planning and reliability analysis of the inspected platforms. Although updating crack size estimates is useful for a known critical location, the ability of the proposed approach to improve estimates of other uncertain parameters (i.e., initial crack size, crack growth parameter, POD, etc.) is much more valuable. The updated distributions of the other uncertain parameters can be used as the prior distributions for the next updating process (next inspection results).

7.4 Future Work

A novel approach is proposed in Chapter 6 of this research to maximise the benefits of the inspection activities by updating all uncertain parameters involved in the fatigue crack model.

The proposed methodology also helps the platform operator/owner to use the Bayesian updating with more confidence. To help the user to implement the proposed approach in practice, guidance is provided for using the approach by explaining the framework, advantages, and limitations.

The proposed model can open a new research direction for Bayesian updating since it considers the credibility of the updating methodology. As future work, the proposed

approach in Chapter 6 can be further developed by making efforts to overcome prevailing limitations. Some of the limitations of the proposed approach are:

- To achieve the best results of the proposed methodology, the user needs to select the mean value of the considered prior distributions for the uncertain parameters close enough to the mean value of the simulated reality distributions.
- The considered standard deviation of the uncertain parameters in the prior distributions needs to be bigger than the simulated reality distributions.

The proposed methodology can properly update the probability of failure, even, in the case of the selection of an inappropriate prior distribution for only one uncertain parameter. If inappropriate prior distributions are chosen for more than one uncertain parameter, the methodology might lead to incorrect results. Further work is required to be carried out to improve the proposed methodology in the case of the selection of inappropriate prior distributions of two or more uncertain parameters.

Moreover, the proposed approach updates the uncertain parameters at one location. As future work, the method can be developed for applying to multiple locations at the same time by suitably non-dimensionalising the input variables such as stress range.

7.5 Concluding Remarks

In this thesis, a comprehensive study is carried out, starting from the component reliability analysis, continuing to the system reliability analysis, and finally updating the reliability analysis by using Bayesian methods to incorporate the new information from the inspection results for offshore jacket structures:

- The reliability analysis at the component level is carried out by considering a fatigue limit state based on the fracture mechanics approach, and the probability of failure of the critical joints are estimated.
- A system reliability approach is presented to estimate the probability of failure of a jacket platform by considering fatigue and extreme wave loads.
- Bayesian framework and the terminology in this context are defined and the probability of failure of a tubular joint is updated by using the common Bayesian approaches (analytical and numerical).

- A new methodology is proposed to update the distribution of all uncertain parameters in the fatigue crack model besides the fatigue crack size. The proposed methodology is verified to some extent with the conventional Bayesian methods and guidance is provided to help the user to implement the proposed approach in practice.
- The credibility of the proposed approach is investigated to find out when the proposed approach works properly and when it might lead to poor results.

REFERENCES

[1] Aghakouchak A.A., Stiemer S.F., “Fatigue reliability assessment of tubular joints of existing offshore structures,” *Canadian Journal of civil engineering,* p. Vol. 28, 2001.

[2] Kam J.C.P., Topp D.A., Dover W.D., “Fracture Mechanics Modelling and Structural Integrity of Welded Tubular Joints in Fatigue,” in *Proceedings, 6th International Offshore Mechanics and Arctic Engineering Symposium, ASME,* 1987.

[3] Etube L.S., "Fatigue and Fracture Mechanics of Offshore Structures", London: Professional Engineering Publishing Limited, 2001.

[4] DNV GL, *SESAM V.7-4,* 2015.

[5] Almar-Naess. A, “Fatigue handbook for offshore steel structures”, Tapir, 1985.

[6] Val D., "Safety, risk and reliability", Heriot-Watt University, 2014.

[7] Shetty N., “System reliability of fixed offshore structures,” A thesis submitted for the degree of Doctor of Philosophy in the faculty of Engineering of the University of London, 1992.

[8] Wang Y., Shi Y., Wang C., Li S., “A New Method for System Fatigue Reliability Analysis of Offshore Steel Jacket,” *Advances in Structural Engineering,* vol. 9, no. 2, pp. 185-193, 2006.

[9] Faber M.H., "Statistics and Probability Theory, In Pursuit of Engineering Decision", Springer, 2012.

[10] Sørensen J.D., "Notes in Structural Reliability Theory And Risk Analysis", Aalborg University, 2004.

[11] Der Kiureghian A., Nikolaidis E., Ghiocel D.M., Singhal S., “First-and Second-order Reliability Methods-Engineering Design Reliability Handbook”, CRC Press, BocaRaton, 2005.

[12] Thoft-Christensen P., Baker M.J., "Structural reliability theory and its applications", Berlin: Springer-Verlag, 1982.

[13] Madsen H.O., Krenk S., Lind N.C., "Methods of Structural Safety", New York: Dover Publications, 2006.

[14] Hasofer A.M., Lind N.C., “An Exact and Invariant First Order Reliability Format,” *Journal of Engineering Mechanics, ASCE,* pp. 111-121, 1974.

[15] Rajasankar J., Iyer N.R., Appa Rao T.V.S.R., “Structural integrity assessment of offshore tubular joints based on reliability analysis,” *International Journal of Fatigue,* pp. p.609-619, 2003.

[16] DNV, “Guideline for offshore structural reliability analysis - General, Appendix B, Report No. 95,” 2018.

[17] Melchers R., “Simulation in time-invariant and time-variant reliability problems,” in *Proceedings IFIP WG 7.5*, Munich, 1991.

[18] Madsen H.O., “Omission Sensitivity Factors,” *Structural Safety*, vol. Vol. 5, no. 1 , pp. 33-45, 1988.

[19] DNV, “Guideline for structural reliability analysis: application to jacket platforms,” report No. 95-3203, 1995.

[20] Newland D.E., "Random Vibrations and Spectral Analysis", London: Longman, 1975.

[21] Bendat J.S., Piersol A.G., "Random Data: Analysis and Measurement Procedures", Wiley-Interscience, 1971.

[22] Langen I., Sigbjsrnsson, R., "Dynamisk Analyse av Konstruksjoner",, Trondheirn: TAPIR, 1979.

[23] DNV, RP-C203, "Fatigue Strength Analysis of Offshore Steel Structures", Det Norske Veritas-Recommended Practice, 2001.

[24] Department of Energy, "Offshore Installations Guidance on Design and Construction", London, 1990.

[25] API RP2A, "Recommended Practice for Planning, Designing and Constructing Fixed Offshore Platforms", American Petroleum Institute, 2007.

[26] Biljaard P. P., “Stresses from radial loads in cylindrical pressure vessels,” *The Welding Journal*, vol. 33, no. 12, pp. 615-623, 1954.

[27] Elliot K., Fessler H., “Photoelastic study of hot spot stresses in tubular joints,” *Cohesive Programme of Research and Development into the Fatigue of Offshore Structures*, 1986.

[28] Kuang J. G., Potvin A. B., Leick R. D. , “Stress concentration in tubular joints,” *Society of Petroleum Engineers*, 1977.

[29] Efthymiou M., “Development of SCF formulae and generalized influence functions for use in fatigue analysis,” *Offshore Tubular Joints Survey*, 1988.

[30] BS 6235, "Code of practice for fixed Offshore structures", British standards Institution, 1982.

[31] DNV, "Rules for the design, construction and inspection of fixed Offshore structures", Det Norske Veritas, 1977.

[32] ISO 19902, "Petroleum and natural gas industries-Fixed steel offshore structures", International Standard, 2007.

[33] Ahmadi H., Lotfollahi-Yaghin M., Aminfar M.H., “Effect of stress concentration factors on the structural integrity assessment of multi-planar offshore tubular DKT-joints based on the fracture mechanics fatigue reliability approach,” *Ocean Engineering*, p. p.1883–1893, 2011.

[34] Pillaia T.M., Prasad A.M., “Fatigue reliability analysis in time domain for inspection strategy of fixed offshore structures,” *Ocean Engineering* , vol. 27 , p. 167–186, 2000.

[35] Dover W.D., Dharmavasan S., “Fatigue and Fracture Mechanics Analysis of T and Y joints,” in *Offshore Technology Conference, OTC 4404*, Houston, 1982.

[36] Austin J.A., The Role of Corrosion Fatigue crack growth Mechanisms in Predicting Fatigue life of Offshore Tubular Joints, University College London, PhD Thesis, Department of Mechanical Engineering, 1994.

[37] Schutz W., “Problems in the prediction of fatigue crack propagation under realistic load sequences,” *European Offshore Steels Research Seminar,* The Welding Institute, UK, 1978.

[38] Newman J.C., Raju I.S., “An empirical stress-intensity factor equation for the surface crack,” *Engineering Fracture Mechanics,* vol. 15, no. 1-2, pp. 185-192, 1981.

[39] Cheaitani M.J., Bolt H.M. , “Evaluation of stress intensity factor solutions for offshore tubular joints.,” in *Proceedings of the 15th International Conference on Offshore Mechanics and Arctic Engineering, Vol. III, pp. 521–532*, 1996.

[40] Lee M.M.K., Bowness D. , “Stress intensity factors for weld toe cracks in tubular joints,” in *Proceedings of the Fifth International Conference on Engineering Structural Integrity Assessment,* Cambridge, 2000.

[41] Khalili H., Oterkus S., Barltrop N., Bharadwaj U., Tipping M., “System reliability calculation of jacket platforms including fatigue and extreme wave loading,” *Trends in the Analysis and Design of Marine Structures, Parunov & Guedes Soares © Taylor,* 2019.

[42] Milne I., Ritchie R., Karihaloo B.L., Comprehensive Structural Integrity, Elsevier Science, 2003.

[43] Lancaster J.F., Metallurgy of Welding, 6th edition: Woodhead Publishing, 1999.

[44] Tipple C., Thorwald G., “Using the Failure Assessment Diagram Method with Fatigue Crack Growth to Determine Leak-before-Rupture,” in *SIMULIA Customer Conference,* Providence RI, USA, 2012.

[45] Hoh H.J., Pang J.H.L., Tsang K.S., “Failure Assessment Diagram (FAD) analysis of fatigue test results for X65 welded joints,” *MATEC Web of Conferences - FATIGUE 2018,* vol. 165, no. 21011, 2018.

[46] Anderson T.L., Fracture Mechanics: Fundamentals and Applications, CRC Press, 2017.

[47] BS 7910, Guide to methods of assessing the acceptability of flaws in metallic structures, 2013.

[48] Kirkemo F., “Applications of probabilistic fracture mechanics to offshore structures,” *Applied Mechanics Reviews,* vol. 41, p. 61–84, 1988.

[49] Siddiqui N.A., Ahmad S., “Fatigue and fracture reliability of TLP tethers under random loading,” *Marine Structures,* pp. p.331-352, 2001.

[50] Karadeniz H., “Uncertainty Modelling in the Fatigue Reliability Calculation of Offshore Structures,” *Reliability engineering and system safety,* vol. 74, pp. 323-335, 2001.

[51] Lin H., Chen G., Wang Z., Yang L., “Integrality Assessment of Tubular Joints in Aging Offshore Platform Based on Reliability Theory,” *Advanced Materials Research,* pp. pp 238-242, 2012.

[52] Dong W., Moan T., Gao Z., “Fatigue reliability analysis of the jacket support structure for offshore wind turbine considering the effect of corrosion and inspection,” *Reliability Engineering and System Safety,* vol. 106, pp. 11-27, 2012.

[53] Wirshing P.H., Light M.C., “Fatigue under wide band random stresses,” *ASCE Journal of the Structural Division,* vol. 106, p. 1593–1607, 1980.

[54] Dover W.D., “Variable amplitude fatigue of welded structures, Fracture mechanics, current status, future prospects,” Cambridge, 1979.

[55] Wirsching P., “Fatigue Reliability for Offshore Structures,” *Journal of Structural Engineering, ASCE,* vol. 110, no. 10, 1984.

[56] Shabakhty N., “System Reliability of Jack-Up Platforms under Fatigue and Fracture Failures,” in *Proceedings of the ASME 27th International Conference on Offshore Mechanics and Arctic Engineering,* Portugal, 2008.

[57] Wordsworth A.C., “Stress concentration factors at K and KT tubular joints,” *Fatigue in Offshore Structural Steel, ICE,* 1981.

[58] Department of Energy, "Background to new fatigue design guidance for steel welded joints in offshore structures", London, 1984.

[59] Carpinteri A., Paggi M., “A unified interpretation of the power laws in fatigue and the analytical correlations between cyclic properties of engineering materials,” *International Journal of Fatigue,* vol. 31, p. 1524–1531, 2009.

[60] Cortie M., Garrett G., “On the correlation between the C and m in the Paris equation for fatigue crack propagation,” *Engineering fracture mechanics,* vol. 30, p. 49–58, 1988.

[61] Gurney T. R. , Fatigue of welded structures, CUP Archive, 1979.

[62] Amirafshari P., Optimising Non-destructive Examination of newbuilding ship hull structures by developing a data-centric risk and reliability framework based on fracture mechanics, Glasgow: A thesis presented in fulfilment of the requirements for the degree of Doctor of Philosophy, University of Strathclyde, 2019.

[63] Tanaka K., Matsuoka S., "A tentative explanation for two parameters, C and m, in Paris equation of fatigue crack growth," *International Journal of Fracture,* vol. 13, p. 563–583, 1977.

[64] Baker M., Stanley I., "Assessing and modelling the uncertainty in fatigue crack growth in structural steels," Health and Safety Executive Research Report RR643, Norwich, 2008.

[65] Rt Software, Department of civil engineering, University of British Columbia (UBC), 2013.

[66] Thoft-Christensen P., Murotsu Y., "Application of Structural System Reliability Theory", Springer, 1986.

[67] Reality Engineering, USFOS, V.8-8, 2015.

[68] Ditlevsen O., "Narrow Reliability Bounds for Structural Systems," *Journal of Structural Mechanics,* vol. 4, pp. 453-472, 1979.

[69] Kurian V.J., Wahab M.M.A., Kheang T.S., Liew M.S., "System reliability of existing jacket platform in Malaysian water," *Applied Mechanics and Materials,* vol. 567, pp. 307-312, 2014.

[70] Karamchandani A., "Systems reliability of offshore structures including fatigue and extreme wave loading," *Marine Structures,* vol. 4, pp. 353-379, 1991.

[71] Márquez-Domínguez S., Sørensen J.D., "System reliability for offshore wind turbines: fatigue failure," in *Proceedings of the ASME 2013 32nd International Conference on Ocean, Offshore and Arctic Engineering*, France, 2013.

[72] Bomel Ltd., "System-based calibration of North West European annex environmental load factors for the ISO fixed steel offshore structures code 19902," 2003.

[73] Oakley A., Brown M., Warren P.A., Barltrop N.D.P., "optimised inspection scheduling for offshore structures, a probabilistic approach," 1992.

[74] Manuel L., Schmucker D.G., Cornell C.A., Carballo J.E., "A reliability-based design format for jacket," *Marine Structures,* vol. 11, pp. 413-428, 1998.

[75] Murotsu Y., "Automatic generation of stochastically dominant modes of structural failure in frame," *Structural safety,* vol. 2, 1984.

[76] Melchers R.E., Tang L.K., "Dominant failure modes in stochastic structural systems," *Structural Safety,* vol. 1, p. 127–143, 1984.

[77] Kim D.S., Song J., Koh H.M. , “System reliability analysis using dominant failure modes identified by selective searching technique,” *Reliability engineering and system safety, ,* vol. 119, 2013.

[78] Rabi S.D., “Offshore structural system reliability under changing load pattern,” *Applied Ocean Research,* vol. 13, no. 3, 1991.

[79] Mathworks, MATLAB, R2017a.

[80] Eurocode 1, “Basis of design and actions on structures,” 1993.

[81] DNV, “Structural reliability analysis of marine structures, Classification note 30.6,” 1992.

[82] Moan T., “Reliability-based management of inspection, maintenance and repair of offshore structures,” *Structure and Infrastructure Engineering,* vol. 1, no. 1, pp. 33-62, 2005.

[83] Fayyazi A., Aghakouchak A.A., “Calculation of probable extreme wave height during life time of offshore platforms in the Persian Gulf,” *Sea engineering journal,* 2014.

[84] Warrens, M.J., *Similarity coefficients for binary data : properties of coefficients,coefficient matrices, multi-way metrics and multivariate coefficients,* Netherlands: PhD Thesis, Universiteit Leiden, 2008.

[85] Lotsberg I., Sigurdsson G., Fjeldstad A., Moan T., “Probabilistic methods for planning of inspection,” *Marine Structures,* vol. 46, pp. 167-192, 2016.

[86] Dover W.J., Rudlin J.R., “Defect characterisation and classification for the ICON inspection reliability trials,” in *Conference Offshore Mechanics & Arctic Engineering, Vol. 2, p. 503-508,* 1996.

[87] Rudlin J.R., Austin J., “ Topside inspection project: Phase I final report. Offshore Technology Report OTN 96 169,” Health & Safety Executive, UK, 1996.

[88] Visser W. , “POD/POS curves for non-destructive examination, offshore technical report OTO 2000/018,” Health & Safety Executive, UK, 2002.

[89] NORSOK N-006, “Assessment of structural integrity for existing offshore load-bearing structures,” 2015.

[90] DNVGL-RP-C210, “Probabilistic methods for planning of inspection for fatigue cracks in offshore structures,” 2015.

[91] Manzocchi M., Stacey A., Shetty N., “Reliability-Based Assessment For Fatigue Integrity Management,” in *Proceedings of the ASME 27th International Conference on Offshore Mechanics and Arctic Engineering,* Estoril, Portugal, OMAE 2008.

[92] Karadeniz H., Toğan V., Daloğlu A., Vrouwenvelder T., “Reliability-based optimisation of offshore jacket-type structures with an integrated-algorithms system,” *Ships and Offshore Structures,* vol. 5, no. 1, pp. 67-74, 2010.

[93] T. Bayes, “An essay towards solving a problem in the doctrine of chances,” *Philosophical Transactions of the Royal Society of London,* vol. 53, no. 1, p. 370–418, 1763.

[94] Yuen K., “Bayesian Methods for Structural Dynamics and Civil Engineering”, John Wiley & Sons, 2010.

[95] Jeffreys, H., "Theory of Probability (3rd Edition)", Oxford, UK: Oxford Clarendon Press, 1961.

[96] Cox, R. T., "The Algebra of Probable Inference", Baltimore, MA: Johns Hopkins Press, 1961.

[97] Jaynes, E. T., “Prior probabilities,” *IEEE Transactions System Science and Cybernetics,* vol. 4, no. 3, p. 227–241, 1968.

[98] Jaynes, E. T., "Probability Theory with Applications in Science and Engineering", St Louis, MO: Washington University, 1974.

[99] Jaynes, E. T., "Bayesian methods: General background In Maximum Entropy and Bayesian Methods in Applied Statistics", Cambridge, UK: Cambridge University Press, 1968.

[100] Papadimitriou, C. and Katafygiotis, L. S., "Bayesian modeling and updating. In Engineering Design Reliability Handbook", CRC Press, 2004, pp. Chapter 22, pp. 22-1–22-20.

[101] Spiegelhalter, D. J., Abrams, K. R. and Myles, J. P., "Bayesian Approaches to Clinical Trials and Health-Care Evaluation", Chichester, UK: John Wiley & Sons, Ltd, 2004.

[102] Woodworth, G. G. , "Biostatistics: A Bayesian Introduction", Hoboken, NJ: John Wiley & Sons, Inc., 2004.

[103] Mendenhall, W., Beaver, R. J. and Beaver, B. M., "Introduction to Probability and Statistics", Belmont, CA: Duxbury Press, 2005.

[104] Melchers R.E., "Structural reliability analysis and prediction", Wiley, 1999.

[105] Gelman A., Carlin J.B., Stern H.S., Rubin D.B., "Bayesian data analysis", 2nd edition, Chapman and Hall/CRC Press, 2009.

[106] Hamada M.S., Wilson A.G., Reese C.S., Martz H.F., "Bayesian Reliability", Springer, 2008.

[107] Lunn D., Jackson C., Best N., Thomas A., Spiegelhalter D., “The BUGS Book, A practical introduction to Bayesian analysis”, Chapter 5, CRC Press, 2012.

[108] Kelly D., Smith C., "Bayesian Inference for Probabilistic Risk Assessment", Springer, 2011.

[109] Baroth J., Schoefs F., Breysse D., "Construction Reliability, Safety, Variability and Sustainability,, John Wiley & Sons, 2011.

[110] Li M., Meeker W.Q., “Application of Bayesian Methods in Reliability Data Analyses,” *Journal of Quality Technology,* 2014.

[111] O’Hagan, “Guidance on best practice”, Chapter 11, Wiley & Sons, 2006.

[112] Damien P., Dellaportas P., Polson N.G., Stephens D.A., "Bayesian theory and applications", Chapter 1, Oxford Publication, 2013.

[113] Raiffa H., Schlaifer R. , Applied Statistical Decision Theory, Boston: MA: Harvard University, 1961.

[114] Wilson A., Fronczyk K., “"Bayesian Reliability Combining Information",” Institute for Defense Analyses, 2016.

[115] Rossi R.J., “Mathematical Statistics : An Introduction to Likelihood Based Inference,” New York, John Wiley & Sons, 2018, p. 227.

[116] Di Francesco D., “Bayesian Data Analysis of Imperfect Information for Decision-Theoretic Approaches to Structural Integrity Management,” A thesis submitted for the degree of Doctor of Philosophy, University of Surrey, 2021.

[117] Rocca J., “Overview of the Bayesian inference problem in statistics: Bayesian inference problem, MCMC and variational inference,” Towards Data Science, 2019.

[118] Coyle P., “Towards Data Science,” 2018. [Online]. Available: https://towardsdatascience.com/what-is-bayesian-statistics-used-for-37b91c2c257c.

[119] Madsen H.O., “Stochastic modeling of fatigue crack growth and inspection,” in *Probabilistic methods for structural design*, Netherlands, Kluwer Academic Publishers, 1997, pp. 59-83.

[120] Zhao Z., Haldar A., “Bridge fatigue damage evaluation and updating using non-destructive inspections,” *Engineering Fracture Mechanics,* vol. 53, no. 5, pp. 775-788, 1996.

[121] Zhang R., Mahadevan S., “Model uncertainty and Bayesian updating in reliability-based inspection,” *Structural Safety,* vol. 22, pp. 145-160, 2000.

[122] Heredia-Zavoni E.; Montes-Iturrizaga R., “A Bayesian Model for the Probability Distribution of Fatigue,” *Journal of Offshore Mechanics and Arctic Engineering,* vol. Vol. 126, 2004.

[123] Peng T., He J., Xiang Y., Liu Y., Saxena A., Celaya J., Goebel K., “Probabilistic fatigue damage prognosis of lap joint using Bayesian updating,” *Journal of Intelligent Material Systems and Structures,* vol. 26, no. 8, p. 965–979, 2015.

[124] Garbatov Y., Guedes Soares C., "Bayesian Updating in the Reliability Assessment of Maintained Floating Structures," *Journal of Offshore Mechanics and Arctic Engineering,* vol. 124, pp. 139-145, 2002.

[125] Zárate B.A., Caicedo J.M., Yu J., Ziehl P., "Bayesian model updating and prognosis of fatigue crack growth," *Engineering Structures,* vol. 45, p. 53–61, 2012.

[126] Karandikar J.M., Kim N. H., Schmitz T.L., "Prediction of remaining useful life for fatigue-damaged structures using Bayesian inference," *Engineering Fracture Mechanics Journal,* p. p. 588–605, 2012.

[127] Schmitt W., Wellein R., "Model of the Flaw Size Distribution in Welds," *Nuclear engineering and design,* 1982.

[128] Ichikawa M., "A theoretical study of flaw size distributions," *Reliability Engineering,* vol. 9, no. 4, pp. 221-228, 1984.

[129] Casciati F., Colombi P., Faravelli L., "Fatigue Crack Size Probability Distribution via a Filter Technique," *Fatigue and fracture of engineering material & structures,* vol. 15, no. 5, pp. 463-475, 1992.

[130] Tanaka M., Kato R., Kayama A., "Size distribution of surface cracks and crack pattern in austenitic steel plates fatigued by cyclic bending," *Journal of Materials Science,* vol. 37, no. 18, p. 3945–3951, 2002.

[131] Python V.3.7, www.python.org.

[132] Moan T., Song R., "Implications of Inspection Updating on System Fatigue Reliability of Offshore Structures," *Journal of Offshore Mechanics and Arctic Engineering,* p. Vol. 122, 2000.

[133] Walter G., Augustin T., "Bayesian Linear Regression — Different Conjugate Models and Their (In)Sensitivity to Prior-Data Conflict," *Statistical Modelling and Regression Structures,* pp. 59-78, 2009.

[134] JCSS, Fatigue models for metallic structures, Joint Committee on Structural Safety, 2011.

[135] Rudd J.L., Gray T.D., "Quantification of fastener-hole quality," *Journal of Aircraft,* vol. 15, no. 3, pp. 143-147, 1978.

[136] Yang J.N., Manning S.D., "Statistical distribution of equivalent initial flaw size," in *Proceedings of the Annual Reliability and Maintainability Symposium*, 1980.

[137] Torregosa R.F., Hu W., "Probabilistic risk analysis of fracture of aircraft structures using a Bayesian approach to update the distribution of the equivalent initial flaw sizes," *Fatigue & Fracture of Engineering Materials and Structures,* vol. 36, p. 1092–1101, 2013.

[138] Cross R., Makeev A., Armanios E., “Simultaneous uncertainty quantification of fracture mechanics based life prediction model parameters,” *International Journal of Fatigue*, vol. 29, p. 1510–1515, 2007.

[139] Li M., Meeker W.Q., Hovey P., “Joint Estimation of NDE Inspection Capability and Flaw-Size Distribution for In-Service Aircraft Inspections,” *Research in Nondestructive Evaluation*, vol. 23, p. 104–123, 2012.

[140] Macheret Y., Teichman J., “Improved Estimation of Aircraft Probability of Failure,” in *IEEE Aerospace Conference*, 2008.

[141] Carr P., Busby P.L., Cresswell S.M., “A unified probabilistic approach to design and inspection of offshore steel structures,” in *Third International Symposium on Integrity of Offshore Structures*, Glasgow, Scotland, 1987.

Appendix A. Common Conjugate Distributions

A.1. Introduction

Within the Bayesian framework, the parameter θ is treated as a random quantity. If a prior distribution for θ, is shown by $f(\theta)$; the posterior distribution, $f(\theta|x)$ can be obtained via Bayes' theorem as:

$$f(\theta|x) = \frac{f(x|\theta) \times f(\theta)}{f(x)} \tag{A.1}$$

Where $f(x|\theta)$ is the likelihood function.

The posterior distribution itself involves computing an integral to normalise the posterior. To obtain the posterior, the following integral must be computed:

$$f(x) = \int f(x|\theta) f(\theta) d\theta \tag{A.2}$$

Which is an integral with respect to the prior.

The basic idea of conjugate priors (given a likelihood function) is to choose a family of prior distributions in a way that the integral of the Eq.(A.2) can be obtained analytically. Based on the Bayes' theorem, the posterior distribution is obtained by multiplying the likelihood function to the prior distribution up to a constant of proportionality. If the posterior distribution has the same distribution as the prior, it is said that the prior is conjugate to the likelihood.

Conjugate models are great because the exact distribution of the posterior is easily obtained and it has an analytical solution. The use of conjugate priors allows all the results to be derived in closed form. Although for the complex models, the computational considerations may be important, there may be little choice to use conjugate priors. Moreover, there are also other reasons not to use conjugate priors.

One of the main disadvantages of using conjugate priors is that conjugate priors involve relatively strong assumptions. Indeed, conjugate priors minimise the impact of the data on the posterior. Therefore, it is important to perform sensitivity analysis to assess how strongly the posterior is influenced by the prior. If the posterior is not influenced strongly by the prior, then it can be used with more confidence. On the other hand, if the posterior is affected intensely by the prior, great care should be taken

to assess whether an expert is comfortable with these priors. Otherwise, it is better to consider other kinds of priors or gather more data to lessen the effect of the prior. Commonly used conjugate prior distributions are shown in Table A.1.

Table A.1. Common conjugate priors

Likelihood	Uncertain Parameter	Prior Distribution	Posterior Distribution
Binomial	Success probability (π)	Beta	Beta
Poisson	Rate (λ)	Gamma	Gamma
Normal	Mean (σ^2 known)	Normal	Normal
Normal	Variance (μ known)	Inverse Gamma	Inverse Gamma
Normal	Mean and Variance (μ, σ^2)	Normal Inverse Gamma	Normal Inverse Gamma
Exponential	Rate (λ)	Gamma	Gamma

A.2. Binomial Model with Unknown Success Probability

A.2.1. Posterior Distribution

Let's consider the likelihood function has a binomial distribution with an uncertain parameter of π (success probability). The probability mass function (PMF) of the binomial distribution is:

$$P(X = x) = \binom{n}{x} \pi^x (1-\pi)^{(n-x)} \tag{A.3}$$

where x is the number of successes and n is the number of trials.

For a binomial model with unknown success probability π, Beta distribution is selected as a prior since the beta distribution is conjugate to the binomial distribution. Two parameters are needed to specify the beta prior distribution, and these will be denoted α and β. Therefore, the probability distribution of the uncertain parameter (π) before incorporating new data is:

$$f(\pi) = \frac{\Gamma(\alpha+\beta)}{\Gamma(\alpha) \times \Gamma(\beta)} \times \pi^{(\alpha-1)} \times (1-\pi)^{(\beta-1)} \tag{A.4}$$

Conceptually, α can be thought of as the number of failures and $(\alpha+\beta)$ is the number of trials over which these failures occurred.

Mean value and standard deviation of the uncertain parameter (π) is calculated as:

$$E[\pi] = \frac{\alpha}{\alpha+\beta}; \qquad Std[\pi] = \sqrt{\frac{\alpha\beta}{(\alpha+\beta)^2(\alpha+\beta+1)}} \tag{A.5}$$

Now, assume new information is available which includes the data consisting of x failures in n trials. The posterior distribution of uncertain parameter (π) can be obtained based on Bayes' rule as:

$$\begin{aligned} p(\pi|x) &\propto p(x|\pi) \times p(\pi) \\ &\propto Binomial\,(n,\pi) \times Beta(\alpha,\beta) \\ &\propto \left[\binom{n}{x}\pi^x(1-\pi)^{(n-x)}\right] \times \left[\frac{\Gamma(\alpha+\beta)}{\Gamma(\alpha)\times\Gamma(\beta)} \times \pi^{(\alpha-1)} \times (1-\pi)^{(\beta-1)}\right] \\ &\propto \pi^{(x+\alpha-1)} \times (1-\pi)^{(n-x+\beta-1)} \end{aligned} \tag{A.6}$$

Which is a $Beta\,(x+\alpha, n-x+\beta)$ distribution. Therefore, when x failure happens in n new trials, the posterior distribution is a Beta distribution with below parameters:

$$\begin{aligned} \alpha_{post} &= \alpha_{prior} + x \\ \beta_{post} &= \beta_{prior} + (n-x) \end{aligned} \tag{A.7}$$

A.2.2. Non-Informative Prior

When there are no strong prior beliefs about the unknown parameters, the small values of α_{prior} and β_{prior} correspond to a broader, non-informative prior distribution. In this case, a prior distribution is selected in a way that gives equal weight to all possible values of the parameters (uniform distribution). For the binomial model, a non-informative prior is $Beta\,(1,1)$which corresponds to a uniform distribution over the [0, 1] interval.

As an example, assume the failure model of pipes under the condensation-induced water hammer (CIWH). A binomial model with uncertain failure probability (π) will be used. The value of π could be any value in the interval [0, 1]. Therefore, a non-informative Beta prior with $\alpha_{prior} = \beta_{prior} = 1$ is selected. Imagine, new information indicates that of 2 failures happened in 110 experiments. The posterior distribution for the uncertain failure probability (π) can be obtained based on Eq.(A.7):

$$\alpha_{post} = \alpha_{prior} + x = 3, \qquad \beta_{post} = \beta_{prior} + (n-x) = 1 + (110-2) = 109$$

Figure A.1 shows the prior and posterior distribution for the parameter of interest (π). The expected value for π after updating is obtained based on Eq.(A.5) equal to:

$$E[\pi_{post}] = \frac{\alpha_{post}}{\alpha_{post} + \beta_{post}} = \frac{3}{112} = 0.0268$$

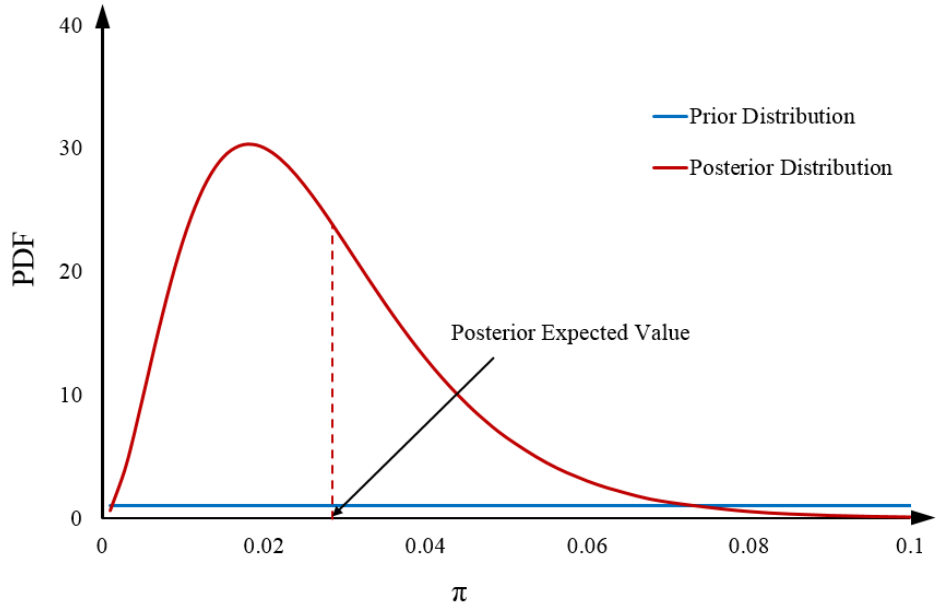

Figure A.1. Prior and posterior distribution for parameter of interest (π)

A.2.3. Effect of Number of Additional Data

Let's look more closely at how the prior and the posterior expected value relate to each other:

$$E[\pi_{post}] = \frac{\alpha_{post}}{\alpha_{post} + \beta_{post}} = \frac{\alpha_{prior} + x}{\alpha_{prior} + \beta_{prior} + n} \quad (A.8)$$

Regarding $n_{prior} = \alpha_{prior} + \beta_{prior}$, Eq.(A.8) can be written as:

$$E[\pi_{post}] = \frac{\alpha_{prior} + x}{\alpha_{prior} + \beta_{prior} + n} = \frac{\alpha_{prior} + x}{n_{prior} + n} = \frac{\alpha_{prior}}{n_{prior} + n} + \frac{x}{n_{prior} + n} \quad (A.9)$$

In Eq.(A.9), the first and second expressions show the contribution of the prior and new data on the posterior, respectively. It shows that if the number of failure in new data (x) is greater than the prior number of failure (α_{prior}), data has a greater effect on the posterior. This is a general phenomenon: as n increases, the posterior distribution gets more concentrated and the likelihood dominates the prior, otherwise, the prior is dominant.

To take into account the effect of the number of additional data, imagine the prior parameters for the unknown parameter are $\alpha_{prior} = 2$ and $\beta_{prior} = 18$. Therefore, prior characteristics of the uncertain parameter are:

$$E[\pi_{prior}] = \frac{2}{2+18} = 0.1; \qquad Std[\pi_{prior}] = \sqrt{\frac{2 \times 18}{(20)^2(21)}} = 0.065$$

In the next step, the new information is provided. Two cases are considered to take into account the effect of the number of additional data on the posterior.

Case (1): One failure in five trials

The expected value and the standard deviation for the posterior are obtained as:

$$E[\pi_{post}] = \frac{\alpha_{prior}}{n_{prior}+n} + \frac{x}{n_{prior}+n} = \frac{2}{20+5} + \frac{1}{20+5} = 0.12$$

$$Std[\pi_{post}] = \sqrt{\frac{(2+1) \times (18+4)}{(25)^2(26)}} = 0.063$$

Case (2): One failure in forty trials

The expected value and the standard deviation for the posterior is:

$$E[\pi_{post}] = \frac{\alpha_{prior}}{n_{prior}+n} + \frac{x}{n_{prior}+n} = \frac{2}{20+40} + \frac{1}{20+40} = 0.05$$

$$Std[\pi_{post}] = \sqrt{\frac{(2+1) \times (18+39)}{(60)^2(61)}} = 0.027$$

Figure A.2 shows how the posterior distribution of the unknown parameter changes when new data is available in two considered cases. As it can be seen from the figure, when few observations are provided, the prior dominates on the posterior results. However, when the number of new information increases, the posterior distribution shifts toward observation (new data). Moreover, the amount of variance will be decreased when new data is provided. New data cause uncertainty reduces.

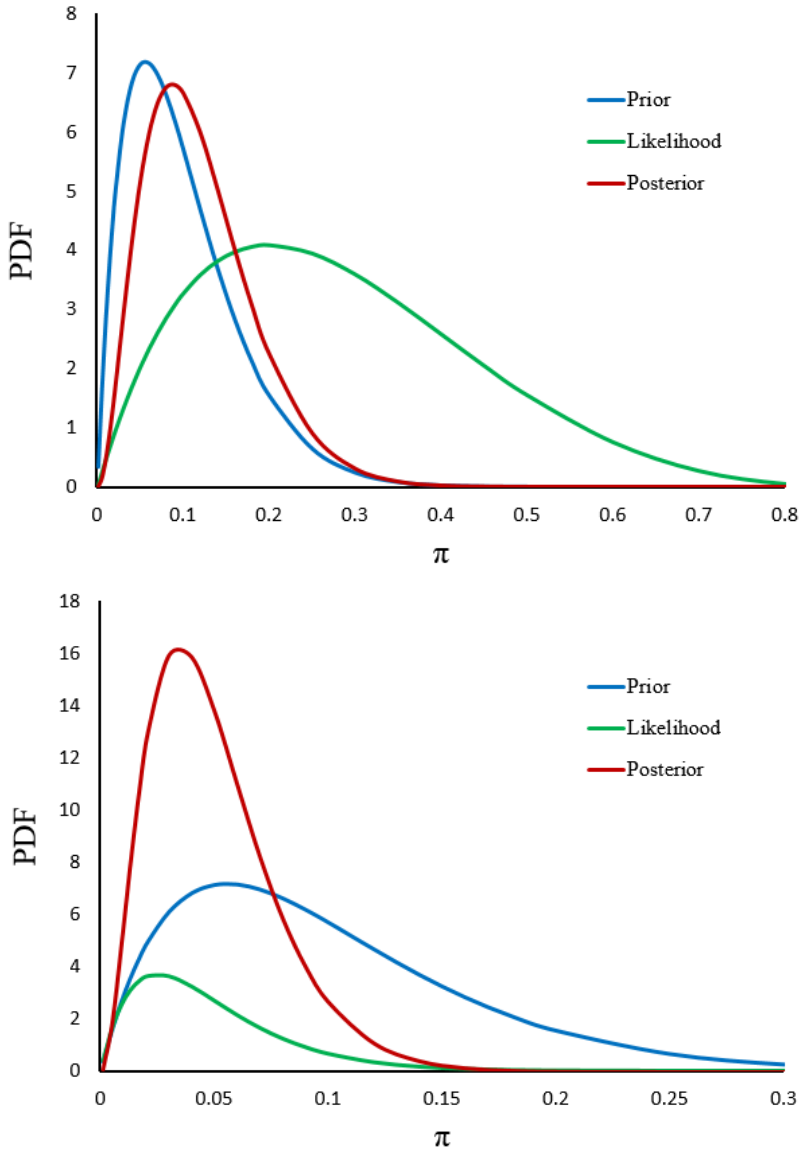

Figure A.2. Posterior distribution in Case 1 (top) and Case 2 (bottom)

A.3. Normal Model with Unknown Mean (Known Variance)

A.3.1. Posterior Parameters

Suppose it is intended to estimate a model where the likelihood of the data is normal with an unknown mean μ and a known variance σ^2. The parameter of interest is μ.

A conjugate Normal prior on μ, with mean μ_0 and variance τ_0^2 can be used here:

$$\begin{aligned} f(\mu|x,\sigma^2) &\propto f(x|\mu,\ \sigma^2) \times f(\mu) \\ &\propto Normal\ (\mu,\ \sigma^2) \times Normal\ (\mu_0, \tau_0^2) \end{aligned} \tag{A.10}$$

Let θ represent the parameter of interest which in this case is μ.

$$
\begin{aligned}
f(\theta|x) \propto & \\
& \left[\prod_{i=1}^{N} \frac{1}{\sqrt{2\pi\sigma^2}} \times \exp\left(-\frac{(x_i-\theta)^2}{2\sigma^2}\right)\right] \times \left[\frac{1}{\sqrt{2\pi\tau_0^2}} \times \exp\left(-\frac{(\theta-\mu_0)^2}{2\tau_0^2}\right)\right] \\
& \propto \exp\left[-\sum_{i=1}^{N} \frac{(x_i-\theta)^2}{2\sigma^2} - \frac{(\theta-\mu_0)^2}{2\tau_0^2}\right] \\
& \propto \exp\left[-\frac{1}{2}\left(\sum_{i=1}^{N} \frac{(x_i-\theta)^2}{\sigma^2} + \frac{(\theta-\mu_0)^2}{\tau_0^2}\right)\right] \\
& \propto \exp\left[-\frac{1}{2\sigma^2\tau_0^2}\left(\tau_0^2 \sum_{i=1}^{N} (x_i-\theta)^2 + \sigma^2\,(\theta-\mu_0)^2\right)\right] \\
& \propto \exp\left[-\frac{1}{2\sigma^2\tau_0^2}\left(\tau_0^2 \sum_{i=1}^{N} (x_i^2 - 2\theta x_i + \theta^2) + \sigma^2(\theta^2 - 2\theta\mu_0 + \mu_0^2)\right)\right]
\end{aligned}
\tag{A.11}
$$

Now, by multiplying the $2\theta x_i$ term in the summation by n/n, the equations can be obtained in terms of the mean of the observations ($\bar{x}$) as:

$$
\begin{aligned}
f(\theta|x) & \propto \exp\left[-\frac{1}{2\sigma^2\tau_0^2}\left(\tau_0^2 \sum_{i=1}^{N} (x_i^2 - 2\theta\frac{N}{n}x_i + \theta^2) + \sigma^2(\theta^2 - 2\theta\mu_0 + \mu_0^2)\right)\right] \\
& \propto \exp\left[-\frac{1}{2\sigma^2\tau_0^2}\left(\left(\tau_0^2 \sum_{i=1}^{N} x_i^2\right) - \tau_0^2 2\theta N\bar{x} + \tau_0^2 N\theta^2 + \theta^2\sigma^2 - 2\theta\mu_0\sigma^2 + \mu_0^2\sigma^2\right)\right]
\end{aligned}
\tag{A.12}
$$

Since $\mu_0^2\sigma^2$ and $\tau_0^2 \sum_{i=1}^{N} x_i^2$ do not contain θ, it can be represented as a constant k, which will be dropped into the normalising constant.

$$
\begin{aligned}
f(\theta|x) \;\propto\; & \exp\left[-\frac{1}{2\sigma^2\tau_0^2}(\theta^2(\sigma^2+\tau_0^2N) - 2\theta(\mu_0\sigma^2 + \tau_0^2N\bar{x}) + k)\right] \\
\propto\; & \exp\left[-\frac{1}{2}\left(\theta^2\left(\frac{\sigma^2+\tau_0^2N}{\sigma^2\tau_0^2}\right) - 2\theta\left(\frac{\mu_0\sigma^2 + \tau_0^2N\bar{x}}{\sigma^2\tau_0^2}\right) + k\right)\right] \\
\propto\; & \exp\left[-\frac{1}{2}\left(\theta^2\left(\frac{1}{\tau_0^2} + \frac{N}{\sigma^2}\right) - 2\theta\left(\frac{\mu_0}{\tau_0^2} + \frac{N\bar{x}}{\sigma^2}\right) + k\right)\right]
\end{aligned}
\tag{A.13}
$$

Let's multiply by $\left(\frac{1}{\tau_0^2} + \frac{N}{\sigma^2}\right) \Big/ \left(\frac{1}{\tau_0^2} + \frac{N}{\sigma^2}\right)$ to simplify the θ^2 term:

$$
\begin{aligned}
f(\theta|x) \;&\propto\; \exp\left[-\frac{1}{2}\left(\frac{1}{\tau_0^2}+\frac{N}{\sigma^2}\right)\left(\theta^2\left(\frac{\frac{1}{\tau_0^2}+\frac{N}{\sigma^2}}{\frac{1}{\tau_0^2}+\frac{N}{\sigma^2}}\right)-2\theta\left(\frac{\frac{\mu_0}{\tau_0^2}+\frac{N\bar{x}}{\sigma^2}}{\frac{1}{\tau_0^2}+\frac{N}{\sigma^2}}\right)+k\right)\right] \\
&\propto\; \exp\left[-\frac{1}{2}\left(\frac{1}{\tau_0^2}+\frac{N}{\sigma^2}\right)\left(\theta^2-2\theta\left(\frac{\frac{\mu_0}{\tau_0^2}+\frac{N\bar{x}}{\sigma^2}}{\frac{1}{\tau_0^2}+\frac{N}{\sigma^2}}\right)+k\right)\right] \\
&\propto\; \exp\left[-\frac{1}{2}\left(\frac{1}{\tau_0^2}+\frac{N}{\sigma^2}\right)\left(\theta-\left(\frac{\frac{\mu_0}{\tau_0^2}+\frac{N\bar{x}}{\sigma^2}}{\frac{1}{\tau_0^2}+\frac{N}{\sigma^2}}\right)\right)^2\right]
\end{aligned}
\tag{A.14}
$$

Eq.(A.14) looks like the density function of a Normal distribution with the following parameters:

$$
\begin{aligned}
&Posterior\ Mean: && \mu_1 = \frac{\frac{\mu_0}{\tau_0^2}+\frac{N\bar{x}}{\sigma^2}}{\frac{1}{\tau_0^2}+\frac{N}{\sigma^2}} \\
&Posterior\ Variance: && \tau_1^2 = \left(\frac{1}{\tau_0^2}+\frac{N}{\sigma^2}\right)^{-1}
\end{aligned}
\tag{A.15}
$$

The prior mean μ_0 and the posterior mean μ_1 are related to each other as:

$$
\begin{aligned}
\mu_1 = \frac{\left(\frac{\mu_0}{\tau_0^2}+\frac{N\bar{x}}{\sigma^2}\right)}{\left(\frac{1}{\tau_0^2}+\frac{N}{\sigma^2}\right)} \;&=\; \frac{\frac{\mu_0\sigma^2+\tau_0^2N\bar{x}}{\tau_0^2\sigma^2}}{\frac{\sigma^2+N\tau_0^2}{\tau_0^2\sigma^2}} \;=\; \frac{\mu_0\sigma^2+\tau_0^2N\bar{x}}{\sigma^2+N\tau_0^2} \\
&= \left(\frac{\sigma^2}{\sigma^2+N\tau_0^2}\right)\mu_0+\left(\frac{\tau_0^2\bar{x}}{\sigma^2+N\tau_0^2}\right)N
\end{aligned}
\tag{A.16}
$$

A.3.2. Effect of Number of Additional Data

Figure A.3 shows how the posterior distribution of the unknown parameter (μ) changes when new data is available. In this figure:

- $\mu = unknown \sim Normal\ (\mu_0 = 0, \tau_0^2 = 0.2)$
- $\sigma^2 = known = \ 0.3$
- $\bar{x} = 1$

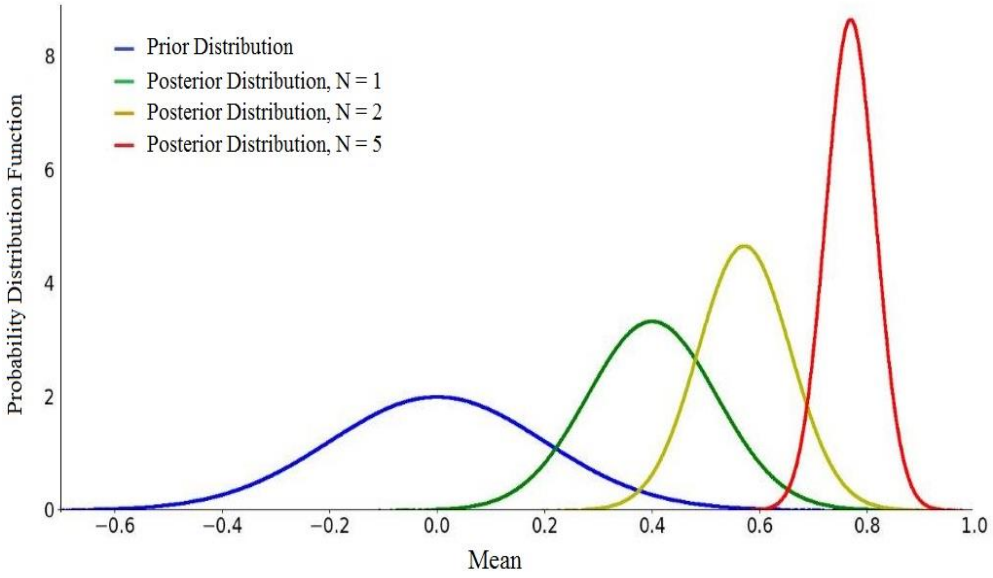

Figure A.3. Effect of the number of additional data on the posterior distribution

It can be seen that the data quickly overwhelms the prior when the number of additional data increases. In fact, as N increases, data mean dominates prior mean (Eq.(A.16)). Moreover, as the number of data increases, the uncertainty of the posterior is reduced (posterior becomes narrower).

A.3.3. Effect of Prior Variance

Figure A.4 shows how the posterior distribution of the unknown parameter (μ) changes regarding the prior estimation for variance (τ_0^2).

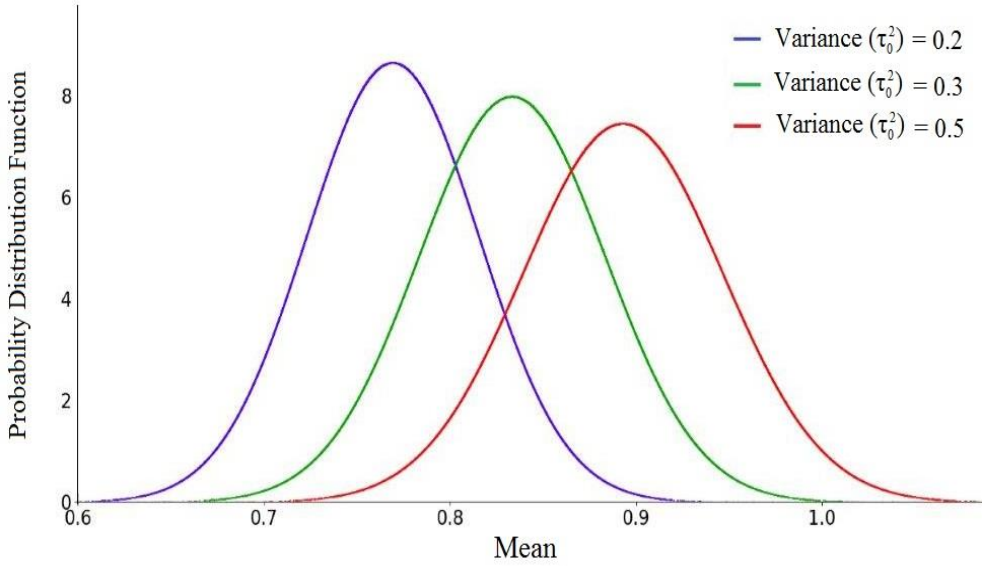

Figure A.4. Effect of prior variance on the posterior distribution

It can be seen that as τ_0^2 decreases (less prior variance), the prior mean becomes more important (Eq.(A.16)). When less prior variance is considered, the posterior distribution shifts to the left ($\mu_0 = 0, \bar{x} = 1$).

A.4. Normal Model with Unknown Variance (Known Mean)

Now it is intended to estimate a model where the likelihood of the data is normal with an unknown variance σ^2 and a known mean μ. The parameter of interest is σ^2.

A conjugate inverse gamma prior can be used for the unknown variance with shape parameter α_0 and scale parameter β_0.

$$\begin{aligned} f(\sigma^2|x,\mu\,) \;&\propto\; f(x|\mu,\,\sigma^2) \times f(\sigma^2) \\ &\propto Normal\;(\mu,\,\sigma^2) \times Invgamma\;(\alpha_0,\beta_0) \end{aligned} \tag{A.17}$$

Let θ represent our parameter of interest which in this case is σ^2.

$$\begin{aligned} f(\theta|x) \propto\; & \left[\prod_{i=1}^{n} \frac{1}{\sqrt{2\pi\theta}} \times \exp\left(-\frac{(x_i-\mu)^2}{2\theta}\right)\right] \times \left[\frac{\beta_0^{\alpha_0}}{\Gamma(\alpha_0)} \times \theta^{-(\alpha_0+1)} \times \exp\,(-\frac{\beta_0}{\theta})\right] \\ \propto\; & \left[\prod_{i=1}^{n} \theta^{-\frac{1}{2}} \times \exp\left(-\frac{(x_i-\mu)^2}{2\theta}\right)\right] \times \left[\theta^{-(\alpha_0+1)} \times \exp\,(-\frac{\beta_0}{\theta})\right] \\ \propto\; & \left[\theta^{-\frac{n}{2}} \times \exp\left(-\frac{\sum_{i=1}^{n}(x_i-\mu)^2}{2\theta}\right)\right] \times \left[\theta^{-(\alpha_0+1)} \times \exp\,(-\frac{\beta_0}{\theta})\right] \\ \propto\; & \left(\theta^{-(\alpha_0+\frac{n}{2}+1)}\right) \times \exp\left[-\left(\frac{\beta_0}{\theta} + \frac{\sum_{i=1}^{n}(x_i-\mu)^2}{2\theta}\right)\right] \\ \propto\; & \left(\theta^{-(\alpha_0+\frac{n}{2}+1)}\right) \times \exp\left[-\left(\frac{2\beta_0 + 2\left(\frac{\sum_{i=1}^{n}(x_i-\mu)^2}{2}\right)}{2\theta}\right)\right] \\ \propto\; & \left(\theta^{-(\alpha_0+\frac{n}{2}+1)}\right) \times \exp\left[-\left(\frac{\beta_0 + \left(\frac{\sum_{i=1}^{n}(x_i-\mu)^2}{2}\right)}{\theta}\right)\right] \end{aligned} \tag{A.18}$$

Eq.(A.18) represents the density function of an inverse gamma distribution with the following parameters:

$$\alpha_1 = \alpha_0 + \frac{n}{2}$$
$$\beta_1 = \beta_0 + \frac{\sum_{i=1}^{n}(x_i - \mu)^2}{2} \tag{A.19}$$

A.5. Exponential Model with Unknown Rate

Now, suppose the likelihood of the data is exponentially distributed. The unknown parameter here is the rate parameter (λ). In this case, a conjugate Gamma prior can be used for λ. Gamma distribution has two parameters, α, and β:

$$f(\lambda) = \frac{\beta^{\alpha}}{\Gamma(\alpha)} \lambda^{\alpha-1} e^{-\beta\lambda} \tag{A.20}$$

The posterior distribution is obtained as:

$$\begin{aligned} f(\lambda|x) &\propto f(x|\lambda) \times f(\lambda) \\ &\propto Exp\ (\lambda) \times Gamma\ (\alpha, \beta) \end{aligned} \tag{A.21}$$

Let θ represent our parameter of interest which in this case is λ.

$$\begin{aligned} f(\theta|x) &\propto \left[\prod_{i=1}^{N} \theta e^{-\theta x_i}\right] \times \left[\frac{\beta^{\alpha}}{\Gamma(\alpha)} \theta^{\alpha-1} e^{-\beta\theta}\right] \\ &\propto \left[\theta^{N} e^{-\theta(x_1+\cdots+x_N)}\right] \times \left[\frac{\beta^{\alpha}}{\Gamma(\alpha)} \theta^{\alpha-1} e^{-\beta\theta}\right] \\ &\propto \left[\theta^{(\alpha+N-1)}\right] \times \left[e^{-(\beta+\sum_{i=1}^{N} x_i)\theta}\right] \\ &\propto \left[\theta^{(\alpha+N-1)}\right] \times \left[e^{-(\beta+N\bar{x})\theta}\right] \end{aligned} \tag{A.22}$$

Eq.(A.22) represents the density function of a Gamma distribution with the following parameters:

$$\begin{aligned} \alpha_1 &= \alpha_0 + N \\ \beta_1 &= \beta_0 + N\bar{x} \end{aligned} \tag{A.23}$$

where N is the number of additional data and $\bar{x}$ is the mean value of N additional data.